A Study into Vibrations of Turbocharger Blading with A Lacing Wire

by

Xu Wang

A Doctoral Thesis

Submitted in partial fulfilment of the

requirements for the award of

Doctor of Philosophy

of the

Loughborough University of Technology

September 1994

Abstract

The vibration of a turbocharger blade and dynamic characteristics of bladed packets connected by a lacing wire have been studied. The study was carried out using three analytical and experimental methods. They are: Modal Testing, Electronic Speckle Pattern Interferometry (ESPI) and Finite Element Analysis (FEA).

Vibration modes of a turbocharger blade with aerodynamic profile, with and without a lacing wire, were identified using model blades with simplified geometry. The separation of coupled modes was achieved using ESPI tests.

The modes of vibrations of bladed packets were identified. The effect of inter-blade coupling through a lacing wire is that a cluster of sub-modes are generated in bladed packets corresponding to each fundamental mode of the free-standing blade, the number of the sub-modes being equal to the number of blades in the packet. Apart from the fundamental sub-mode, the vibration of all other sub-modes are out of phase with different phase relations.

The stiffness of the lacing wire and its location with respect to the blade make great contributions towards certain mode clusters in terms of mode shapes and natural frequencies.

The nonlinearity of the stiffness of the deformed lacing wire caused by centrifugal force was established. The coupling of this nonlinearity with different vibration amplitudes, due to different phase relation, results in the dynamic mistuning in lacing wire stiffness. This mistuning is considered to be a major attribute in reducing the responses at resonance.

Acknowledgements

Publications from This Work

1. Chapman and Wang: "Interpretation of Experimental and Theoretical Data for Prediction of Mode Shapes of Vibration Turbocharger Blades", Proc. of the ASME Conf. on Mechanical Vibration and Noise: Bladed Disk Assemblies, Boston, U.S.A., Sept. 1987. Edited by Kielb. R., Crawley, E. and Simonis, J.

    Also appears in Trans ASME, Journal of Vibration, Acoustics, Stress, and Reliability in Design, Vol 110, pp 53-58, Jan. 1988.

2. Chapman and Wang: "Development of a Laboratory Exercise to Investigate Vibration Characteristics of Turbine Blading", Proc Sixth British Conference on the Teaching of Vibration and Noise, pp 153-162, July 1988.

3. Chapman and Wang: "Theoretical and Experimental Determination of Natural Frequencies of Laced Blading", Proc of the Conference on Modern Practice in Stress and Vibration Analysis, Liverpool, UK. April 3- 5, 1989.

4. Chapman and Wang: "Vibration Analysis of Laced Blades", Proc of ASME Conference on Mechanical Vibration and Noise, Montreal, Sept, 1989.

5   Chapman and Wang: "Vibration Behavior of Laced Turbocharger Blading," Proc of the 3rd IFToMM Conf on Rotordynamics, Sept. 1990, Lyon, France.

6. Chapman, G. M., Swain, E., Wang, X., Yang, M., "Vibration Reduction of blading Using Interconnecting Elements", Rotordynamics' 92, Proceedings of the International Conference on Rotating Machine Dynamics, Venice, April, 1992, pp 270-277.

iv

Contents

Contents

Contents

Contents

Contents

List of Figures

List of Tables

List of Tables

Chapter 1

Introduction

Vibration in a mechanical structure arises if a periodic or non-periodic change in applied forces takes place, the severity of the vibration depending on the magnitude of this change in forces and their frequencies. Turbomachinery is particularly subject to this change which is a direct threat to its reliability.

1.1 Importance of the Reliability of Turbomachinery

The availability and safety of large modern power generating and industrial condensing turbines are dependent on the performance of their last stage. As these turbines form the basis of power and industrial processing plants their reliability and high efficiency are most important.

Long down-times due to damage will lead to high operating losses. The cost of these outage times is normally much greater than the repair cost of the turbomachine.

It is obvious that not only high operating efficiency is required, but also the reliability of turbomachine components is a major consideration. These two factors influence the economics of a turbomachine. If the availability could be increased by one percent the plant-efficiency also increases from 0.2 to nearly 2 percent depending on the utilization factor and the type of fuel used in the power plant [198].

Commercial reasons have encouraged the production of larger output turbines with little or no increase in weight or size. In these high power turbines the mechanical and thermal loadings increase and the resulting stresses get near the upper safety limit of the turbine materials. This causes a decrease in the stress life and may lead to a fatigue failure. These additional loadings and the unsteady modes of operation must be taken into consideration when designing a turbine without risk of

failure.

In marine operations, the generations of two-stroke and four-stroke engines introduced or refined in 1980s have aimed to achieve the following improved qualities over their low speed and medium speed precursors:

■   the ability to burn residual fuels of continually declining quality;

■   improved engine reliability under various operating conditions; and

■   flexibility of operation at different loads or ratings with increased emphasis on part-load conditions.

A significant contribution in achieving those aims has come from developments in turbochargers and turbocharging systems. Medium-speed four-stroke engines generally operate at rather higher boost pressure ratios than the two-stroke. High turbocharger efficiency is necessary in order to maintain low valve temperatures and of course to assist in the attainment of low fuel consumption. High rotational speeds and turbine temperatures must be adequately countered by improvements in the design of the turbocharger rotating assembly and bearings. As part of the power generating system, the reliability of the turbocharging system forms the basis of a durable and reliable operation.

Turbine blade failures have been a significant cause of unit unavailability and expense to the power generating industry. In a survey conducted by The Electric Power Research Institute (EPRI) in United States [172], it was found that, for the years 1970-1981, there were 216,380 hours of reported downtime for the 192 units included in the sample. The total cost of replacement parts, as estimated by the 69 reporting utilities, was $87,456,000 and the break-down costs are normally much more than the cost of repair.

Damage-statistics show that with 40% the runner-blades demand the greatest portion of the overhaul-costs caused by individual steam turbine parts. Blade vibrations are the most frequent causing factors. A particular damage factor can be seen at the low pressure (LP) stage of condensing turbines. Besides the high static loads by centrifugal and aerodynamic forces, the LP-blades are exposed to additional dynamic loads whose intensity and appearance could not have been predicted satisfactorily. Over 79% of all blade related outages occurred in the low Pressure turbines and 75% of those occurred in the L-0 and L-1 rows in fossil units [45].

Fleeting and Coats [63] reported their experiences on the blade failures that occurred in the HP turbines of RMS "Queen Elizabeth II" in 1968. This ship left the manufacturers on 19 November 1968 and failures occurred quite early on 24 December 1968 during the ship's maiden voyage from Tail O' the Bank, resulting in a complete damage to the 9th and 10th stage starboard HP turbine rotors. This failure is attributed by them to resonances of the blade packet in the respective stages with nozzle excitation.

Frank [64] reported considerable damage that occurred when a 600 MW turbo-set was restarted after a general inspection. The major overhaul was carried out after 25000 hours of service. Before pressing the machine into service, the electrical overspeed protection device was checked to respond at the preset 108% of the nominal speed. Then the speed was reduced to check the mechanical overspeed protection device set to switch the turbo-set off at about 110% of the rated speed. Just before attaining this mark, the machine exploded. The generator shaft at the turbine end ruptured over half its length and broke in the middle. Two fractures had occurred at the exciter end of the shaft. The shafts of three low pressure sections were fractured both at the turbine and the generator ends. The medium pressure section was also broken at the generator end. The high pressure section of the turbine was not affected. The incident has been attributed to a sudden instability in the train

of shafts, which may have been caused by a blade fracture in the last low-pressure stage or the breakage of a bearing. The turbo-set damage alone is estimated to be $40 million. A study conducted by Dewey and Rieger [44] reveals that high cycle fatigue alone is responsible for at least 40% failures in high pressure stages of steam turbines.

A critical review of the various problems with present day jet aircraft reveals that those associated with blades emerge high in order of importance. Gas turbine blades can fail if they are subjected to alternating forces having frequencies near their important resonant frequencies. The danger of resonances of blades or blade packets in working machines, and the consequential failure due to fatigue, is too well known to require amplification.

1.2 Importance of Turbine Blades

The most critical component of any turbomachine is the blading. Blades are the instruments by which a compressor or turbine fulfils its function and they are usually exposed to the most hostile environment in the whole machine. In turn, one of the most difficult to control is the dynamic loading to which the blades are subjected. These two facts combine to present us with a major problem to be overcome in the design and operation of turbomachinery: that of preventing excessive blade vibration levels under operational conditions. The essential problem is simply stated: the structural integrity of blading is of primary importance as the loss of a single blade will generally cause extensive secondary damage. Modern turbomachinery must run at high speeds of prolonged periods of time and so blades vibrating at frequencies typically between 100 and 20,000 Hz will undergo a large number of cycles in a relatively short time (500 Hz for 6 hours exceeds 10^7 cycles). The possibility of fatigue failure is thus of primary concern and design techniques

must ensure that the vibration levels experienced during operation will not induce fatigue failure of any blade during the life of the machine.

Therefore, an intimate knowledge and understanding of the vibration characteristics of the blades in their operating environment is essential for eliminating vibration problem conditions.

1.3 Sources of Excitation in Service

In service, blade vibrations are most likely to be excited by the unavoidable non-uniformities of steam flow and pressure around the annulus either upstream or downstream of the moving blades, but may also sometimes be excited by rotor movements. The possible causes for turbine blade excitation are:

a)   Non-uniform pressure distributions in the inlet and exhaust piping.

b)   steam extraction points

c)   unequal spacing between guide blades at the parting plane

d)   pitch errors

e)   change in radial clearance due to warping of the housing

f)   jet excitation

g)   non-uniform wake shed behind a row of blades due to the loss distribution and the change of the angle of attack of the rotating blade row

h)   flow disturbance due to probes

i)   partial admission

j)   self excited vibration such as flutter

All these discontinuities have a periodic nature. Regardless of the pattern of the exciting forces, they will be repeated periodically, one or more times for each revolution of the turbine. These discontinuities can be analyzed into different harmonic components, which cause a periodically varying force acting on the moving blades.

The predominant dynamic load is the source of the operation principles on which the machine is designed. When a rotor blade passes across the nozzles of the stator, it experiences fluctuating lift and moment forces repeatedly at a frequency given by the number of nozzles multiplied by the speed of the machine. The blades are very flexible structural members, in the sense that a significant number of their natural frequencies can be in the region of possible nozzle excitation frequencies.

1.4   Blade Safety against Vibrations

1.4.1   Freedom from Resonance in the Operating Range

Every turbine stage, without exception, is designed such that the natural frequencies of practical importance are clear of resonance with significant excitation frequencies. For long blades, the wheel mode frequencies are designed to be clear of the relevant low multiples of running speed. This signifies that the natural frequencies of no runner blade of the turbine to be allowed to correspond to whole

multiples of the rotational frequency and needs a precise knowledge of the natural frequencies of all the turbine stages.

Though a machine can be normally designed to avoid resonance at its steady operating speed, it experiences resonances several times during the starting and shutting down of the machine, i.e. whenever the instantaneous speed of the machine gives rise to a nozzle excitation coinciding with the blade frequencies. Thus it is not infrequent to find major shut-downs of these machines arising because of blade failures.

1.4.2 Reduction of Vibration Stress Using Damping Elements

It may be possible to design a machine with constant rotational speed as for example a turbine driving a generator, so that no lower blade mode in the turbine at the operating point is in resonance with a rotational harmonic. But it is not possible with a machine which has a range of rotational speed of 60 to 110 percent of the rated speed as for example a turbine driving a compressor.

Vibrations of turbocharger blades is a problem for turbocharger manufacturers since it is very difficult to avoid all dangerous resonances. Operating experience with large turbochargers driven by the pulsed pressure system of energy transmission from engine to turbocharger identifies pressure forces with a wide range of frequency components [38]. Coupled with these gas-borne excitation frequencies are further excitation frequencies generated as a consequence of blade pass frequencies (e.g. the frequency at which rotor blading passes the stationary nozzle blading). It follows therefore that components within the turbocharger can easily be excited at any of one of the many natural frequencies associated with its constituent parts.

All these excitation sources increase the difficulties associated with the design

8

of bladed disk assemblies and have caused designers to consider the inclusion of damping devices in the blading assemblies with the objective of reducing possible damage to operating systems.

In particular, with the considerable increase in the power weight ratio of the machines, one uses the damping or binding elements in such machines and also in constant speed machines. Continuous blade-to-blade connection round the whole circumference is provided, either by shrouding, or for the longest blades by inter-connecting rods, to avoid the complexities associated with packets. Mostly these are provided in the top third of the blade height, and in recent times in gas turbines damping elements are provided at the foot region of the blade.

1.5 Use of Lacing Wires

The forms of damping elements include riveted shrouds, binding/tie/lacing wires, lashing pins and snubbers. The effectiveness of such elements in practice is confirmed from many operating machines.

One method for minimising blade vibration is to employ lacing wires threaded between a group of blades on the disk. Irrespective of detailed design, as indicated by Chubb [36], there are two main categories of mechanical blade vibration dampers -- those designed as part of the initial concept of the unit and those introduced as a necessary emergency measure to control unacceptable vibration that was not expected initially. It is perhaps in this latter application that the true value of lacing in the design of turbomachine buckets is to be found. It gives a relatively simple modification that at least gives a moderately long-life blade, although at the expense of performance penalties and an increase in the number of failure sensitive parts. The location of the lacing wire hole in the blade must be carefully considered to

ensure safe stress levels when full load conditions are met. Also the position must be such that maximum advantage is gained from the damping characteristics at the wire/blade interface without weakening the blade by introducing high stress concentrations in highly stressed areas.

The basic design of lacing wires is that there is a continuous wire that runs through some portion of the blade above the retaining disk as illustrated in Figure 1.1.

The large amount of literature (see Chapter 2) on the vibrations of turbine blades, relating both to theoretical and experimental research, bears witness to the enormous amount of work done in this field. In spite of this, the need to modify existing bladed disks, in order to forestall breakdown or, at any rate, to improve vibratory performance, provides the demand in establishing better understanding of the vibrations of blade packets. Theoretical research has to overcome the obstacle represented by the dimensions involved to ensure sufficient accuracy in calculating the frequencies. This applies particularly when packets of blades have to be examined, whose frequency range becomes denser and narrower as the number of blades forming the packet increases.

In addition, the modifications that can be made in a bladed disk that is already installed in order to prevent damaging vibrations can, in practice, only be concentrated within the limitations imposed by the blades themselves and, especially, imposed by the way in which they are grouped together in packets. Theoretical research on bladed disks therefore involves the need to look thoroughly into the part played by these limitations, particularly by the shroud in influencing the natural frequencies and on the corresponding configurations taken on by the system and the stress states connected with those configurations.

1.6 The Objective of This Study

The intention of this study was to establish:

■ the nature of the modes of vibration for an assembly of blades coupled by a lacing wire

■ typical vibration response characteristics of such an assembly

■ the effects of a lacing wire on the modes of vibration of free standing blades

■ the primary interest here lies in studying how the blades interact with each other, to see how the natural frequencies of a completed assembly of blades are related to those of a single blade.

1.7 Overall Project Solution Strategy

The primary aim was to understand the vibration characteristics of turbine blading with lacing wires. It was noticed that the modes of vibration of bladed assembly were very complicated. The complexity arises from the complicated shape of turbine blades due to aerodynamic design and stress requirement, minor differences among blades in the same assembly and in particular, the inter-blade coupling elements.

In order to understand the complex modes of vibration of bladed assembly, it was considered necessary to understand the nature of vibration modes of a free standing blade with complex geometric shape. In addition to the purpose mention above, the aim of this step was also to justify the analytical techniques proposed and

to verify the interpretation of results obtained from using these techniques. The work is reported in Chapters 4 and 5.

Then the investigation would be expanded to study the effects of a lacing wire on a single blade. The understanding of modes of vibration of a single blade under the influence of a lacing wire could be established and the modification on the modes of vibration of free standing blades due to the lacing wire could be identified. This work is reported in Chapter 6.

Finally, the study into the understanding of vibration characteristics of a blade packet assembly connected by a lacing wire was carried out and reported in Chapter 7. The final conclusion is given in Chapter 8.
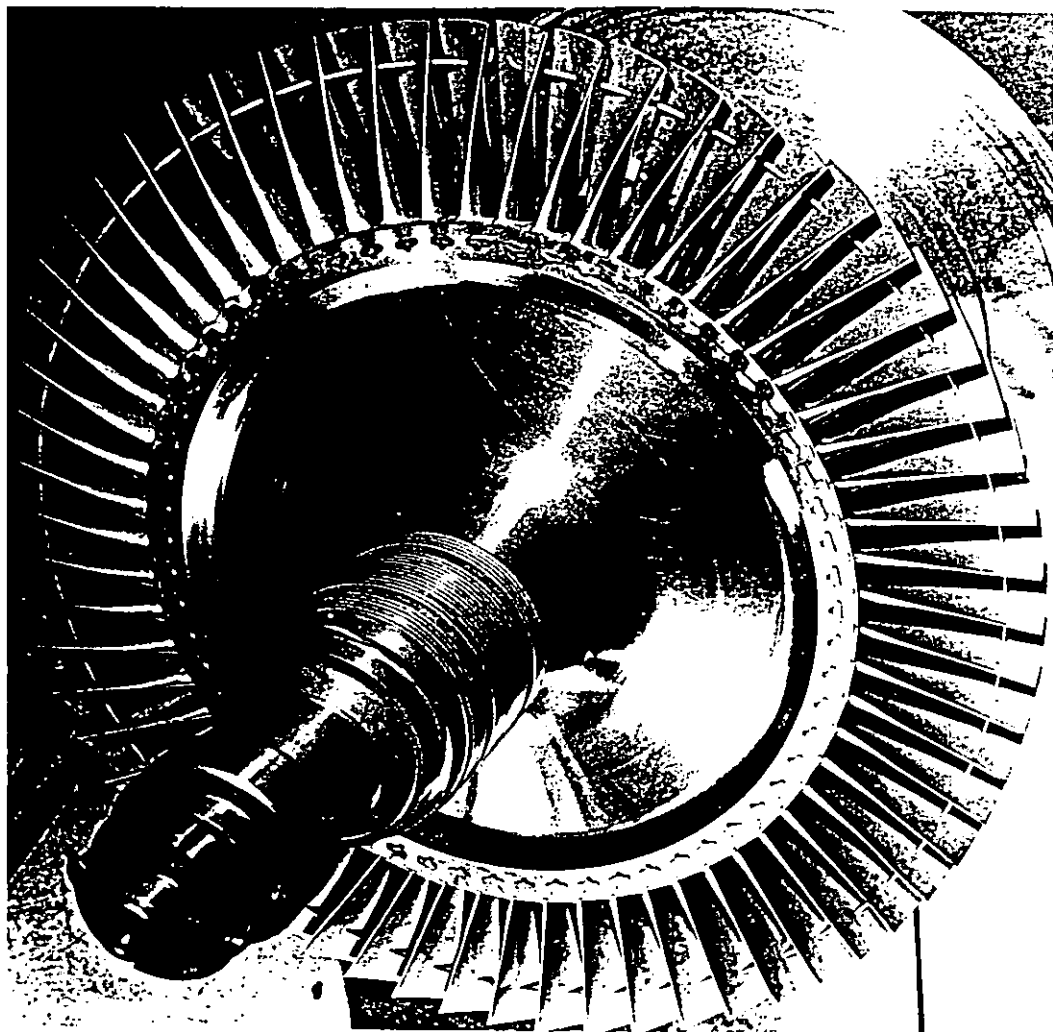
Figure 1.1   A typical bladed disk assembly with lacing wires

Chapter 2

Review of Previous Work

2.1   Introduction

2.1.1   Technical Description of the Problem

2.2   Single Blade Vibrations

2.2.1   Analytical Solutions

2.2.1.1 Timoshenko Theory

2.2.2   Effects of Taper

2.2.3   Vibrations of Rotating Blades

2.2.4   Effects of Pretwist

2.2.5   Root Flexibility

2.3   Coupled Blade Vibrations

2.3.1   Bladed Disk Assemblies

2.3.1.1 Mistuning

2.3.1.2 Mode Splitting

2.3.1.3 Rogue Failure of Turbine Blades

2.3.2   Vibrations of Blade Packet Assemblies

2.4   Conclusion

Figures

14

2.1 Introduction

Turbine blades are major components in turbomachinery. The numbers of blades in any turbomachine can be up to thousands. Their sizes and shapes vary significantly in order to meet the very demanding criteria imposed by industries. They operate in very hostile environment which is subjected to vibration excitations. The failure of a single blade may cause considerable secondary damage to the turbomachine and consequently, results in high costs for repair and more importantly for long period of break-down.

It is also relevant to consider the extent of the problem of blade vibration: the majority of large turbomachines are either gas turbines (all forms of transport, power generation) or steam turbine (power generation). In round numbers there will be about 20 stages of rotating blades in an aircraft gas turbine, representing a total of some 2,000 blades, and there will be in the order of 5000 blades in the 60 stages of a typical 660 MW steam turbine. A major airline with a fleet of 150 jet aircraft will have some 500 engines in use, and a further 150 in reserve, representing between 10,000 - 15,000 stages and a total of 1,000,000 to 1,500,000 rotating blades. The extrapolation of these basic figures clearly indicates a very large number of blades currently in use, and helps to explain why there has been (and continues to be) much attention given to the treatment of blade vibration problems.

2.1.1 Technical Description of the Problem

Figure 2.1 represents a typical fan blade. The blade has considerable twist along its length. It has curvature (camber) in the direction transverse (chordwise) to its length, but negligible curvature in its longitudinal (spanwise) direction. Typical cross-sections are aerofoil shapes, varying in thickness along the chord. The

15

thickness and curvature both vary along the length of the blade, decreasing from the fixed root towards the free end. The width of the blade also varies along the length. The particular blade shown in Figure 2.1 is relatively long compared with its width (i.e., large aspect ratio), although much shorter ones are also utilized.

The blade is attached at its root to a circular disk by means of a dovetail joint. Typically, 30-40 blades will be attached circumferentially about the periphery of the disk, forming one stage of the turbomachine. The disk and its attached blades rotate at large angular velocity (Ω) about an axis perpendicular to the plane of the disk. As a result of centrifugal forces arising from the rotation, there is a small, but significant, amount of blade untwisting. This causes the attached shroud to lock with those of adjacent blades and adds stiffness to the individual blades. In some applications, such as steam turbines, lacing wires may be used in place of shrouds.

An aircraft gas turbine engine will have many stages. The fan blades described above will be followed by numerous compressor stages, with blades having aspect ratios varying between 5 and 1. Subsequently, the combusted gas encounters turbine blades (or buckets) having thick, highly cambered cross-sections and operating at high temperatures. Figure 2.2 shows a highly-twisted, actual turbine blade, with cross-sections taken at the root, the free end, and midway along the blade.

2.2 Single Blade Vibrations

If a blade is relatively long, it may be modelled as a beam. If there is no contact between adjacent shrouds and if the disk is relatively stiff, the beam may be considered as cantilevered. Though a turbine blade is loosely mounted on the disk, the root gets encastered due to the centrifugal force, thus almost satisfying the

cantilever fixed end conditions. Therefore, a single free-standing blade can be considered as a pre-twisted cantilever beam with an asymmetric aerofoil cross-section mounted at a stagger angle on a rotating disk and considerable useful information for frequencies and mode shapes are obtainable from a relatively simple beam model.

Coupled bending-torsion vibrations occur when the centre of flexure does not coincide with the centroid as in the aerofoil blade cross-section and the vibrations are coupled between the two bending modes because of pretwist. The problem becomes further complicated because of second order effects such as shear deflections, rotary inertia, warping of the cross section, root fixing and Coriolis accelerations. In general the equations of motion will be six coupled-partial-differential equations [154] coupled between the two bending deflections, the two shearing deflections, the torsional deflection and the longitudinal deflection. The warping function will be obtained by a modified Poisson equation, taking into account the dynamic conditions of the blade. Thus, theoretically it is a difficult task to determine the natural frequencies of an actual turbine with all the effects mentioned.

Most of the early work was carried out on free standing single blades with the aim to identify their natural frequencies and mode shapes

2.2.1 Analytical Solutions

The exact analytical solutions, which are only available for a few simple cases, provide an invaluable basis for comparison when assessing the validity of numerical methods. The starting solution for a simple stationary blade is obtained from the classical Euler-Bernoulli beam [190] with cantilever boundary conditions for bending vibration and St. Venant's non-circular rod for torsional vibrations [190], [191].

Typical examples using a classical approach of solving the differential equations of motion of a cantilever blade under very simplified conditions are Ward [204], Wrinch [211], Meyer [116] on tapered beams and Sutherland and Goodman [176] on the effects of shear and rotary inertia. Energy methods of continuous systems are very powerful in the solution of turbine blade problems. Different versions of energy methods are Rayleigh [26] Rayleigh-Ritz [42], Galerkin [141], Lagrange [83], Reissner [153], and Nemat-nassar [92] based on the basic Hamiltons's principle. Other methods used for solving differential equations of motion of cantilever blades are Integral equation approach [94], Perturbation [109] and Collocation [141] procedures. The literature in this area is reviewed by Rao [142, 144, 145 and 146].

Discrete model approaches were widely used to obtain solutions of turbine blade vibration problems. Methods employed, such as Holzer and Myklestad, use a trial and error procedure to determine the frequencies. The applications of these methods can be found in [178, 158, 90, 152] on Holzer-Myklestad, [113, 114] on Station Function method, [187, 132, 179] on Matrix method, [30, 31] on Finite Difference and [47, 183] on Finite element method.

2.2.1.1 Timoshenko Theory

A large amount of the published literature on vibration of beams is limited to Bernoulli-Euler theory which does not account for the effects of shear deformation and rotary inertia. The concept of rotary inertia was introduced by Rayleigh and later extended by Timoshenko who, using conventional Newtonian approach, obtained an equation allowing for both shear deflection and rotary inertia.

Boley and Chao [20] obtained some solutions of the Timoshenko beam equations under four types of loadings using Laplace transformation, taking into

account of the effects of shear deformations and rotary inertia. A comparison with the corresponding results of the Bernoulli-Euler theory were briefly presented. Studies using very similar methods were reported by other authors [43, 117, 194].

After demonstrating the application of Rayleigh-Ritz and Galerkin methods in the solutions for a hinged-hinged beam [74], Huang [75] obtained the solutions for free flexural vibrations of finite beams including the effects of shear and rotary inertia for various cases of simple beams. Similar work were reported by other authors [35, 12, 77, 41, 7, 48, 74].

Lee [93] applied an extended minimum principle and the Schwartz integration method to flexural vibration of a wedge with rotary inertia and shear. The upper and lower bounds of the first two eigenvalues were established. The effects of rotary inertia and shear were clearly demonstrated against the classical Kirchhoff solution.

Hutchinson and Zillmer [78] developed an exact solution for the vibrations of rectangular parallelepiped. They [79] also used this solution as a basis of comparison for the Timoshenko beam theory and a plane stress approximation developed in their work.

2.2.2 Effects of Taper

The feature of taper in turbine blade vibration has been studied by many researchers. Lateral vibrations of cantilever beams with variable cross-sections were studied as early as 1888 by Meyer [116]. The solutions of this problem were sought in the following years by many others such as Ward (1913) [204], Wrinch (1922) [211], Conway (1946) [39] Nobuo (1957) [124], Wang (1966) [201], Downs (1977) [49], Arvind and Gupta (1985) [11].

Exact solutions are given by Cranch and Adler [32] for beams ranging linearly in both depth and width. Taylor [180] gave power series solutions of blade natural frequencies for the case of a uniform beam and a completely tapered beam. Mabie and Rogers [104] solved the differential equation of vibration of tapered beams with different boundary conditions using Bessel functions and tabulated the results of the first five vibrational frequencies for different breadth and depth taper ratios.

Rao [140] used the Galerkin method to calculate the fundamental natural frequencies of beams tapered in depth. A computing process employing Ritz-Galerkin method was used by Rao and Carnegie [149] to determine the first three lateral frequencies of tapered cantilever beams.

Collocation method was applied by Rao [141] to obtain first three natural frequencies of tapered cantilever beams with rectangular cross-section and showed close agreement with the results produced by the Ritz-Galerkin process. Banks and Kurowski [14] solved eigenvalue problem of the transverse vibration of double tapered beam with different boundary conditions following McKenna's [111] approach.

A variety of numerical methods have been used. Myklestad [120] presents an approximate method for calculating the frequencies and mode shapes of cantilever beams. The beam is modelled as a series of lumped masses and results are obtained by an iterative calculation procedure. Myklestad notes that for accuracy in the higher modes, at least eight significant figures are required in the calculation. Thomson [187] uses a similar method to Myklestad but models the tapered beam as a series of uniform stepped segments. Housner and Keightley [73] applied the Myklestad procedure to determine the first three modes of a tapered beam.

Finite element solutions, using Euler theory, for various assumed deformation shapes are given by Lindberg [99], Klein [87], Krishna [88] and Krishna and Prabhakara [89]. None of the solutions given are particularly accurate and those of Krishna and Krishna and Prabhakara, who assume a linear displacement function, are at best poor.

Downs [49] uses dynamic discretization to calculate the frequencies, mode shapes and stress distribution patterns for cantilever beams possessing both linear width and/or depth taper. Results are presented for both Euler and Timoshenko theory and comparisons with exact solutions wherever available show the method to provide results of extremely high accuracy.

Most published analytical results for tapered beam elements have been limited to a few cross-sectional shapes and simplest sets of end conditions. Arvind and Gupta [11] derived the stiffness and consistent mass matrices for tapered beam elements of any cross-sectional shape. The utilization of these stiffness and mass matrices of good accuracy would enable designers to minimise the efforts involved in computing the dynamic response of tapered beams to arbitrary forcing functions.

Bernoulli-Euler theory and Bessel functions were used by Banerjee and Williams [13] to obtain explicit expressions for the exact dynamic stiffnesses for axial torsional and flexural vibrations of a range of tapered beams. These exact dynamic stiffnesses enable members with taper to be included in exact frequency calculations. However, shear deflections and rotary inertia were neglected and the effect of any axial force on the flexural behaviour had also been neglected.

Torsional vibration of cantilever tapered beams with various cross-sections were investigated by Walker (1938) [199], Vet (1962) [195], Rao (1965) [139], Rao, Belganmkar and Carnegie (1970, 1972) [147, 151].

21

2.2.3 Vibrations of Rotating Blades

The simplest representation of a rotating blade is a uniform, straight, cantilever beam having vibrational displacements which are perpendicular to the plane of rotation. The radially directed body force adds to the elastic restoring forces, causing the square of the natural frequencies to increase approximately proportional to the square of the rotation speed. This eigenvalue problem is widely formulated and can be found in several vibrations textbooks. The differential equation is linear, but has variable coefficients. No exact, closed form solution is known.

In a relatively early paper Boyce [22] showed how the problem could be generalized to accommodate a finite disk radius, and how upper and lower bounds for the frequencies can be determined. Another early, related paper is the one by Plunkett [132]. Sutherland [175] demonstrated in an early paper the effects of a destabilizing (i.e. frequency reducing) body force arising due to the local component of circumferential displacement, on natural frequencies when the beam vibrates in the plane of rotation. The approach was later generalized by others to account for motions having components in both directions [102, 19, 161, 101].

A lot of work has been carried out by Carnegie [30, 27, 28, 29, 148, 150, 152] to treat the vibrating blade as a beam in a thorough and rational manner, especially for the general types of blades having both camber and pretwist and therefore, coupling among all modes. His early analytical works [27, 28, 29] were principally devoted to deriving consistent and complete sets of equations of motion. Subsequently Rao [148, 150, 152], Banerjee [13] and others [100, 115, 118, 119, 134, 138, 192, 197, 203, 205, 207] have done much to establish the effects of pretwist, camber, taper, and hub radius, together with rotational velocity, upon the free vibration frequencies and mode shapes of rotating, beam-like blades.

Coriolis effects have been included by a number of analysts [28, 29, 148, 150, 197, 9, 8, 82], yielding differential equations of motion which are nonlinear. However, there appears to be considerable disagreement concerning the importance of these effects in blade vibration problems.

The most simple two-dimensional model is the rotating rectangular plate which is particularly well suited to represent the chordwise bending modes of a blade, which beam models cannot predict. However, other modes will be poorly estimated due to the lack of both camber and twist. This problem received excellent treatment by Dokainish and Rawtani [46] who showed the effects of rotation velocity, disk radius, aspect ratio, and "setting angle" (angle between the normal to the plate and the axis of rotation). Results for this problem were also obtained by Henry and Lalanne [70] and by Nagamatsu and Michimura [122], and equations of motion were derived by Wang [202].

The problem of a rotating, cantilevered, shallow, circular cylindrical shell of rectangular planform was analyzed by Leissa, Lee, and Wang [97], thereby showing the effects of the various parameters on a cambered blade.

Almost all of the two dimensional analyses described above used the finite element method. This approach is, of course, widely used in all areas of modern structural analysis, and is particularly well suited to cope with blades of general configuration, including arbitrary curvatures and pretwist, variable thickness and irregular shapes.

All three dimensional analyses of rotating turbomachine blade vibrations to date have been by means of finite element models. This typically entails utilizing "solid" or "brick" elements containing nodal points through the thickness, as well as along the middle surface coordinates of the blade. These elements are well suited

23

for thick blades, but lack accuracy for thin blades.

The first known application of three dimensional finite elements to the present problem was by Bossak and Zienkiewicz [21] who applied their isoparametric element to the rotating flat plate problem. Almost simultaneously Thomas and Mota Soares [185] demonstrated the "super-parametric" element on the rotating twisted plate, and presented further results for this problem, as well as for the cambered shell having taper across its width, in subsequent papers [186, 184].

Although the use of three dimensional finite elements typically results in a large number of degrees of freedom, with correspondingly large eigenvalue determinants, there are techniques available for reducing the size of the problem. One procedure is to eliminate tangential inertia, from consideration. This technique is effective for shells having shallow curvature [95]. However, it also results in the loss of blade modes which are predominantly chordwise displacements. Another very useful procedure reduces the numbers of degrees of freedom by eliminating some (and even most) of the nodal displacements in favour of certain "master" displacements [21].

2.2.4 Effects of Pretwist

If the blade has pretwist, uncoupled bending modes in flapwise and chordwise directions are not possible. Both the lateral deflections are always coupled and coupled bending-bending vibrations occur. In addition there is a modification of beam bending and torsional stiffness properties due to pretwist. The modification of beam stiffness properties is considered by Chen Chu [34], Goodier and Griffin [66] and Downs [80] and the coupling of modes clearly demonstrated.

There are a large number of publications dealing with the free vibrations of

24

pretwisted beams having rectangular cross-sections [96]. In many cases the beam theories used are capable of handling cross-sections of arbitrary shape, such as the aerofoil profiles of turbomachinery blades. In a few cases shear deformation and rotary inertia, which decrease the frequencies, are accounted for and become important for the flapwise bending modes of thick beams and for the edgewise bending modes of thin or thick beams.

The application of beam theory for purposes of vibration analysis is limited to relatively long and thick blades. For short and thin blades two dimensional mathematical representation is required.

Twisted plates which give close presentation of thin turbine blades have received considerable attention by researchers. In an early paper Reissner and Washizu [157] applied shallow shell theory to the torsional vibrations of thin plate having small pretwist angles. They showed that a relatively small amount of pretwist may have a considerable effect on the torsional frequencies of thin, twisted plates.

Leissa, Lee and Wang [98] developed a shallow shell theory for blades of arbitrary curvature, and used the Ritz method with algebraic polynomial displacements for the case of a twisted plate. One advantage of the Ritz method is that the chosen displacement functions need not satisfy the free edge boundary conditions.

Deep shell theory was applied to the vibrations of twisted plates by Petricone and Sisto [129,130], using right helicoidal shell co-ordinates. Numerical solutions were obtained by the Ritz method with orthogonal, algebraic polynomials for the displacements.

Large amount of studies on twisted plates were carried out using two or three

dimensional finite element methods. In some early work by Rawtani and Dokainish [155, 156, 47] partially conforming, triangular plate elements were used. Nagamatsu and Michimura [122] also used triangular elements. MacBain [105] used quadrilateral plate elements. Shell elements have also been used [199, 167, 193]. Three dimensional finite element analyses of vibrating twisted plates were reported in [185, 128, 6].

2.2.5 Root Flexibility

Though a turbine blade is loosely mounted on the disk, the root gets encastered due to the centrifugal force, thus almost satisfying the cantilever fixed end conditions. A few researchers have considered the effects of elastic, rather than fixed, constraints at the root [23, 119, 165]. Still others have treated the blade having one end pinned (i.e., simply supported) and the other free [18, 65, 159]. Several have modelled attached shrouds by suitable lumped masses [118, 138, 197, 65]. Quite a few have included the effects of shear deformation and rotary inertia in their analyses [28, 118, 138, 192, 203, 65, 9], thereby making them applicable for relatively shorter blades.

Effect of hub radius on the vibrations of a uniform bar was studied by Boyce and Providence (1956) [23] using the Rayleigh-Ritz method and the Southwell technique. The study showed that the frequencies depended almost linearly on the hub radius for various rotational speeds.

In calculating coupled bending and torsional vibrations in a twisted, rotating blade, Montoya (1966) [119] assumed the fixing plane of a fir-tree root mounting at the narrowest point directly above the first scallop. This treatment considered the flexibility of a large part of the root in the calculation and proved to be a close representation. This technique was adopted in this study.

26

2.3   Coupled Blade Vibrations

It is now widely recognized that the vibration of turbomachinery blading cannot be adequately described by the analysis of a single blade. In order to be able to predict the vibration of blades under operating conditions, and to interpret measurements of vibration actually experienced, it is necessary to consider the behaviour of the complete bladed disk assembly.

2.3.1   Bladed Disk Assemblies

Considerable research has developed methods for the vibration analysis of the complex shaped blading of modern turbomachinery. However, the analysis on the complete bladed disk assembly in order to study turbine blade vibrations is not well established, the main reason being that inter-blade coupling through the disk and shroud contributes significantly to the nature of the basic vibration properties.

Early attempts were made by Stodola (1927) [173] and Smith (1949) [164] to study these vibration characteristics, but full solutions of the equations were not obtained. While the vibrations of a rotating disk are well known from classical studies, the geometry and method of attachment to the shaft, and of the blades are all influencing factors on the behaviour. The coupling between the turbine disk and blades causes the blade packet to exhibit more complex vibration than previously considered. Although it is the intention of this project to study the inter-blade coupling through disk, it is important to introduce the work done on this subject, because this coupling will inevitably exist in the experimental model of blade packet assemblies.

2.3.1.1 Mistuning

No survey of this important subject can be complete without a discussion of the phenomenon of mistuning. Under certain excitation conditions, the nominally identical blades on a rotor stage do not experience equivalent response amplitudes [3]. This is contrary to theoretical predictions made on the assumption that all the blades on a stage, having been designed to the same specifications, are practically identical. But in reality, the inevitable small differences among such blades can greatly affect their vibration characteristics when they are coupled together.

The recognition of blade-to-blade differences in modal characteristics dates back at least 20 years when Whitehead [208] considered its influence on torsional flutter of a system of blades represented as single degree-of-freedom oscillators. An upper limit to the effect of mistuning was found, which shows that the amplitude on one blade may increase by a factor of roughly $\frac{1}{2}(1+\sqrt{N})$, where N is the number of blades in the row. Under normal circumstances, the amplitude will not increase by more than about 20 percent.

The effects of mistuning of the blades around the disk have been considered by a number of researchers [8, 209, 51, 168, 54, 62, 85, 1, 56]. While it is known that mistuning can lead to stress increases, there is no consensus on the magnitude of such escalation. Various figures have been presented from 1.55 increase over the tuned state in [61]; 2.21 in reference [67] and 2.82 in [50].

A series of papers have discussed this at various conferences to determine how closely tuned a set of blades should be to minimise forced response levels, but to avoid flutter. Several authors in the volumes edited by Ewins and Srinivasan [53] (1983), and Kielb and Rieger [86] (1985) made useful contributions to this field.

Included in the first volume is a useful paper by Afolabi [3] who resolved some of the contradictions in the forced response characteristics of mistuned

assemblies reported by previous research [61, 67, 50, 209]. This was based on dividing the response spectrum of the blades on the disk into three classes, and making a critical study of the vibration characteristics of each. It agreed that the blades with maximum mistuning are most likely to experience maximum amplitudes, except in the cross-over zones between classes II and III.

2.3.1.2 Mode Splitting

Dual mode or mode splitting phenomenon is one of the effects of mistuning. Ewins [55] found this phenomenon in an effort to study the effects of mistuning and damping on vibration characteristics of bladed disk assemblies. It was found that the mistuning of a bladed disk resulted in a natural frequency splitting in certain of its modes of vibration and, further, that deliberate detuning might be employed to induce such behaviour or, equally, to suppress it.

Experimental study carried out by Stange and MacBain [171] on a simplified bladed-disk model confirmed the phenomena. It was found that, apart from many of the same vibratory characteristics as a perfectly tuned disk, a disk with some circumferential variation in mass (or stiffness or damping) will exhibit dual resonant modes each of which will have slightly different frequencies and a preferred orientation with respect to the disk.

2.3.1.3 Rogue Failure of Turbine Blades

Another effect of mistuning combined with excitation is rogue failure of turbomachine blades. The localization of vibrations due to the influence of small structural irregularity was studied by many researchers [56, 2, 71, 72, 15]. It has been shown that, for weakly coupled systems, structural irregularity leads to the confinement of vibration to the vicinity of the source, for all modes of vibration.

The vibration confinement is closely related to the problem of rogue blade failure in turbomachinery.

Isolated failure of one or two blades has been known to occur at a service life that is well within the predicted safety limit. Subsequent examinations of the failed blades have revealed in such cases that they suffered vibration at excessively high stress levels while all other blades on the same stage were still stressworthy. The blades exhibiting such a markedly different behaviour are referred to as "rogue blades" [174], while the failure itself may be termed a "rogue failure", to differentiate it from other types of failure such as the conventional "fatigue failure". or failure due to "foreign object damage".

The two main characteristics which distinguish a rogue failure from other modes of failure are (a) the severe localization of vibration around only one or two blades, so that while the failed blades are vibrating at dangerously high levels, all other blades on the same disk are virtually at rest and (b) the amplitudes of the failed blades are several times larger than expected.

Using receptance analysis on a lumped mass parameter system, Afolabi [5] reported that vibration localization phenomenon had been shown to exist in bladed disk assemblies with stronger inter-blade coupling. Under certain unfavourable conditions, the forced response amplitudes of nominally identical blades become extremely unequal. At such times, severe vibration is localized around one or two blades. When the localization is compounded with a substantial amplitude increase, an unexpected failure of some rogue blade could result.

2.3.2 Vibrations of Blade Packet Assemblies

Another aspect of the vibrations of turbomachine blading is the effects of

30

grouping blades into packets by inter-blade connecting elements at mid-span or the tip of the blades. The blades are in general connected by shroud rings or lacing wires, so as to form packets. The failures of these blade packets have given rise to the theoretical consideration of blade packet vibrations. A packet of blades vibrates in such a way that the independent modes of the blades and shroud are coupled and therefore exhibits more complex dynamic behaviour than a free-standing blade.

The first determination of the group frequencies and mode shapes of a six and a twenty-blade group was reported by Smith [164] in 1948. He made a two dimensional free vibrational analysis in the tangential direction using the dynamic stiffness matrix method. The blade was treated as a beam and was separated from covers at their joints. The equilibrium equations were written in terms of the blade tip deflections and slopes. It was significant in that he established the approach and identified the group frequencies for the first time, but the analysis was limited as it was a two dimensional beam model. In addition, the exact solutions were not sought owing to the algebraic complexity of the resulting form of equations. Ellington and McCallion [52] simplified Smith's analysis by using finite difference calculus to the special case of a blade group with a tie wire which joins the blade tips together.

The first well-known blade group design paper was by Prohl [136]. He presented a method of calculating natural frequencies, mode shapes and bending stresses for three dimensional free and forced vibrations in the tangential and axial directions. The blade group was modelled by lumped masses and concentrated inertias and the blade was broken into n stations and the mass of one cover section was added to the tip blade section. A modified Holzer technique was used to calculate the natural frequencies and mode shapes. This analysis followed the approach of Smith and is extended to consider axial and torsional vibrations, but higher order effects and more importantly the coupling between bending and torsion motions of the blade was disregarded. Other studies into blade group were reported

31

in [206, 162, 143].

The method of analysis by Prohl was developed by Deak and Baird [42] for calculating a laced group of rotating exhaust blades. It included three dimensional coupled tangential and axial free vibrations with root stiffness. This method gives all of the natural frequencies and mode shapes including both flexural and torsional motions. The importance of the effects of disk and centrifugal stiffening in long exhaust blades was clearly demonstrated. Blade to blade coupling does occur through the lacing wires. The frequencies calculated by this method were compared with experimental results with good correlation. Some judgement was required to define the effective point of fixity in the disk rim and the effective lacing wire constraints. The complicated root of the blade was replaced by an equivalent beam encasement.

Same as Prohl's approach, the blade was represented by a series of concentrated masses connected by massless elastic elements. For blades with complex profile this approach is not able to provide detailed analysis on complicated mode shapes of coupled modes. In addition great efforts are required to obtain the solutions of eigenvalue equations, which presents the difficulty in its applications.

Huang [76] developed a computational procedure for calculating the free vibration of rotationally periodic structures with various types of connecting elements using transfer matrix method. The equations of motion for coupled bending and torsional vibration of a twisted blade proposed by Montoya [119] were adapted to calculate the dynamic stiffness matrix. Circumferentially closed packets of turbine blades coupled by lacing wires in different connections were calculated. The forced vibration and condition of resonance of a closed structure of blades on a disk under time-periodic excitation were discussed.

The vibration characteristics of blade group due to inter-blade coupling were not discussed and the effects of damping by lacing wires were not included. As the structure was considered as periodically closed, a lot of group frequencies could not be reflected in the study. Other work on rotationally periodic structure were reported by Cmolnickov [37], Pfeiffer [131] and Namura [123].

Butkovic [24] obtained an expression of the stiffness coefficient between blade and damping wire. The first natural frequency of tangential vibrations of ten blades grouped and tied by a damping wire with assumed contact stiffness between blades and damping wire were calculated by using finite element technique combined with transfer matrix method. Then the contact stiffness were verified by comparing the calculated natural frequencies with the ones obtained in tests. The use of the stiffness coefficient in other modes of vibration is in doubt as its justification was only based on the first tangential mode where the displacements of all blades in the group are in phase. Blade to blade coupling due to damping wire was not considered in this work.

The finite element method was used by Thomas and Belek [182] to study the vibration characteristics of a packet of shrouded blades of rectangular cross-section. The beam elements were given flexural and extensional degrees of freedom. A method of predicting the frequencies of vibration of a blade packet was introduced. The effects of various blade-shroud weight, flexural rigidity, and length ratios between the blades and shrouds on the blade packet frequencies of vibration were investigated. The results presented show close agreement with experimental results and good comparison was made with other research results. It concluded that the general behaviour of a packet of blades could be predicted from a frequency inference diagram plotted for a two-bladed packet.

Same as the work reported by Smith [164] and Prohl [136], the shroud was

attached to the tip of the blade. Therefore, the conclusions made may not represent the dynamic characteristics of tie wire laced at part-span of the blade. Comparing the methods introduced above with each other, the finite element method is seen to be ideal for the dynamic analysis of blade packets.

Nagarajan and Alwar [121] used three dimensional isoparametric quadratic elements to analyze the vibration of blade packets. As the packets were considered to be three dimensional structures, all the natural modes were determined, including the packet modes due to the presence of the shroud. These were found to occur both in bending and in torsion. The vibration characteristics of two different blade packets were considered in the paper. The first was the same as modelled by Thomas and Belek. In addition to the modes previously identified, torsional batch modes were obtained. The second packet considered consisted of two thick curved steam turbine blade connected by a shroud. The mode shapes and natural frequencies were obtained, and could be clearly classified. It showed that high precision element can represent effectively the true aerofoil surfaces of blades and give torsional batch modes in addition to the batch modes in bending, it could be of considerable use in further detailed studies of blade packets.

Mayer [110] investigated the vibration behaviour of an axial blading connected by lashing pins, cover bands or shroud segments using numerical calculations and by experiments. Natural frequencies and natural modes taking into account centrifugal effect are calculated using the finite element method combined with the wave propagation technique [112, 181], which largely reduces the number of degrees of freedom. The experiments were carried out using semi-conductive strain gauges and a special process technique. Good agreement were found between computed frequencies and measured resonant frequencies for the different configurations.

The study above was confined to fixed configurations of blade packets with periodically closed connections. It showed that finite element analysis is a very powerful tool in studying vibrations of blading. However, the study did not fully reveal the effects of connecting elements in packets and their dynamic characteristics due to limited configurations.

A number of studies based on previous work was reported by Ewins [58, 60] of the effects on bladed disk vibration properties of grouping blades into packets by inter-blade elements. A simple mass-spring model [50] was used to establish the relation of dynamic characteristics between simplified models of packeted bladed disk assemblies and a continuously shrouded bladed disk. It showed that most of the packeted assembly modes did not have the simple nodal diameter shape as in the case for a continuously-shrouded assembly. Instead, each mode contains several diametral components. Certain modes were split into pairs with different natural frequencies due to packeting and the mode to split was related to the number of blades in each packet in the assembly. This work demonstrated that judicious manipulation of blade numbers, or packet numbers, may well minimise the forced vibration levels of a given assembly at known and unavoidable engine order excitations.

2.4 Conclusion

It can be seen that a great amount of work has been carried out to study the dynamic characteristics of turbomachine blading. Some representative work reported are reviewed here in order to set the background for this research.

Blade vibration analyses have traditionally focused on the properties of a single blade cantilevered at its root. Although we are not really concerned here with

the vibration properties of isolated blades, they are of important relevance to those of blade packets, because the latter are conveniently grouped into families of modes, each of which is associated with a parent blade mode. Thus, while the natural frequencies of a single blade do not necessarily provide good estimates of those for an assembly, it is appropriate to know them and their associated mode shapes. Traditionally identified as flap, edgewise or torsion cantilever modes, the modes of many modern blades are less easily categorised because current designs are so complex in shape that motion in all three directions becomes highly coupled and many modes can only be classified as 'bending-bending-torsion'.

In their working environment, blades form part of an assembly - in the simplest case consisting of a packet of blades connected by a shroud band, but more generally as complete stage or bladed disk with several packets. For many such assemblies, the useful vibration data are those which relate to the whole assembly.

The vibration of blade packets are very different from that of a free standing blade due to the coupling through the blade disk and the inter-blade connections. While the former has received a lot of attention in recent years, the understanding of the latter was found to be inadequate, especially in the cases with part-span lacing wires, as shroud bands or lashing pins have received some good investigations.
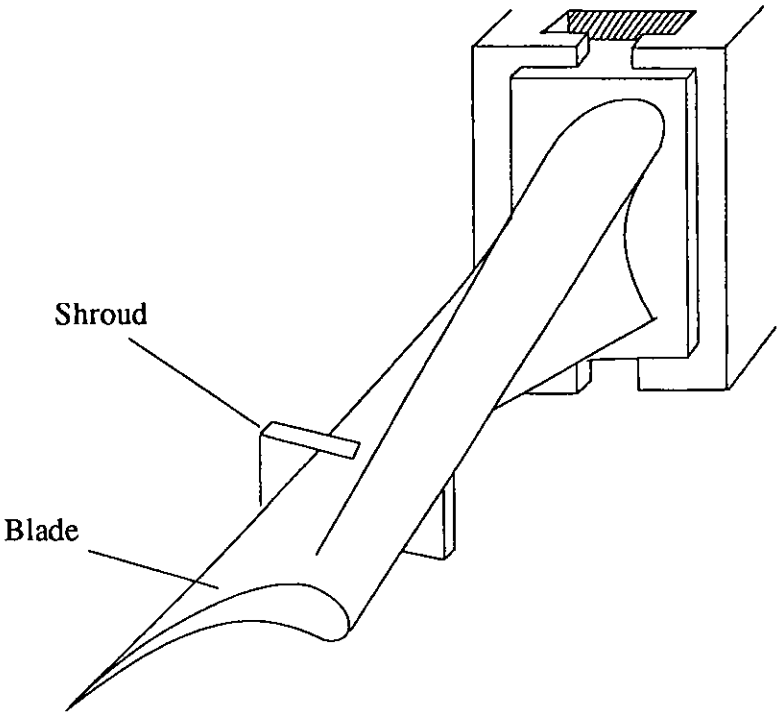
Figure 2.1 Typical shrouded fan blade
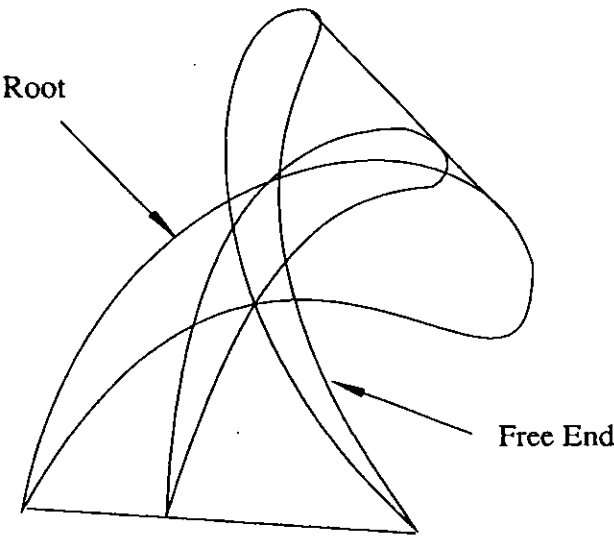
Figure 2.2 Typical blade cross-sections

Chapter 3

Analysis Techniques and Theoretical Background

3.1   Introduction

3.2   Modal Testing

    3.2.1   Modal Properties

    3.2.2   The Frequency Response Function

    3.2.3   The Fast Fourier Transform (FFT) Analyser

    3.2.4   Determination of Modal Parameters

    3.2.5   Excitation of Structures

    3.2.6   Measurement of the Response

    3.2.7   Instrumentation

3.3   Laser Interferometry Techniques

    3.3.1   Basic Principle of ESPI

    3.3.2   Image Reconstruction

    3.3.3   ESPI and Vibration Measurement

    3.3.4   Instrumentation

3.4   Finite Element Method for Natural Frequency Prediction

3.4.1   The Finite Element Method

3.4.2   The Eigenvalue Equation

3.4.3   Master Degrees of Freedom --- Eigenvalue Economization

3.5   Mode Shape Classification

3.6   Conclusion

Figures

3.1 Introduction

The study of dynamic characteristics of turbine blading with lacing wires was carried out using three powerful vibration analysis techniques. They are Modal Testing, Electronic Speckle Pattern Interferometry (ESPI) and Finite Element Analysis. Modal testing and ESPI were used to establish dynamic characteristics of turbocharger blades. Finite element modelling was carried out to build up mathematical presentation of the blades. The dynamic characteristics of the FE models were justified by experimental results. In order to study and establish the vibration feature of the blades, it was considered necessary to employ all three methods because each method has its own limitation and disadvantages.

The first two methods are experimental techniques which are able to identify dynamic characteristics of a mechanical system. Modal testing technique requires attachment of transducers to the mechanical structures under test hence introducing mass modification into the system. This modification may result in large errors in detected dynamic characteristics if, for instance, the effective mass of the system under testing is relatively small. Moreover, the sensitivity of accelerometers varies with the direction of their movements. In the cases where displacements are not completely in line with the principal axis of accelerometers some displacement components are not seen by the accelerometers and great care is required in interpreting modal testing results.

ESPI technique detects displacement of a structure by processing interferometry pattern of laser speckle reflected from the surface of the structure under testing. It does not suffer from mass modification owing to the attachment of transducers but for the type of ESPI used in this study, its sensitivity only lies in the axis of the camera lens.

Mathematical modelling of vibration of turbine blades with a lacing wire was carried out using the finite element method. Close presentation of turbine blade geometry in F.E. modelling was made difficult by aerodynamic profile of the blades. Assumptions had to be made in modelling at blade-disk and blade-lacing wire interfaces.

The discussion above clearly reveals that an in-depth understanding of all techniques used plays an important role in correct interpretation of experimental and theoretical results. This chapter will introduce some basic concepts and principles of the three techniques used in this study.

3.2 Modal testing

Modal analysis is the process of determining the inherent dynamic characteristics of a mechanical system (natural frequencies, damping factors, and mode shapes) and using them to formulate a mathematical model of the system's behaviour. The analysis is based on the fact that the vibratory response of a linear system can be expressed as the sum of a set of simpler constituent motions, called the natural modes of vibration. The degree of participation of each mode in the overall motion is determined by the properties of the excitation source. This principle of modal superposition was first used by the eighteenth-century mathematician Daniel Bernoulli in the analysis of distributed parameter systems.

Modal analysis embraces both analytical and experimental techniques. The rapid development of data acquisition and processing capabilities has led to major advances in the experimental aspect of the field, which has become to be known as modal testing.

41

Structural frequency response testing, also known as 'modal analysis', has become an integral part of the development and testing of a wide range of industrial and consumer products [69]. It is an essential tool for the definition and solution of many types of structured dynamics problems, such as fatigue, vibration and noise. Ewins has given a complete discussion on modal testing in his book [59].

Most structures vibrate. In operation all machines, vehicles and buildings are subjected to dynamic forces which cause vibrations. Very often the vibrations have to be investigated, either because they cause an immediate problem or the structure has to be 'cleared' to a 'standard' or test specification. For instance, the blading in large turbocharger is subjected to vibration excitation origination from pulsations in the exhaust gas stream coupled with the blade pass frequencies. This raises a problem to be overcome in the design and operation of turbomachinery: the prevention of excessive blade vibration levels under operation conditions. Therefore the investigation into blading vibration is required.

Two of the analysis methods in structural frequency response are signal analysis and system analysis. The signal analysis is the process of determining the response of a system, due to some generally unknown excitation, and of presenting it in a manner which is easy to interpret. The frequency spectrum description of how the vibration level varies with frequency can then be checked against specifications. This type of testing will give results which are only relevant to the measured conditions. The result will be a product of the structural response and the spectrum of an unknown excitation force, it will give little or no information about the characteristics of the structure itself.

An alternative approach is the system-analysis technique in which a dual-channel FFT analyser can be used to measure the ratio of the response to a measured input force. The frequency response function (FRF) measurement removes

the force spectrum from the data and describes the inherent structural response between the measurement points. A set of FRF measurements made at defined points on a structure can build up a picture of response. The technique used to do this is modal analysis. Simply stated, modal analysis is the process of characterising the dynamic properties of an elastic structure by identifying its modes of vibration. Once the dynamic properties of an elastic structure have been characterised, the behaviour of the structure in its operating environment can be predicted and, therefore, controlled and optimized.

Modal analysis has been widely used for three reasons:

1)   Modal analysis provides experimental support for the verification and adjusting of the mathematical models of the structure. The mathematical models, which are equations of motions based on an idealized analytical model of the structure, are used to simulate and represent the dynamic performance of the structure. Their accuracy can be physically checked by experimental measurements on the actual structure. Although the mathematical model allows the designer to check the effects of changes in mass, stiffness and damping, the correct prediction of dynamic performance of the structure has to be given by the mathematical model which predicts the same behaviour that is actually measured. It is reasonable to extend the use of the model for simulation, thus reducing the expense of building hardware and testing each different configuration. This type of modelling plays an important role in the design process.

2)   Modal analysis is a powerful tool to locate structural weak points. It can be used to test the most effective product design for avoiding failure. This often eliminates the tedious trial and error procedures that arise from trying to apply inappropriate static analysis techniques to dynamic problems.

3)   Modal analysis provides information which is essential in eliminating unwanted noise or vibration. With the knowledge of the dynamic characteristics of the structure such as where are the natural frequencies and what are the mode shapes, further study can be carried out to remove the natural frequencies from the range of the excitation or to limit the maximum amplitude within the safety requirement.

3.2.1 Modal Properties

Most vibration problems are related to resonance phenomena, where the operational forces excite one or more resonances. Resonances, or the modes of vibration, in the range of excitation are the potential problems.

An important property of modes is that any forced or free dynamic response of a linear system can be reduced to a discrete set of modes. An FRF measurement made on any structure will show its response to be a series of peaks. The individual peaks, with identifiable centre-frequencies, indicating that they are modes. Each mode can be regarded as the response of a single-degree-of-freedom (SDOF) structure. It is known that each SDOF model is associated with a frequency, a damping coefficient and a mode shape. These are the Modal Parameters:

■   modal frequency
■   modal damping
■   mode shape

The modal parameters of all the modes, within the frequency range of interest, constitute a complete dynamic description of the structure. The modes of vibration represent the inherent dynamic properties of a free structure. (a structure on which there is no forces acting).

44

3.2.2 The Frequency Response Function

One very efficient model of a linear system is a frequency domain model, where the output spectrum $X(\omega)$ is expressed as the input spectrum $F(\omega)$ modified by a system descriptor $H(\omega)$

$$X(\omega) = H(\omega)F(\omega)$$

This system descriptor $H(\omega)$ is called the Frequency Response Function (FRF), and is defined as:

$$H(\omega) = \frac{X(\omega)}{F(\omega)}$$

$H(\omega)$ is the complex ratio between output and input, as a function of frequency ω. The FRF can be considered as a complex weight. It operates on the amplitude and the phase of the sum of sinusoidal input signals and produces an output which is the sum of the modified sine waves with the same frequency, as illustrated in Figure 3.1. With linear systems, any input/output spectrum can be considered to be the sum of sinusoid functions. The FRF describes the dynamic properties of a system independent of the signal type used for the measurement. The FRF is therefore equally applicable to harmonic, transient and random excitation.

3.2.3 The Fast Fourier Transform (FFT) Analyser

Digital Fourier analysers are essential tools for modal testing. The ability of these systems to quickly and accurately measure a set of structural frequency response functions and then operate on them to extract modal parameters offers a powerful way to set up a modal model of the structure. A summary of the processes

in FFT analyser is shown in Figure 3.2 and is described as follows.

The measured force input signal f(t) and displacement output signal x(t) as the function of the time, are both fed into the dual channels of the FFT analyser. These signals are digitized, filtered and sampled. The length of the time of recording and sampling rate determine the frequency range and the resolution of the analysis. Then signals are windowed (box A) to overcome the leakage problem which is a direct consequence of the need to take only a finite length of time history coupled with the assumption of periodicity. The window functions taper the data at both the beginning and end of each record to make the data more suitable for block analysis. The weighted sequence is transformed to the frequency domain as spectra, $F(\omega)$ and $X(\omega)$ in box B, by the used of a Discrete Fourier Transformation. They are complex which can be expressed as amplitudes and phases. Some averaging technique has to be used to remove some noise. Autospectra G_{ff} and G_{xx} are obtained, as shown in box C1 and C3, by multiplying a spectrum by its complex conjugate and by averaging a number of independent products. A Cross Spectrum is calculated by multiplying the complex conjugate of one spectrum by a different spectrum (box C2). The Cross Spectrum is complex, showing the phase shift between the output and input, and a magnitude representing the coherent product of power in the input and output. The noise in either input (force) or output (response) can be removed during the averaging process of the Cross Spectrum.

Cross Spectrum between the force and response, together with the Autospectra of the force and response provide the elements needed for FRF and Coherence estimates.

To minimising the effect of noise at the output (response $X(\omega)$), the best FRF estimator is (box D1)

$$H_1 \equiv \frac{G_{fx}(\omega)}{G_{ff}(\omega)} = \frac{F*X}{F*F}$$

in which averaging process of the Cross Spectrum reduces the noise at $X(\omega)$. As the number of averages is increased, H_1 converges to the true H.

Similarly, to minimising the effect of noise at the input (force $F(\omega)$), the best FRF estimator is, as shown in box D3

$$H_2 \equiv \frac{G_{xx}(\omega)}{G_{xf}(\omega)}$$

The input noise is removed from the Cross Spectrum during the averaging process. As the number of averages is increased, H_2 converges to the true H.

Since $G_{xf}(\omega)$ can average out the noise components in either $X(\omega)$ or $F(\omega)$, the following inequality must be true if there are noise contributions in measured signals

$$|G_{fx}(\omega)|^2 \le G_{xx}(\omega)G_{ff}(\omega)$$

This relationship gives rise to the definition of the Coherence Function

$$|\gamma(\omega)|^2 \equiv \frac{|G_{fx}(\omega)|^2}{G_{xx}(\omega)G_{ff}(\omega)}$$

where $0 \le \gamma(\omega)^2 \le 1$

At a frequency ω, γ is 1.0 if there is no noise in either $F(\omega)$ or $X(\omega)$; and is

47

zero if there is only noise in either measured signals. This is actually a parameter describing the degree of linear relationship between measured input and output signals. This property of the Coherence Function can be used to detect a number of possible errors in mobility measurements.

3.2.4 Determination of Modal Parameters

The modal frequencies are determined simply by observing the FRF. The spectrum exhibits high and sometimes sharp peaks at resonance frequencies, as shown in Figure 3.3(b).

The determination of the modal damping is not so simple. Finding the 3dB bandwidth is one of those methods. But on a lightly damped structure, this method does not work accurately since the resonances are sharp and the peaks are too narrow for accurate measurements of the bandwidth on the structure. However, this problem can often be overcome by using the zoom facility to obtain sufficient frequency resolution for the measurements.

The determination of mode shapes needs additional measurements on selected points over the structure. The imaginary part of the FRF spectrum indicates two facts: a) the height of the peaks represents the amplitude of vibration modes at the measuring point; b) the positive and negative signs of the peaks indicate that the amplitude of vibration modes is in or out of phase with the excitation at the measuring point. Therefore, the peaks in the spectrum describe the behaviour of the structure at the measuring point for different modes within the frequency range of investigation. Then measurements from selected points over the structure can define the mode shapes of the structure.

This procedure is schematically demonstrated in Figure 3.3. A cantilever is

48

shown in Figure 3.3(a) where an accelerometer is mounted at positions A to C in turn and hammer impact is applied at position A. The imaginary part of FRF spectra of the cantilever including the first three natural frequencies with respect to three impact positions are given in Figure 3.3(b). The imaginary peaks of the spectra, representing the amplitude and the direction at the position of measurement are re-plotted in Figure 3.3(c) for each natural mode of vibration. The curves obtained by linking the peaks together give the mode shapes of first three natural modes of vibration. This procedure was used in this study in determining the natural frequencies and mode shapes of turbine blades.

3.2.5 Excitation of the Structure

To obtain an FRF, the ratio of the input excitation transform to the output response transform, it is necessary to excite the structure with vibrational energy. The three most common ways of exciting a structure are transient, random and swept sine excitation.

Transient excitation is most often achieved by using an instrumented hammer. A sharp blow given by the hammer will excite a range of frequencies. The sharper the impact, the larger the frequency range produced. The frequency range may be varied by adjusting the hammer tip material and the effective hammer mass. The maximum frequency limit that may be achieved using a hammer is about 5 kHz. The input force is measured by a piezoelectric force transducer situated just behind the tip of the hammer. The hammer impact test is quick, as the hammer impact point can be moved to determine the mode shape, inexpensive and can give excellent results.

Large structures may become damaged if large peak forces are necessary to excite them. It should also be noted that a flexible structure can rebound when

struck causing a double hit on the hammer. Such a result is extremely undesirable and should be discounted.

Another method of exciting transiently is to apply strain to the structure and then release it, thus exciting with a step function, which is theoretically continuous in the frequency domain, although in practice a perfect step function is not achieved.

Random and swept sine excitation require the use of an electromagnetic excitor. The excitor is driven by a signal generator, usually incorporated within the FFT analyser. The excitor attachment is slightly more complicated in this case; a rigid attachment of the excitor to the structure will introduce a large extra mass. For this reason excitors are usually mounted so that force is transmitted through a needle or "stinger" which is flexible in the transverse direction. In this way the structure is free to move at this point in the five degrees of freedom other than the excitation direction. It should be noted that it is very important that the force transducer is located on the structure's side of the needle for a good reading.

Random excitation, or pseudo random excitation when the signal is periodic, are good tests, as all the resonances over the frequency range should be covered. Zoom analysis is easy to perform, maximising the amount of energy going into the structure. The mounting of the piezoelectric excitor is the main problem as the connection to the structure needs to be rigid to minimise the input noise. For this test it is usual to move the response transducer around on the structure to determine the mode shape.

Sine sweep testing is slower than random excitation as the sinusoidal signal has to be swept across the frequency range but the technique does get the maximum possible energy in to the structure hence producing a high signal to noise ratio. The rate of sweep may be controlled manually or automatically to get the best results.

3.2.6 Measurement of the Response

The most common method of measuring the output transform, the response, is by measuring the structural acceleration at a point using an accelerometer and then electrically integrating the signal to find the displacement. A low mass accelerometer may be easily attached to the structure with wax and should not alter the modal mass greatly. An important point is to place the accelerometer in the correct orientation to measure the correct component of the acceleration. A typical modal testing set-up is illustrated in Figure 3.4.

3.2.7 Instrumentation

A Nicolet 660A dual channel Fast Fourier Transform (FFT) Analyser was used in this study, its control panel is shown in Figure 3.5. It has no storage capability and therefore, all experimental results were plotted using a Tek Tronic 4662 plotter. The analyser was used to identity the FRF of turbine blades under impulse, sine wave and white noise excitations.

The force transducer used was a Bruel and Kjaer type 8200. It is a unidirectional piezoelectric device with a nominal upper frequency limit of 20 kHz. It is shown in Figure 3.6 and its frequency response characteristics are shown in Figure 3.7.

The accelerometer used was a Bruel and Kjear type 4374 as shown in Figure 3.6. This is a unidirectional piezoelectric device which has a nominal upper frequency limit of 20 kHz. Its frequency response characteristics are shown in Figure 3.8.

51

B & K 2635 type charge amplifiers shown in Figure 3.6, were used to amplify the signal from accelerometers and force transducers.

A Hewlett Packard 3330A frequency signal generator was used to generate sinusoidal signal between 0 Hz to 20 kHz. PA100 power amplifiers were used to amplify the signal in order to drive exciters. They are shown in Figure 3.9.

An instrumented hammer was used for the impulse excitation technique, as shown in Figure 3.6. Note that the force transducer is behind the hammer tip, in order to obtain the force reference as closely to the test piece as possible. The tip material used for the blade excitation is mild steel, whilst there are three tips shown. The mass behind the hammer may be altered depending on the amount of energy required to stimulate the structure.

An electromagnetic excitor (Ling Dynamic Systems model V201) was used for alternative excitation. The excitor has to be clamped to a rigid surface or suspended freely with a rigid attachment to the structure. Very low frequencies (of the order of 10 Hz) can not be produced by the excitor. The needle or stinger should be as thin as possible to minimise the input noise and extra mass, but thick enough to transmit sufficient energy. It was found that a needle diameter of 1.0 mm was suitable, whilst a diameter of 0.6 mm was too thin.

Excitations were applied to test pieces using hammer testing, white noise and sine-wave sweeping excitations in the modal testing experiment. The test pieces were firmly clamped down on the surface of a vibration isolated test bench while they were excited. This was the case in both modal testing and ESPI experiments. In the ESPI testing, manually controlled sine-wave excitation was preferred in order to identify modal parameters.

3.3 Laser Interferometry Techniques

Laser interferometry techniques which have been developed in the past 20 years have offered additional powerful measurement tools for stress and vibration analysis. Holographic Interferometry (HI) and Electronic Speckle Pattern Interferometry (ESPI) are well known means for static and vibration analysis. They are different from accelerometers and strain gauges, as they are non-contact techniques, which gives the advantage that the structure under test is not modified by the addition of mass.

The early vibration analysis by the wave reconstruction technique dates back to 1965 by Powell and Stetson [135] (1965) and a recent report was given by Lacitignola et al [91] (1986). Basic techniques of vibration measurement on disks and turbine blades using holography were described. To detect rotating objects such as the bladed turbine disk, a pulsed laser was used and derotating techniques were developed. A holographic vibration study of a rotating propeller blade using a spinning-hologram technique was reported by Sikora and Mendenhall [163] (1974).

MacBain et al [107] (1979) presented another approach using pulsed laser holograph in conjunction with an image derotator. These methods are proved to be effective and they produce high resolution fringe pattern pictures. However, one significant restriction of HI is the need for the chemical processing of the data recording medium. Whilst the use of a high resolution medium gives better results than conventional ESPI, for many applications in engineering it is of more importance to be able to perform interactive analysis. This is different when it takes up to 15 minutes to process a holographic plate after exposing it. During experimental work interactive analysis can reveal more information than the analysis of a single frozen interferogram. What may take hours with holographic

53

interferometry takes minutes with ESPI.

Early development of ESPI was reported by Butters and Leendertz [25] (1971). The method reported was based on Speckle Pattern Interferometry with optical to electronic interfacing by means of a modified closed-circuit television arrangement, which was the initial stage of ESPI. Jones and Wykes [84] (1980) discussed general basis for the systematic design and optimization of ESPI, and Soares [166] (1986) gave a review on the improvements on ESPI techniques to further its technical capabilities and resolve some of the inconveniences of HI in industrial applications. A very good introduction to ESPI was given by Lokberg [103] (1980) who discussed the basic principles, modes of operation and applications of ESPI.

3.3.1 Basic Principle of ESPI

ESPI can be defined as image holography with an in-line reference beam where the TV system has replaced the film as the recording medium, while the reconstruction is done by electronic processing.

Since optical layout of ESPI is similar to image holography and the later is a well know technique, a summary of the principle of ESPI is given below step by step as illustrated in Figure 3.10, where the two processes are compared.

In Image Holography (IH) a coherent beam is split into two beams, an object beam and a reference beam. The object beam reflected from the object is focused onto or very close to the film. To get interferometric sensitivity (or to make the recording holographic) the reference beam also impinges on the film. The image and the reference wave interfere, creating very complicated patterns of closely spaced lines in the image of the object. The pattern is photographically recorded on the

film. The line spacing d in this interference pattern is given roughly by $d = \lambda/\theta$, where λ is the laser wavelength and θ is the angle between the two waves. In IH this angle can be large as the resolution of the film can be down to 0.2 μm. If the object is vibrating during the exposure as shown in Figure 3.10, the averaged intensity of the interferogram is as shown in Figure 3.10a. The fine variations represent the interference spacing, while the slowly varying envelope in the fringe contrast is caused by the optical path length variations due to object vibration. The film recording this interferogram is then converted by chemical development into corresponding variations in transmittance, refractive index or thickness.

Comparing with the IH, the recording step in ESPI is identical. However, the poor resolution of the TV system, which is approximately a factor of one hundred lower, requires that the details in the interferometric pattern are within the resolution limit of the TV system. With a fixed wavelength, this can only be achieved by reducing the angle θ between the object and reference waves. This is obtained by closing down the aperture of the imaging lens (to f:16 or smaller) and placing the reference wave in-line with the object wave (Figure 3.10b). The last feature can be accomplished by using a beam splitter as shown in Figure 3.11. If the object vibrates in a similar way to Figure 3.10a, the light intensity recorded by the TV system will also be similar except the fringe spacing (or the speckle) will be much coarser. The TV exposure results in a charge distribution across the target which is subsequently transformed into a proportional current variation by the TV scanning. This process takes the place of the exposure and development of the film in IH.

3.3.2 Image Reconstruction

In IH the image reconstruction is achieved by placing the developed film, the hologram in the reference wave and covering the object wave. The reference wave going through the hologram, which is a fine complex grating, refract and reconstruct

the wave front of the object wave. Therefore, a reconstructed image of the object can be seen at the plate. Now considering the vibrating bar again, due to the vibratory movement the envelope of the fringe pattern at certain position is very narrow (Figure 3.10a), which means that the pattern at certain amplitude values had very low or zero contrast. This results in a fringe pattern with light and dark regions covering the reconstructed object as the light intensity of the reconstructed object is roughly proportional to the fringe contrast in the hologram. The vibration amplitude across the object can be deduced from these patterns.

In ESPI, the optical wave front reconstruction is replaced by electronic processing of the video signal (Figure 3.10b, lower half). First, the DC component (and some low frequency noise) is removed by high-pass filtering with a lower frequency. Then the filtered signal is full-wave rectified. The effect of the electronic processing is to change the depth of modulation in the original video signal into corresponding high and low signals on a varying carrier. (The whole process is roughly equivalent to AM demodulation in radio receivers.) The processed video signal is fed into the TV monitor where the object covered with exactly the same bright and dark fringes as in holography except that the image is less well defined.

Figure 3.11b shows an ESPI recording of the vibration of a turbocharger blade. The blade vibrates in its fundamental flapping mode - a movement which is quite similar to the vibrating bar used as an example in Figure 3.10. The node at the base is the brightest or zero-order fringe; each bright fringe thereafter represents about a quarter wavelength increased amplitude. Thus we can interpret the fringe patterns just as we read the height contours on an ordinary map. The maximum amplitude at the tip of the blade to be 10/4 wavelengths which corresponds to 1.3 μm with $\lambda = 0.5146$ μm.

It is evident from Figure 3.11b that ESPI gives a lower image quality than

56

holography, which limits the details and number of fringes which can be resolved across the image of the test object. However, this is outweighed by the advantages of TV registration, namely: real-time presentation, short exposure (normally 1/25 s †) and high repetition rate (25 Hz†). († = European TV standard)

As a result we observe the interferogram (almost) immediately after it has been recorded, with an exposure which is short compared to ordinary holography, a new hologram being created each 1/25 s. These properties, combined with the high-sensitivity, non-contact and nondestructive properties of the holographic method, make ESPI a unique measuring tool in its different modes of operation.

3.3.3 ESPI and Vibration Measurement

The main elements of a standard ESPI layout is shown in Figure 3.11a. The beam from the laser is split into two by a beam splitter BS_1. The reflected beam is expanded and used to illuminate the object. The object is imaged by a chopped-down lens system L through a wedge-shaped beam splitter BS_2 on to the TV target. The transmitted beam through BS_1 is reflected by mirrors M_1 and M_2, expanded and finally reflected by BS_2 on the TV target in-line with the object-image wave (BS_2 is wedge shaped to avoid back reflection hitting the object). The image-interferogram is then converted to a video signal, processed and fed to the TV monitor as explained earlier.

Vibration measurement represents the most straightforward and common use of ESPI. The instrumentation is simple as only the basic elements in the set-up of Figure 3.11a are necessary to obtain fringe patterns as shown in Figure 3.11b. Real-time presentation is very useful for vibration measurements as the effects of varying parameters such as frequency, phase and excitation level can be observed instantaneously. The combination of short exposure and high framing rate makes the

system very insensitive to external disturbances and object instability.

3.3.4 Instrumentation

The ESPI device VIDISPEC used in this study was developed at Loughborough University and manufactured by Ealing Electro-Optics. Its optical path and basic components are very similar to that shown in Figure 3.11a using a 10 mW HeNe laser. In addition, it has a powerful digital store and an electronic processor to enhance image quality.

Figure 3.12 shows the Optical Unit of the VIDISPEC System mounted at the end of a vibration isolated testing bench, with its top cover removed to reveal its components. It is capable of illuminating objects up to 300 mm diameter. VIDISPEC measures the deformation of displacement of an object in a direction defined by the illumination and viewing geometry. In its standard configuration, the instrument is sensitive only to out of plane displacement. Any movement from 0.3 to 12 micrometres (μm) can be accurately measured. However, by re-referencing the system at 12 μm intervals, deformations over a very much wider range (up to the point of destruction if necessary) can be monitored. VIDISPEC was used to identify modes of vibration of turbine blades in this study. A time averaged fringe pattern was obtained showing contours of constant vibration amplitude. The interval between contours is 1/4 of the wavelength of the laser light (0.3 micrometres with a HeNe laser). The performance of an object over a wide frequency range was explored very quickly using this technique.

The Electronics Unit (known as the memory store) of the VIDISPEC System controls the mode of operations. It has 64K RAM individual chip memory and 256K RAM total memory with sampling rate of 9 MHz. Two modes of operation are available for different applications. The time averaged mode is achieved by freezing

only the reference beam in the memory store with the speckle pattern from the surface of the object moving relative to the frozen reference. Because the fringe pattern represents instantaneous vibration amplitudes, a wide frequency range can be swept through in this mode and resonant modes can be identified. The subtraction mode is used to enhance fringe patterns by recording a reference state of the object before the excitation is applied. The subtraction mode can provide fringe patterns with much better quality. The video monitor, shown with the memory store in Figure 3.9, has the resolution of 800 TV lines with a bandwidth of 10 MHz. Shown in Figure 3.13 is a SONY high resolution reel to reel tape recorder. It was used to record the real-time measurement, mainly vibration measurement, for post-processing. The frequency generator and signal amplifier are also shown in Figure 3.9.

3.4 Finite Element Method for Natural Frequency Prediction

In order to predict the system natural frequency it was necessary to generate a mathematical model for the blading. As presented in Chapter 2, a lot of different mathematical approaches were used to predict the natural frequencies of single blade or multi-blade structures. Early works were mostly carried out using Euler equations and energy methods treating single blades as beams.

For blades with complex profile, two dimensional or even three dimensional mathematical modelling are required and finite element analysis was proven to be very useful. It was decided that the FE method be used to carry out the mathematical study.

3.4.1 The Finite Element Method

The finite element method is the most powerful numerical technique available today for the analysis of complex structural and mechanical systems. It is used to obtain numerical solutions to a wide range of problems. The finite element method is used for both static and dynamic analysis.

The classical method of analysis in elasticity involves the study of an infinitesimal element of an elastic body. Relationships among stress, strain and displacement for the infinitesimal element are developed that are usually in the form of differential equations that apply to each point in the body. These equations must be solved subject to appropriate boundary conditions. In other words, the approach is to define and solve a classical boundary value problem in mathematics. Problems in engineering usually involve very complex shapes and boundary conditions. Consequently, for such cases, the equations cannot be solved exactly, but must finally be solved by approximate methods; for example, by truncated series, finite differences, numerical integration, etc. All these approximate methods require some form of discretization of the solution.

The formulation of finite element solutions recognizes at the outset that discretization is likely to be required. The first step in application of the method is to discretize the domain into an assemblage of a finite number of finite size *elements* (or subregions) that are connected at specified node points. The quantities of interest (usually nodal displacements) are assumed to vary in a particular fashion over the element. This *assumed* element behaviour leads to relatively simple integral equations for the individual elements. The integral equations for an element are evaluated to produce algebraic equations in terms of the displacements of the node points. The algebraic equations for all elements are assembled to achieve a system of equations for the structure as a whole. Appropriate numerical methods are then used to solve this system of equations.

60

In a dynamic analysis the effects of inertia forces are considered in the calculation. These are proportional to acceleration and their inclusion leads to an equation that has time-varying terms, giving a dynamic response. In order to define such a problem the minimum information that the user has to specify is the stiffness of the system and the inertia of the system. In addition any real system will contain damping that dissipates the vibrational energy and, probably, a time-varying set of loads known as the forcing function.

3.4.2 The Eigenvalue Equation

The mathematical base of finite element method uses frequency solution algorithm. A brief summary of the theory is given below [125].

The equations of motion may be expressed in matrix form:

$$[M]\{\ddot{u}\} + [C]\{\dot{u}\} + [S]\{u\} = \{F(t)\} \tag{3.1}$$

where [M], [C] and [S] refer to the mass, damping and stiffness matrices respectively. u is the system displacement and is the function of time t. F(t) is the external excitation. To find the undamped natural frequencies we get

$$[M]\{\ddot{u}\} + [S]\{u\} = \{o\}$$

A principal mode occurs if the entire system executes synchronous harmonic motion at a natural frequency ω.

$$Let \quad u = A\sin\omega t$$

$$then \quad \dot{u} = \omega A\cos\omega t$$

$$also \quad \ddot{u} = -\omega^2 A\sin\omega t$$

We may substitute

$$\{\ddot{u}\} = -\omega^2\{u\}$$

and rearranging

$$[-\omega^2\,[M] + [S]]\,\{u\} = \{\o\} \tag{3.2}$$

This is the eigenvalue problem and the equation has a solution when the determinant is zero. For each eigenvalue found there is an accompanying eigenvector, corresponding to the mode shape at that frequency. The eigenvalues are important physically because they define those frequencies at which the structure wants to vibrate, that is those frequencies that should be avoided in the forcing function.

There are several ways of finding the solution of the determinant. It is important to find the method which is least computer intensive. It would be possible to produce a graph of $|\{[S] - \omega[M]\}|$ versus ω to find where the zero values are and hence the natural frequencies. This would be extremely time consuming. A better technique is to transform equation (3.2). We proceed by factorising [M] to obtain

$$[M] = [L][L]^T$$

where [L] is a lower triangular matrix, and $[L]^T$ is its upper triangular transpose. We

62

then transform the degrees of freedom {u} using

$$\{u'\} = [L]^T \{u\}$$ (3.3)

Equation 3.3 is substituted into equation 3.2 and {u} is eliminated. On premultiplying by $[L]^{-1}$ we obtain

$$([S'] - \omega^2 [I]) \{u'\} = \{o\}$$ (3.4)

where [S'] is the symmetric matrix $\quad [S'] = [L]^{-1}[S]([L]^{-1})^T \quad$ and [I] is a unit matrix.

Equation 3.4 can be much more efficiently solved.

Whilst this is considerable faster it is still too time consuming when considering structures with more than 100 degrees of freedom.

3.4.3 Master Degrees of Freedom --- Eigenvalue Economization

The method that is typically used to overcome this problem is eigenvalue economisation. Almost all the degrees of freedom in a very large eigenvalue problem have little effect on the mass matrix. Thus the equation may be reduced if the inertia effects of certain degrees of freedom are ignored, so long as the stiffness terms are retained. (see for example [81]). To do this displacements are divided into master degrees of freedom u_m which will be retained, and slave degrees of freedom u_r which are to be reduced out. Equation 3.2 becomes:

$$\left[\begin{matrix} S_{mm} & S_{mr} \\ S_{rm} & S_{rr} \end{matrix}\right] - \omega^2 \left[\begin{matrix} M_{mm} & M_{mr} \\ M_{rm} & M_{rr} \end{matrix}\right]\left\{\begin{matrix} u_m \\ u_r \end{matrix}\right\} = \left\{\begin{matrix} \varnothing \\ \varnothing \end{matrix}\right\}$$

Ignoring the slave inertia we have

$$[S_{rm}]\{u_m\} + [S_{rr}]\{u_r\} = \{\varnothing\}$$

To eliminate $\{u_r\}$, the static energy

$$\text{S.E.} = 0.5\{u_m\}^T[S_m]\{u_m\} \quad \text{and} \quad \text{K.E.} = 0.5\{u_m\}^T[M_m]\{u_m\}$$

Where, dropping the matrix bracket nomenclature,

$$S_m = (S_{mm} - S_{mr} \, S_{rr}^{-1} \, S_{rm}) \text{ and}$$

$$M_m = (M_{mm} - M_{mr} \, S_{rr}^{-1} \, S_{rm} - S_{mr} \, S_{rr}^{-1} \, M_{rm} + S_{mr} \, S_{rr}^{-1} \, M_{rr} \, S_{rr}^{-1} \, S_{rm})$$

producing the master system equation

$$([S_m] - \omega^2[M_m])\{u_m\} = \{F_m\} \tag{3.5}$$

The elimination of the $\{u_r\}$ terms is not carried out during the matrix inversions due to the time involved, but beforehand in the frontal solution. The master degrees of freedom may be chosen automatically by calculating the ratio S_{ii}/M_{ii}, where S_{ii} refers to the leading diagonal term for freedom i. If the ratio is large then the node is well supported and unlikely to vibrate much.

Once the matrix has been inverted and the eigenvalues solved, the original

equation (eq. 3.1) may be substituted into and solved for.

Master degrees of freedom were used in the FE analysis in this study in order to reduce the computing time. Because the main interests were with the first few fundamental modes in both single and multi-blade analysis, the reduction in the degree of freedom will not have unacceptable effects.

3.5 The Mode Shape Classification

The modes of vibration of a structure are defined by three modal parameters, they are the natural frequency, the mode shape and the damping coefficient. The mode shapes describe the amplitude of the degree of freedom relative to each other at a resonance. It represents the relative motion of different parts of the structure when it is excited into one of its natural modes of vibration. The traditional classification of the mode shapes in turbine blade vibrations is used in this study and briefly introduced in this section.

In the study of the vibrations of turbine blades, mode shapes were often found having similar features due to the similarity in the geometry of the blades. it is convenient to categorise mode shapes according to their different features. They are usually defined as the flap modes, the torsional modes, the edgewise modes and the spanwise mode. They are discussed and illustrated below using a straight cross-section blade.

The Flap Mode

Two typical flap modes are illustrated in Figure 3.14. The main feature of the flap mode is that the blade flaps out of its own plane (plane YZ in Figure 3.14a).

One end of the blade is fixed and the other is free. The displacements are in XZ plane. The order of the flap mode is defined by the number of nodal lines across the blade. The first flap (1F) mode has one nodal line located at the root of the blade and the second flap (2F) mode shown in Figure 3.14f has two nodal lines. The first one is at the root of the blade and the second appears near the tip of the blade. Generally, the NF mode has N number of nodal lines.

The Torsional Mode

In torsional modes, the blade twists about its longitudinal axis, generating a vertical nodal line from the tip of the blade to its root, as shown in Figure 3.15a. A horizontal nodal line at the root also appears as the root is fixed. The order of the torsional mode is related to the number of horizontal nodal lines. The Nth torsional mode has N horizontal nodal lines including the first one at the root. The first and the second torsional modes (1T and 2T) are shown in Figure 3.15 (a) and (b) respectively. The torsional mode is an out-of-plane mode.

The Edge Mode

When vibrating in the edge mode as illustrated in Figure 3.16, the motion of the blade remains in its own plane (YZ plane). One end of the blade is fixed and the other is free. The natural frequency of the fundamental edge mode (1E) is usually higher than that of the 1F mode, because the bending stiffness of the blade in YZ plane is much larger than that in the XZ plane. The definition for the higher order of the edge modes is similar to that of the flap modes. It is noticed that the higher order edge modes are usually above other major modes and are very often not included in the frequency range of the interest.

The Spanwise Mode

Another in-plane vibration is that the blade stretches itself along its longitudinal axis, as demonstrated in Figure 3.17. The blade remains in its plane (YZ plane). The natural frequency of the spanwise mode is normally much higher than those of other fundamental modes, i.e., the 1F, 2F, 1T and 2T.

The mode classification introduced above is demonstrated on a simplified blade with straight cross-section. The real turbine blades have aerodynamic profiles with taper, camber and pretwist in geometry. Therefore the mode shapes are expected to be distorted.

3.6 Conclusion

The theories of the experimental and analytical methods used in this study were briefly discussed in this Chapter. The experimental set-up and the identification of natural frequencies of turbine blades by ESPI and modal testing were presented. It was very important to understand the principles of the methods used in order to obtain and interpret data correctly. As the main techniques have been discussed here, the following Chapters will mainly report on the study into the vibrations of single turbocharger blade and multi-blade packets.
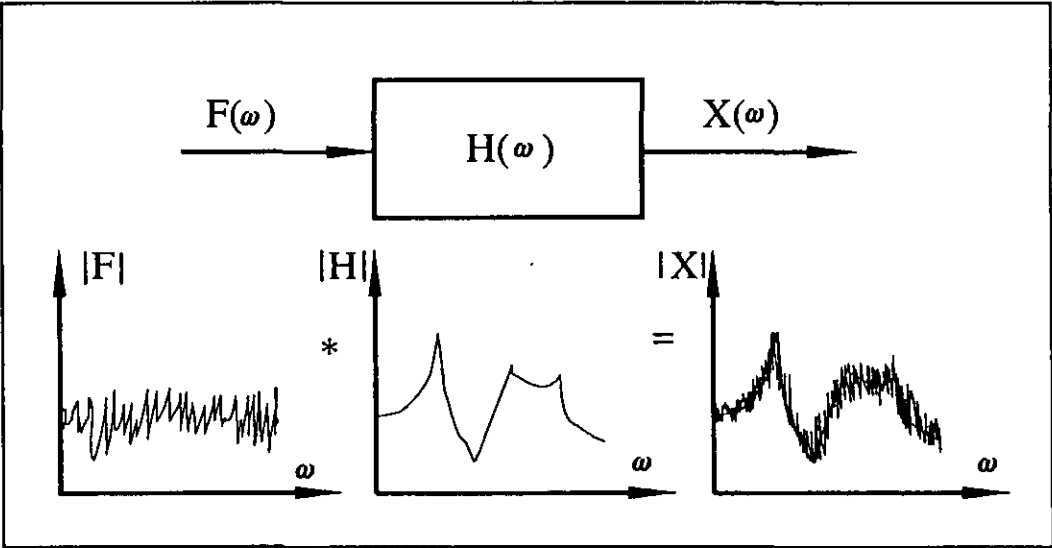
Figure 3.1 Frequency Response Function H(ω)
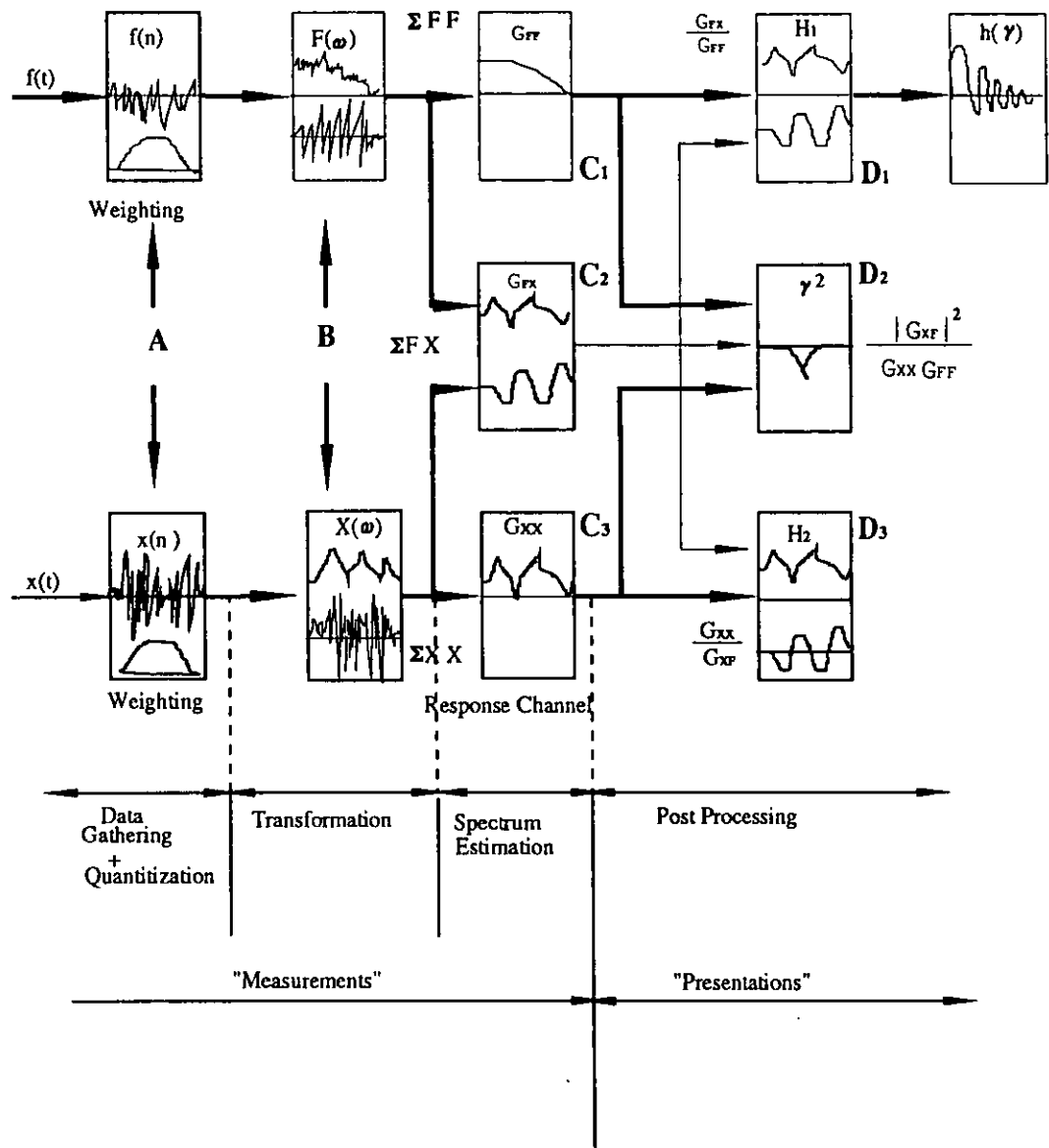
Figure 3.2 Signal processing in FFT analyzer.

Figure 3.3 Identification of mode shapes using imaginary part of FRF.

Ⓐ , Ⓑ , Ⓒ   Locations of accelerometer on the beam
f_1, f_2, f_3 Natural frequencies of the beam

a Locations of accelerometer and hammer impact
b Imaginary part of FRF detected at each location
c Mode shape at first three natural frequencies
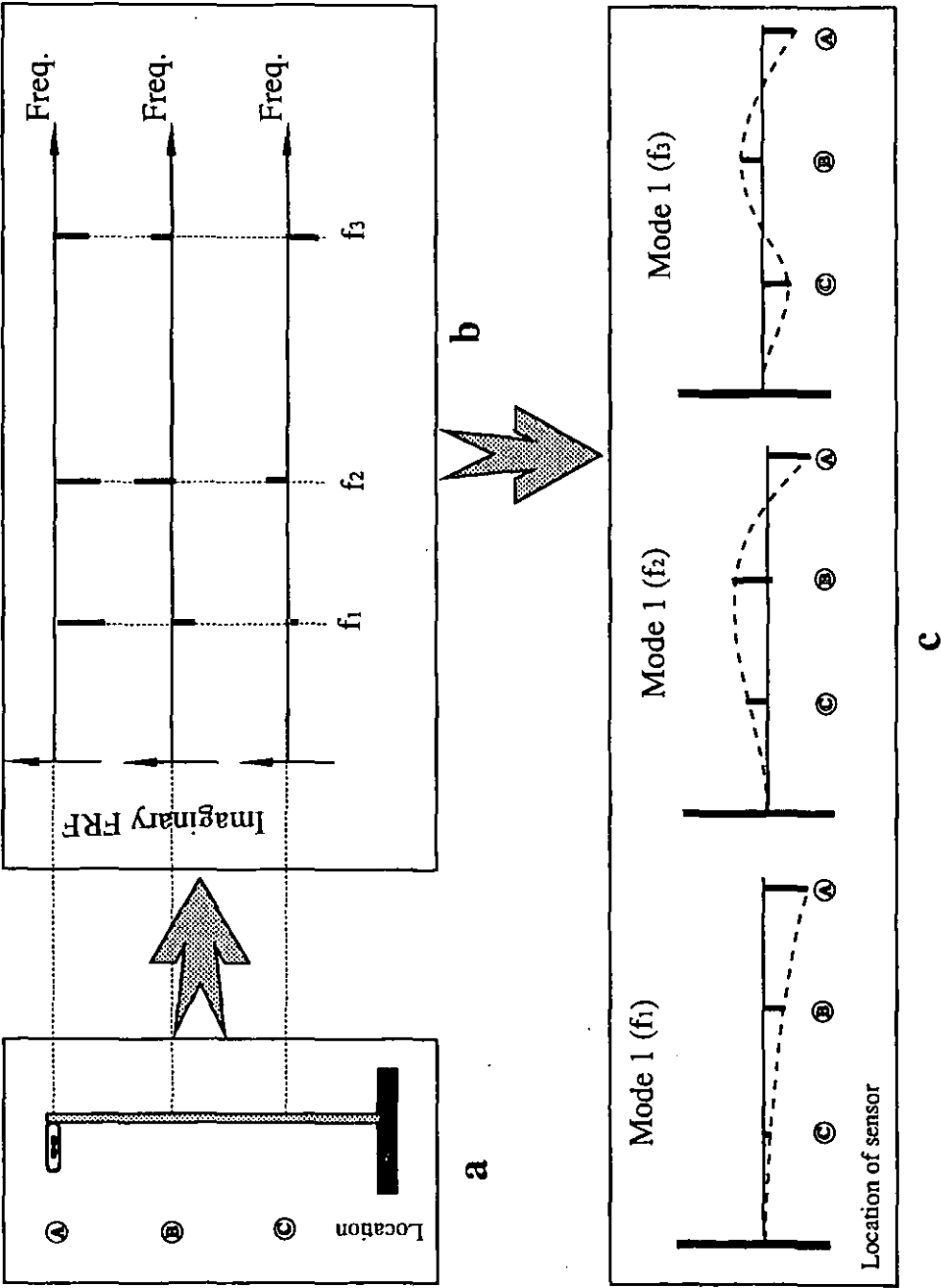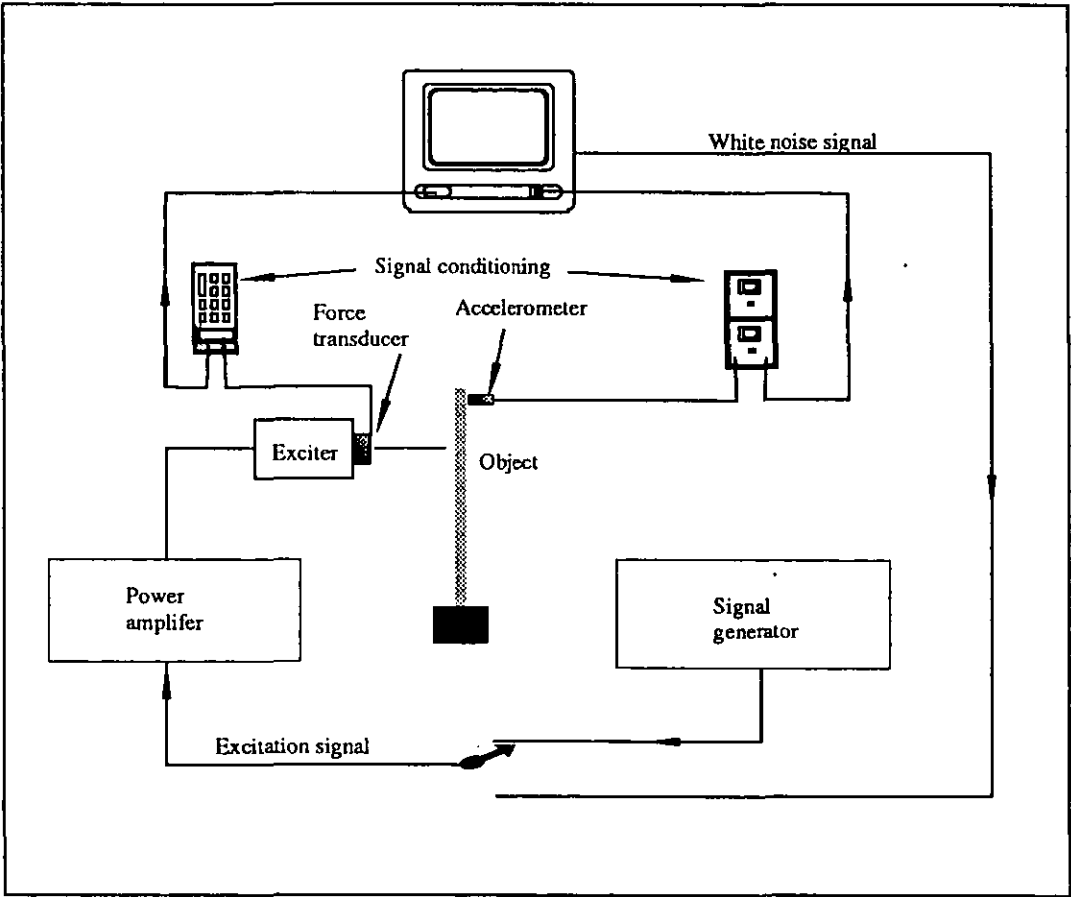
Figure 3.4   Illustration of modal testing set-up
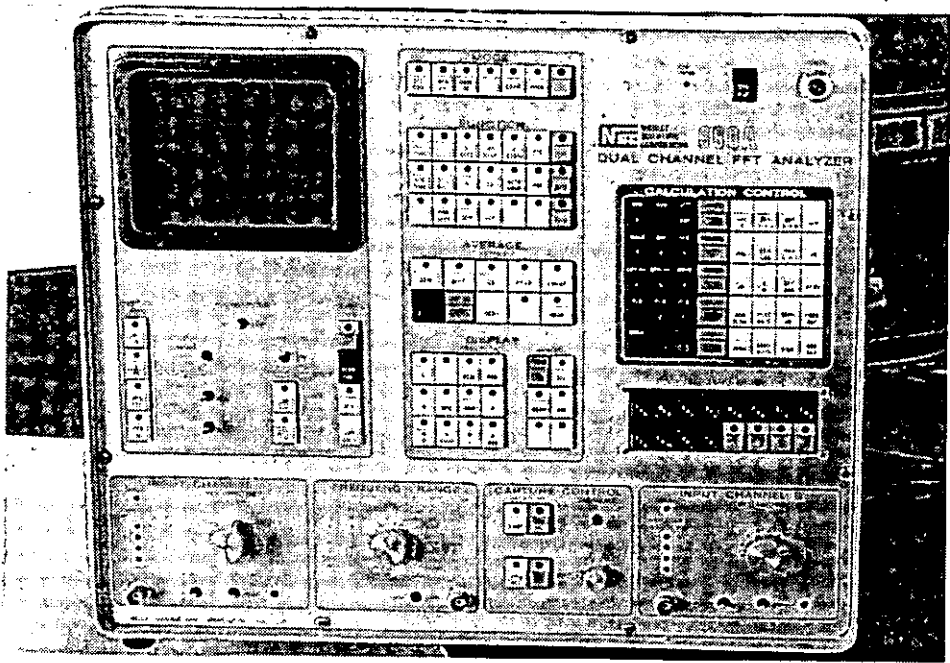
Figure 3.5   The control panel of Nicolet 660A dual channel FFT Analyzer
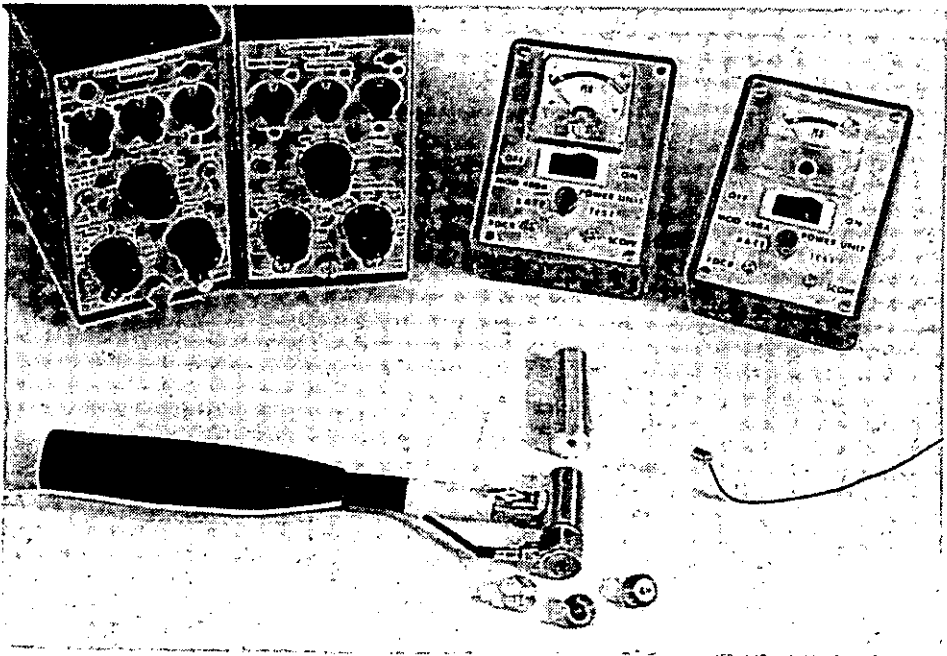
Figure 3.6   Instruments used in modal testing experiments
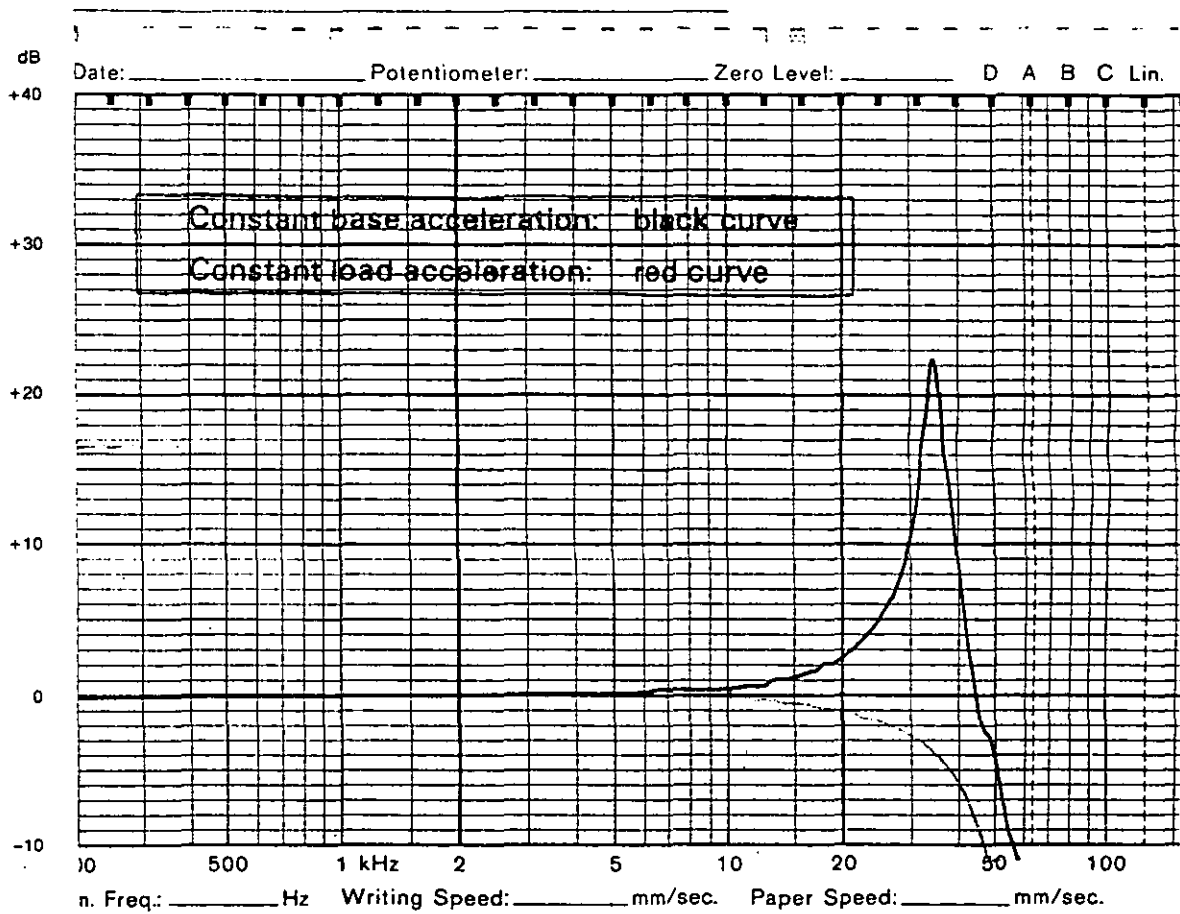
Figure 3.7   Frequency response characteristics of Bruel and Kjaer force transducer 8200 type

Typical Temperature Sensitivity Deviation:
(Piezoelectric Material PZ 27)
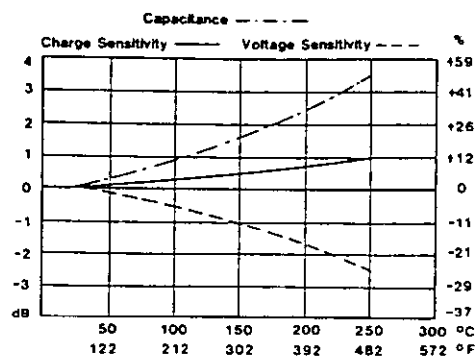
Typical Frequency Response Curve of 4374:
(Corrected for response of 4290)
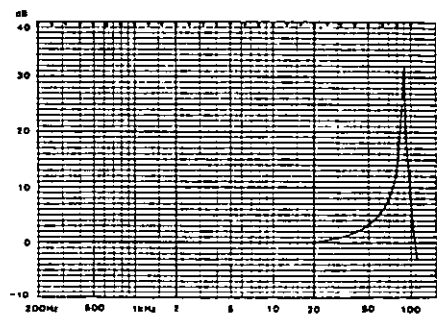
Schematic Drawing of Exciter 4290:
(Modified laboratory reference)
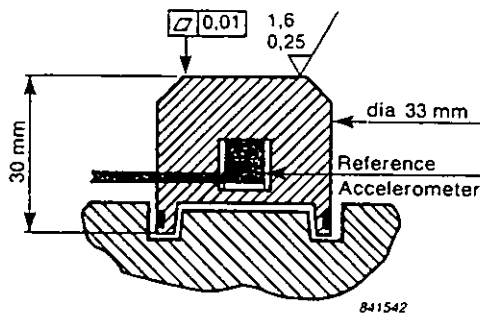
Material: Beryllium

Mass of Exciter Table: 38 gram

Mounting Technique:
Examine the mounting surface for cleanliness and smoothness.
If necessary, machine surface to tolerances shown in schematic drawing of calibration table.
Use quick setting Methyl Cyanoacrylate Adhesive for mounting. Apply adhesive sparingly to one surface and apply pressure to set. Sets in 5–15 seconds

Figure 3.8   Frequency response characteristics of Bruel and Kjaer

accelerometer 4374 type
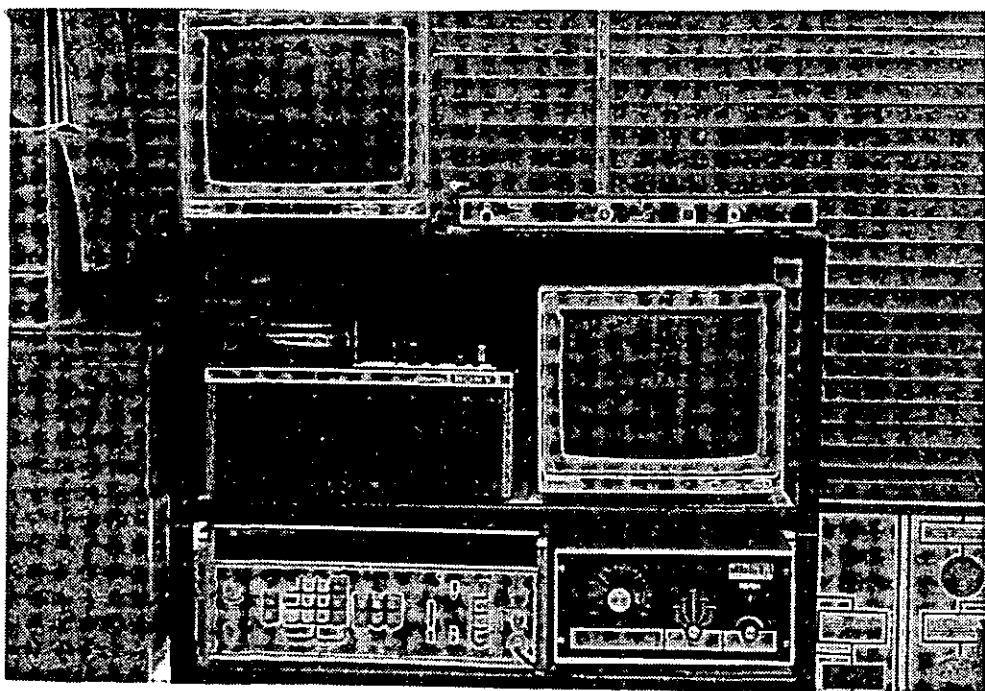
Figure 3.9   Instruments used in ESPI tests

(a) Image holography
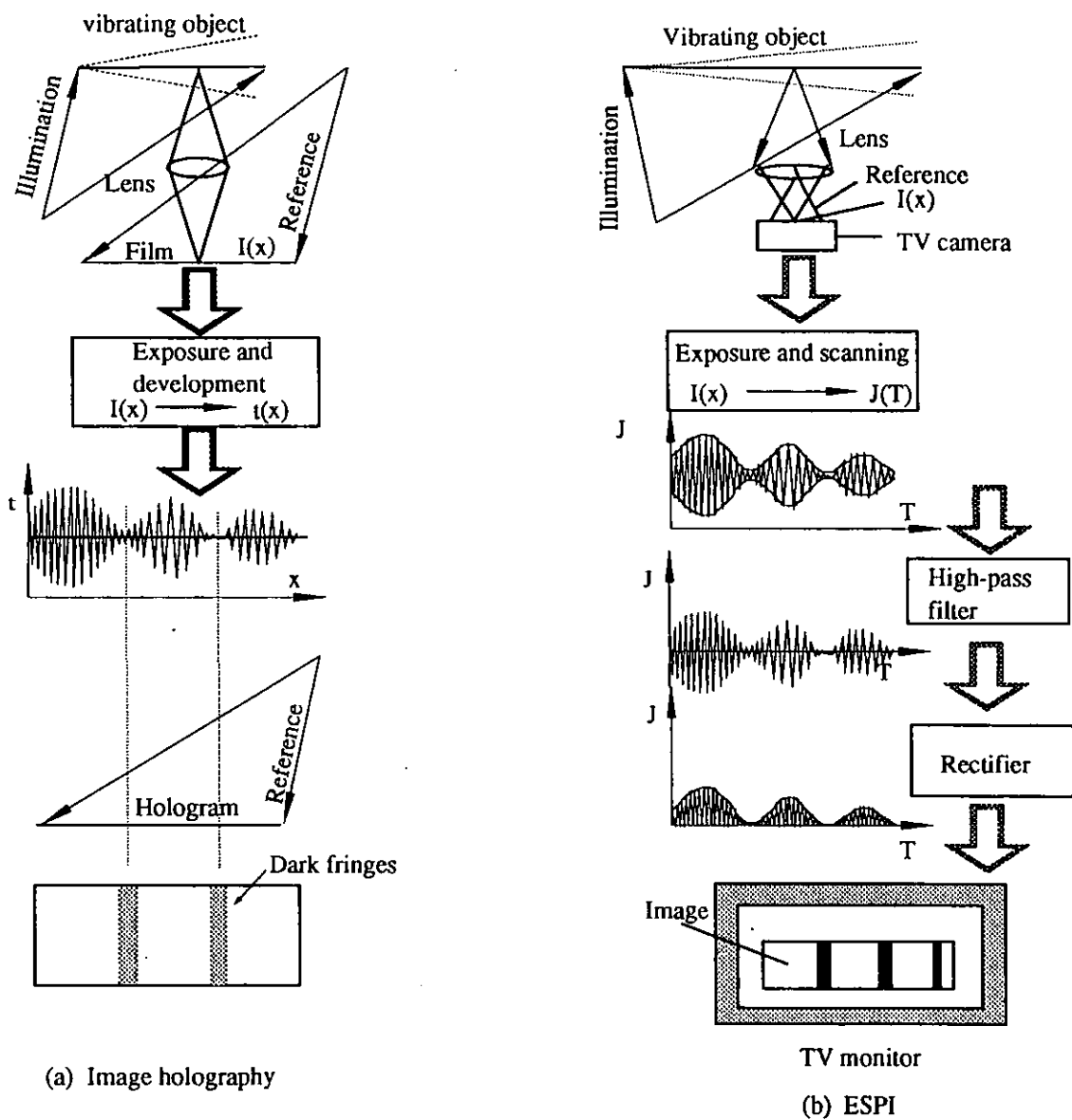
(b) ESPI

Figure 3.10 Principle of Electronic Speckle Pattern Interferometry
compared with Image Holography
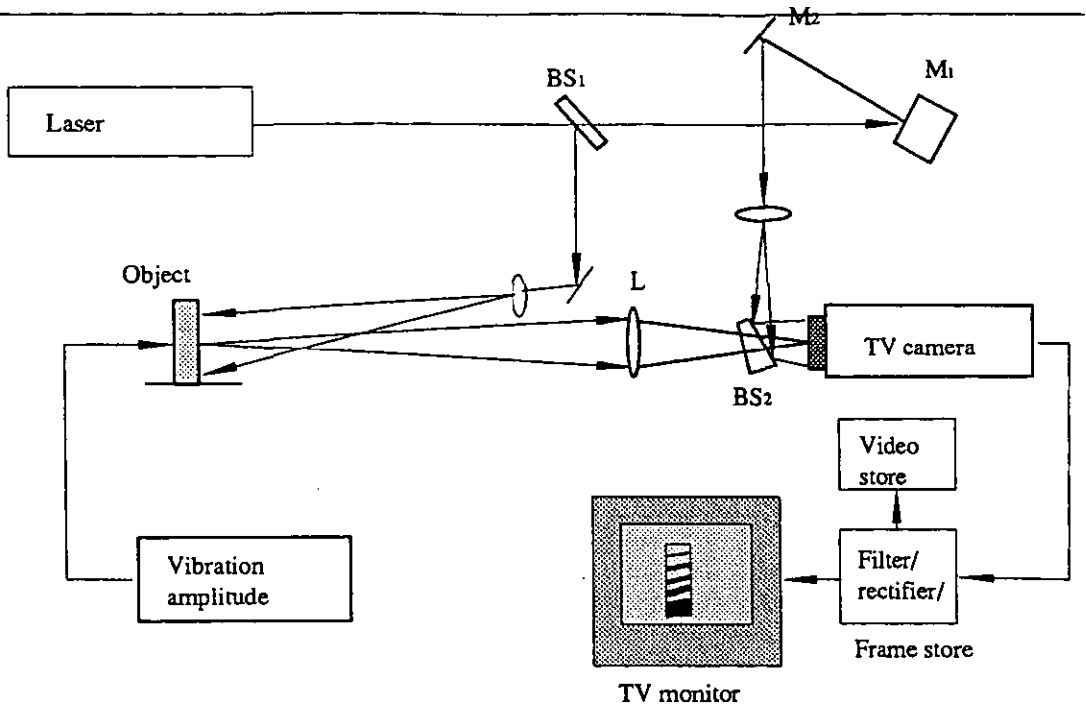
Figure 3.11a Basic elements of ESPI set-up
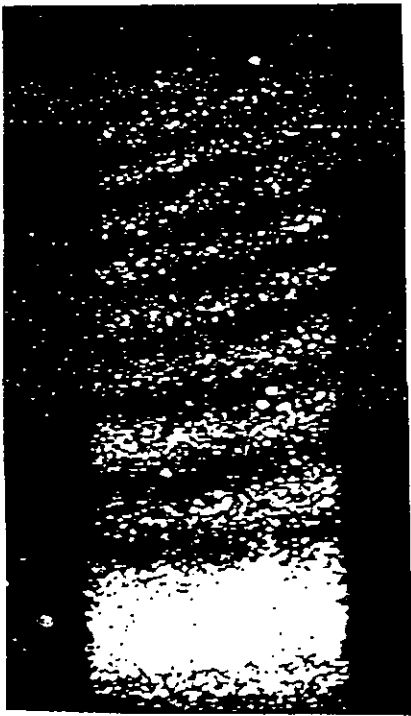
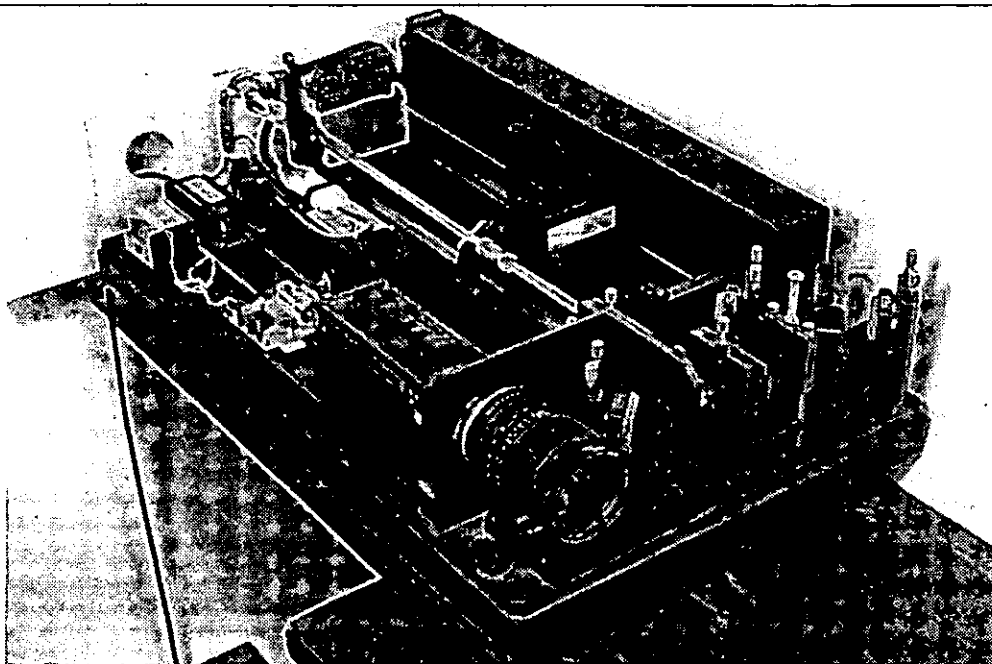Figure 3.11b ESPI recording of the vibration of a turbocharger blade

Figure 3.12 Optical Unit of the VIDISPEC system

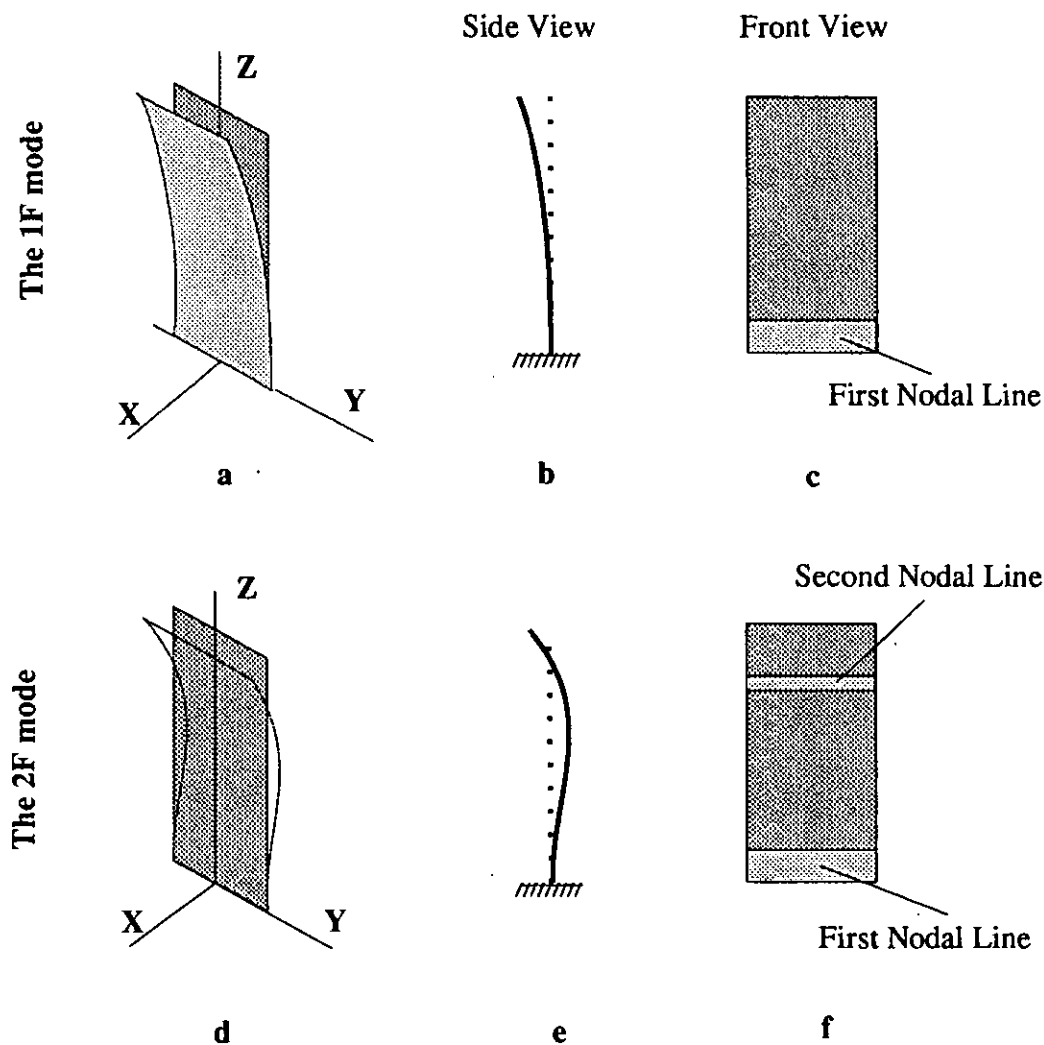Figure 3.13 SONY high resolution reel to reel tape recorder

Side View   Front View

The 1F mode

Z

X   Y

a   b   c

First Nodal Line

Second Nodal Line

The 2F mode

Z

X   Y

d   e   f

First Nodal Line

Figure 3.14 The flap modes in turbine blade vibrations
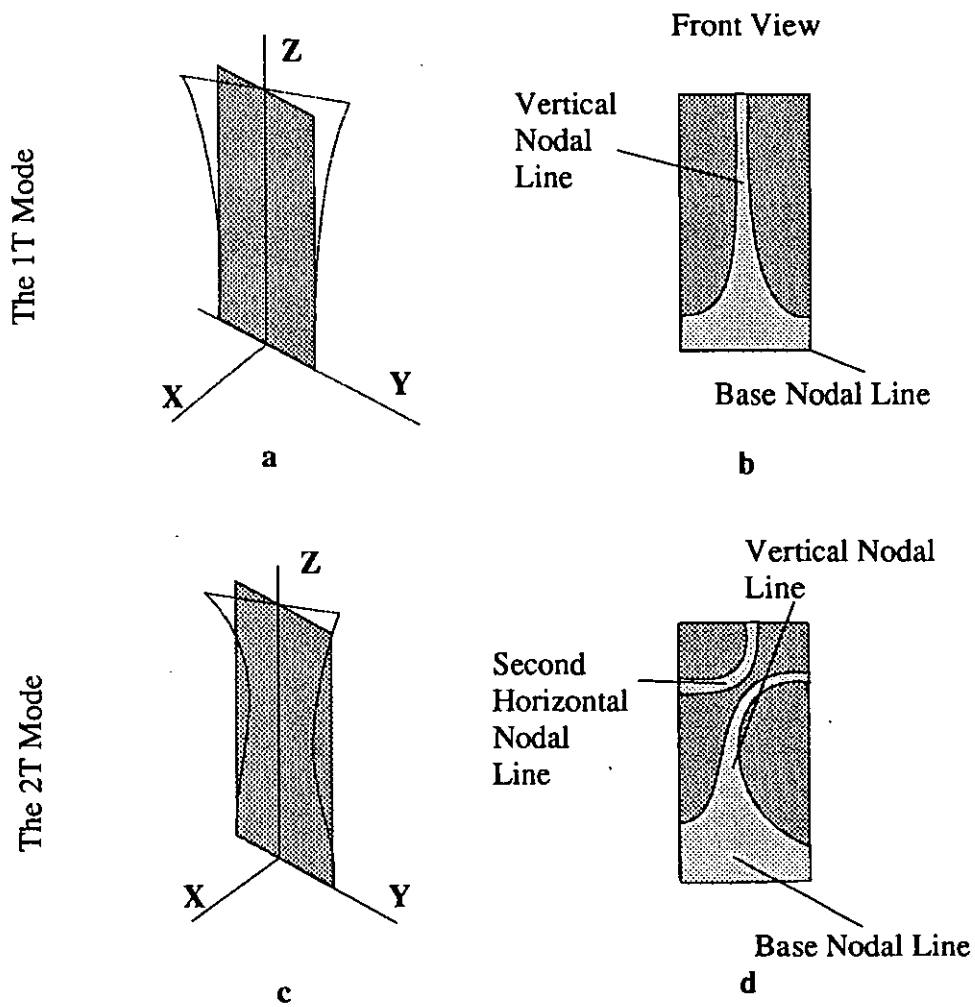
Figure 3.15 The torsional modes in turbine blade vibrations

Front View

a

b
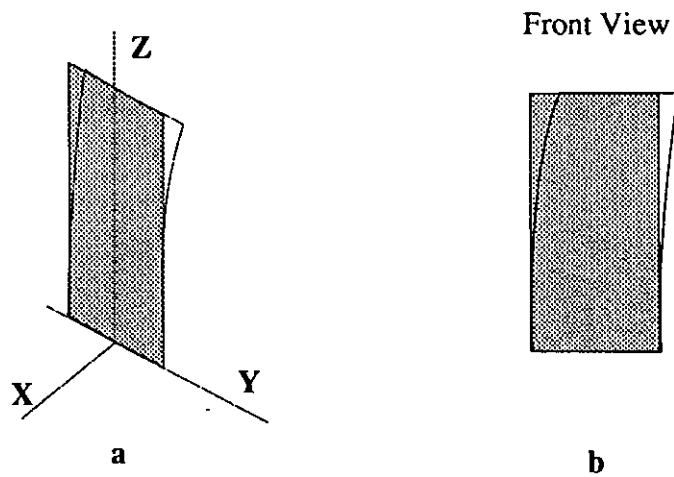
Figure 3.16 The first edge mode (1E) in turbine blade vibrations

Front View

a

b
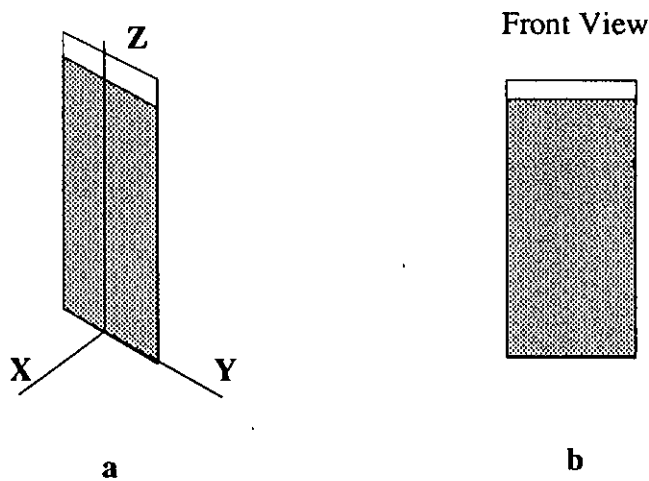
Figure 3.17 The first spanwise mode (1S) in turbine blade vibrations

Chapter 4

The Initial Study into Vibration Characteristics of a Single Turbocharger Blade

4.1   **The Blade K**

4.2   **Investigation by Modal Testing**

4.3   **Investigation by the E.S.P.I.**

4.4   **Investigation By the Finite Element Analysis**

        4.4.1   Computing Hardware

        4.4.2   Computing Software.

        4.4.2.1 The Structure of PAFEC

        4.4.2.2 Module Explanation

        4.4.3   Prime Interactive Graphics System (PIGS)

        4.4.4   Initial FE Analysis of the Blade K

4.5   **Initial Attempt at Classification of Modes for the Blade K**

4.6   **Discussion on Initial Investigation**

4.7   **Conclusion**

        Figures

The initial study was carried out on a turbocharger blade, noted as blade K. The aim of the initial investigation was to identify modal parameters of blade K using modal testing, ESPI and finite element analysis. It was considered necessary to use three techniques in order to obtain a good understanding of their theories and applications.

4.1 The Blade K

A turbocharger blade, blade K as shown in Figure 4.1 , was selected to be the model of this study. It was removed from its disk and mounted via its fir-tree root on to a holding block. The lacing wire was also removed leaving a hole of 3.2 mm diameter in the blade at 13 mm from the blade tip on the central line along its length. The blade is 91 mm long and 32 mm wide. It is twisted and tapered along its length, tapered and cambered across its width. A force was applied to the base of the root of the blade via two bolts to ensure that the fixing of the blade was as near as possible representative of the real operating condition for rotating blades. In this initial study, blade centrifugal loading was not considered for simplicity. Its finite element model was called BLDK.

4.2 Investigation by Modal Testing

The initial investigation was started with modal testing. Natural frequencies and mode shapes were firstly identified by using hammer impulse excitation. The response was detected by a miniature accelerometer attached to the blade at various positions. Both excitation and response were fed into Nicolet 660A FFT analyser via their amplifiers. The experimental set-up is schematically illustrated in Figure 4.2. The holding block was clamped on a vibration isolated testing bench.

A mesh was drawn on the surface of blade K in order to identify the natural frequencies and mode shapes. The hammer impulses were applied at different nodes on the mesh while the accelerometer was attached at the top corner of the trailing edge. This is effectively same as hitting the blade at one position while the accelerometer is attached at different nodes on the mesh. However, the former application could avoid potential poor attachment of the accelerometer due to frequent change of positions. It also provided more control on identifying anti-node positions when hitting at or near an anti-node. Consideration of the real and imaginary components of the transfer function of the processed transient data located some natural frequencies and gave some indication of mode shapes associated. A typical set of results detected was shown in Figure 4.3(a).

Modal testing was also carried out using white noise (random) and sinusoidal sweeping excitations. An electro-magnetic exciter driven by either a white noise signal or a sinusoidal signal was used to excite the blade via a fine push rod as shown in Figure 4.4. For white noise excitation, the output from the accelerometer, attached at different nodes of the mesh, together with the input signal from the force transducer connected between the exciter and driving probe were sent into and processed by the FFT analyser. This experimental set-up is shown in Figure 3.4 and the instrumentation used was discussed in Section 3.2.7. The results are shown in Figure 4.3(b).

For sinusoidal excitation a sweeping sinusoidal signal was fed into the exciter which drove blade K via the push rod at a node while the accelerometer was attached either at the top corner of either the leading edge, or the trailing edge of the blade. Frequencies causing resonant responses were recorded and are illustrated in Figure 4.3(c).

The distance between adjacent nodes was constrained, with the limiting factor

being the hammer impact diameter. Also impulses to the blade could not be repeated exactly for each sample in each averaging procedure. Thus errors associated with hammer testing for small components were highlighted. For example, nodal lines identified by hammer testing had to be made up by discrete nodal points.

It was noted that quality of input signals could be very poor, especially when excitation was applied at near anti-node positions. The averaging facility in Nicolet was fully utilised to ensure good quality input signals when white noise excitation was applied. 16 to 100 samples were used in averaging process in order to generate one response curve before it was processed.

Such tests were considered to be extremely useful guides to identify natural frequency values and mode shapes but large discrepancies on results were found. For instance, there appeared to be 7 resonances in between 1451 Hz and 2831 Hz identified by modal analysis in Figure 4.3. Three of them looked like the second flap mode but further study was apparently required to reveal the true nature of the modes of vibration of blade K.

4.3   Investigation by the E.S.P.I.

A second series of tests were conducted using the comparatively modern technique of ESPI. This has the advantage that instantaneous real-time speckle pattern images can be viewed on a television screen. The patterns are representative of the deformed modal patterns.

Blade K was mounted in front of an ESPI rig and was excited by an electro-magnetic exciter via a fine push rod driving at either of the top corners of the blade. A continuously swept sine wave signal generated by a digital signal generator

was fed into the exciter and laser speckle interference fringe patterns representing local amplitudes of responses were displayed on the monitor screen. These fringe patterns clearly showed the nodal lines at resonances. Two sets of results are given in Figure 4.3(d).

It was found that some modes at the higher frequency ranges were easy to identify. For example natural frequencies of the modes at about 7300Hz and 9860Hz shown in Fig. 4.3(d) did not vary with different excitation location. But in the middle and lower frequency range the results were rather confusing. Double natural frequencies and mode shapes for the torsional mode were found as shown in Fig. 4.3(d) from 4500Hz to 5300Hz. The variation of this mode was found to be related to the excitation position. The same phenomena was found for the mode at about 2600Hz. Natural frequencies and mode shapes are inherent characteristics of a component. They are not related to the excitation. If the detected responses change with the location of excitations, then they are not the true natural frequencies. Therefore further studies about the effects of excitation position on dynamic characteristics of turbocharger blade were carried out.

4.4 Investigation by the Finite Element Analysis

4.4.1 Computing Hardware

The major limitations on the accuracy of finite element models in general is the mesh size and the number of elements used. These factors themselves depend on the maximum cpu time that can be used on a particular computer and the memory file space available. Another factor of the overall speed of job completion is the job turnaround time which depends on the ease of use of the operating system and the available editors.

The computers used for the finite element calculations of the project were the Prime 75 and the Apollo 3000 Domain. On each of the computers, the finite element package PAFEC had been installed, with the more recent computers having a newer version.

The computer that was used at the start of the project was the Prime 750. The Prime used Primos 19.4 as its operating system and its main editor was qedx. The operating system was user friendly, but as qedx was a line editor, most file editing was performed by transferring files to the Honeywell Multics and using a screen editor, emacs. The Prime disc space available varied between 25000 Units and 70000 Units corresponding to 51.2 Mbytes and 143 Mbytes respectively, depending on the student requirements. This was sufficient for all single job runs but insufficient to allow the use of the PAFEC option "restart" where the solution of an eigenvalue problem is performed in stages. The Prime ran 4 batch queues for finite element jobs, having maximum cpu times of 5 mins, 17 mins, 50 mins and 9 hrs 6 mins. This last maximum was dependent on the hardware, therefore, could not be changed. The Prime was initially the only mainframe available for finite element calculations at Loughborough University, so the maximum size of the finite element model was governed by this maximum cpu time, and the computer's processing speed.

The Prime 750 was discontinued after two years of the project. Before the Hewlett-Packard computer was installed, the Apollo 3000 Domain was used as an alternative. This consists of 20 to 30 work stations, each with its own processor and memory. Each workstation, or node, is connected to each other, so that one node may draw the entire processing power of the other nodes if they are not being used. The operating system is Aegis level 9.7, and the editor used an Apollo design, both of which were exceptionally easy and flexible to use. The maximum disc space was sufficient for successful job completion. The speed of the Apollo was significantly

87

better than the Prime, cutting the cpu time from 9 hours to about 5 hours.

4.4.2 Computing Software.

The standard solution technique for vibration problems is by using finite elements in the eigenvalue equation. A brief review of the theory is given in section 3.4.

Several finite element packages are available commercially, each with its own advantages and disadvantages. The requirement for the project was the ability to solve for the eigenvalues and eigenvectors. The package which was available in-house, PAFEC, has the above ability and so was chosen for the model software.

4.4.2.1 The Structure of PAFEC

PAFEC uses different phases at different times within the overall solution algorithm. Different phases are relevant to different applications. For eigenvalue problems, the following phases listed in Table 4.1 would be required [126].

The data is read in from a series of modules, each module defining some parameter of the system. A brief explanation of some of the modules is given in Table 4.1.

The two main analysis types available are static analysis, (stress analysis and thermal analysis), and dynamic analysis, (natural frequency and mode shape identification, Sinusoidal response and transient response). Additional specialist analyses include non-linear analysis, (plasticity, creep, large displacement and prestressed eigenvalue prediction), cyclical symmetric analyses, axisymmetric analysis, multi-level substructure analysis, lubrication analysis and boundary integral

solution technique. Documentation of the analyses types may be found in reference [126].

Phase 1	Read	Data modules are read in and stored on the backing store.
Phase 2	Paf-blocks	Auto mesh generating facility
Phase 4	House Keeping	The constraints on the system are considered and the degrees of freedom are numbered.
Phase 6	elements	The elemental stiffness and mass matrices are stored.
Phase 7	Solution	The equations are decoupled and solved.
Phase 8	Out Draw	The displacements are drawn.

Table 4.1 Phases required by eigenvalue problem and post processing.

Solution with different damping forces and the same system matrix is possible using the restart facility, which solves for the new forces whilst using the previously inverted matrix. This typically reduces the computational time by an order of magnitude.

4.4.2.2 Module Explanation

Control   This module is different from all the rest as it does not define any parameter of the structure, but acts as a guide to the solution. The restart option is defined in this module.

Nodes The nodes are defined within a particular axis set. They may be generated automatically by using the PIGS [127] option, (see below).

Elements Various types of elements are available, corresponding to the geometry

and application involved. The element may be distorted away from its basic shape to a degree, but there are limitations, which if exceeded will result in an error message in the output files and failure of execution.

Modes.And.Frequencies This defines how many frequencies are solved for, and how many masters are used for the solution.

Restraints Other constraint modules include ENCASTRE and NO.CONSTRAINTS.

Material PAFEC has standard materials, but others may be defined to improve accuracy, or to change element stiffness.

Dynamics.Graph This defines which nodes and directions are drawn.

Masters The master degrees of freedom are automatically generated, but should be supplemented with those defined in FORCE and DYNAMICS.GRAPH, above.

The major limitation with PAFEC, as with other packages, is its accuracy with respect to elemental size. Finite element packages are inherently an upper bound solution, so the predicted frequencies will tend to be over-estimates.

4.4.3 Prime Interactive Graphics System (PIGS)

PIGS is a pre and post-processor applicable to PAFEC. As a preprocessor pigs may generate the finite element structure and input data files. As a post-processor, finite element output may be analyzed. Documentation of the pigs facility is detailed in PIGS manual [127].

4.4.4 Initial FE Analysis of the Blade K

Great effort was made to build up the initial F.E. model of blade K. The drawing of cross sections of blade K was used to generate the mesh. Top, middle and bottom cross sections were selected to form the F.E. mesh. Key nodes were located on the boundaries of cross sections and their coordinates were given by measuring the drawing. Based on these key nodes, the mesh was automatically generated, as shown in Fig. 4.5, by using PAFBLOCK module in PAFEC data preparation program. The F.E. model of blade K is called BLDK.

This F.E. model was built up with the idea that the geometry of blade K should closely model the dynamic characteristics in 3 dimensions to allow for the complex geometry of blade K, resulting in coupled vibration. Thus 3-dimensional brick elements (element type 37110) with 20 nodes per element were used to build up the initial 120 element model as shown in Fig. 4.5, which had 2115 degrees of freedom.

The number of elements used was kept to the minimum in order to reduce the computing time, whilst the accuracy of the modelling had to be maintained at a reasonable level. Large error would occur if elements used were largely distorted. Therefore, the longest side to the shortest side ratio of the elements was no bigger than 5 as recommended by PAFEC. This dictated the maximum size of elements at the trailing edge hence the total number of elements used.

The three dimensional brick element was also selected for the following reasons:

■   when the bladed packet is analyzed as a solid structure, the analysis leads to results that are closer to the experimental results; the natural mode shapes of

91

structures can be established in space co-ordinates;

■ as the three dimensional analysis covers not only bending modes but also torsional and longitudinal modes, the analysis will be more extensive, so that all the blade natural frequencies and coupled packet frequencies can be estimated for a blade packet. Similar to packet modes in bending, packet modes in torsion and edgewise can also be established.

■ as this high precision element can represent effectively the true aerofoil surfaces of blades and hence model the coupling of bending and torsional modes.

The root of BLDK was fully constrained and the centrifugal force was not considered; though in reality a more representative support condition is that the blade is constrained by the interface between the top surface of the fir-tree root element. It was thought possible to compensate for this effect by either extending the root of the mathematical model below the base of the blade or by applying more flexible constraints to the base of the model.

The third set of results illustrated in Figure 4.3(e) was produced by F.E. analysis which proved to be the key link in the interpretation of the three sets of results. This was because it enabled the author to identify mode shapes in the conventional method of bending or flap modes (F), edge modes (E), torsional modes (T) and span-wise modes (S).

4.5 Initial Attempt at Classification of Modes for the Blade K

Indeed, whilst the initial study did not give satisfactory results it proved to demonstrate problems concerning the measurement of dynamic characteristics of a single turbocharger blade. It showed limitations for each technique in detecting or analysing a component and also indicated difficulties with the interpretation of experimental data.

The table of results shown in Figure 4.6 displays all the natural frequencies identified by the three methods of analysis. The conventional methods for classifying nodal patterns [68] was utilized here. Only results which were clearly identifiable are illustrated. By cross-referencing between the results presented in Figure 4.3, it can be seen that only the first flap (1F), second torsional (2T) and possibly 1T modes were positively identified.

Both Modal Analysis and ESPI analysis indicated several resonant responses in the frequency ranges 1100 to 2800 Hz, 4400 to 5600 Hz and 7150 to 7380 Hz. However it was not possible with the data available to classify the mode shapes within these frequency ranges. For instance the natural frequency identified by both experimental methods between 1700 and 2800Hz implied a second flap mode (2F) but this conflicted with the finite element analysis prediction of 5610 Hz for the 2F mode. Also there were three resonances found in between 1000 and 1450 Hz by ESPI whilst there was only one 1F mode predicted by FE analysis.

Moreover, it was noted that each of the experimental techniques failed to detect several modes that were suggested by the finite element analysis. For example, the 2F mode at 5610 Hz suggested by FE analysis was not positively detected by modal analysis and ESPI. Review of the experimental procedure confirmed that this was not a consequence of too fast a scan rate which was a particular problem associated with the method of excitation used in the ESPI tests.

93

4.6 Discussion on the Initial Investigation

It was considered at this point in time that some small discrepancies among identified frequencies were due to improper excitation, mass modification and poor modelling of boundary condition in FE analysis.

Several natural frequencies, clearly predicted by finite element analysis were not detected by experimental techniques because both measurement techniques had an element of polarisation in the method by which they sensed vibration. The accelerometer associated with the modal analysis measurements was only capable of detecting vibration in a plane perpendicular to the surface to which it was attached, whilst the ESPI detection capability was polarised to view only out-of-plane motion. Clearly, therefore, the modal analysis results would lack information on vibration mode shapes which caused the contact point of the accelerometer to move at right angles to its direction of sensitivity (i.e. approximately in the blade edge mode) whilst the ESPI results would suggest out of plane motion (i.e. blade flap motion) for an inclined plane moving in-plane (i.e. blade edge mode).

For instance, because of the twist of blade K, the edgewise movement at lower part of the blade may cause components of motion normal to the surface of the upper part of the blade. These components are measured as bending motion by the accelerometer giving a confusing indication. For the same reason, a nodal line may be presented by ESPI measurement and the edgewise mode may look like a flap mode.

Minor differences in determined frequencies can be attributed to the method of excitation, mass of the accelerometer and even to a poor choice of equivalent blade height in the finite element analysis. However the larger discrepancies and

interpretation of the mode shapes identified with some of the results required far more consideration. Furthermore there was variation of mode shapes and natural frequencies for some modes (e.g. at 4400 Hz up to 5600 Hz), caused by the changing of excitation positions. Thus a thorough understanding of excitation technique and justified interpretation of experimental data were required by further study.

4.7 Conclusion

The study of a free standing turbocharger blade was started using modal testing, ESPI testing and finite element analysis. It was seen from the initial results that the vibration of a turbine blade with a complex profile was very complicated. The large discrepancies in some of the results obtained using different techniques suggested the limitation of each technique. Hence a better understanding of the experimental techniques used was required, in order to correctly carry out the experiments and interpret their results.

Assisted by FE analysis, the 1F, 2T and 1T modes were identified. Several resonant responses were detected by both modal testing and ESPI analysis in between 1100 to 2800Hz, 4400 to 5600Hz and 7150 to 7380Hz, depending on the location of excitations. The detected mode shapes were complex and they vary with the location of excitations. It was concluded from the above study that a more fundamental study was required to establish the understanding of the effects of complex profile, location of excitations and the coupled mode vibrations. This study is presented in Chapter 5.
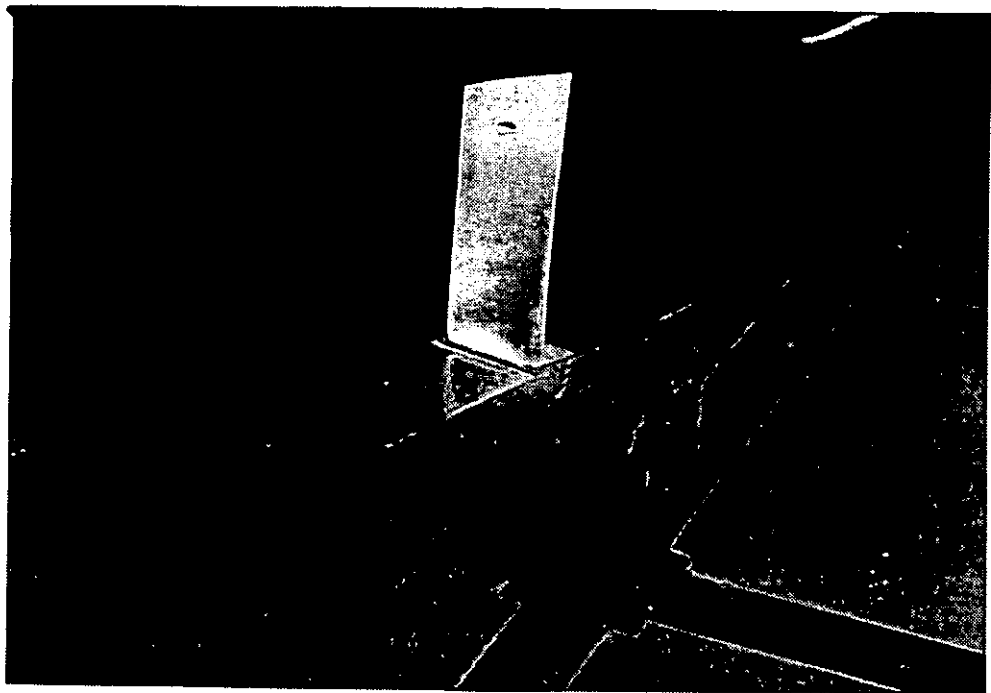
Figure 4.1 Single turbocharger blade
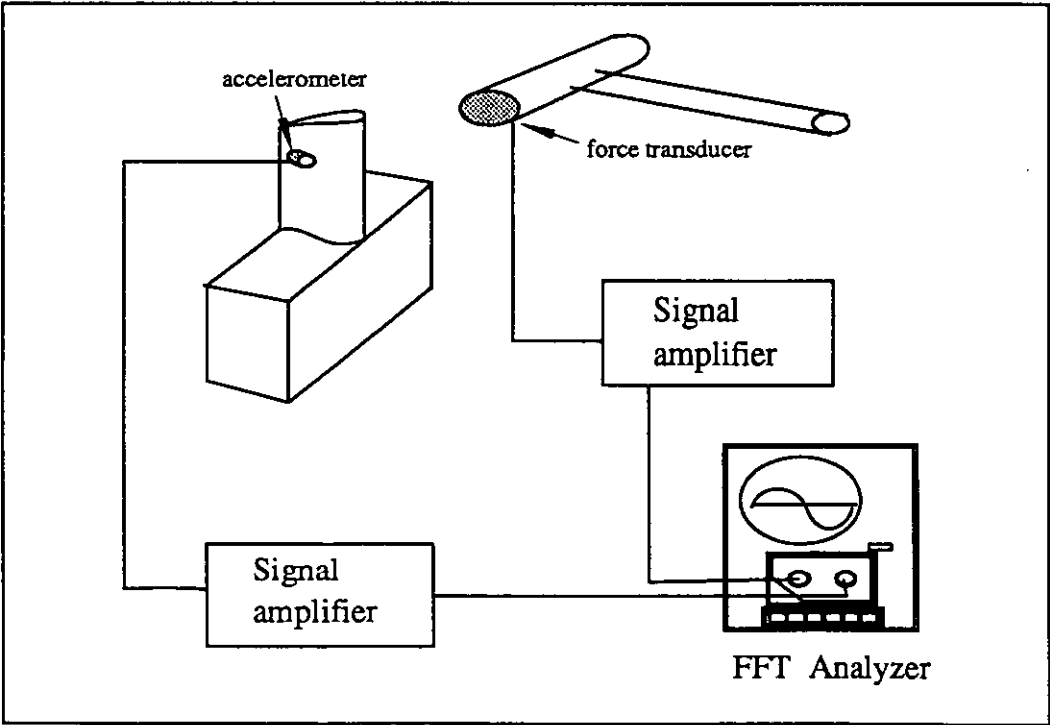
Figure 4.2 Experimental set-up of modal testing using hammer impulse excitation
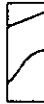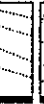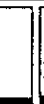
	Excitation Method		Sensor Location	Frequency (Hz)							
				1000	2000	3000	4000	5000	6000	7000	Above
a	Modal Analysis	Impulse		1050	2300		4250		6850		
b		White Noise		1180 / 1725	2800			5000		7600	9600
c		Sinusoidal	Leading Edge	1173 / 1451	2727		4371	4881		7423	
			Trailing Edge	1116 / 1753	2831	3741	4413	5673		7150	9985
d	E.S.P.I. Analysis	Sinusoidal at Trailing Edge		1074 1266 1450	2650 2722		4532	5336		7382	9892
		Sinusoidal at Leading Edge		1078 1256 1438	2374 2748		4402 4476	5032		7270	9846
e	F.E. Analysis			1290	2960		4710	5610			9030

Figure 4.3 Initial results of the natural frequencies of blade K
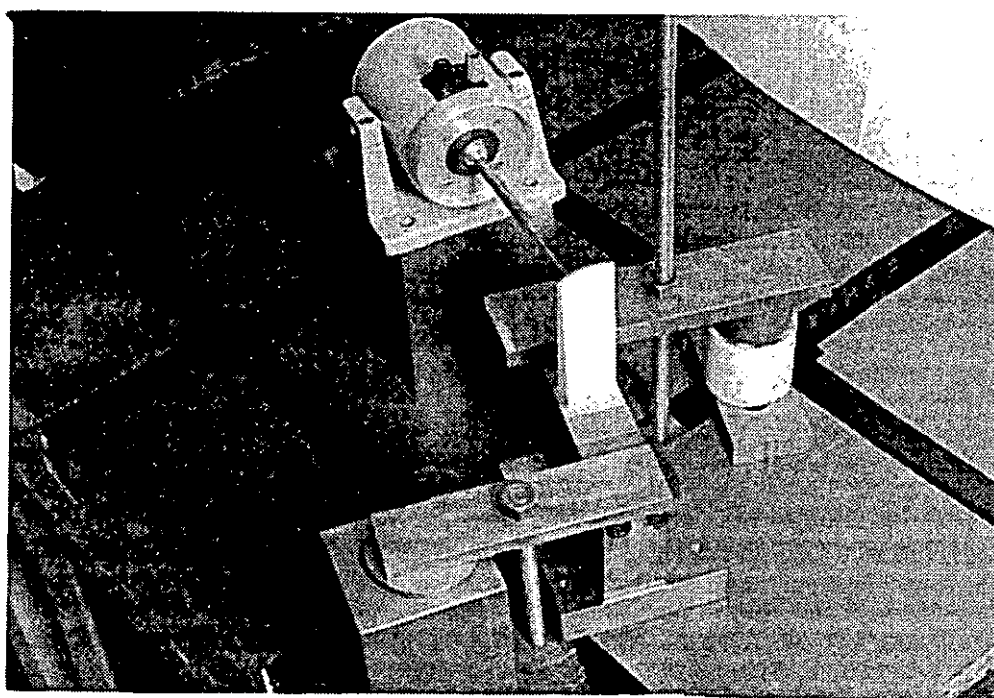
Figure 4.4   Excitation to a blade by a fine pushing rod
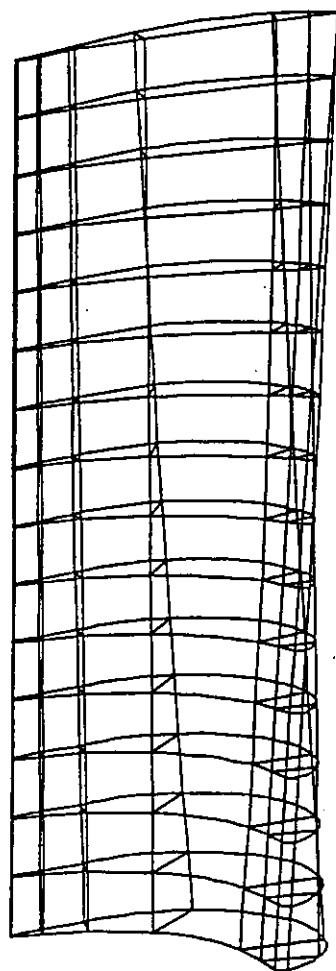
Figure 4.5   Finite element model of blade K

Analysis Method	Detected Mode Frequency (Hz)					
	1F	1E	1T	2F	3F	2T
Modal	1050		4250		6850	9600
E.S.P.I.	1070					9840
F.E.	1290	2960	4710	5610	9030	10800

Figure 4.6 Initial attempt at classification of modes for a turbocharger blade

Chapter 5

Further Investigation into Simplified Blades and the Blade K

5.1 Key Factors in the Vibration Mode Identification

    5.1.1   Design of Simplified Model Blades

5.2 Investigation by ESPI and Separation of Coupled Modes

    5.2.1   Consideration of Excitation positions

    5.2.2   Separation of Coupled Modes

    5.2.3   Theoretical Consideration of coupled mode vibrations

5.3 Finite Element Models of Simplified Model Blades and the Blade K

    5.3.1   F.E. Mode Shape Identification Using PIGS.

5.4 Summary of Results

    5.4.1   Effects of the Complex Profile

5.5 Further Consideration Into the Interpretation of Modal Analysis Results

5.6 The Improvement of the F.E. Model of the Blade K

    5.6.1   Number of Elements

    5.6.2   Type of Elements

101

5.6.3   Modelling of the Root of the Blade K

5.6.4   Material Properties of Elements

5.7   Conclusion

Figures

5.1 Key Factors in the Vibration Mode Identification

Further consideration of problems with identifying vibration modes revealed that the complex geometric shape of blade K and the uni-directional sensitivity built in experimental and theoretical analysis methods were the key factors resulting in difficulties of mode identification.

The complexity of the blade shape greatly distorted the mode shapes from normal classical mode classifications such as flap modes, torsional modes etc. Furthermore the complex shape, especially twisting factor increased the difficulty of data interpretation for both experimental and theoretical approaches since all techniques are uni-directional. An accelerometer can only detect the motion in its sensitivity direction and it was attached with its axis of sensitivity normal to the surface of blade K. ESPI technique is only able to monitor out-of-plane motion and mode shapes of F.E. models can be seen on a screen which is only two dimensional. Hence the difficulty of mode identification is greatly increased. In addition, there were modes which were so close to each other in frequency that they were coupled and gave coupled mode shapes which could not be identified without the knowledge of standard mode shape understanding for the blade K. To overcome these difficulties, the further study started with simplified blade models.

5.1.1 Design of Simplified Model Blades

Instead of studying the blade K the further investigation was carried out on a set of simplified blade models as shown in Figure 5.1. The aim was to simplify the complex shape of the blade K and to find out the influence of complex geometric shape factors on standard mode shapes before the further study was extended to the

blade K. Each of the seven simplified blade models possesses one feature in the complexities of the blade K. As shown in Figure 5.1 they are:

APL1 uniform rectangular cantilever blade with 5mm thickness,

APL2 cantilever blade tapered across the cross-section with 6mm and 2mm thickness at leading and trailing edge respectively,

APL3 cantilever blade tapered along the length with 8mm and 2mm thickness at the bottom and the top cross-section respectively,

APL4 uniform cantilever blade with added twist along its length with 5mm thickness,

ASH1 uniform cantilever blade cambered across the cross-section with 5mm thickness,

ASH2 cantilever blade cambered and tapered across the cross-section with 6mm and 2mm thickness at leading and trailing edge respectively,

ASH3 cantilever blade cambered across the cross-section and tapered along the length with 8mm and 2mm thickness at the bottom and top cross-section respectively.

They are 91mm long with a block-like root machined from one piece of mild steel and 31mm wide.

A blade holding block as shown in Figure 5.2 was made to hold the blade root. Two bolts in the main block can push the movable jam-blocks and lock the

root of the blades into the mechanism. The blade can be easily replaced when the holding block is clamped on a testing bench.

5.2 Investigation by ESPI and the Separation of Coupled Modes

All the simplified blades and blade K were tested using ESPI. The blade under test was mounted tightly in the holding block which was itself fixed on the vibration isolated testing bench. An electro-magnetic exciter connected to a sine wave generator and amplifying system was used to stimulate the blade via a fine push rod touching on the blade in specific positions. Results obtained are illustrated in Figure 5.3.

5.2.1 Consideration of Excitation Positions

The ESPI experiment was firstly carried out on model blade APL1. It was found that modes of vibration detected by ESPI were sometimes related to the positions of excitation. In order to obtain correct modal parameters, relation between position of excitation and resulted mode shapes was studied.

The relation of symmetry between the load, the structure and the displacement generated was used to justify the selected positions of excitation for different modes of vibration. The relation is explained in Figure 5.4. A simply supported beam is shown in Figure 5.4 (a). The beam is symmetric about axis X-X. The beam deforms symmetrically if it is under symmetrical load as shown in Figure 5.4 (b), whilst skew-symmetric displacement takes place under skew-symmetric load as shown in Figure 5.4 (c).

As shown in Figure 5.5 (a), APL1 is symmetric about plane X-Y and so symmetric load was needed to excite symmetric mode shapes such as flap modes. Therefore, the chosen positions of excitation for flap modes were considered in plane XOY (Figure 5.5 (c)). For skew-symmetric modes such as torsional modes and edge modes, non-symmetric stimulation was required. The positions were chosen off the central OY line (Figure 5.5 (b)).

Using the excitation discussed above, the 1F, 3F and 4F modes were easily identified at 471Hz, 8354Hz and 15984Hz respectively, with the excitation applied along the central axis. These results are presented in the first row of Figure 5.3. The 2T and 3T mode were located at 8925Hz and 15794Hz by placing the push rod at either of the top corners of the model blade.

5.2.2 Separation of Coupled Modes

Difficulty was encountered in the frequency range from 2500Hz to 3500Hz where many mode shapes were found when excitation was applied at various locations. One example of a distorted mode shape at 5032 Hz is illustrated in Figure 5.6.

Mode shapes and natural frequencies are modal parameters determined by physical properties of the structure in question. They do not vary with excitation position. But in the case of two modes being very close to each other, both modes are activated by stimulation near their natural frequencies. The mode shape is the combination of the two modes. The contribution from each mode to the coupled mode shape depends on the frequency and also the position of the excitation. The contribution of the mode nearer to the excitation frequency is more than the other mode whose natural frequency is relatively far away. For the same excitation amplitude, response is much larger if the excitation is applied at an anti-node

position. Theoretically a mode can not be excited if stimulation is placed at nodal positions.

The above understanding suggested that the modes found between 2500Hz and 3500Hz could be the result of the coupling of two modes with closely spaced natural frequencies. It was thought that natural frequencies of the two modes were so close to each other that they both were excited easily at the same time when the excitation frequency was in their range. The distorted mode shapes consisted of the components of the first torsional mode and the second flap mode. The mode shape of the 1T mode, according to the analysis of symmetry, should be a nodal line along the central axis from the tip to the bottom of the blade and the 2F mode shape which is symmetric to the central axis should be two horizontal nodal lines, with one line at the bottom and the other located at about two third of the blade height. The predicted mode shapes of 1T and 2F mode are presented in Figure 5.7 (a) and (b) respectively. Finite element prediction, which will be discussed in the next section, confirmed the above analysis.

Considerable care was exercised to separate coupled modes. It was found that the blade had to be excited at several locations for each natural frequency under investigation. Obviously attempting to excite a mode by stimulating at its node would prove to be pointless but for the situation when two frequencies overlapped, it was possible to stimulate the other frequency by this method. A method of separating the modes was developed in the tests by choosing an excitation point on the nodal line of the mode not required, whilst measuring the vibration amplitude of the other natural frequency.

The first torsional mode was found to be a very strong mode which could not be avoided even when the push rod was placed on the nodal line. However, the 2F mode was identified at 3132Hz by placing the push rod at a location where minimum

amplitude of vibration for 1T mode was achieved and where maximum amplitude for 2F mode took place. These are shown at location L_1 and L_2 in Figure 5.7(b). The 1T mode was recorded at 2865Hz when the excitation was applied on the top nodal line for the 2F mode and at a point off the central axis, shown as L_3 in Figure 5.7 (a). Identified mode shapes are presented in the first two rows in Figure 5.3. The application of this method was necessary for mode identification with APL2 and APL3. The method proved extremely effective for the turbocharger blade illustrated as BLDK in Figure 5.8 and helped to clarify the confusing problems in initial investigation.

In the tests on simplified blades it was found that coupled modes, particularly where natural frequencies were close to each other, were very easily excited. Nodal lines were shifted at frequencies both below and above the two very close modes. This explained why the results in Figure 4.3(d) indicated a range of frequencies around 4400 to 5600Hz for the initial tests on the blade K. The detected frequencies were in fact the frequencies of coupled modes which occurred with one frequency just below the 1T mode of 4510Hz and the other frequency just above the 2F mode of 4594Hz (Figure 5.3, BLDK by ESPI). This is a classic phenomenon illustrated effectively in the paper by Grinsted [68].

5.2.3 Theoretical Consideration of Coupled Mode Vibrations

As coupled mode vibrations are very often found in this study, further consideration on the vibration of coupled modes was given in order to establish better understanding. Coupling is the term used in mechanical vibration to indicate a connection between equations of motion. Coupled mode shapes may occur when selected coordinates are coupled due to dynamic and/or static coupling.

Coupling is related to the coodinates used in the equations of motion. If

principal coordinates are used, at the natural frequencies, the equations of motion are completely separate. Each principal mode corresponds to one natural frequency or eigenvalue of the frequency equation. There are the same number of principal coordinates as there are equations of motion and principal modes, so each equation of motion is separate from every other. Only one coordinate, or any of its derivatives, with respect to time appear in each equation of motion.

It is necessary to remember that a set of principal coordinates exist for every linear vibration system, but they may defy our geometric interpretation. It is possible to decouple any set of equations of motion by using principal coordinates. However, it is often preferable to use a coupled system with coordinates that can be visualized than a decoupled system with principal coordinates that cannot. The uni-directional sensitivity of the ESPI technique and the classification of mode shapes of blades in Section 3.5 determine that the mode shapes presented are in the Cartesian coordinate system. As this system may not be the decoupled system for all modes of the blade vibration, some modes may be coupled. The selection of coordinates has no effect on eigenvalues or mode shapes.

The 'compounded' mode shapes also occur in the system with two or more equal natural frequencies. Because they are not generated by dynamic/static coupling, the word 'coupled' is not the most appropriate. However, in terms of the mode shapes, they are still the combination of two (or more) normal mode shapes. For simplicity, the term 'coupled mode' is still used in this thesis.

One example is provided by a particle which is constrained to move in a plane and is controlled by two light springs which lie in the plane and are mutually perpendicular, as shown in Fig. 5.10(a). If the excitation force $F = F_0 \sin\Omega t$ is applied to the particle at an angle θ as shown, the equations of motion of the particle are

$$m\ddot{x}+k_1 x=F_0\cos\theta\sin\Omega t$$
$$m\ddot{y}+k_2 y=F_0\sin\theta\sin\Omega t$$

(5.1)

If the spring stiffness k_1 and k_2 are different, then the system has two natural frequencies, $\omega_1 = \sqrt{(k_1/m)}$ and $\omega_2 = \sqrt{(k_2/m)}$, the corresponding principal modes being motions along the axes of the two springs. The particular solutions to equation (5.1) are a steady-state oscillation of the same frequency Ω as that of the excitation. They can be assumed to be of the form

$$x=A_1\sin(\Omega t+\phi_1), \qquad y=A_2\sin(\Omega t+\phi_2)$$

(5.2)

where A_1 and A_2 are the amplitude of oscillation of the particle in ox and oy direction respectively and ϕ_1 and ϕ_2 are the phase of the displacements with respect to the exciting force.

The amplitude and phase in equation (5.2) are found by substituting the equation into the differential equation (5.1). The amplitudes in ox and oy directions are

$$A_1=\frac{F_0\cos\theta}{k_1-m\Omega^2}, \qquad A_2=\frac{F_0\sin\theta}{k_2-m\Omega^2}$$

(5.3)

These equations can be further expressed as

$$\frac{A_1}{F_0}=\frac{\cos\theta/k_1}{1-(\Omega/\omega_1)^2}, \qquad \frac{A_2}{F_0}=\frac{\sin\theta/k_2}{1-(\Omega/\omega_2)^2}$$

(5.4)

The phase angles are not given as they are not the major concern of this discussion.

The equations (5.4) reveal that the response amplitudes in x and y directions are functions of the angle θ. If the excitation F(t) is applied only in x direction as shown in Figure 5.10(b), $\theta = 0$, thus $\sin\theta = 0$, therefore A_2/F_0 is always zero. The response will only be in x direction. Similarly, if F(t) is applied in y direction, the response in x direction will be zero. The response amplitudes are also functions of the frequency ratio Ω/ω_i, $i = 1, 2$. When $\cos\theta$ and $\sin\theta$ are not zero, the resonant responses can be found at $\Omega = \omega_1$ or $\Omega = \omega_2$. However, the resonant response in x or y direction will not occur if the excitation is not applied in that direction. This relation provides the possibility of identifying the mode shapes of the modes with closely spaced natural frequencies.

If $k_1 = k_2$, equal roots are found in the characteristic equation, the corresponding eigenvectors are not unique and a linear combination of such eigenvectors may also satisfy the equations of motion. This means that any straight line motion of the particle in the xoy plane becomes possible and may be regarded as a principal mode. As any motion not in line with ox and oy axes is the combination of the simultaneous motions in ox and oy directions, their mode shapes appear as coupled modes.

If the natural frequencies of the two modes are closely spaced, i.e. $k_1 \approx k_2$, the excitation shown in Figure 5.10(a) will result in two coupled modes at $\Omega = \omega_1$ and $\Omega = \omega_2$ due to the resonant response of both modes. The contribution from each mode to coupled mode shapes depends on the frequency ratio Ω/ω_i (i = 1, 2) and the direction of excitation θ. If the direction of the excitation is changed, the resonant responses of the two coupled modes will change.

This explains some confusing results obtained in ESPI tests given in Section 4.3. When the natural frequencies of two modes are close to each other, the resonant responses found are two coupled modes. In addition, more than two resonances of

coupled modes were often detected if the position of excitation was moved around. (see Fig. 4.3(d) between 4500 Hz and 5300 Hz). This is because the contribution to the resonant response of the coupled modes from each constituent mode is related to the position of excitation.

5.3 Finite Element Models of Simplified Model Blades and the Blade K

A full finite element analysis was conducted on all the blades. All the simplified blades were constrained as cantilevers. They all were modelled by three-dimensional 20 node brick elements, using different meshes. A 1x6x15 mesh was used for APL1 and APL2. A 1x6x10 mesh was used for APL3, APL4, ASH1, ASH2 and ASH3. The number of elements used in BLDK was reduced from 120 to 90. Different coordinate systems were used in mesh forming. ASH1 and ASH3 were built with cylindrical coordinate while the others were formed with cartesian coordinate. The results of the analysis (associated with ESPI results.) are shown in Figure 5.3.

5.3.1 F.E. Mode Shape Identification Using PIGS.

Viewing the mode shapes and interpreting the modes was enhanced by use of an interactive graphics package (PIGS). PIGS is designed to work with PAFEC F.E. package for both pre-processing and post-processing. In mode identification of F.E. models of simplified blades, the backing store file created by computing was firstly retrieved by PIGS and then was processed for further analysis. The mesh of the F.E. model of a blade and deformed structure of the blade for any mode specified can be displayed on the screen. The viewing angle can be selected in any direction.

Mode shapes of simplified blades were easily identified and they are illustrated in Figure 5.3.

The 1F, 1T and 2F modes of BLDK were identified at 1290Hz, 4710Hz and 5810Hz respectively. But it was difficult to identify specific mode shapes for BLDK particularly the 2T and 3F modes as bending, edgewise and torsional displacements were coupled such that there was no single viewing angle available from which the real mode shape could be identified. An example of the possible display is shown in Figure 5.11(a). A better understanding of the fully deformed shape was obtained by taking sections at several height locations of the blade. Viewing them from the top, superimposing the deformation of the section for the frequency under investigation, rotating the sections into appropriate viewing angles so that nodal points on sections could be identified and then drawing nodal lines along nodal points. This time consuming technique is illustrated in Figure 5.11 (b) and (c), which proved extremely useful in interpreting mode shapes of turbocharger blades from F.E. analysis. The 2T and 3F modes were then identified at 10800Hz and 9030Hz respectively.

5.4 Summary of Results

A summary of results of mode shapes and natural frequencies of simple blades and blade K is shown in Figures 5.3 and 5.12. Results for different blades for APL1 to ASH3 are shown in different rows in Figure 5.3 and results for blade K are illustrated in the bottom row. Different modes can be found in different columns and the value of natural frequencies are located just below the diagrams of associated mode shapes. Results for the same blades by different analysis methods are grouped together. The uniform cantilever was used to set up the reference standard for modal patterns using the conventional flap mode(F), edge mode(E), Torsional mode(T) and

spanwise mode(S) designations.

5.4.1 Effects of the Complex Profile

Good agreement of mode shapes and natural frequencies of simplified blades between results of ESPI and F.E. analysis was found. The influence of the change of geometry on mode shapes has been identified. The presence of taper across the cross-sectional area is clearly seen to skew the nodal lines in mode shapes of APL2.

For the 1T mode, the skewed nodal line starts from the middle of the tip and ends at the right hand bottom corner of the blade since the leading edge (right hand) is thicker than the trailing edge. The higher location of the top nodal line of the 2F mode on the leading edge confirms the larger stiffness on this side of the blade.

The distortion of the 2T and the 3F mode shapes of APL2 proves to be the key references for identifying the same modes of blade K. The taper from root to tip in the APL3 blade forces the nodal line towards the tip in flap modes. The twisted uniform cantilever APL4 demonstrates the ability of the twist to raise the natural frequency without substantially affecting the shape of the modal pattern. However it is possible that different degrees of twist could alter adjacent natural frequencies so that combination frequencies occur. This phenomenon was originally reported by MacBain [105] (1975) and has recently been quantified by MacBain J. et al [108] (1985). Similar conclusions can be obtained from the results for the tapered shell elements which also highlight the distortion of the modal patterns with geometry change of the blade.

Of particular interest are the results associated with the 2T and 3F modes as these have close natural frequencies in most of the models and the frequencies do not necessarily occur in the same sequence for all blades. For example, the natural

114

frequencies of the 2T mode of APL1 and APL4 are higher than those for the 3F mode, whilst in the rest of the cases they are lower.

The natural frequencies and mode shapes of blade K were identified. Eight mode shapes obtained using ESPI are illustrated in the row under BLDK in Figure 5.8. This is essential in order that the correct location of blade lacing wire can be specified. For the convenience of reference, identified modes of free standing blade K is also drawn in Figure 5.12. One frequency detected for blade K at 2394 Hz and predicted by finite element analysis at 2960 Hz caused considerable difficulty in interpretation as the ESPI investigations identified a clear nodal line (shown as 1E mode at 2394 Hz in Figure 5.12) of a similar form that could be expected for the 2F mode whilst the finite element analysis failed to identify this nodal line.

Initial attempts to view this mode by considering the finite element analysis predicted deformed shapes in which discrete points in the section appeared to have zero deflection and therefore suggested the possibility of a node. However by increasing the amplitude allowable for deflections in the finite element investigation it was shown that the nodal point appeared to shift. In reality no node existed as the intersection of the deformed and un-deformed components of the vibration analysis was not comparing the absolute motion of identical points. The detection of this false mode was a function of the angle chosen to view the section.

This error also occurs with the use of ESPI investigations. As explained in section 3.3.1, ESPI technique used in this study was only able to monitor out-of-plane motion. For a curved surface of blade K, ESPI could give false presentation of motion as illustrated in Figure 5.13. If the blade is vibrating in edgewise mode in plane x-x, ESPI will detect displacement *ab* due to the curvature of the surface. In truth the displacement *ab* suggested by the ESPI investigation is non-existent as the laser with its uni-directional view cannot distinguish between

115

different points of the viewed object.

5.5 Further Consideration into the Interpretation of Modal Analysis Results

In modal analysis, an accelerometer can only detect motion in its sensitivity direction and it was attached with its axis of sensitivity X-X perpendicular to the surface of blade K, as shown in Figure 5.14. The normal vector of the surface varies at different locations on the blade due to the complexity of its shape. As a consequence, the sensitivity of the sensor to the same mode shape is also location dependent. Figure 5.14 shows the top cross-section of blade K which is moving edgewise. The accelerometer at location (a) can detect component *oa* of acceleration *ob*, whilst at location (b), it can sense no acceleration as its axis of sensitivity in x-x direction is normal to *ob*. Therefore, this edgewise mode of vibration could be mis-interpreted as flapwise mode.

Based on the work reported above, a paper was presented at the 1987 ASME International Vibrations Conference in Boston, USA. It was also published in the Journal of Vibrations, Acoustics, Stress and Reliability in Design. Jan, 1988 [33].

5.6 The Improvement of the F.E. Model of the Blade K

Though good agreement on mode identification for simplified blade models from both experimental and theoretical approaches was found and the vibration modes of the blade K were identified, discrepancies between the natural frequencies for the blade K obtained by ESPI tests and F.E. analysis were still considerable. For instance, the F.E. calculated natural frequency is 24% higher than that obtained by ESPI test for the 1E mode, 26% higher for the 2F mode, 10% higher for the 2T

mode and 25% higher for the 3F mode. This large disagreement suggested that further study should be carried out to improve the finite element model of the blade K. Also the computing time for BLDK was 100 minutes in CPU time which was equivalent to 9 hours computer run time in practice for one calculation. This long computing time had to be shortened in order that a multi-blade model could be calculated in a reasonable time.

5.6.1 Number of Elements

There are 90 Elements used in BLDK model as shown in Figure 5.11 (a). Using a large number of elements ensured the accuracy of the initial modelling. But to reduce the computing time it was considered necessary to establish the minimum number of elements with a reasonable accuracy.

It was found that for the three dimensional elements available in the PAFEC package, the biggest ratio of the longest side to the shortest side should be kept within 15:1. This limitation conditions the minimum number of elements required to faithfully model the blade K. The thickness of the trailing edge of the blade is very thin hence the shortest side of the element is about 1mm long. This gives 15mm as the length of the longest side. The height of the blade is 91mm. Therefore the blade at least has to be divided into about 7 portions. In the width direction the cross-sections are divided into 3 parts to ensure a reasonable geometric representation for the modelled blade. Thus overall 21 elements were used to model the blade K. The new models are named under ASP as a prefix followed by a number. The mesh of ASP4 is illustrated in Figure 5.15 and the results for the natural frequencies are given in Table 5.1. Considerable time saving was achieved with ASP4, reducing the CPU time to 17 minutes.

5.6.2 Type of Elements

The complex geometry of the blade K creates considerable difficulty in finding a proper type of element which is able to describe the motion of the blade. Two segments from the tip and the bottom of the blade K are plotted in Figure 5.16 which reveal that though it could be treated as a two dimensional problem at the upper part of the blade, the thickness at the lower part of the blade should not be neglected. The 3D element (37110 type) used in previous models is able to process both 3D and 2D analysis but is very time consuming and expensive. Therefore other types of elements were considered and tested to improve the model of the blade K.

Shell elements were considered as the best alternative. Curved eight node thick shell element (46210 and 46110 types) and three node flat facet shell element (41320 type) were tried. 41320 elements are basically designed for thin shell applications. They were used in conjunction with other shell elements to model the upper part of the blade. It was found that it was difficult to model cambered cross-sections by flat elements unless a large number of elements was used, which was in conflict with the idea of reducing the computing time. 46210 elements can be used in generally curved shell problems for the intermediate range between full three dimensional and thin shell behaviour. They are generally curved thick shell elements with four corner nodes and four midside nodes defining the middle surface of the shell. 46110 elements are similar but with a triangular shape. It was found that the mesh generating module in PAFEC was not compatible with the 46210 type of elements, which meant that the mesh had to be generated manually. The results of modelling using 46210 elements were far less satisfactory. Considering the great amount of work to be done manually for each improvement on the shell model of blade K and the poor accuracy of the modelling, the following study was carried out using 3D elements.

118

Currently the 3D element (37110) used is a generally shaped brick type with six curvilinear faces and twelve edges. There are eight corner nodes and one midside node on each of the edges, giving twenty nodes in all. The element is easy to use as it can be built into the mesh generating module in the PAFEC data preparation program. Once the mesh for the blade K was constructed, other 3D elements could also be used since coordinates of all nodes had been generated by PAFEC.

One of the elements considered was an eight node 37100 type with six faces and twelve straight sides, which belonged to the same family of 37110 elements. A model called A8NK2 was created using 40 elements. The natural frequency results calculated are listed in Table 5.1. Comparing A8NK2 results with those obtained

MODE (Hz)	1F	1E	1T	2F	CPU(min)
ESPI	1255	2392	4510	4994	
BLDK	1290	2960	4710	5610	138
ASP4	1360	3080	4780	5920	17
A8NK2	1771	3429	4891	8051	7
ASPRT12	1226	2482	4643	4984	11.5

Table 5.1   Natural frequencies calculated by different FE models and the CPU times used

from the model ASP4, it can be seen that though the CPU time of A8NK2 was only about 7 minutes, which is about 10 minutes shorter, natural frequencies were much higher. This implied that using more elements with few nodes in each element gave a poorer model than using less elements with more nodes in each element.

Another approach employed the use of 16 node 37130 elements which have

119

two opposite faces with a midside node on all four edges but there are no midside nodes in the third direction. This element is useful when the stresses vary less in one of the directions than the other two, which is the case with the blade K as it is thin in depth and consequently there is less stress variation in this direction. Great effort was made to work out coordinates of nodes from the output file of ASP4 model in order to generate the mesh composed of 37130 elements manually, as the PAFBLOCK module would not work with this type of element. The application of 37130 elements was proved to be successful in a new F.E. model which will be discussed in the next section.

5.6.3 Modelling of the Root of Blade K

Along with the investigation into the number and types of elements which could be used to build up the F.E. model of the blade K, the study was also extended to find out the importance of modelling the fir-tree root.

Blade K and simplified blade models have been modelled as cantilever blades vibrating in flexure and torsion. Afolabi pointed out, in his study [4] in 1986, that in such treatments, the influence of root flexibility on natural frequencies and mode shapes of vibration is ignored. In practice, however, the flexibility at the root of a blade is not always negligible, especially in bladed disk assemblies with complex fixtures like fir-tree or pin-joint roots.

Effects of root flexibility on the vibration of isolated cantilevered systems have been investigated in several studies. MacBain and Genin [106] has shown in their studies that natural frequencies are lowered with the inclusion of root flexibility. In practice, unless exceptionally good clamping is enforced, the measured resonant frequencies are lower than the actual cantilever frequencies to an extent which depends on the prevailing flexibility at the clamped root.

120

The blade K is mounted into the holding block at its fir-tree root and vertical forces are applied upwards by two bolts acting beneath the root creating a tight interface, similar to the conditions experienced during operation. However, the measured resonant frequencies by ESPI on the testing bench were the experimentally determined frequencies for the system under the test, whilst previous F.E. models predicted only cantilevered natural frequencies with no allowance for blade root mounting. Simple analysis indicated that the interface between the slot of the block holding the blade and the root of the blade takes place within the root teeth and the resultant of the restraint may well occur below the platform between the blade and the root as shown in Figure 5.17. This suggested that the previous models might have missed out a very important factor in the modelling.

Several approaches were exercised using different type of elements and different numbers of elements to model the root. The names of the new models with fir-tree root began with ASPRT followed by a number. Three 8-node 37100 elements were firstly used to build up the root of ASPRT9 which was composed of 21 16-node 37130 elements. Then the number of elements for the root increased to five in ASPRT8. Finally using one 24-node 37140 element, which is a further extension of 37130 having two midside nodes instead of one, for the root was tested in ASPRT12. The best results, in terms of natural frequencies being close to experimental values and short CPU time, were achieved by model ASPRT12. The identified mode shapes and natural frequencies are given in Table 5.1. The mesh of ASPRT12 is illustrated in Figure 5.18.

5.6.4 Material Properties of Elements

PAFEC F.E package automatically provides a number of material properties in SI units. Further materials can be added for local usage. If a material provided is required then the material number should be given in the appropriate module.

Some of the standard material properties are listed in Table 5.2. The material properties used in modelling simplified blades and blade K was taken from material number 1 for mild steel.

Common Name of Material	Mat. Num.	Young's Modulus E Nm⁻²	Poisson's Ratio NU -	Mass Density RO kg m⁻³	Coefficient of Thermal Expansion ALPHA °C⁻¹	Hysteretic Damping MU -
Mild Steel	1	209E9	0.3	7800	11E-6	.005
Stainless Steel	2	195E9	0.3	7700	12E-6	.005
Cast Iron	3	125E9	0.25	7100	12E-6	.005
Aluminium	4	68.5E9	0.33	2695	24E-6	.01
Aluminium Alloy	5	70E9	0.33	2800	22E-6	.01
Aluminium Alloy	6	75E9	0.33	3000	20E-6	.01
Titanium	7	110E9	0.3	4533	8.5E-6	.005

Table 5.2   Standard material properties included in the pafec scheme.

5.7 Conclusion

The understanding of vibration characteristics of blade K has been established in this chapter. The fundamental modes of vibration have been identified as 1F, 1E, 1T, 2F, 2T and 3F.

The effects of taper and pretwist on mode shapes have been shown by studying the mode shapes of simplified model blades, which model the geometric

features of blade K. This study has provided the fundamental understanding in the vibration of free standing turbine blades.

One effect of changing the geometry of a blade is that different modes of vibration can be placed very close in frequency domain. The study has revealed that two coupled modes occur outside of the frequency band between the two closely spaced natural frequencies alone, while the latter disappear. An experimental technique of mode separation has been developed and successfully applied to simplified blades and blade K.

The study has shown that both modal testing and ESPI techniques are polarized in detecting displacements. They may see vibration motion in one direction while the blade is moving in the other due to the pretwist of the blade. Thus thorough understanding of the techniques used is required for correct interpretations.

Finite Element model of blade K was justified and simplified. With the better understanding of experimental techniques and justified F.E. models of simplified blades and blade K, the investigation began to study vibration characteristics of blade K with a lacing wire.
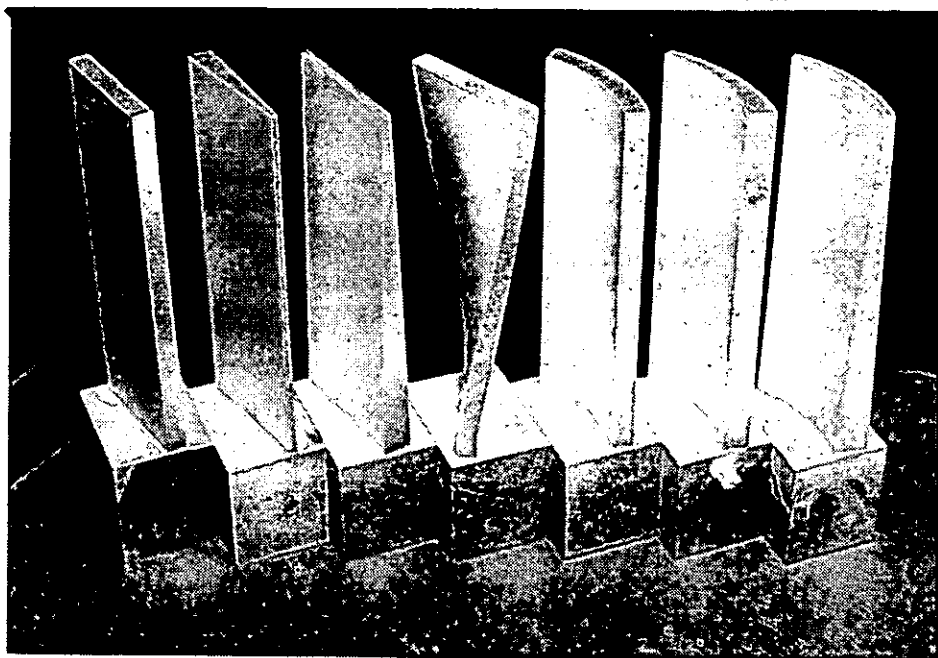
Figure 5.1   Simplified blades with different geometry features
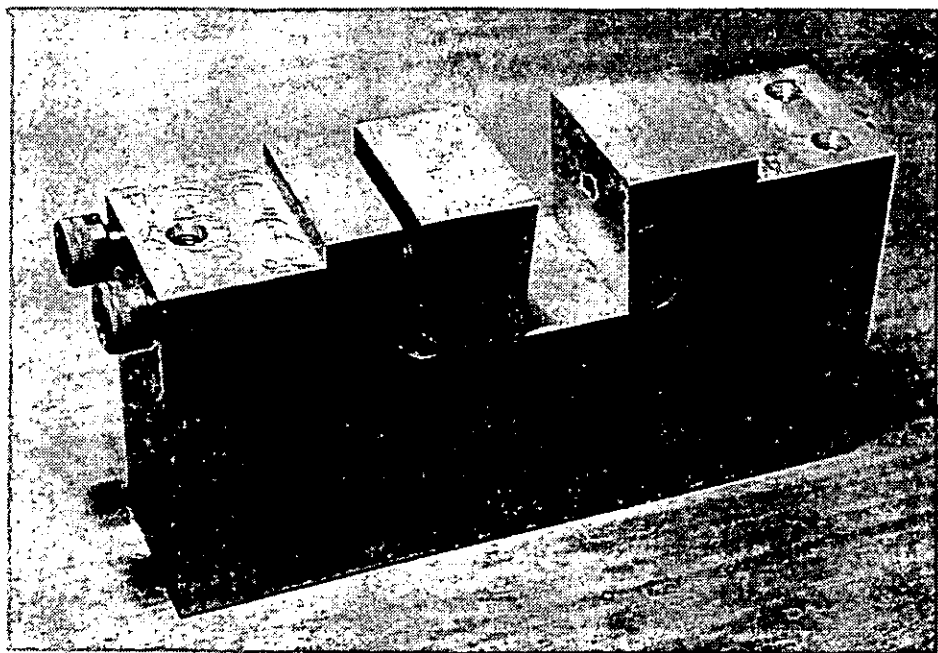
Figure 5.2   The holding block and wedges

125

	1F		1T		1E		2F		2T		3F		2E		1S		3T		4F		#	
	F.E.	Laser	F.E.	Laser	F.E.	Laser	F.E.	Laser	F.E.	Laser	F.E.	Laser	F.E.	Laser	F.E.	Laser	F.E.	Laser	F.E.	Laser	F.E.	Laser
APL1	504	471	2820	2865	2930		3120	3132	8900	8925	8740	8354	14200		15600		16300	15794	17300	15984		
APL2	449	400	2330	2290	2970		2800	2843	7830	7440	6750	6321	10100		15800		12300	11314	13900	12488		
APL3	952	1070	3600	3684	4400		3670	3714	7910	7762	8780	8570	16200		20300		14000	13481	16800		15400	15300
APL4	503	480	2920	2904	2100		4559	3604	9037	8918	7796	7306	15713		15436		16216	15464	17177	15060	24554	
ASH1	620	552	2590	2830	3190		3720	3547	8520	8439	9970	9313	14200		15400		15700	15348	19000		24500	
ASH2	580	500	2270	2577	3090		3440	3535	6990	7204	8840	8710	14200		15400		12500	12544	15100	14935		
ASH3	1090	1172	3540	3890	4480		4470	4677	8010	8490	10500	10000	16400				14400	14552	19200		15800	16809
BLDK	1290	1255	4710	4510	2960	2392	5610	4708	10800	9824	9030	7746					17200	15400	14200	11968		

Figure 5.3 Mode shapes obtained for blades
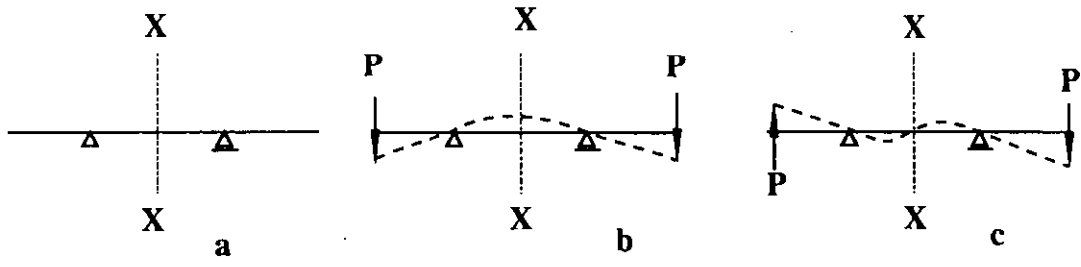
Figure 5.4 Displacement of symmetric structure under symmetric
and skew-symmetric loading
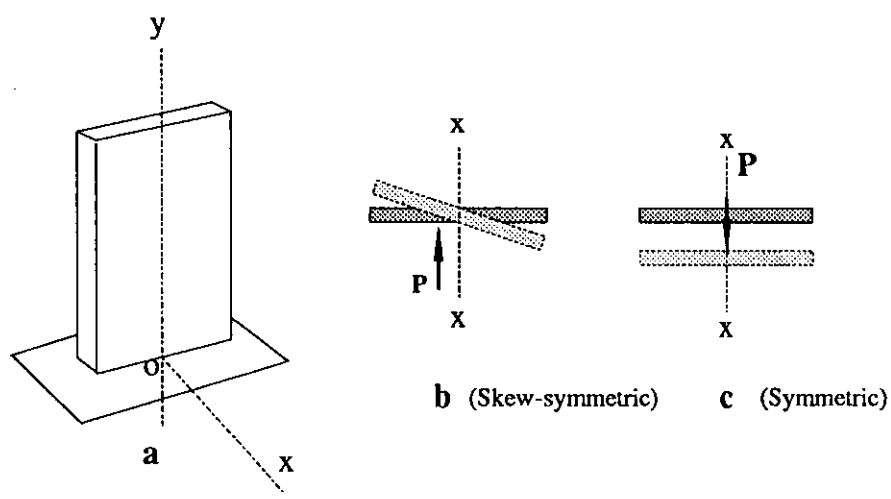
Figure 5.5   Model blade APL1 and its symmetric and skew-symmetric
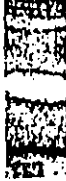displacement about X-Y plane under different loading.
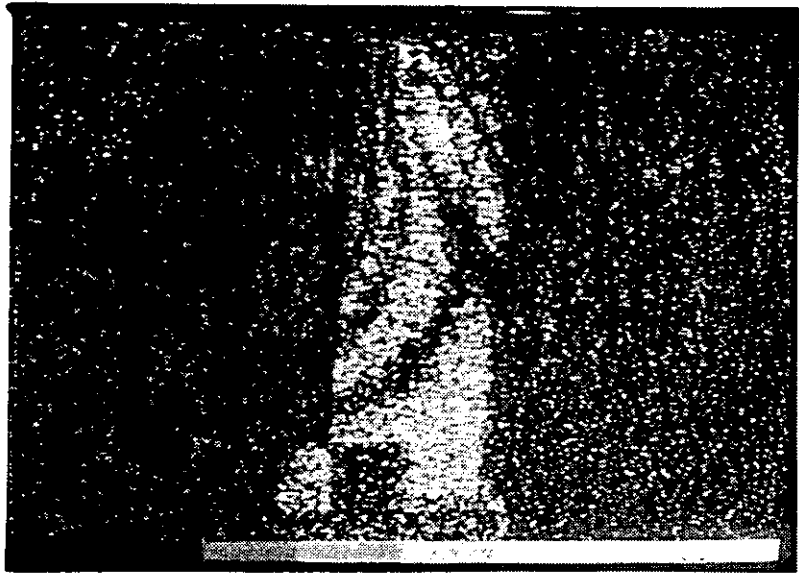
Figure 5.6 Unidentified mode shape
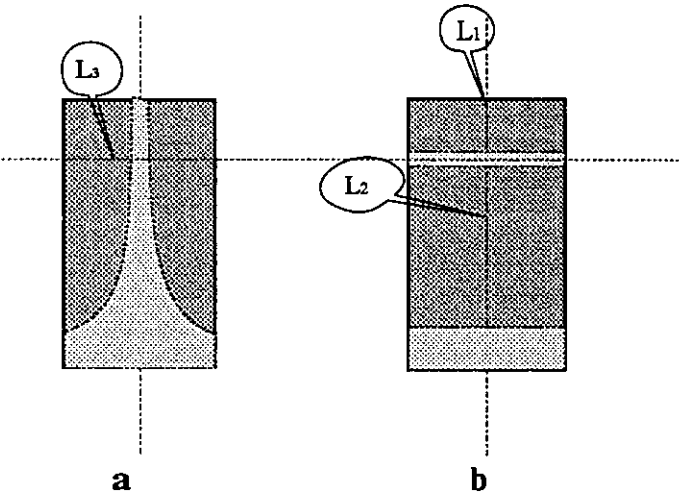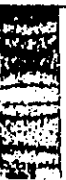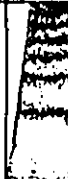
Figure 5.7 Predicted mode shapes of (a) 1T mode at 2865 Hz and
(b) 2F mode at 3132 Hz and excitation locations L1, L2 and L3

APLI	IF 497	IT 2873	2F 3039	3F 8354	2T 8925	3T 15820	4F 15984
BLDK	IF 1232	IE 2394 / IT 4503	2F 4708	3F 7248	2T 9824	3T 15400	4F 11968
2T MODE	APLI 8925	APL2 6321	APL4 8834	ASHI 8569	ASH2 7142	ASH3 8506	BLDK 9824
3F MODE	APLI 8354	APL2 7498	APL4 7396	ASHI 9225	ASH2 8692	ASH3 9916	BLDK 7248

Figure 5.8   Classification of modes
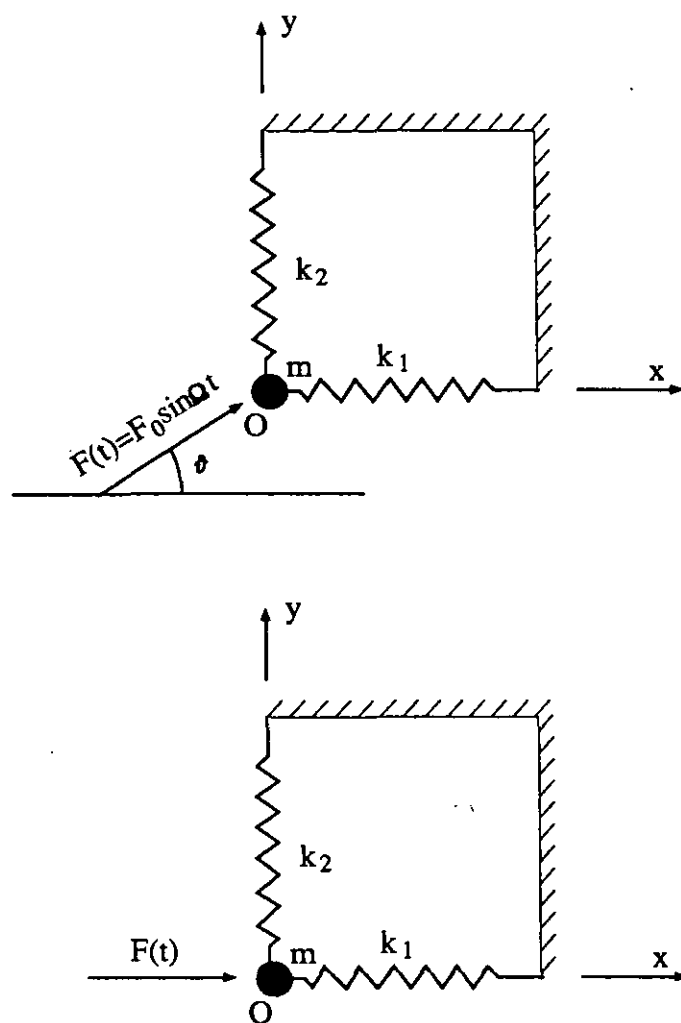
Figure 5.10 A system with two equal natural frequencies

a	**b**	**c**
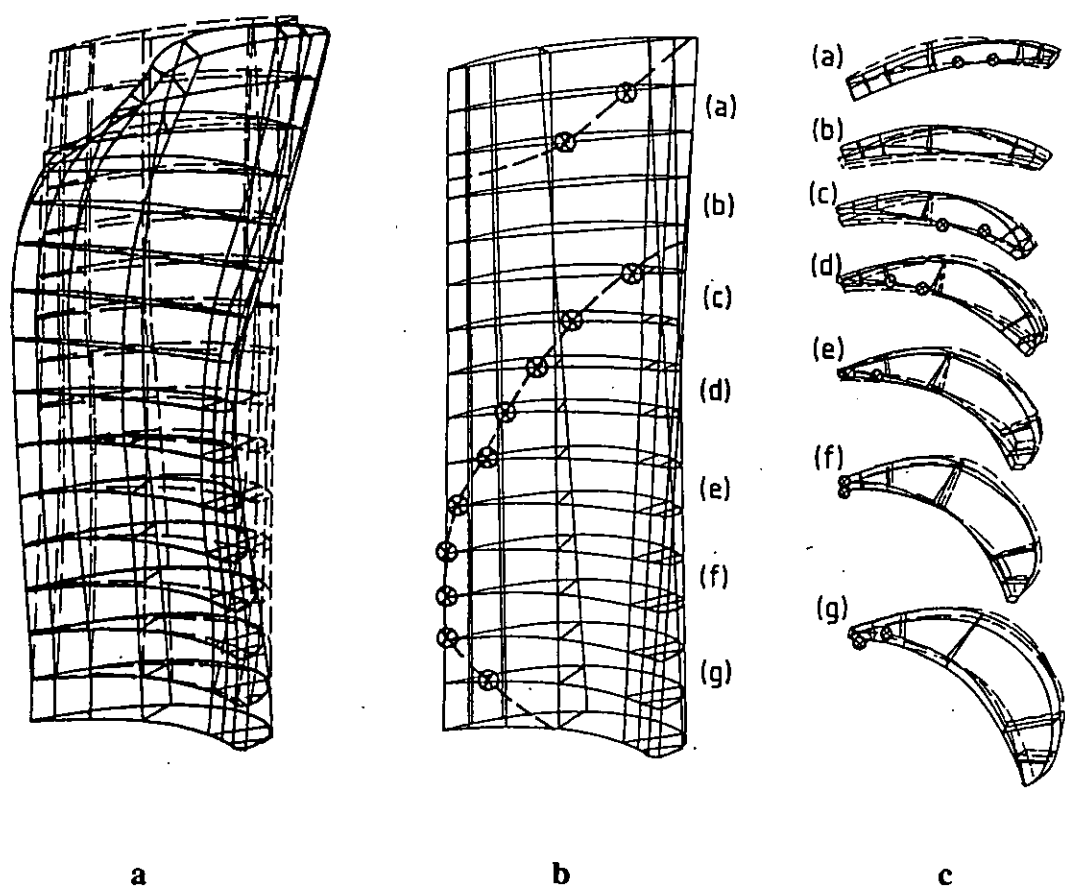
Figure 5.11   Interpretation of finite element analysis predicted mode shape for blade K at 9030 Hz 3F mode
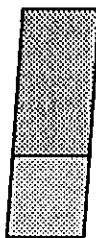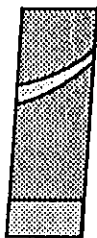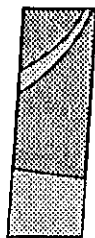
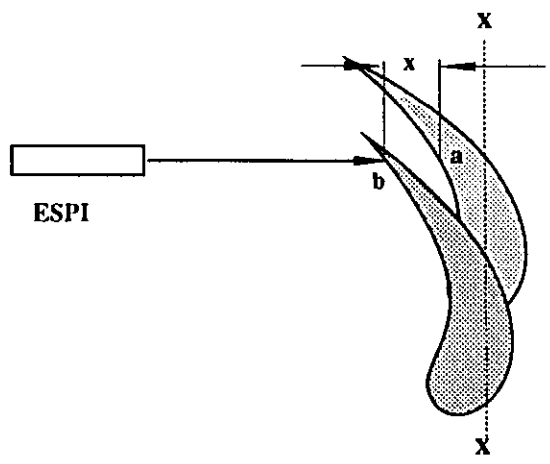| MODE	1F	1E	1T	2F	
ESPI	1232	2394	4503	4708	Hz
FE	1290	2960	4710	5610	Hz
MODE	3F	2T	3T	4F	
ESPI	7248	9824	15400	11968	Hz
FE	9030	10800	17200	14200	Hz

Figure 5.12 Natural frequencies (Hz) and mode shapes of free-standing blade K
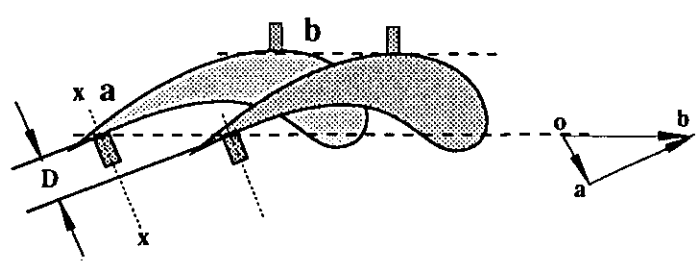
Figure 5.13 Uni-directional view by ESPI

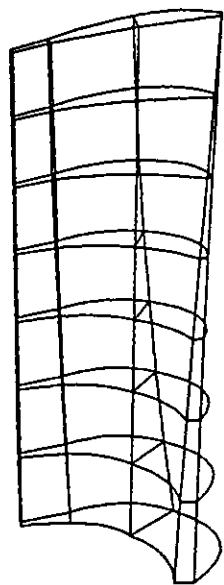Figure 5.14 Uni-directional sensitivity of accelerometers

Figure 5.15 F.E. model ASP4 of blade K
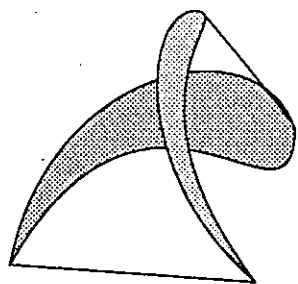

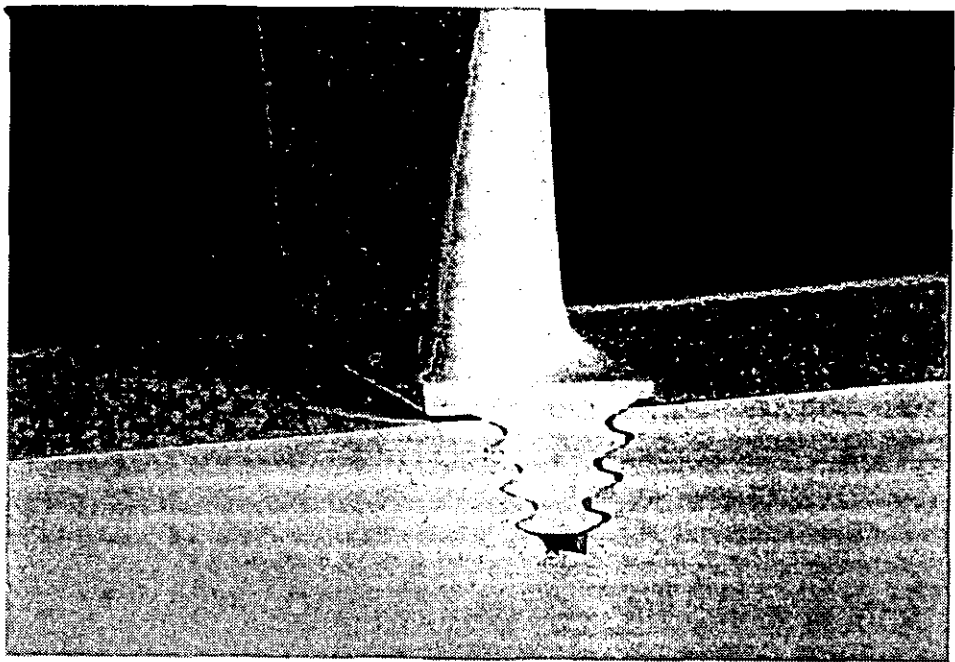Figure 5.16 Top and bottom cross-sections of blade K

135

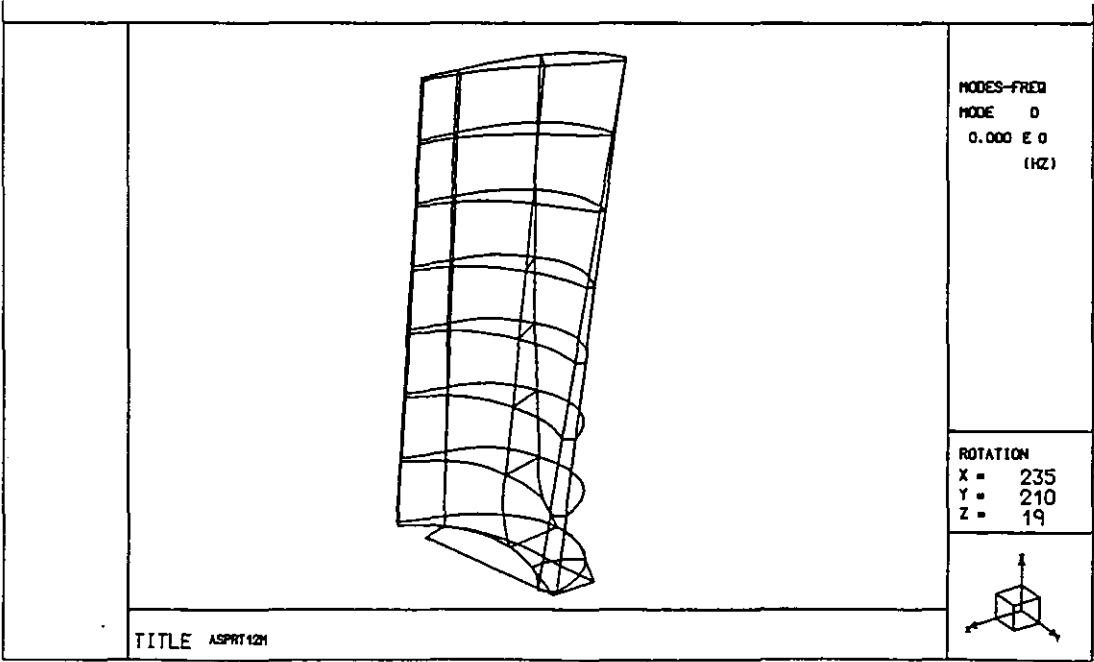Figure 5.17   The fir-tree root of blade K

Figure 5.18   FE model ASPRT12 of blade K with root

Chapter 6

Investigation into Single Blades with Lacing Wires

6.1   Introduction

6.2   Design of Simplified Blades with a Lacing Wire Hole

6.3   Design of the Lacing Wire Loading Rig

6.4   The Initial ESPI Test

6.5   FE Modelling of Simplified Blades with a Lacing Wire

6.5.1· Fundamental Assumptions

6.5.2   Calculation of Spring Stiffness

6.5.2.1 Longitudinal Stiffness

6.5.2.2 Lateral Stiffness

6.5.2.3 Torsional Stiffness

6.5.3   FE Modelling Criteria

6.5.3.1 Number of Elements

6.5.3.2 Spring Locations

6.5.3.3 Spring Stiffness Used in the Initial Models

6.5.4   Initial Results and the FE Model Improvement

6.5.4.1 Initial Results

6.5.4.2 Discussion of Initial Results of ESPI Tests and FE Modelling

6.5.4.3 Improvement of FE Models

6.5.4.4 Improvement of Lacing Wire Locking Mechanism

6.6   Further Results and Discussion

6.6.1   Coupled Modes introduced by the Lacing Wire

6.6.2   Excitation from the Side of the Blade

6.6.3   Identification of Mode Shapes

6.6.3.1 Definition of the Flap Mode Shapes

6.6.3.2 Identification of Mode Shapes

6.6.4   Effects of the Lacing Wire on Single Blade Vibration

6.6.4.1 Effects of the Lacing Wire Location on Flap Modes

6.6.4.2 Effects of the Lacing Wire Stiffness on Flap Modes

6.7   Investigation into Blade K with a Lacing Wire

6.7.1   First ESPI Test on the Blade K with the Lacing Wire

6.7.2   FE Model of the Blade K with the Lacing Wire

6.7.3   Second ESPI Test on the Blade K and the Summary of Results

6.8   Conclusion

Figures

6.1 Introduction

Having considered the vibration characteristics of a free standing single turbocharger blade, the next step was to investigate the effects of lacing wires on the blade. The study was carried out by using ESPI and FE modelling. With the experiences of studying a single turbocharger blade, the investigation started again from simplified blades, then moved onto the blade K.

6.2 Design of Simplified Blades with a Lacing Wire Hole

The design criteria of simplified blades were similar to those of blade APL1 model. The blade was straight cross-section, 92mm high, 31mm wide and 5mm thick. The root block was 30mm high and 34mm wide. The thickness was 20mm at the top platform of the root block and 24mm at the bottom section. The taper in depth was considered to give better clamping at the root block. The blade and the root block were machined out of one piece of mild steel. A hole of 3.3mm in diameter was designed on the central line of the blade at different heights as illustrated in Figure 6.1. The dimension of the lacing wire was 3.1 mm. To allow sliding between the wire and the hole, the dimension of the hole was a little bigger than that of the wire. The distance of the holes from blade root platform and names of simplified blades are indicated in Figure 6.2. The lacing wire was located at 31.4% (APL16), 35.6% (APL15), 50% (APL14), 68.9% (APL13), 83.7% (APL11) and at 94.6% (APL12) of blade height from its bottom.

A setting angle of 12 degrees was designed to simulate the setting angle at the root of blade K. Blade K is pretwisted with a 12 degree setting angle at the root and 55 degrees at the top section. At the section where the lacing wire goes through,

it is approximately 50 degrees.

The investigation into simplified blades with a lacing wire was to establish basic understanding of the effects of lacing wires on vibration mode shapes and frequencies on fairly simple models so that the knowledge could be used to analyse turbocharger blades of complex geometric shape. It was not necessary at this stage to introduce a large setting angle into the system. On the contrary, a large setting angle would cause experimental difficulties since a viewing angle had to be available for ESPI tests, which will be explained in detail in Section 6.3.

6.3 Design of the Lacing Wire Loading Rig

To carry out experimental investigations into the vibration of blades with a lacing wire, the following basic conditions have to be satisfied: a) the wire going through the blade under test has to be fixed at two ends relative to the testing bench so that no displacements occur when the blade is in vibration, b) simulated centrifugal force has to be applied to the blade via the wire.

A wire loading rig, as illustrated in Figure 6.3, was designed to meet the above requirements. The rig is composed of two frames, top and bottom frames. The top frame , where the wire is locked in, can slide vertically with its freedom in the horizontal plane being restrained by the bottom frame. Consequently, the wire can not move as a rigid beam in the horizontal plane but is free to move vertically. When a blade in the holding block is loaded in the rig as shown in Figure 6.4, vertical displacement of the top frame is restricted by the wire which passes through the blade being firmly clamped on the testing bench. A pulling force of 700 Newton was applied via a pulley system illustrated in Figure 6.5 to the top frame, and its upwards displacement transferred the force to the blade via the lacing wire with

tension and shear forces to simulate the centrifugal force occurred in the rotating lacing wire.

The interested running speed of a bladed disk where the blades and the lacing wires are employed is 18000 rpm. The centrifugal force resulting from this speed is 1400 Newtons. As the capacity of the pulley system was limited and also it was proved that it was not necessary to apply a full load to lock the wire into the blading, i.e. no slippage between the wire and the hole in the blade, 700N was chosen to be used in this study.

6.4 The Initial ESPI Tests

The experimental rig with simplified blades was set up in front of the VIDISPEC on the bench. An electro-magnetic exciter was employed to excite the blade as in previous ESPI tests as shown in Figure 6.6. Blades were excited at different locations on the rear face by a fine push rod connected to the exciter. Tests were carried out on each simplified blade from APL11 to APL16.

In the test for each specific blade, the blade held in the holding block was put between top and bottom frame and clamped down firmly onto the bench, then a lacing wire was threaded through the hole on the blade and was locked into the top frame by screws as shown in Figure 6.7(a). 700N weights were gradually loaded into the pulley system pulling the wire upwards. To insure that the force applied was fully loaded to the blade via the wire, not to the resistant force of friction in the joint mechanism between top and bottom frames, shaking impact was applied to the rig. When the rig was fully loaded and extended, top and bottom frames were locked with each other by the locking mechanism. As the distance of the lacing wire to the blade top varies from 5mm to 70mm which was more than 3 quarters of the blade

141

length, joint mechanisms with different lengths were made as shown in Figure 6.8.

The initial ESPI results are shown in Table 6.1. The ESPI results of APL1 blade model, a simplified blade without lacing wires, are also listed in the table as a reference. We shall discuss the results together with results of FE modelling in the following sections.

MODES	1F	1T	1E	2F	2T	3F
APL1	471	2865		3132	8925	8354
APL16	578	2809		3743	8886	9193
APL15	678	2818		4546	8778	8600
APL14		2925		5260	8868	8250
APL13	2175	2933		4235	8706	9388
APL11	5094	2957		2957	8785	8236
APL12	2435	2996		6026	8787	10374

Table 6.1   Natural frequencies (Hz) of Simplified blades with A Lacing Wire Obtained by Initial ESPI Tests

6.5 F.E. Modelling of Simplified Blades with a Lacing Wire

6.5.1 Fundamental Assumptions

Considering the way that the lacing wire works, there were two possibilities as indicated by Wachter [198]:

a)   friction damping,

b)   a lacing wire is locked in the blade and hence alters significantly the vibration characteristics of the system.

Friction damping was not investigated in this study for the following reasons:

a)   when there is friction damping, the blade's natural frequencies may not vary significantly from the frequencies of the free-standing blade.

b)   the FE package PAFEC used in this study is not able to carry out natural frequency analysis with the friction of variable friction coefficient.

c)   the interesting operational speed of the turbocharger in which the blade under study is employed is around 18000 rpm. Consequently the centrifugal force exerted on each blade by the lacing wire is 1400N. The ESPI test which will be discussed later proved that no slippage occurs above 700N's loading.

Whether the slippage between the lacing wire and the blade occurs depends on the following factors as noticed by Provenzale [137]:

a)   friction between the lacing wire and the blade, resulting from the lacing wire being held outward by centrifugal force,

b)   Displacement of the blade in vibration at the lacing wire location, and

c)   blade-to-blade phase angle. If the friction is bigger than the force required to stretch and compress the lacing wire over the displacement equal to the amplitude of blade vibration at the lacing wire location as illustrated in Figure 6.9, then the wire is locked in the blade.

Friction is produced by the lacing wire being held outward by centrifugal force which is proportional to the square of the rotating speed of the rotor. Amplitude of vibration is the displacement response of the blade to the excitation and depends on the relationship between natural frequencies and excitation frequencies. It is not directly proportional to the running speed. Therefore, when rotating speed is higher than a certain critical value, the friction is large enough to restrain the displacement at the lacing wire location. Then the wire is locked.

In this study it was assumed that the wire was locked into the blade and it was intended to find out how the wire altered the vibration characteristics of a single blade.

6.5.2 Calculation of Spring Stiffness

Huang [76] calculated the free vibration of rotationally periodic structures with various types of connection elements by a transfer matrix method. He considered the lacing wire as segments of wires with hinged ends as shown in Figure 6.10. In the work done by Wildheim [210] a lacing wire was treated as a massless beam in between blades and only static stiffness of the wire was considered. In this study, the lacing wire was modelled as massless springs hinged in between blades.

6.5.2.1 Longitudinal Stiffness

A lacing wire is a continuous beam when it loosely rests in holes in the blades. When the disk rotates, the centrifugal force acting on the lacing wire pushes it outwards. The friction produced by centrifugal force stops relative sliding between blades and the lacing wire. If the lacing wire hole is slightly bigger in dimension than that of the wire, which is true in most cases because of the wear between them during operation, then there is no bending moment applied to the blade by the lacing

wire at the points of interface. Thus the connection between blades and the lacing wire could be considered as hinged.

Now the calculation for the longitudinal stiffness of the wire is straightforward. As shown in Figure 6.11, assuming there are no displacements for blade i-1 and blade i, the displacement in x direction for blade i+1 is δ which is the elongation of the wire L_i. If P represents the tensile force, E is the Young's modulus of the lacing wire and A is the cross-sectional area of the wire, then the relation between elongation and tensile force, according to Hooke's law, is

$$\delta = \frac{PL_i}{EA}$$

(6.1)

which is

$$P = \frac{EA}{L_i}\delta$$

(6.2)

For a linear spring, the relation between external force and deformation is

$$P = K_i\delta$$

(6.3)

where K is the spring stiffness.

Comparing equations 6.2 and 6.3, the longitudinal stiffness of the lacing wire is

$$K_l = \frac{EA}{L_l}$$

(6.4)

In the first attempt at modelling the lacing wire, the length of the wire was considered 25mm long as illustrated in Figure 6.7. The material of the wire used in the ESPI test is steel hence the value of E is $209 \times 10^9 N/m^2$. The dimension of the wire is 3.1 mm, thus the value of K_l is obtained by the following calculation:

For circular cross-section, $$A = \frac{\pi D^2}{4}$$

(6.5)

Substitute eq. 6.5 and values of E and L_i into eq. 6.4, the longitudinal stiffness of the lacing wire is given by:

$$K_l = \frac{E\pi D^2}{4L_l} = 6.31 \times 10^7 N/m$$

(6.6)

6.5.2.2 Lateral Stiffness

For lateral stiffness calculation, different phase relations among blades have to be considered. There are two possibilities of phase relations among blades, which are illustrated in Figure 6.12 (a) and (b). Taking coordinate axes x and y as shown, the angle θ_1 in diagram (a) between the lacing wire and axis x at the connecting point of blade (i+1) is not zero and neither is θ_2, while in diagram (b), both of them are zero. These two different phase relations can be simplified as illustrated in Figure 6.12 (c) and (d).

146

K_{yc}. Now we shall calculate the lateral stiffness of the lacing wire K_{yc} in the case shown in Figure 6.12c. Timoshenko [189] studied the deflection of laterally loaded symmetrical beams and gave the differential equation of the deflection curve denoted by:

$$EI_z \frac{d^2y}{dy^2} = -M$$

(6.7)

with regard to the coordinate system in diagram (c) of Figure 6.12. The bending moment M at any point x is:

$$M = \frac{1}{2}Px \qquad for \quad 0 \leq x \leq \frac{L}{2}$$

Substitution of M in eq. 6.7 gives

$$EI \frac{d^2y}{dx^2} = -\frac{1}{2}Px$$

By integrating this equation we obtain

$$EI \frac{dy}{dx} = -\frac{1}{4}Px^2 + C_1$$

(a)

and

147

$$EIy = -\frac{1}{12}Px^3 + C_1x + C_2$$

(b)

Now we need to determine two constants C_1 and C_2, for their determination we have two conditions, namely that the deflection at each of the two ends is zero and the slope at the middle of the beam is zero as the beam is symmetric to the point of loading. Substituting x = 0 and y = 0 in the expression (b), we find

$$C_2 = 0$$

(c)

Substituting dy/dx = 0 and x = L/2 in the expression (a), we obtain

$$C_1 = \frac{1}{4}P(\frac{L}{2})^2 = \frac{1}{16}PL^2$$

(d)

Substituting the values (c) and (d) of the constants into eqs. (a) and (b) for the deflection curve, we obtain

$$EI\frac{dy}{dx} = -\frac{1}{4}Px^2 + \frac{1}{16}PL^2 \qquad 0 \le x \le \frac{L}{2}$$

(6.8)

$$EIy = -\frac{1}{12}Px^3 + \frac{1}{16}PL^2x \qquad 0 \le x \le \frac{L}{2}$$

(6.9)

The deflection at the position of loading is obtained by substitute x = L/2 in eq. 6.9

148

$$EI\delta = \frac{PL^3}{48}$$

Rearranging this expression, we obtain

$$P = \frac{48EI}{L^3}$$

(a)

Comparing with $P = K_{yc}\,\delta$ gives

$$K_y = \frac{48EI}{L^3}$$

(6.10)

where E is the Young's modulus, I is the second moment of area and L is the length of the beam.

K_{yd} The case in diagram (d) of Figure 6.12 is actually to obtain the deflection δ at the loading location.   It is a statically undetermined problem with six reactive elements, which means the problem has three statically indeterminate elements. However, for ordinary beams, the horizontal components of the reactions can be neglected, which reduces the number of statically indeterminate quantities to two. If we use the method of superposition, then the case can be considered in simpler ways as shown in diagrams (e) and (f) of Figure 6.12. The solution can be obtained by combining the two statically determinate problems shown in diagram (e) and (f). It is evident that the conditions at the built-in ends of the beam AB will be satisfied if the couples M_a and M_b are adjusted so as to make

$$\theta_1 = -\theta_1', \qquad \theta_2 = -\theta_2'$$ (6.11)

Considering the structure and the load are symmetric to the loading point, we know that the deflection should be symmetric too. Hence we obtain

$$\theta_1 = \theta_2 \text{ and } \theta_1' = \theta_2'$$ (a)

Therefore M_a must be equal to M_b. The numbers of statically indeterminate couples are reduced to one, M_a, which can be determined by

$$\theta_1 = -\theta_1'$$ (b)

Substitution of x = 0 in eq. 6.8 gives

$$EI\frac{dy}{dx} = \frac{1}{16}PL^2$$
at x = 0

we obtain θ_1 by rearranging the expression above

$$\theta_1 = \frac{PL^2}{16EI}$$ (c)

To obtain the angle θ_1' in diagram (f), the equation for the deflection curve can be written as below:

$$EI\frac{d^2y}{dx^2} = M_a \qquad\qquad 0 \leq x \leq L$$

(6.12)

The first integration gives

$$EI\frac{dy}{dx} = M_a x + C_1$$

(a)

and the second integration gives

$$EIy = \frac{1}{2}M_a x^2 + C_1 x + C_2$$

(b)

The constants C_1 and C_2 are found from the condition that the deflection vanishes at supported ends. Thus, by substituting x = 0, y = 0 and x = L, y = 0 in eq. (b), we obtain

$$C_2 = 0, \qquad\qquad C_1 = -\frac{1}{2}M_a L$$

Substituting these values in eqs. (a) and (b), we find

$$\frac{dy}{dx} = \frac{M_a}{EI}(x - \frac{L}{2})$$

(6.13)

$$y = \frac{M_a}{EI}(x^2 - Lx)$$

(6.14)

Thus we obtain $\theta_1{'}$ by substituting $x = 0$ in eq. 6.13

$$\theta_1{'} = -\frac{M_a L}{2EI}$$

(6.15)

The static undetermined couple M_a is found by substituting equations 6.15 and 6.11(c) in eq. 6.11(b)

$$M_a = \frac{PL}{8}$$

(b)

Substituting (b) and $x = L/2$ in eq. 6.14 we obtain the deflection at the middle of the beam in diagram (f)

$$\delta_2 = -\frac{PL^3}{64EI} \;(\uparrow)$$

(c)

δ_1 in diagram (e) is given by eq. 6.9(a)

$$\delta_1 = \frac{PL^3}{48EI} \;(\downarrow)$$

(d)

Finally, the summation of equations (c) and (d) gives the deflection at the middle of the beam in diagram (d)

$$\delta = \delta_1 + \delta_2 = \frac{PL^3}{192EI}$$

(6.26)

Rearranging expression (6.26), we obtain

$$P = \frac{192EI}{L^3}\delta$$

(626a)

Hence we find

$$K_y' = \frac{192EI}{L^3}$$

(6.27)

which is the lateral stiffness of the lacing wire subject to the phase relation shown in diagram (b) of Figure 6.12.

Comparing equations 6.10 and 6.27, we find

$$K_y' = 4\frac{48EI}{L^3} = 4K_y$$

For the lacing wire used in the test, the diameter D = 3.1 mm, length L = 50 mm, E = 209x10⁹ N/m². Substituting these values in eq. 6.10, we obtain

$$K_{yc} = 3.638 \times 10^5 \text{ N/m.} \tag{6.16}$$

Hence

$$K_{yd} = 4K_{yc} = 1.455 \times 10^6 \text{ N/m.} \tag{6.19}$$

6.5.2.3 Torsional Stiffness

Torsional stiffness of the lacing wire is also related to phase relations of the blades as shown in Figure 6.13. Apparently the stiffness at location i in case (b) is larger then that in case (a). From diagram (d) we shall calculate the stiffness in case (b).

The beam loaded at the middle by M_o with two built in ends in Figure 6.13(d) can be simplified as a beam, which is half of the original length, with one end built-in and loaded by $M_o/2$ and P_o at the free end as shown in Figure 6.13(e). There are standard solutions for cantilevers loaded at the free end as shown in Figure 6.14, where θ and δ denote deflective angle and deflection at the free end respectively.

This is a statically undetermined problem with one statically undetermined element P_o, which can be determined by the deflection $\delta = 0$ at the free end.

Referencing equations in Figure 6.14, the deflection caused by $M_o/2$ at the free end is

$$\delta_1 = \frac{M_o L^2}{16EI} \tag{6.17}$$

Deflection resulting from P_o at the free end is

$$\delta_2 = -\frac{P_o L^3}{24EI}$$

(6.18)

Summation of δ_1 and δ_2 should be equal to zero, thus $\delta_1 = -\delta_2$ Substituting equations 6.17 and 6.18 we find

$$P_o = \frac{3M_o}{2L}$$

(6.20)

In the same way of referencing equations in Figure 6.14 the deflective angle θ_1 caused by $M_o/2$ at the free end is

$$\theta_1 = \frac{M_o L}{4EI}$$

(a)

and θ_2 caused by P_o at the free end is

$$\theta_2 = -\frac{P_o L^2}{8EI}$$

(6.21)

Substituting eq. 6.20 in eq. 6.21, we obtain

$$\theta_2 = -\frac{3ML}{16EI}$$

(6.22)

Therefore, the summation of equations 6.20 (a) and 6.22 gives the deflective angle θ at the free end in Figure 6.13(e), which is at the middle of the beam in Figure 6.13(d).

$$\theta = \frac{M_o L}{4EI} - \frac{3M_o L}{16EI} = \frac{M_o L}{16EI}$$

(6.23)

Rearranging eq. 6.23, we obtain

$$M_o = \frac{16EI}{L}\theta$$

Hence the torsional stiffness is

$$K_t = \frac{16EI}{L}$$

(6.24)

Substituting $E = 209 \times 10^9$ N/m, $L = 50 \times 10^{-3}$ m and $I = 4.533 \times 10^{-12}$ m^4 in eq. 6.24, we find

$$K_t = 303 \text{ Nm/rad}$$

(6.25)

So far, we have obtained longitudinal stiffness, lateral stiffness and torsional stiffness which are listed below for further reference

Longitudinal stiffness $\qquad K_l = 6.31 \times 10^7$ N/m $\qquad$ (6.6)

Lateral stiffness	$K_{yc} = 3.638 \times 10^5$ N/m	(6.16)
Lateral stiffness	$K_{yd} = 1.455 \times 10^6$ N/m	(6.19)
Torsional stiffness	$K_t = 303$ Nm/rad	(6.25)

6.5.3 F.E. Modelling Criteria

6.5.3.1 Number of Elements

The number of elements used to model each simplified blade was different according to the location of springs.

For initial models named APL1 to APL16, 12 elements were used apart from APL13, of which the number was 14. In addition, two spring elements were used on each blade. The root of the blades was not modelled on the initial models.

The type of elements used for blades was 37110 in PAFEC, which were 20 noded brick elements for three dimensional analysis. The lacing wire was modelled by massless spring elements which had three translational stiffnesses and three torsional stiffnesses.

6.5.3.2 Spring Location

For instance, to model the blade APL16 which is shown in Figure 6.15, the height of the key cross-section relative to the top and bottom sections, was determined first according to the location of the lacing wire. Then the mesh distribution was decided proportionally to the size of two blocks between three cross-sections. The mesh then was generated by PAFBLOCK module in PAFEC [126].

157

Springs were connected to node 12 and 15 in the key section and their outer ends were fixed to earth. Consequently, the springs would change their height when the key section moved up and down. The blade model consisted of two columns of elements joining at the central axis where node 12 and 15 were located. Therefore the springs were ensured to be on the central axis. As another example, APL14 shown in Figure 6.15 was constructed in the same way. The key section this time was at the middle of the full length, hence springs were moved up with node 12 and 15 too.

6.5.3.3 Spring Stiffness Used in the Initial Models

In section 6.5.2, we calculated three stiffnesses of the lacing wire, which were longitudinal, lateral and torsional. But in practice, at the time of this initial modelling, only longitudinal stiffness was considered which was

$$K_l = 6.31 \times 10^7 \text{ N/m} \tag{6.6}$$

6.5.4 Initial Results and the F.E. Model Improvement

6.5.4.1 Initial Results

Six initial models were generated using the criteria described in the previous section. They were named as APL model, numbered from 11 to 16. Natural frequencies and mode shapes were calculated and frequency results are listed in Table 6.2.

6.5.4.2 Discussion of Initial Results of ESPI Test and FE Modelling

Results of initial ESPI and FE modelling were presented in Table 6.1 and

Table 6.2 respectively. Great discrepancies were found between the two groups of results.

MODE	1F	1T	1E	2F	2T	3F
APL1	504	2820	2930	3120	8900	8740
APL16	698	2875	2946	4186	9045	11010
APL15	908	2888	2956	5312	9093	11669
APL14	1404	2887	2957	7404	9079	9098
APL13				5360	9311	10438
APL11	7097	2888	2953	3050	9109	9446
APL12	2484	2892	2959	7691	9109	12929

Table 6.2   Natural frequencies (Hz) of simplified blades with a lacing wire calculated by Initial FE analysis

The first edge (1E) mode was not identified by the ESPI test since only deflections in the viewing directions of ESPI rig could be detected. Good agreement was found in torsional modes (1T and 2T). This confirmed the assumption that very little torsional constraint was applied to the blades by the lacing wire. Because the clearance between the lacing wire and the hole was fairly large, hence the wire under loading was not largely bent while blades were undergoing torsional motion. Therefore in FE modelling, torsional stiffness was not considered. Consequently, changes of frequency for torsional modes were not expected in FE results.

The main concern here was about flap modes. As can be seen in Tables 6.2 and 6.1, corresponding natural frequencies of the 1F mode in FE modelling were higher than those obtained from ESPI. In cases with models APL11 and APL16, they were 40% and 20% higher respectively. Same large discrepancies were also

found with 3F modes.

The disagreement in the initial results indicated that FE models needed to be modified and corrected and if, after the modification, there are still large discrepancies, then the ESPI results will be questioned.

6.5.4.3 Improvement of FE Models

Considering the initial models one thing obviously different from testing models was the direction of the spring stiffness K_t. The initial model was constructed in the coordinate system shown in Figure 6.17(a), which gives the top view of the FE model. Obviously, K_x was in x direction, but the test model was designed having a setting angle which resulted in an angle θ between the axis x' of the local coordinate and axis x of the global coordinate as shown in Figure 6.17(b). Since there was no pretwist the angle θ was equal to the setting angle which was 12° with APL models.

Spring elements had to be connected at nodes which were chosen to be node 12 and node 15 in APL models. With the setting angle θ, node 12 and node 15 were no longer in line with axis x. Therefore, different ways of connecting spring elements to the nodes were considered as illustrated in Figure 6.17(c) and (d). Finally, taking the experience of modelling the ASPRT model, which was the FE model of the blade K with the root, the connection was modelled as shown in Figure 6.17(e). Nodes 12 and 15 were moved to be on x axis. In this case no torsional moment was pre-loaded to the blades. Two coordinate systems were used in the improved models. x'y' was the local coordinate and xy system was the global one as shown in Figure 6.17(f).

In the FE program of improved models, coordinates of nodes were given in

the x'y' system and a setting angle was achieved by giving an angle θ to define the position of the x'y' system in the xy system. New locations of nodes 12 and 15 were decided by using PIGS4. The cross section containing nodes 12 and 15 was displayed on a computer screen. A new location of the nodes was then graphically input from the screen, the new coordinates of the nodes were obtained from PIGS4 information facility.

The coordinates of new nodes 12 and 15 given by PIGS4 were in the xy system. The coordinates in the input file for the construction of models should be in the x'y' system. So these new coordinates needed to be transferred to the x'y' system. The coordinate transferring matrix could be obtained easily from Figure 6.17(f). For a known point p(x,y) in the xy system, its coordinate in the x'y' system was given by

$$\begin{bmatrix} x' \\ y' \end{bmatrix} = \begin{bmatrix} \cos\theta & \sin\theta \\ -\sin\theta & \cos\theta \end{bmatrix} \begin{bmatrix} x \\ y \end{bmatrix}$$

(6.26)

Inputting the new local coordinates of nodes 12 and 15 in the input file we constructed improved FE models of simplified blades.

The second difference between FE models and testing models was that there was no root modelled in the FE models. APL models were treated as cantilevers with one end fully restrained. But as can be seen in Figure 6.1, a root was designed for the blade to be clamped. The root and the blade were made out of one piece of metal and the blade was only clamped at the root as shown in Figure 6.4. The real interface between the root block and the blade holding block was unknown. Since the blade root block was locked in by screws, there must be some clearance, hence the restraint must be lower than the plane where the blade and the root block meet.

The blade root block are modelled using four 20-noded, 3D brick elements (37110 type as shown in Fig. 6.16). The bottom plane of the root was fully restrained. Results of the FE models with improved spring connections and the root block, which were named as APL#NB models, where # represents serial numbers, were shown in Table 6.3.

MODES	1F	1T	1E	2F	2T	3F
APL16NB	688	2864	2366	4122	8934	10330
APL15NB	892	2872	2369	5289	8979	10462
APL14NB	1370	2873	2378	7105	8488	8984
APL13NB	2189	2874	2555	5217	8978	10414
APL11NB	2215	2864	2478	7219	8966	10538
APL12NB	2307	2869	2914	7132	8713	8978

Table 6.3   Natural frequencies (Hz) of simplified blades with a lacing wire calculated by Second FE analysis

6.5.4.4 Improvement of the Lacing Wire Locking Mechanism

Results in Table 6.3 were little lower than those in Table 6.2 but they were still much higher than ESPI results in Table 6.1. This implied that there could be something incorrect about the basic assumptions. Further investigation was carried out to look into the basic parameters of the testing rig and ESPI tests. The lacing wire holding frame was examined again and the attention was drawn to the lacing wire locking mechanism, which is shown in Figure 6.7a. The wire was considered to be locked by top screws and the effective length of the wire was assumed from the surface of the blade to the inner edge of the wire holding frame. Therefore, it

was 25 mm long. Actually, some sliding wear on the wire at edge of the wire holding frame was found which indicated that the wire might not be fully locked during the vibration. This possibility led to the improvement of the mechanism for wire locking.

The secured way of locking the wire into the wire holding frame was shown in Figure. 6.7b, the wire was locked by double nuts at the outer edges of the wire holding frame. This method was more reliable than the one used before so it was known that the wire would not slide. The effective length for longitudinal deflection then was 50mm from the middle of the wire holding frame, where the blade was, to the outer edge of the wire holding frame. Hence the stiffness K_l given by eq. 6.6 became

$$K_l = 3.155 \times 10^{+7} \text{ N/m} \tag{6.27}$$

The value of K_l in all APL#NB models were replaced by eq. 6.27 and new results were listed in Table 6.4. (# = serial numbers)

6.6 Further Results and Discussion

The ESPI tests were carried out again after the wire locking mechanism was improved. Natural frequency results were listed in Table 6.5. Comparing Tables 6.4 and 6.5, it could be seen that the natural frequencies of the FE models were very close to those obtained from the experiment. Natural frequencies of FE modelling were less than 6% higher than those from the ESPI tests except for a few individual cases. This agreement meant that FE models and ESPI tests were both correct and the study into the vibration characteristics of a single blade with a lacing wire could be carried out on the data obtained.

MODES	1F	1E	1T	2F	2T	3F
APL1NB	493	2391	2820	3028	8828	8247
APL16NB	653	2361	2864	3819	8935	9544
APL15NB	847	2378	2873	4708	8981	9583
APL14NB	1308	2401	2876	5710	8983	8444
APL13NB	2155	2537	2877	4498	8979	9488
APL11NB	5517	2382	2868	2897	8976	8505
APL12NB	2243	2528	2869	6662	8967	10103

Table 6.4   Natural frequencies (Hz) of simplified blades with a lacing wire calculated by correct FE analysis

MODES	1F	1E	1T	2F	2T	3F
APL16	577		2809	3743	8886	9193
APL15	728		2812	4582	8733	9502
APL14	1382	2388	2903	5260	8868	8250
APL13	2152	2514	2933	4235	9070	9680
APL11	5122	2316	2957	2941	9269	8225
APL12	2200	2528	2984	6172	8886	9193

Table 6.5   Improved Natural frequencies (Hz) of simplified blades with a lacing wire obtained by ESPI tests

So far, experimental data have been presented in terms of natural frequencies only as listed in Tables 6.1 to 6.5 under the classification of flap modes, an edge mode and torsional modes. To carry out a full analysis, mode shapes had to be considered along with natural frequencies. A full data presentation was given in Figure 6.18.

Names of the simple blade models were given in the top row of Figure 6.18 and they were the headings of columns where mode shapes, relevant natural frequencies and the location of the lacing wire were given. Classical classifications of mode shapes were used and the data of model APL1 which was a simplified blade without lacing wires, was also given to be the reference.

6.6.1 Coupled Modes Introduced by the Lacing Wire

Great care was exercised during the tests and some difficult modes were identified. It was found that with most models apart from APL11, the edge mode was affected by other modes such as 1T and 2F mode. This coupling from other modes gave the edge mode out-plane deflection which was then detected in ESPI tests. As presented in the 1E mode row in Figure 6.18, a nodal line appeared above half of the height of the blade. It looked like the second nodal line of the 2F mode but it was not horizontal. Actually it was the registration of an out of plane component of edge mode deflection coupled by the 2F and the 1T modes because of the contribution of the lacing wire and the setting angle as shown in Figure 6.19(a).

The further study revealed that a force in x' direction is applied by the lacing wire to the blade due to its edgewise displacement. The development of the relation between the force and the displacement are given below.

As shown in Fig. 6.19(b), the deflection of the edge mode at the cross-section of the lacing wire is $\delta_{y'}$. Considering the relationship illustrated in Fig. 6.19(c), we obtain the deflection of the lacing wire in x direction as

$$\delta_x = \sin\theta \; \delta_{y'} \tag{6.28}$$

Since δ_x is very small, δ_y is considered to be normal to δ_x. The acting force

165

of the lacing wire on the blade is given by Hooke's law (eq. 6.3)

$$F_x = \delta_x \, K_l \tag{6.29}$$

Where K_L is the longitudinal stiffness of the lacing wire. From Fig.6.19(d) showing relationship among F_x, $F_{x'}$ and $F_{y'}$, we can obtain the acting force of the lacing wire in x' direction

$$F_{x'} = F_x \cos\theta \tag{6.30}$$

Substituting equations 6.28 and 6.29 in eq. 6.30 gives

$$F_{x'} = (1/2)\sin 2\theta \, K_l \, \delta_{y'} \tag{6.31}$$

This is the force acting on the blade in x' direction by half of the lacing wire. Taking the other half into account, the resultant force from the lacing wire is

$$R_{x'} = \sin 2\theta \, K_l \, \delta_{y'} \tag{6.32}$$

Eq. 6.32 indicates that $R_{x'}$ varies with the setting angle θ, following a sine relationship. A curve is drawn in Fig. 6.20. It takes the maximum when θ equals to $\pi/4$ and the minima occur when θ is equal to zero and $\pi/2$.

In our case, θ is 12°, therefore

$$R_{x'} = 0.41 K_l \, \delta_{y'} \tag{6.33}$$

Eq. 6.33 shows that $R_{x'}$ is in the same quantity level as $K_L \delta_{y'}$, which explains the existence of bending moment in x' direction associated with the edge mode. A

166

front and a side view of the 1E mode of FE model APL14NB in Fig. 6.21 revealed this influence.

6.6.2 Excitation from the Side of the Blade

In the initial ESPI test it was very difficult to identify the edge mode and some other modes were coupled with the edge mode. The reason was that excitations were applied only in the direction of excitation 1 as shown in Fig. 6.19a. As the direction of excitation was normal to the direction of major displacement, the edge mode on most models was not stimulated such as in the cases of APL16 and APL15. Moreover, natural frequencies of those stimulated edge modes varied with different locations of excitation. Hence they were not true natural frequencies. Since the major displacement of the edge mode was in y' direction, excitation from the side of the blade shown as excitation 2 in Fig. 6.19a was exercised.

It was proved that side excitation had provided the key technique to identify the edge mode. Mode shapes of ESPI results were the same as those obtained from FE modelling and the maximum difference of natural frequencies of the 1E mode between two sets of results was within 3%.

The edge mode of APL1 was identified by viewing the blade on one side and exciting it at the other side. Some other modes coupled by the edge mode were also identified by side excitation such as the 1F mode of APL13. Natural frequencies of these modes were close to the natural frequencies of the edge mode of the same models. In the case of APL13 the natural frequency of the 1F mode was 2152Hz (ESPI) which was only 362Hz away from 2514Hz (ESPI) for the edge mode (Figure 6.18). Also in the case of APL12, the natural frequency at 2528Hz (ESPI) for the edge mode was only 328Hz higher than 2200Hz for the 1PF mode. Since both modes were strongly coupled by the edge mode, side excitation was necessary to

stimulate the true mode shapes though they were not edge modes.

The study of the vibration of coupled modes are given in Section 5.2.3. When two independent modes are coupled, they switch into two coupled modes with similar mode shapes composed of the two independent modes. One of the natural frequencies of the coupled modes is higher and the other one is lower than both constituent natural frequencies.

It can be seen from Fig. 6.18 that natural frequencies of the edge mode of all models were not very far away from those of the 1T mode. The average natural frequency of the 1E mode was 2432Hz (FE) and the average natural frequency of the 1T mode was 2897Hz (FE). The difference in between was only 465Hz. Therefore, vibrating at about 2432Hz (FE) all edge modes were affected by torsional vibration which made the second nodal line at the middle of the blade tilted as shown in Fig. 6.18. This influence can be seen in Figures 6.21, 6.22, 6.23 and 6.24.

6.6.3 Identification of Mode Shapes

Most mode shapes were easy to identify such as torsional modes on all models and the 1F modes on the models where the lacing wire was in lower locations. However, difficulties were met in identifying some of the flap modes. Further study into the classification of the flap modes revealed the limitation of the traditional classification and a better understanding of the identification of the flap mode shapes were obtained.

6.6.3.1 Definition of the Flap Mode Shapes

Traditional definition on the flap mode shapes is based on the number of nodal lines across the blade concerned, as illustrated in Figure 6.25. The first mode

with only one nodal line at the bottom of the blade root block at 493 Hz is defined as the 1F mode, the second mode with 2 nodal lines is the 2F mode and three nodal lines indicate the third mode at 8089 Hz as the 3F mode. This way of classification is widely used for its simplicity but it is not always representative. For instance, it can not describe the flap mode shapes of the systems such as the modes of APL12NB shown in Figure 6.24, in which two modes both with two nodal lines were found at 2243 Hz and 6662 Hz and one mode with three nodal lines was found at 10103 Hz, while the mode with only one base nodal line was missing. This confusing identification of the flap mode shape signified that the number of nodal lines could not represent all the features of the flap mode shapes and a better definition of the flap mode shapes was needed.

Further study into a better presentation was carried out. The basic theory of vibration [118] indicates that a linear system can be represented by its characteristic equation, which is derived from differential equations of motion of the system, and the roots of the equation are the characteristic values for the system. The amplitude ratios of the mode of vibration can be found by substituting characteristic values into the displacement equations obtained from putting assumed harmonic solutions into the equations of the motion. The amplitude ratios denote the mode shapes and the square roots of the characteristic values are the natural frequencies corresponding to their mode shapes. Because of the nature of free vibration, only the amplitude ratios, not the amplitude itself, can be determined. The ratios imply two relative features:

a)   the values of the ratios represent the amplitude of vibration at different positions of the system relative to the amplitude of vibration at the reference position for a particular mode of vibration,

b)   the signs of the ratios indicate the phase relations of them, i.e. amplitudes are in the same direction or in the opposite direction. It is these two features

which define the mode shapes.

The traditional definition on the flap mode shape takes the undeformed shape of the system as the reference and considers the number of zero amplitudes to define the mode shape. The relative feature of eigenvectors may not be included in case of complex mode shapes. Moreover, the springs in the system introducing extra restraint make the identification of the flap modes more complicated. The restraint modifies the mode shape of flap modes and their natural frequencies according to its location relative to the mode shapes.

A typical example is that a free-fixed end condition of a uniform beam could be altered into a pinned-fixed condition by applying a hinge at the free end, as illustrated in Figure 6.26. The first pinned-fixed mode, 1PF, has two nodal points at two ends because they are both restrained. The slope of its deflection curve changes its sign once, which is very similar to the 2F mode of the free-fixed beam. For the same reason, the deflection curve of the 2PF mode is similar to that of the 3F mode of a cantilever.

The above study has revealed the importance of the relative feature and they can be described by the variation of the sign of the slope of the mode shape curve. For the nF mode, the sign changes n-1 times. It is also noticed that the pinned-fixed end condition may be introduced by a lacing wire. The special feature of the pinned-fixed (PF) mode shapes is that they are very similar to the flap modes of a cantilever. The slope of the deflection curve changes n times for the nPF mode and the amplitude at the free end is small relative to that at other part of the blade.

For example, the sign of the slope of the curve of the 1F mode (with one nodal line) of APL1NB in Figure 6.25 is equal to or greater than zero. The sign of the slope of the 2F mode (with 2 nodal lines) changes once only and changes twice

for the 3F mode. Furthermore, the unique character of the 1F mode is the bigger amplitude at the free end of the blade and the smaller amplitude near the fixed end of the blade as the result of no sign variation of the slope.

For further reference, the natural frequencies of a uniform beam under free-fixed and pinned-fixed conditions were obtained by solving the Euler equation for the beam [188], without considering the effect of rotary inertia and shear deformation. They are governed by $\omega_n = \beta^2(gEI/w)^{-2}$, where w/g is the mass per unit length of the beam. Number β depends on the boundary conditions of the problem and are given in Figure 6.26.

Using $E = 210\times10^9$ N/m^2, material density $\rho = 7800$ kg/m^3, natural frequencies of simplified blade with different boundary conditions are given by $\omega_n = 140.8(\beta l)^2$ Hz. The first three modes with cantilever and pinned-fixed conditions are listed in Table 6.7. Natural frequencies for free-fixed condition calculated using finite element method are also given in the table for comparison.

Mode/Freq.(Hz)	First	Second	Third
Free-Fixed (Euler)	496	3154	8689
Free-Fixed (FE)	495	3060	8420
Pinned-Fixed	2196	7041	14646

Table 6.7   Natural frequencies of simplified blades by Euler solution

It is interesting to notice that the difference between two sets of results for free-standing blade is within 3%. The error is considered due to the exclusion of the root block of the blade in Euler solution, hence frequencies are higher. The table

also reveals that the frequency of the 1PF mode is lower than that of the 2F mode and the same relation is true between the 2PF and the 3F modes. This suggests that the 2F mode of a free standing cantilever is softened by adding restraint between the second nodal point (the first being at the fixed end) and the free end.

6.6.3.2 Identification of Mode Shapes

In order to help for the flap mode identification, Figure 6.27 was constructed, in which the three flap modes of all APL#NB models were illustrated. With the reference to the APL1NB model, it was not difficult to identify the flap mode shapes of such models as AL16NB, AL15NB and AL14NB.

The difficulty started with the model APL13NB. The 2F mode was identified at 4235Hz (ESPI in Figure 6.18), but a second nodal line vaguely appeared at the middle of the blade at 2152Hz (ESPI, Figure 6.18). The traditional classification based on the number of nodal lines could not explain which was the 2F mode and where was the 1F mode. The F.E. mode shapes of these two modes of APL13NB can be found in Figure 6.27 at 2155Hz and 4498Hz. It can be seen that the side view of the mode shape at 2155Hz was basically the 1F mode. Because of the restriction from springs, part of the blade below the nodal line exhibited a small amount of flap bending opposite to the displacement at the part of the blade above the nodal line. This made the slope of the mode shape curve change its sign but the dominant amplitude was still at the upper part of the blade. The existence of the nodal line at the middle of the blade did not change the basic feature of the mode shape of the 1F mode.

The side view of the mode shape at 4498Hz showed that the sign of the slope genuinely changed once at the position below the springs. Hence, this mode was considered as the 2F mode although the sign intended to vary again at the position

172

of the springs which signified the influence of the springs. Therefore, the 1F mode was located at 2155Hz, the 2F mode was at 4498Hz and the 3F mode was at 9488Hz (F.E.) with APL13NB.

Similarly, the 1F mode and the 2F mode of APL11NB were identified at 5517Hz (F.E.) and 2897Hz (F.E.) respectively. The influence of torsional mode on the 2F mode was very strong since the frequency was very close to the frequency of the torsional mode at 2868Hz (F.E.) as shown in Figure 6.23.

The identification of modes for APL12NB model was also difficult. Mode shapes of the first at 2243Hz, the second (2528Hz), the fourth (6662Hz) and the sixth (10103Hz) modes were plotted in Figure. 6.24. The third mode at 2869Hz (F.E.) was identified as torsional mode. Here again we found the mode switching phenomenon which will be discussed in Section 7.2.4. The frequencies of bending mode and edge mode were very close hence they were fully coupled. Their mode shapes were very similar. It was hard to distinguish between the flap mode and the edge mode. Actually, for coupled modes, mode shapes can not be really distinguished and it is not necessary to identify each of them. In our case these two modes had to be put into a classified position in Figure 6.18. Therefore, the one with more edge mode element under the same maximum displacement was chosen to be the 1E mode which was at 2528Hz. The one at 2243Hz (F.E.) then was considered as a flap mode.

Now the first mode at 2243Hz (F.E.), the fourth mode (6662Hz, F.E.) and the sixth mode (10103Hz, F.E.) had to be identified. Two nodal lines were found both with the first and the fourth mode and three nodal lines were found with the sixth mode. The mode with only one nodal line was missing. This was an indication that the free-fixed boundary condition was transformed to pinned-fixed condition due to the location of the spring being very near the free end. Comparing the first (2243

Hz, FE) and the fourth mode (6662Hz, F.E.) in Figure 6.27 with the PF mode shapes in Figure 6.26, it was clearly seen that they were the 1PF (2243 Hz) and the 2PF (6662 Hz). The sixth mode was identified as the 3F mode because the sign of the slope of the mode shape curve changed twice and the amplitude at free end was still dominant relative to other part.

So far all modes of vibration of simplified blades with a lacing wire were identified and are summarised in Figure 6.18.

6.6.4 Effects of the Lacing Wire on Single Blade Vibrations.

Different modes of vibration are affected differently. For instance the effect of the loaded lacing wire location on torsional modes (1T and 2T) is insignificant as the lacing wire stiffness in the rotational mode is almost non-existent because of the clearance between the lacing wire and the hole in the blade. The effects of the lacing wire on the flap modes of the blade vibration are related to the height of the lacing wire relative to that of the blade.

It was found that the experimental and theoretical analysis carried out on six rectangular cantilevers as illustrated in Figure 6.18 could not fully reveal the true feature of the vibration behaviour of the laced blade. Then more APL#NB FE models were built up with smaller variation of the relative lacing wire height to find out the tendency of the variation of the natural frequencies of the flap modes and mode shapes. The FE results of natural frequencies are listed in Table 6.6.

The good agreement between ESPI and F.E. results in Figure 6.18 suggested that APL#NB F.E. model was reliable. Therefore it was not necessary to do experimental analysis on every F.E. model. Natural frequencies of three flap modes against the relative lacing wire height are plotted into Figure 6.28, in which natural

Relative Spring Height	Freq. Grp 1 Mode	Freq. Grp 2 Mode	Freq. Grp 3 Mode
0.00	495/1F	3060/2F	8420/3F
0.24	653/1F	3819/2F	9544/3F
0.35	847/1F	4708/2F	9583/3F
0.51	1308/1F	5710/2F	8444/3F
0.67	2155/1F	4489/2F	9488/3F
0.73	2840/1F	4210/⊗	9410/3F
0.75	3000/2F	4210/⊗	9160/3F
0.78	3054/2F	4474/1F	8899/3F
0.82	2980/2F	5030/1F	8640/3F
0.84	2897/2F	5510/1F	8500/3F
0.87	2750/2F	6290/1F	8460/3F
0.90	2629/2F	6751/2PF	8913/3F
0.92	2571/1PF	6770/2PF	9570/3F
0.95	2243/1PF	6660/2PF	10100/3F

⊗ = Unidentified mode shapes between the 2F and the 1F modes

Table 6.6   Variation of the natural frequencies of simplified cantilever blade with the height of the lacing wire

frequencies divided into three groups form three curves. The first curve starts at about 500Hz, the second at 3000Hz and the third at 8400Hz. The vertical coordinate denotes the range of frequency from 0 to 10,000Hz whilst the horizontal coordinate, from 0 to 1, represents the relative value of the height of the lacing wire against that of the blade. To simplify the following discussion the relative height of the lacing wire is defined as letter H. The location of the nodal lines of the 2F and the 3F

mode of the blade without lacing wires are also illustrated as dotted lines in Figure 6.28. The frequency line of the 1F, 1PF, 2F, 2PF and 3F modes of free-standing blade APL1NB are also drawn for reference.

Using the definition for the flap mode and pinned-fixed mode discussed in Section 6.6.3.1, most mode shapes were identified and expressed by circular, square and triangle marks on the curves respectively for the 1F, the 2F and the 3F mode. The PF modes are represented by patterned rings. The mode shapes at 4210 Hz in the second frequency group were not identified (Table 6.6).

6.6.4.1 Effects of the Lacing Wire Location on Flap Modes

The three curves in the Figure 6.28 reveals the variation of natural frequencies and mode shapes of three flap modes with the height of the lacing wire.

The first effect of the lacing wire is the mode shape "switching" phenomenon. The first frequency curve starts at 495Hz as the 1F mode from a free cantilever with no lacing wires. Following the first curve, the fundamental first flap (1F) mode switches into the 2F mode when the lacing wire relative height exceeds 73% (H > 73%). Furthermore, the first pinned-fixed mode is exhibited (1PF at H = 95%, Figure 6.29) as the lacing wire location exceeds 90% of the blade height. Simple Euler theory suggests a difference of 4.38 to 1 for frequency ratio between a propped cantilever mode and a pure cantilever mode (Figure 6.26). The detected ratio between APL12NB and APL1NB (Figure 6.18) is 2220 Hz to 474 Hz which is 4.64 to 1. This confirms that the 2F mode is transformed into the 1PF mode due to the restraint by the lacing wire at the end of the blade. Similarly, the second frequency curve starts as the 2F mode then switches into the 1F mode at H = 0.78 and into the 2PF mode when H exceeds 0.90. The third curve starting at 8420 Hz as the 3F mode remains its identity whilst the frequency varies between 8400 Hz and 10100

176

Hz.

The second effect of the lacing wire is to stiffen up or to soften the blade and consequently the natural frequencies for the modes concerned tend to increase or to decrease. As the lacing wire height increases, the natural frequency of the 1F mode increases as the result of the stiffening up on the first curve. At lower attachment points the blade is stiffened but the first flap mode is still detected at higher frequency values. As the attachment point moves up along the blade and the effective free end is shortened, the fundamental mode frequency increases to 5122Hz (ESPI, APL11, Figure 6.18) at H = 0.837 and to 6290 Hz at H = 0.87 (Table 6.6). This effect can be seen in Figure 6.28 by looking at circular marks against the H axis. It shows that the stiffness of the 1F mode can only be increased when a restraint is applied to the free standing blade.

The variation of the natural frequencies of the 2F and the 3F mode can also be found by following the square and the triangular marks respectively against the H axis in Figure 6.28. It is noticed that the frequency of the 2F mode is increased if the lacing wire is connected between the two nodal lines (at H = 0 and H = 0.78), whilst it is decreased when the lacing wire is above the second nodal line (H > 0.78). They can even be lower than that of the 2F mode of a free standing blade. This suggests that the attachment of a lacing wire to a blade can stiffen the blade and soften it as well. This is because the 1PF mode is less stiff than the 2F mode for the same beam (Table 6.7), and applying restraint at the free end of the blade is to transform free-fixed condition into pinned-fixed condition. The variation of the frequency of the 3F mode shows no effect of the lacing wire if it is attached at nodal lines (H = 0.51 and H = 0.87), and higher frequencies are found if it is at other locations.

The variation of the 1F mode shape resulted from the stiffening up by the

177

lacing wire is clearly illustrated by F.E. mode shape plots in Figure 6.29. Moreover, The degree of stiffening up is decided by the distance between the location of the lacing wire and the location of the nodal lines of flap modes. For the 1F mode, the stiffening effect gets stronger when the lacing wire moves away from the nodal line.

For the 2F mode, the maximum stiffening effect is achieved when H is between 0.45 and 0.55 which is the area of the maximum amplitude between the two nodal lines of the 2F mode. If the lacing wire is located close to the second nodal line (H = 0.78), the modes of vibration of the laced blade is almost identical to that of the unlaced blade, which is almost the case for the model APL10NB in Figure 6.29.

In general, small vibration amplitudes result in small load effects from the lacing wire, thus light overall effects. Loading from the lacing wire increases as the connection friction increases. When the position of the lacing wire coincides with the nodal lines, the lacing wire has no effect on that particular mode. Beyond this position, when wire approaches the tip of the blade, the fixed-pinned modes is becoming dominant, Hence, blade vibration can switch from the 1F, 2F modes into 2PF or 1PF.

In some cases however the lacing wire has the effect of raising one mode of vibration to be near to another less affected mode, with the consequence that the two modes interact and produce a vibration mode shape which is a combination of two modes. This was particularly noticeable with the overlapping of the first flap (1F) mode and the first edge (1E) mode for blade APL13. To observe this effect experimentally it was necessary to excite the blade in the edgewise direction in order to stimulate the equivalent flap mode. The finite element analysis also identified this trait as can be seen in Figure 6.22, which clearly shows the mode shape deflecting in both planes simultaneously.

6.6.4.2 Effects of the Lacing Wire Stiffness on Flap Modes

The study into the effects of the lacing wire stiffness on the three flap modes was also carried out using F.E. analysis. The results confirm that flap modes switch into associated PF modes, i.e., 1F --> 2PF and 2F --> 1PF. The results are shown in Figure 6.30. For instance, the 1F mode of APL12NB blade (H = 0.95) at 813Hz when the lacing wire stiffness K_x is 2.9×10^5 switches into the 2F mode at 2243Hz when Kx increases to 2.9×10^7 as shown in diagram (a). The diag. (b) shows that the 2F switches into the 2PF. It can be seen that the increase of the stiffness pulls the free end of the 1F and the 2F mode shape back towards the static position. The distance between nodal lines is reduced and the natural frequencies hence increased.

The 3F mode remains in the same mode shape (Figure 6.30c). This is because the stiffness of the restraint provided by the spring is inadequate to transform the blade into a pinned-fixed condition. This is reflected by the much lower frequency achieved at 10100 Hz comparing with 14646 Hz (Table 6.7) for the 3PF mode. The 3PF mode shaped can be obtained by further increase of spring stiffness. However, vibration amplitude can be seen largely reduced by the increase of the spring stiffness.

It is considered that the understanding of the features discussed above is very important. This understanding may be used as a base on which the control of resonant amplitudes could be exercised by optimising the position and the stiffness of a lacing wire.

6.7   Investigation into the Blade K with the Lacing Wire

In previous chapters , we have discussed the vibration of simplified blades

and established the basic understanding of characteristics of blade K without the lacing wire. In this chapter, we have investigated simplified blades with a lacing wire. In the light of the knowledge acquired, we are going to study the vibration characteristics of blade K with a lacing wire.

6.7.1 First ESPI Test on the Blade K with the Lacing Wire.

In previous sections we have discussed experimental investigation into simplified blades by using ESPI techniques. The blade K was tested in exactly the same way as shown in Figure 6.6. 700N load was applied to the blade via the wire. The blade was excited at various locations. When the blade K was first tested, the lacing wire was locked by a screw on the top surface of the wire holding frame. Natural frequencies and mode shapes were illustrated in Figure 6.31. Where there were two natural frequencies given under the same mode shapes meant that exciting at different locations, more than one "natural frequency" could be found for the same mode shape. One could be stronger than the other. Which was the one closer to the true natural frequency had to be decided later.

6.7.2 F.E. Model of the Blade K with the Lacing Wire

In Section 5.6, the F.E. model of blade K was developed as shown in Figure 6.32. The F.E. model of the K blade with a lacing wire could simply be set up by connecting springs to the blade.

The distance of the lacing wire hole from the top of the blade is 13mm. This gives the z coordinates of the nodes to which spring elements were connected. At the beginning springs were connected to one node, node 401 as shown in Figure 6.33(a), which is a top view of one cross-segment of ASPRT20 F.E. model. The

180

cross-segment consisted of brick elements 11, 18, 28 and spring elements 27 and 28 which were connected to the segment at node 401. Outer ends of the springs were fixed to earth. Figure 6.33(b) gives the full view of ASPRT20 model. In this stage of the investigation, the ESPI test on blade K was carried out when the lacing wire was locked by screws from the top surface of the wire holding frame as shown in Figure 6.7(a). So corresponding spring stiffnesses were $K_x = 6.3 \times 10^7 \text{N/m}$ (longitudinal) $K_y = 1.46 \times 10^6 \text{N/m}$ (lateral) and $K_t = 303 \text{Nm/rad}$ (torsional). Mode shapes and natural frequencies were shown in Figure 6.31.

Large differences of both mode shapes and natural frequencies between F.E. results of ASPRT20 model and ESPI results of the first test on blade K were found with the first three modes. For instance the mode shapes of the first mode did not appear like each other. Natural frequencies of the second mode were 20% apart. This large error indicated that further study of modelling was necessary.

Model ASPRT21 as shown in Figure 6.34 (a) and (b) was set up to find out the effect of connections between springs and the blades. Springs were connected at both faces of the blade at node 401 and node 403. F.E. results of ASPRT21 model were illustrated in Figure 6.31. Comparing results of ASPRT21 with those of ASPRT20 we found differences in mode shapes (second and third mode). This implied that the connection of springs to the blade played an important part in F.E. modelling.

The lacing wire can be considered to be locked at two outer edges of the lacing wire hole on the blade when the centrifugal load is large enough. Therefore, the springs in F.E. model should be connected to the blade at both faces and both springs should be in line. The study of Figure 6.34(b) clearly showed that the above requirements could not be met without amending the blade model.

181

To create the connecting nodes for springs in correct locations, two triangle 12 noded 3D elements (element type 37230) were added to the FE model in conjunction with 16 noded 37130 elements. The location of element 27 and element 28 are shown in Figure 6.35(a) and the top view of a cross-segment including element 18 and 27 showing the spring connection with the blade was illustrated in Figure 6.35(b). Spring element 30 was connected at node 403 on the rear face of the blade and spring element 29 was connected at node 493 on the front face of the blade. Nodes 493 and 494 were created by using 37230 triangle elements.

This F.E. model was called ASPRT32 and its results were shown in Figure 6.36. Comparing Figure 6.36 with Figure 6.31, we found out that all mode shapes apart from the first one were very similar to those obtained from the ESPI test and natural frequencies were within 10% in difference. But why the mode shapes of the first mode were different and the second mode shapes were not quite alike remained unclear.

The answer came from Section 6.5.4.4. It was found in the investigation into simplified blades with the lacing wire at different locations that the wire locking mechanism was not reliable. Therefore this was improved by locking the wire by screw nuts at two ends of the wire on the outer edges of the wire holding frame as shown in Figure 6.7(b). As discussed in Section 6.5.4.4, the longitudinal stiffness, associated with the improved wire locking, was $K_x = 3.155 \times 10^7$ N/m. Replacing new K_x into ASPRT32 F.E. model data file, we obtained ASPRT34 ----- the F.E. model of the blade K with a lacing wire.

6.7.3 Second ESPI Test on the Blade K and the Summary of Results

After the improvement of the wire locking mechanism, the ESPI test on K blade was carried out again under the guidance of the computer results of ASPRT34.

182

Both experimental and theoretical results were presented in Figure 6.37.

Comparing Figure 6.37 with previous F.E. and ESPI results (Figures 6.31 and 6.36), we found one major difference. Mode 4 and mode 5 exhibit very similar mode shapes and their natural frequencies were very close in the ESPI test. In previous F.E. studies only one mode was found at about 7800Hz. But the ASPRT34 model with new spring stiffness gave two modes with similar mode shapes at 7189Hz and 8782Hz. Great difficulties were met in the ESPI test to identify them since they were only 110Hz apart in frequency.

Classification for modes was rather difficult since mode shapes were largely altered by the lacing wire. The influence of the lacing wire on torsional modes was not very significant if we compare Figure 6.37 with results of unlaced blade K in Figure 5.12. The differences in frequency with laced blade against the unlaced for the 1T mode was 7.4% higher for ESPI results and 1.9% lower for F.E. results, in which centrifugal force was not considered. For the 2T mode at about 10418 Hz, the maximum difference was 3.6%, the rising of natural frequencies of the 1T and the 2T modes was due to the simulated centrifugal force which stiffened up the blade and consequently brought frequencies up, and was because of experimental errors which came from different clamping and excitation at different times of testing.

The first flap mode at 1290Hz (FE, Figure 5.12) of the free standing blade K disappeared in laced case where the first mode at 2539Hz (F.E.) was more like the 1E mode of the unlaced blade. Mode shapes of torsional modes basically remained the same as the lacing wire goes through the area of the blade K where the amplitude of vibration was zero or very small for torsional modes. The second mode at 4170Hz (ESPI) in the laced case appeared like the 2F mode at 4708Hz (ESPI, Fig. 5.12) in the unlaced case but in fact, it was the development of the 1E mode of free standing blade K affected by the lacing wire. To support this argument, different

183

spring stiffnesses were used in the ASPRT34 model and their mode shapes and natural frequencies of the first two modes were illustrated in Figure 6.38.

Figure 6.38 revealed the variation of the 1F and the 1E mode shapes upon the spring stiffness. AS12 was the model without springs and AS45 was the one with calculated stiffness of the lacing wire. Then the spring stiffness of the models in between were increased from zero to 3.0×10^7 N/m. The development of the 1F mode when stiffness increased was that the stationary area (nodal line) at the fixed end of the blade expanded, as the nodal line became wider (AS41 and AS42). Then a nodal line grew out from the stationary area and the mode shape ended up like the one at 2416Hz which was very similar to the 1E mode of AS12. The mode shape of the 1E mode of free standing blade K was the one at 2480Hz. Since the blade was largely twisted, the edgewise displacement at the lower part of the blade caused displacement component in the direction of the flap mode at the upper part of the blade. Hence a tilted nodal line appeared across the width. When the blade was stiffened up, this tilted nodal line moved upwards and was broken from the stationary area at the root of the blade (1E at 2814Hz). The finishing mode shape was the one at 4304Hz.

This variation of mode shapes upon the stiffness of the spring confirmed that mode shapes were closely linked with natural frequencies. The existence of a lacing wire stiffened up the blade hence relevant natural frequencies were raised. At the same time mode shapes developed into the ones associated with those frequencies. The basic format of the mode shape was decided by frequency range (and vice versa). Then the mode shapes were also modified by extra constraints.

Therefore, the first mode at 2539Hz (FE) of the blade K with a lacing wire in Figure 6.37 exhibited a mode shape similar to the 1E mode of the unlaced blade K, as 2539Hz was in the frequency range for the 1E mode of the blade K. It was

184

classified as the 1E mode. The second mode at 4170 Hz (FE) showed the 2F mode shape at 4708 Hz of free-standing blade K in Figure 5.12 and was identified as the 2F mode. It was noticed that the natural frequency of the 2F mode of laced blade K was lower than that of the free-standing one. This was true in this specific case where the lacing wire was connected to the blade 13mm below the tip and was on the central axis. The discussion in Section 6.6.4.1 concluded that the lacing wire might lower the natural frequencies of free-standing blades depending on its location.

6.8 Conclusion

The study into the effects of a lacing wire on a single blade and the vibration characteristics of single laced blade were carried out in this chapter. The FE model of the blade K with a loaded lacing wire was established and justified by experiments using ESPI technique. Modes of vibration of blade K with a loaded lacing wire were identified.

It was found that the relative height of a lacing wire had great effects on the flap modes in their mode shapes and natural frequencies. Employment of a loaded lacing wire to a free standing blade may increase the natural frequency of flap modes or may decrease those of the second and the third flap modes. It may also transform flap modes of a free-standing beam into pinned-fixed modes. When the lacing wire changes its location from the bottom of the blade to the top of the blade, the 1F mode switches into the 2PF mode while the 2F mode switches into the 1PF mode. The frequencies of the two modes change across with each other when the lacing wire is located near the nodal line of the 2F mode.

Coupled modes due to the introduction of a lacing wire with a setting angle were found. When the natural frequency of the 1F mode was raised near that of the

1E mode because of the restraint applied by the lacing wire, the two modes were found to be coupled with each other and both exhibited very similar mode shapes with the 1F and 1E features.

In order to understand mode shapes modified by the loaded lacing wire, the classification of the flap modes were studied and an alternative way of classifying flap modes were suggested. This new definition helped in identifying the flap mode shapes modified by the lacing wire and the trend of variation of mode shapes.

Together with Chapters 4 and 5, the study into single blade vibration has been completed. The investigation is then extended to multi-blade vibration in Chapter 7.
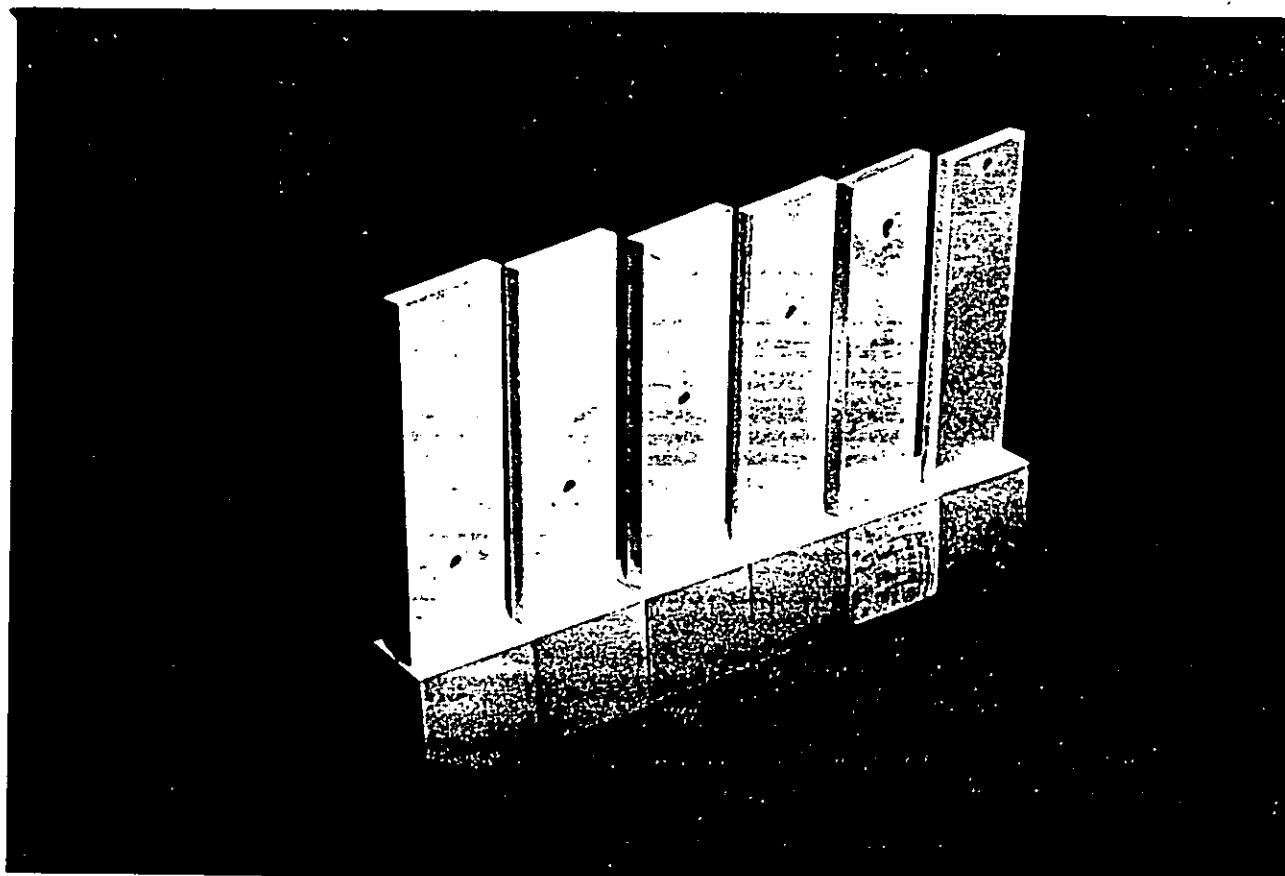
Figure 6.1   Simplified blades with lacing wire holes
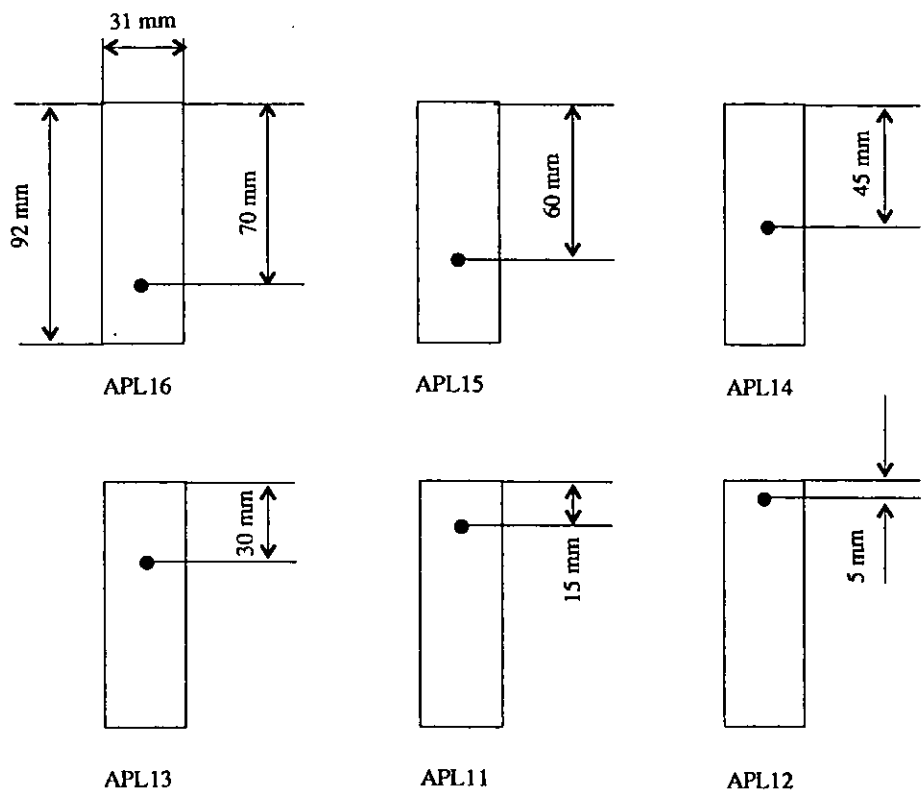
figure 6.2 Simplified blades with the lacing wire hole and their dimensions
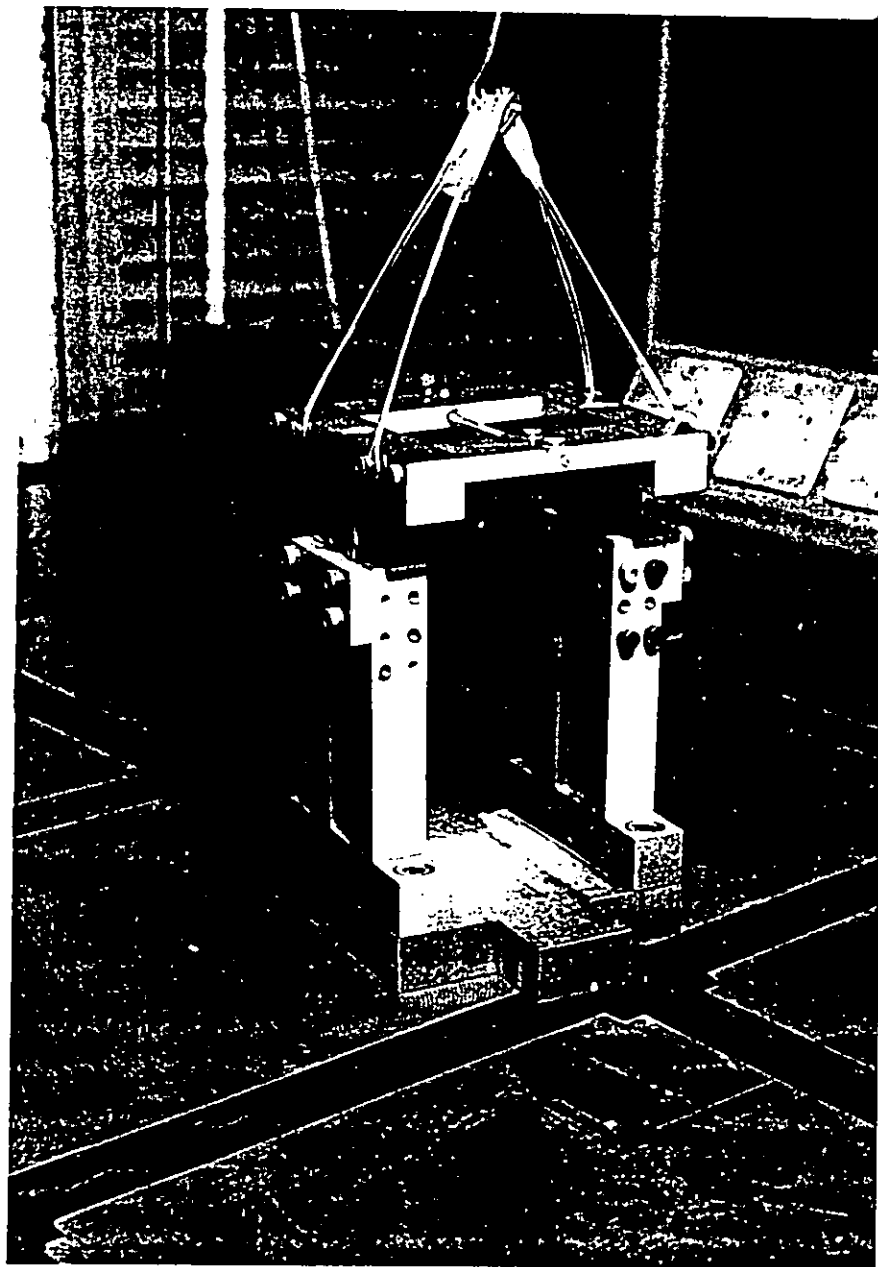
Figure 6.3　　Lacing wire loading rig
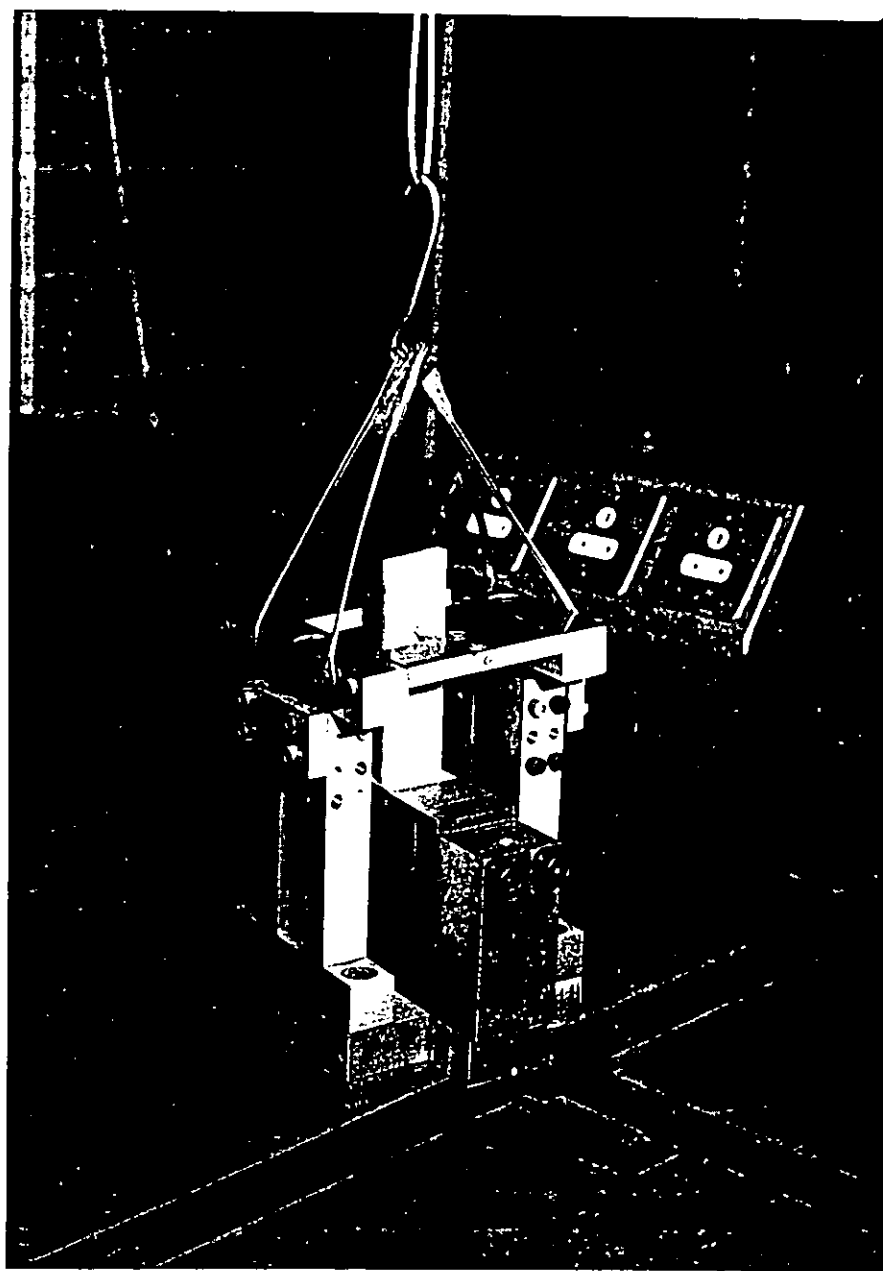
Figure 6.4   A simplified blade with lacing wire
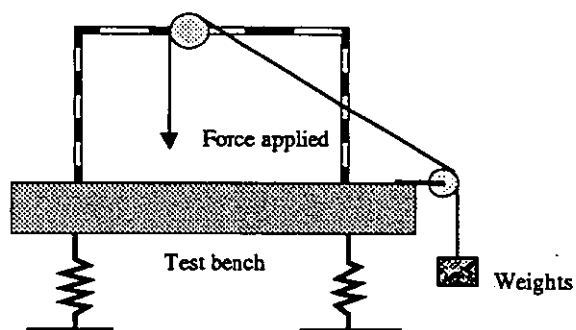
Figure 6.5 The pulley system to apply force to the lacing wire
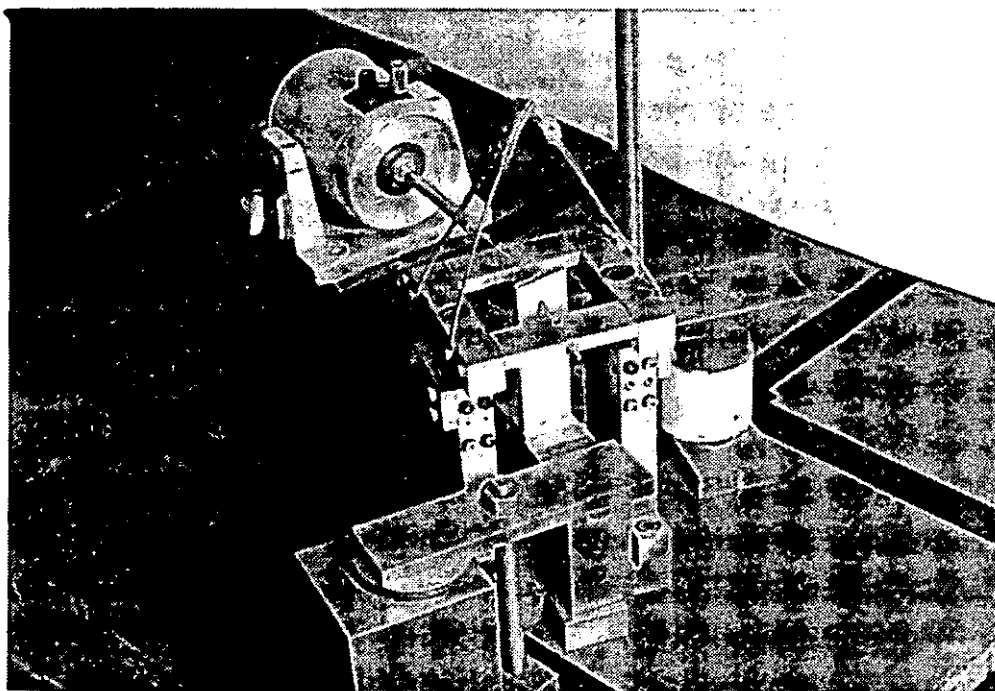
Figure 6.6 Excitation to a simplified blade with a lacing wire

skrew   nut

a) initial design   b) improved design
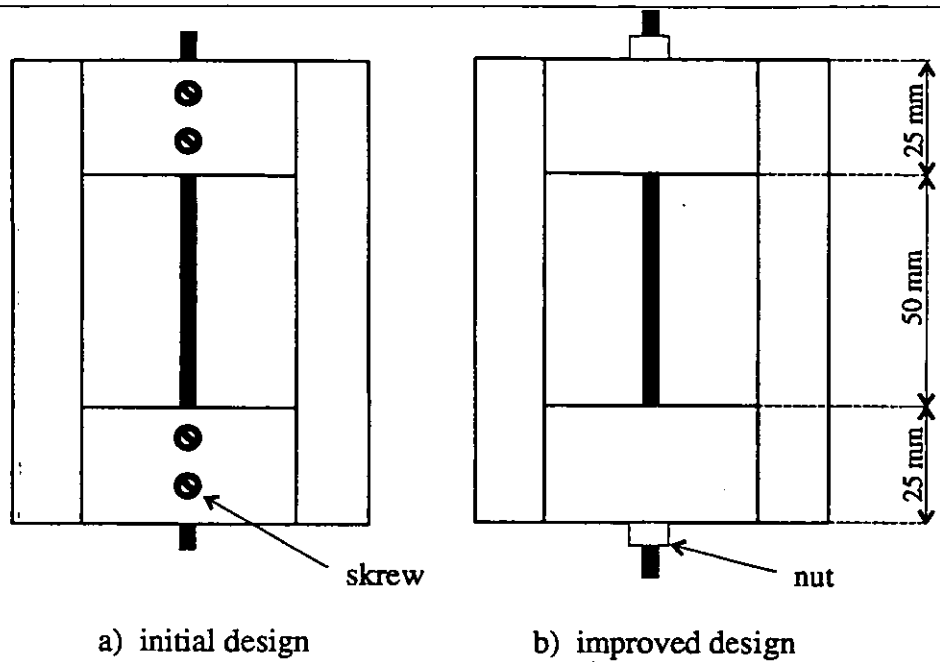
Figure 6.7 Top frame of the lacing wire locking mechanism
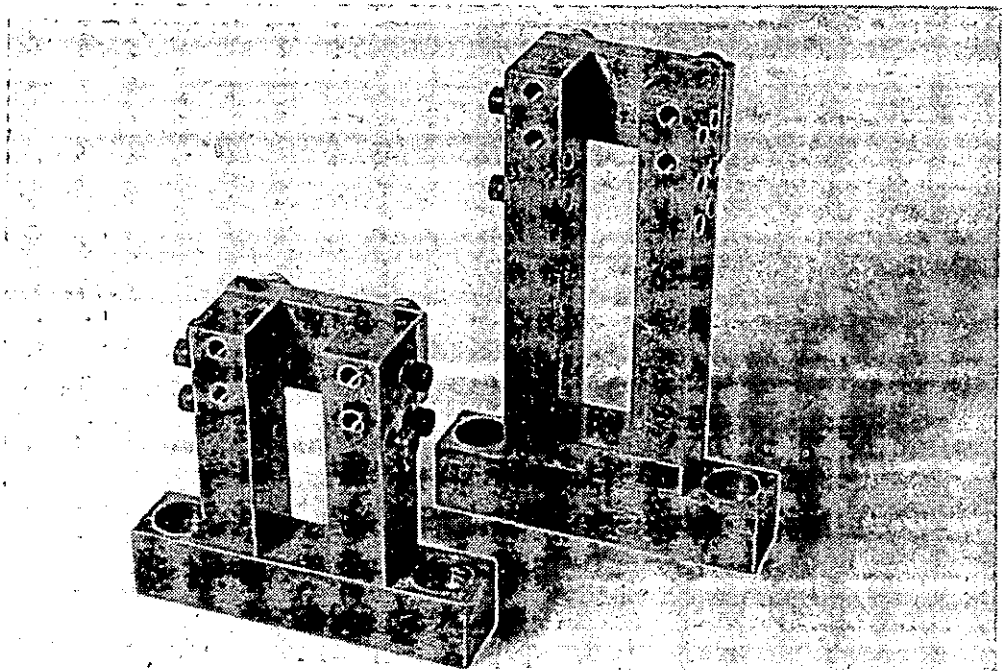
Figure 6.8 Sliding guides used in the lacing wire loading rig
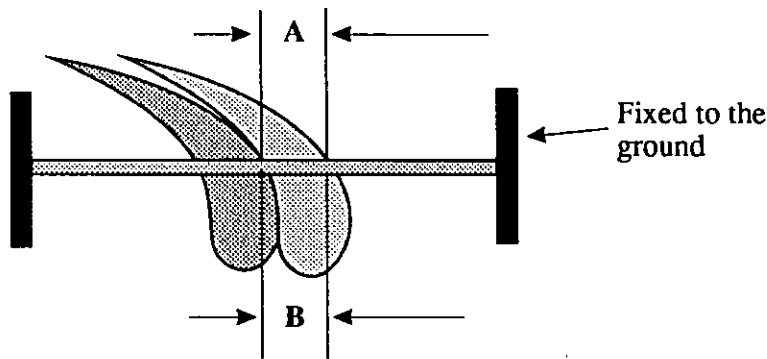
Figure 6.9   Vibration amplitude A and lacing wire deformation B
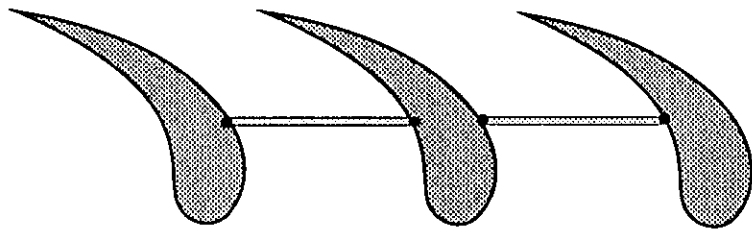
Figure 6.10 Lacing wire considered as hinged segments
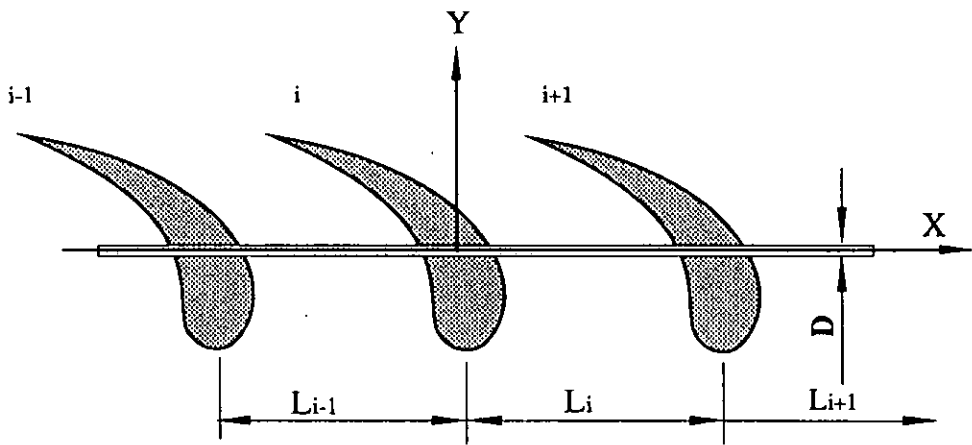
Figure 6.11 Calculation of longitudinal stiffness of the lacing wire
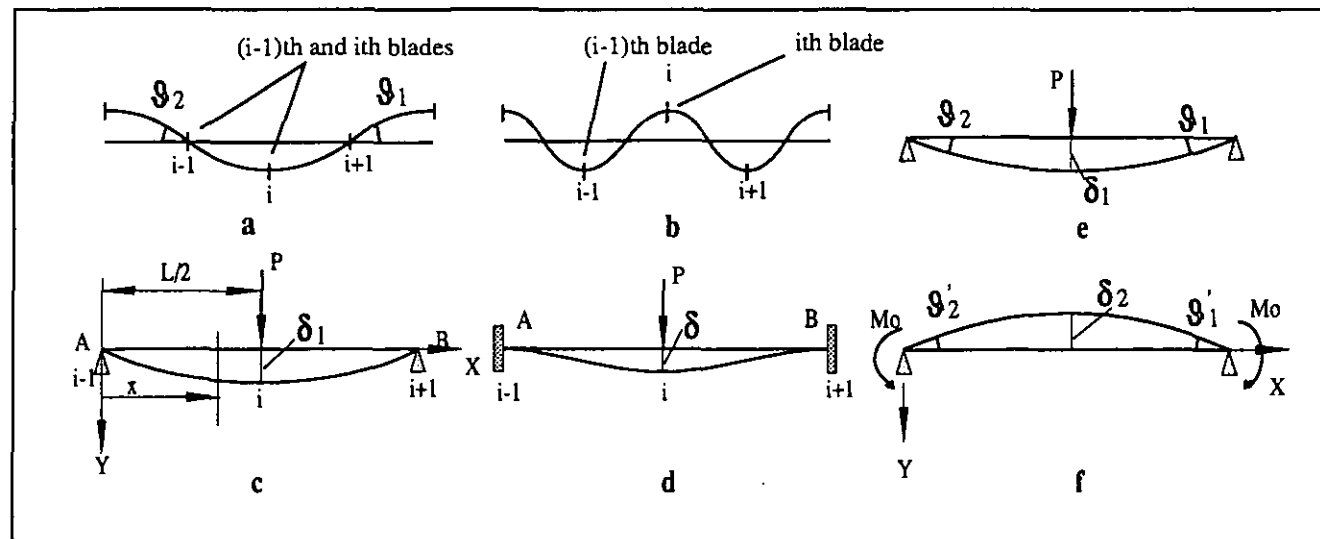
Figure 6.12 Blade phase relations and calculation of lateral stiffness of the lacing wire
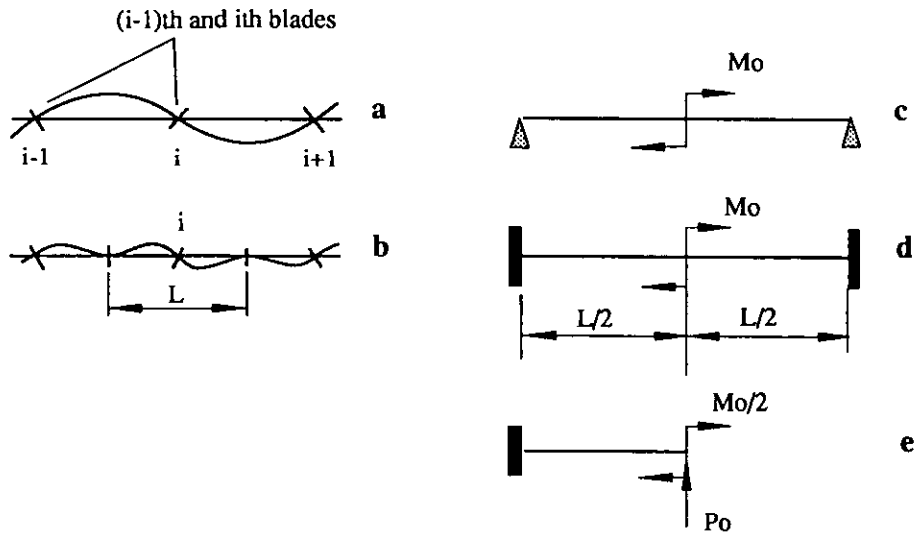
Figure 6.13 Phase relations in torsional mode and the calculation of the torsional stiffness
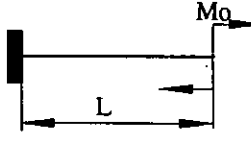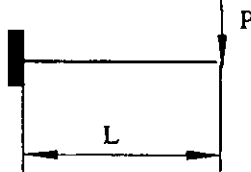
		ϑ_L	δ_L
a		$\dfrac{MoL}{EI}$	$\dfrac{MoL^2}{2EI}$
b		$\dfrac{PoL^2}{2EI}$	$\dfrac{PoL^3}{3EI}$

Figure 6.14 Deformation of a cantilever under Mo and Po
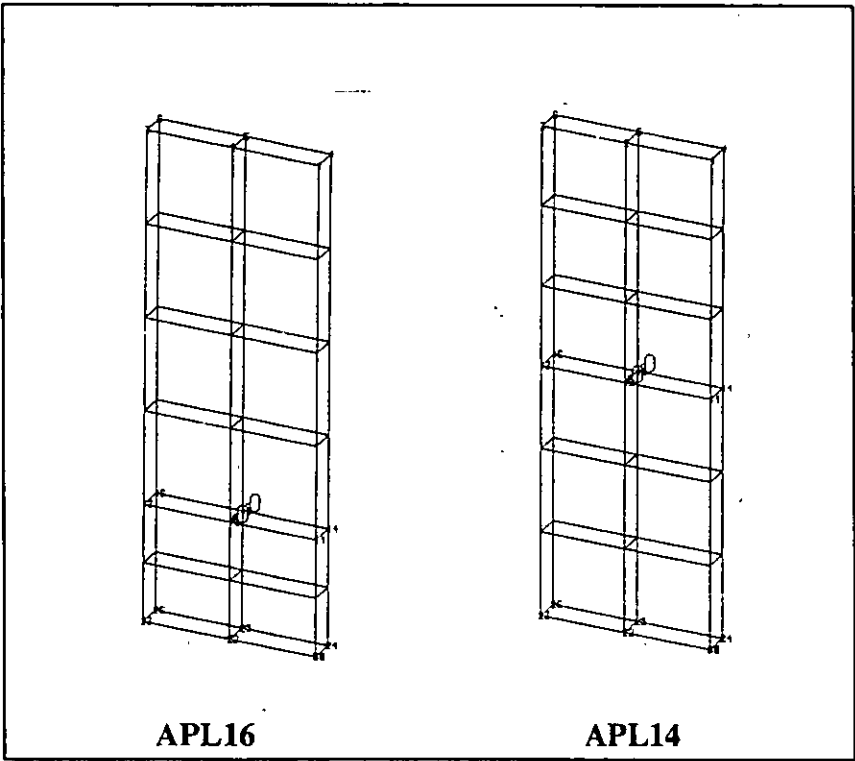
APL16   APL14

Figure 6.15   Finite element models of simplified blades with a lacing wire
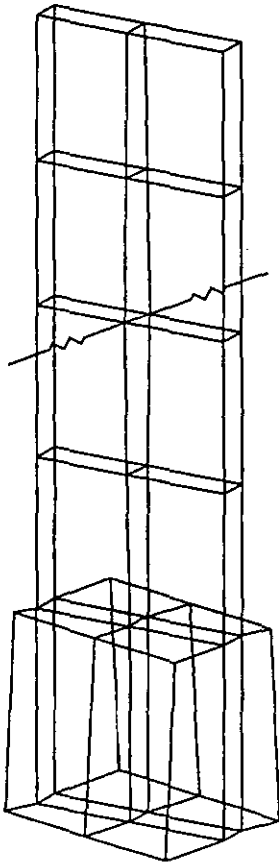
Figure 6.16   Finite element model APL14NB
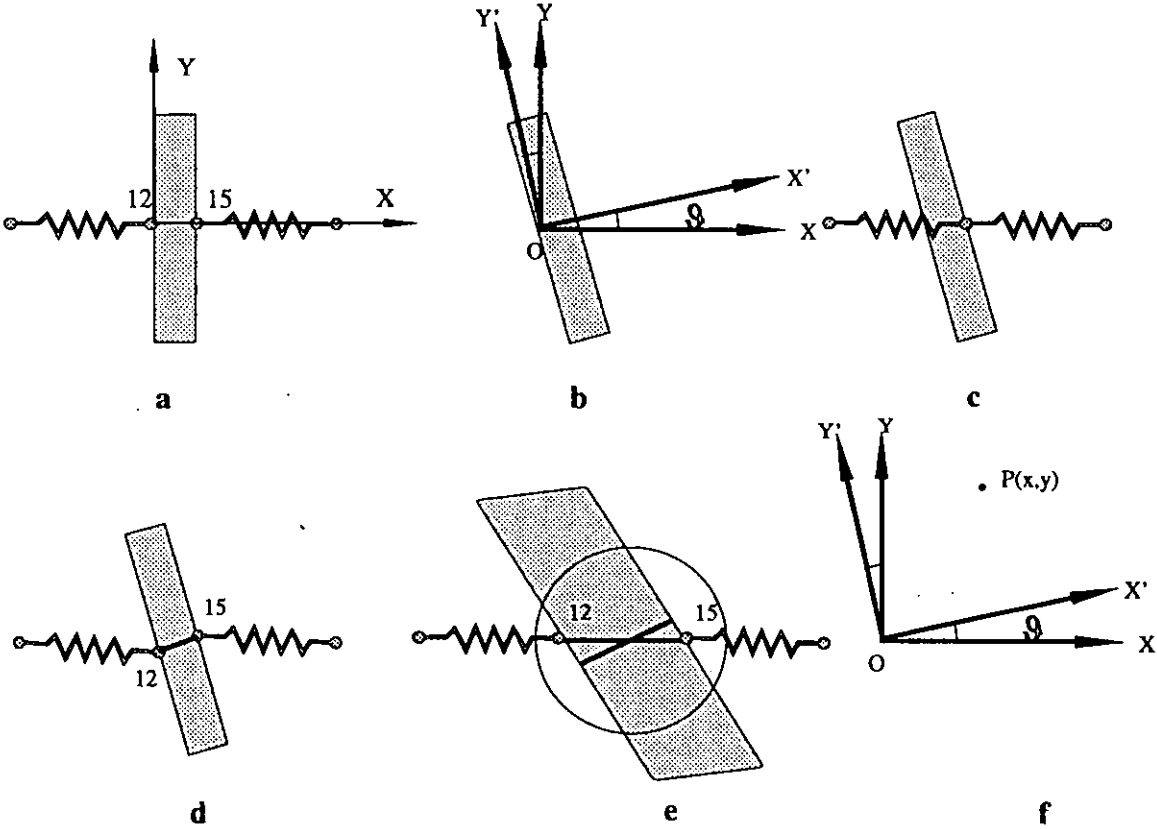
Figure 6.17 The improvement on the FE modelling of lacing wires
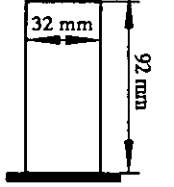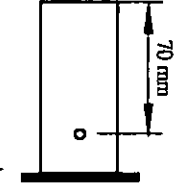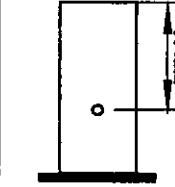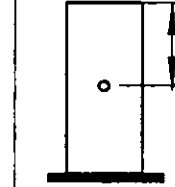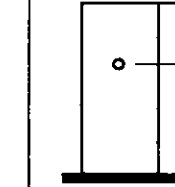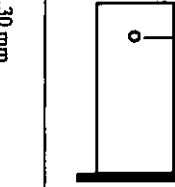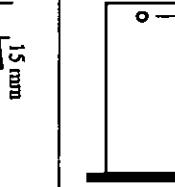
Figure 6.18 Modal patterns and natural frequencies (Hz) of rectangular blades with a lacing wire

199
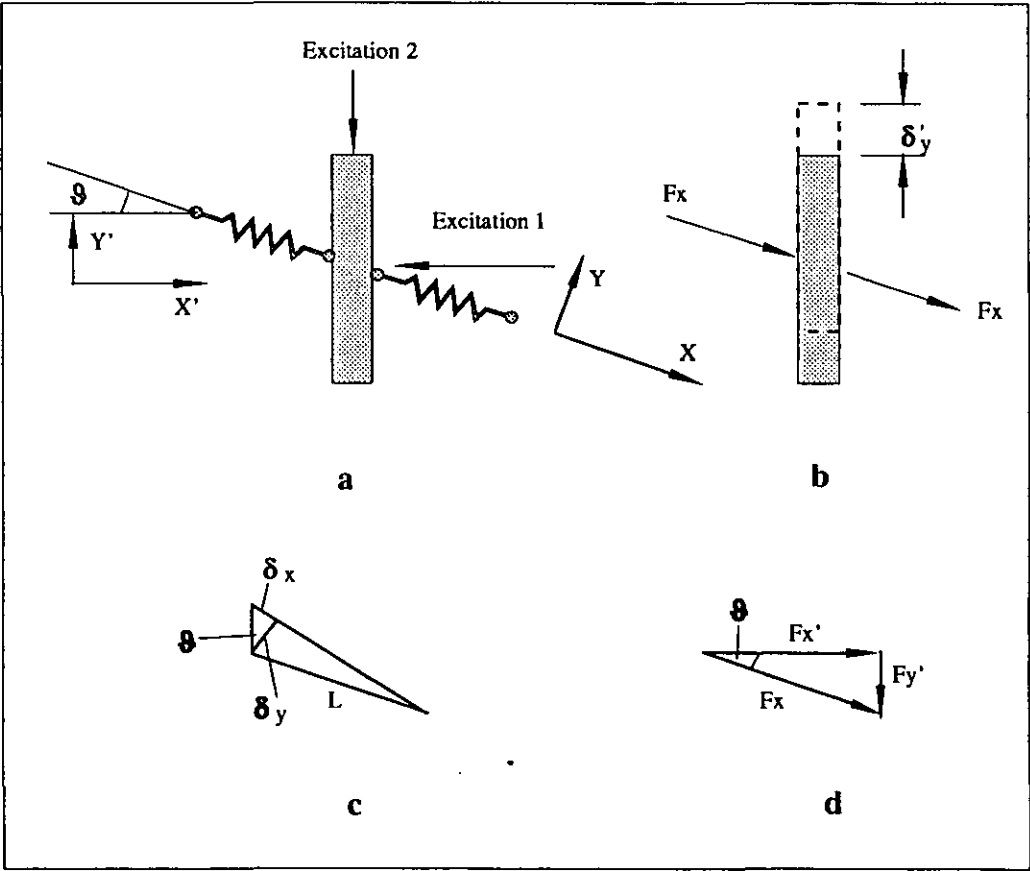
Figure 6.19 Longitudinal force generated by the lacing wire due to edgewise
displacement of the blade
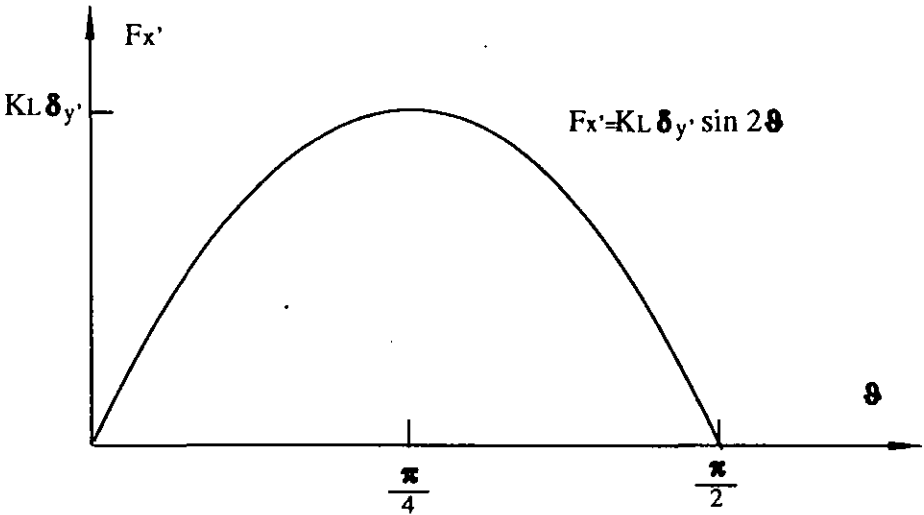
Figure 6.20 Variation of the lacing wire stiffness force Rx' with edgewise displacement $\delta_{y'}$

front view   side view
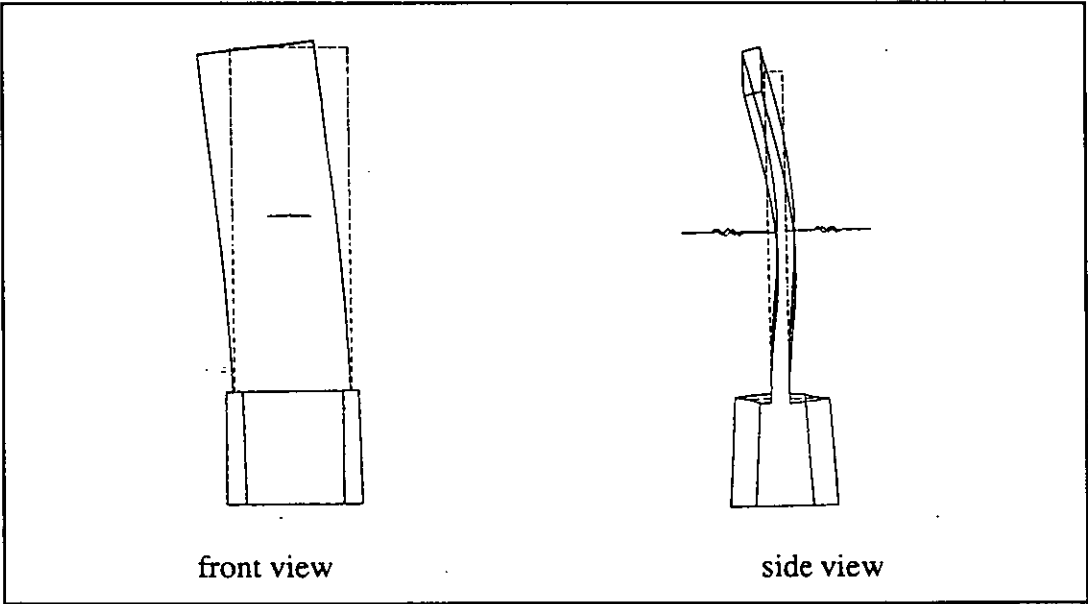
Figure 6.21   1E mode at 2400 Hz of FE model APL14NB

2155 Hz / 1F	2537 Hz / 1E
2877 Hz / 1T	4489 Hz / 2F
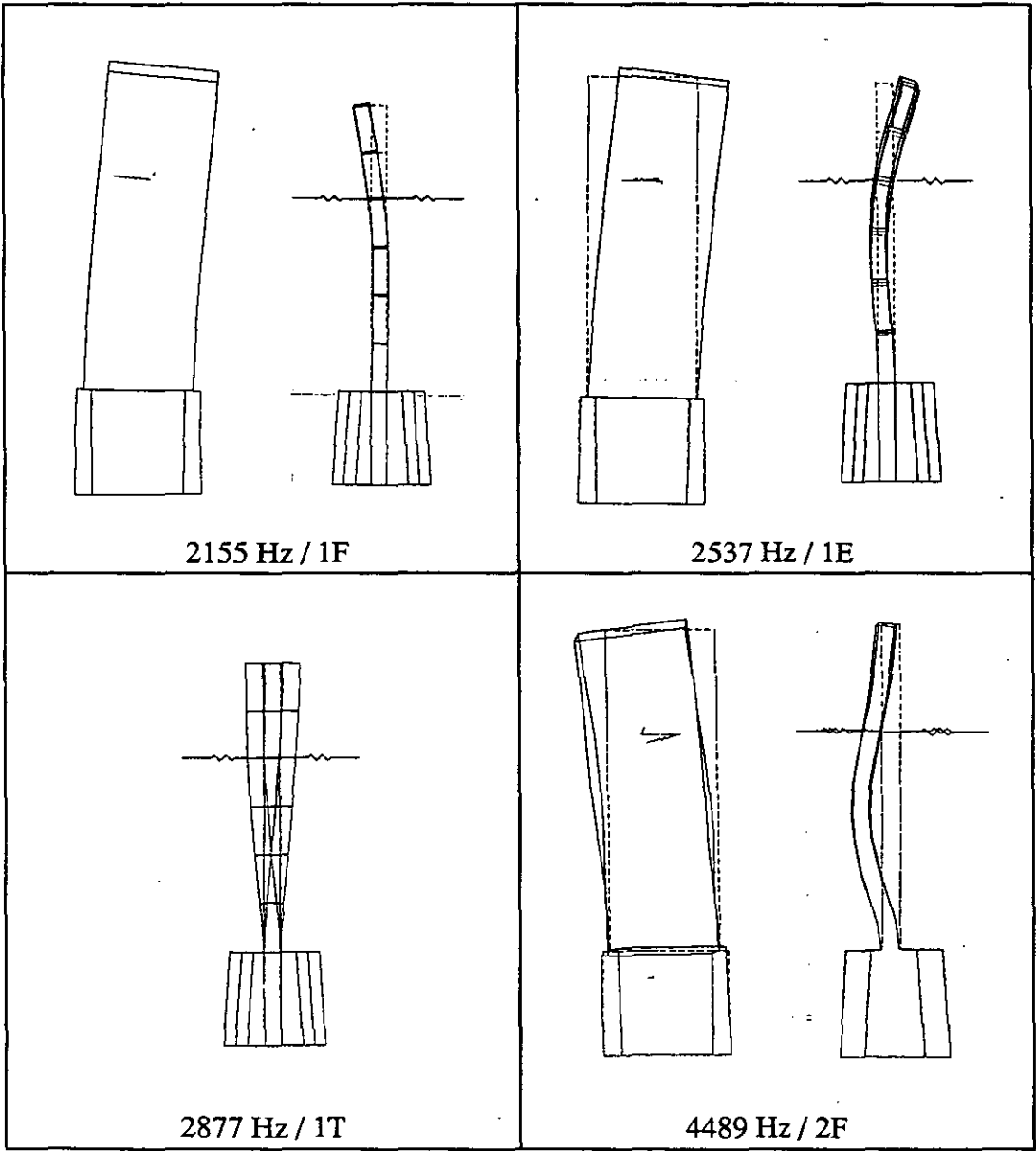
Figure 6.22   First four modes of FE model APL13NB

5517 Hz / 1F	2382 Hz / 1E
2868 Hz / 1T	2897 Hz / 2F
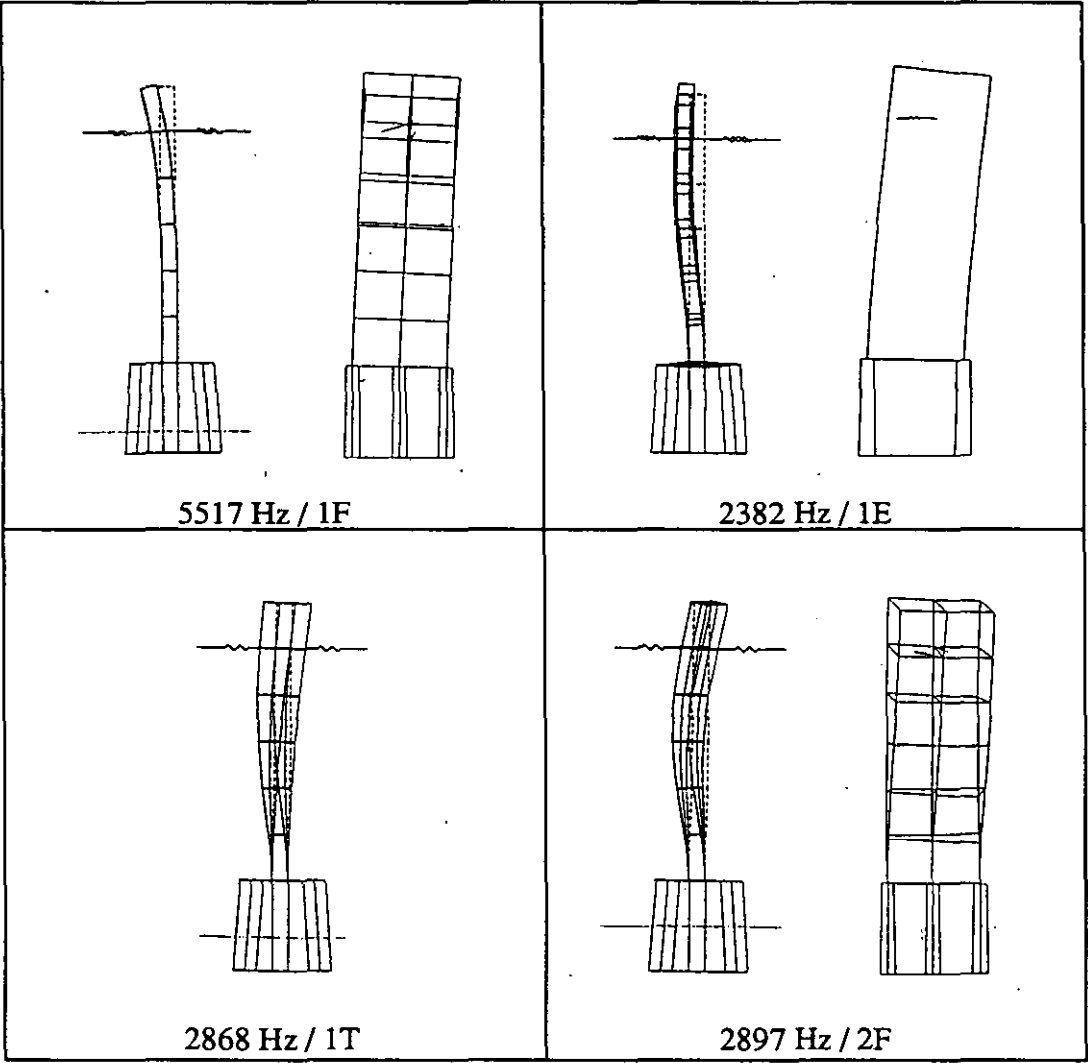
Figure 6.23 First four modes of FE model APL11NB

10103 Hz / 3F

2528 Hz / 1E

2869 Hz / 1T

2243 Hz / 1PF   6662 Hz / 2PF
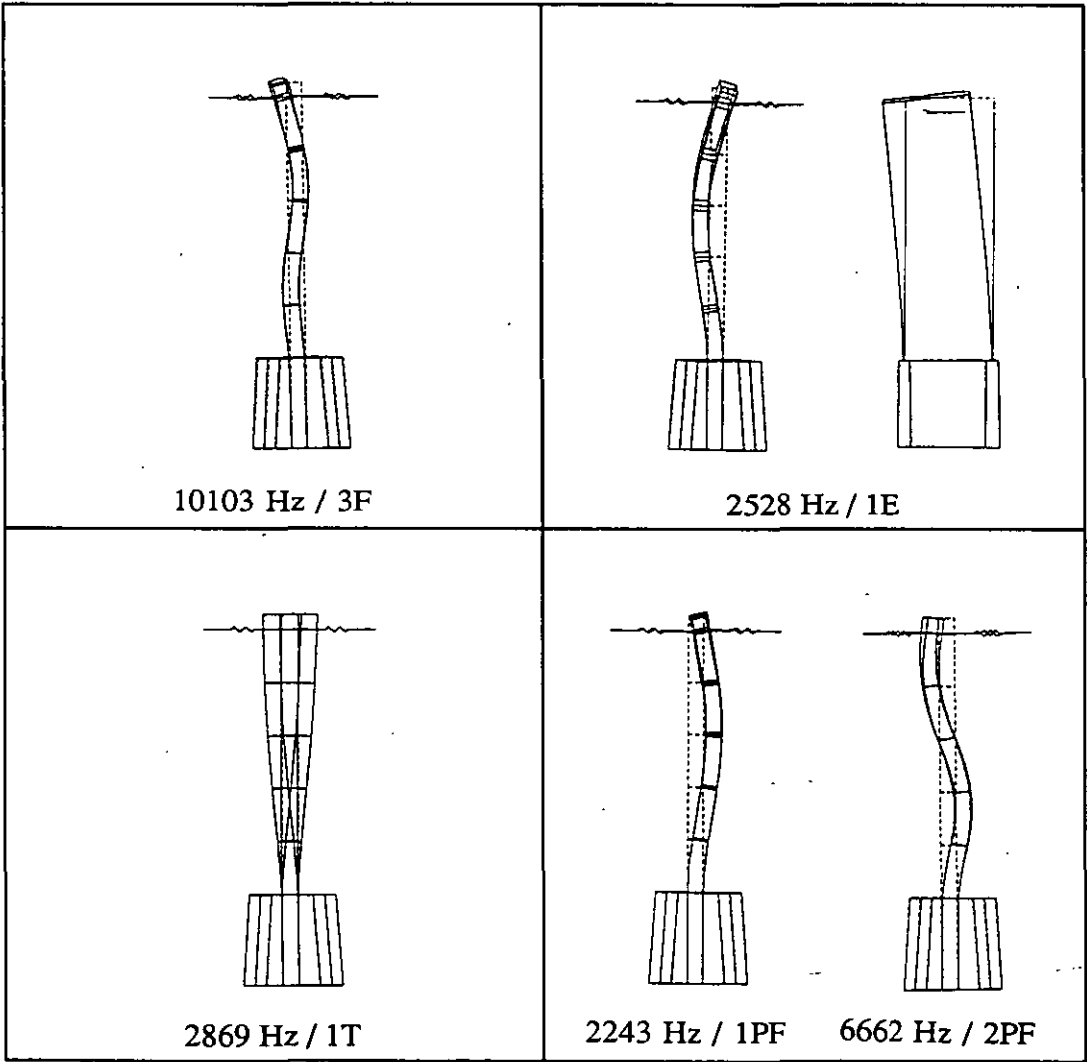
Figure 6.24   Mode shapes of FE model APL12NB

| 493 Hz / 1F | 3028 Hz / 2F | 8247 Hz / 3F |
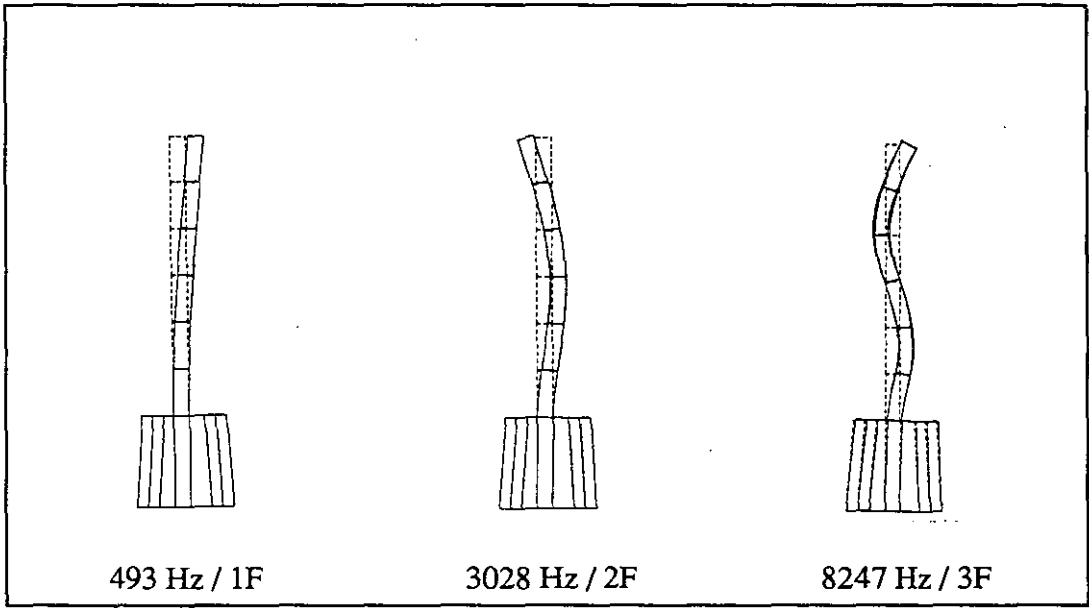
Figure 6.25   Side view of the flap modes of FE model APL1NB

MODE	1	2	3
Free-Fixed			
$(\beta l)^2$	3.52	22.4	61.7
Pinned-Fixed			
$(\beta l)^2$	15.4	50	104

Figure 6.26 Natural frequencies and mode shapes of a uniform beam with free-fixed and pinned-fixed boundary conditions

207
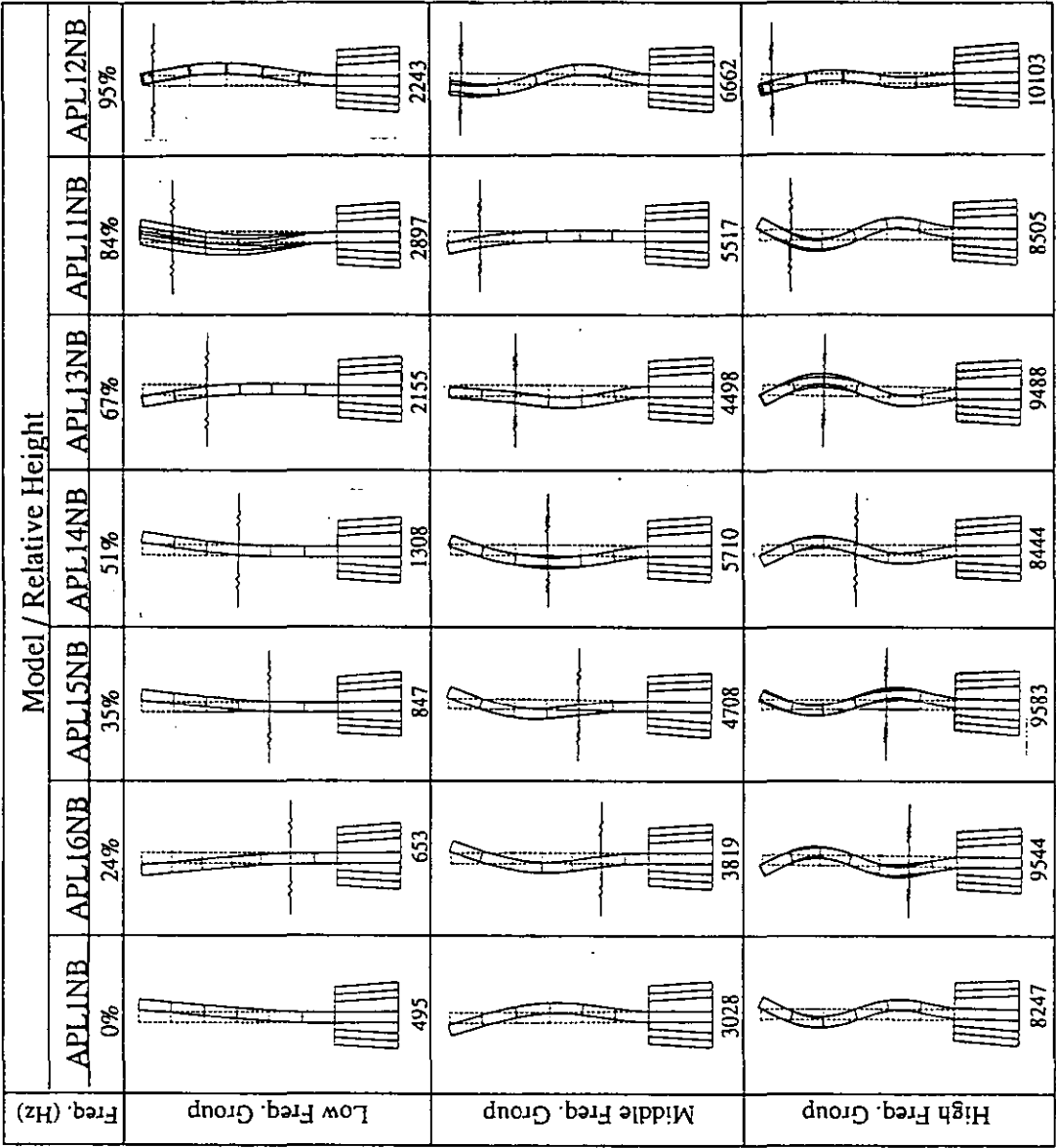
Figure 6.27   The flap modes of simplified blades with a lacing wire at different heights
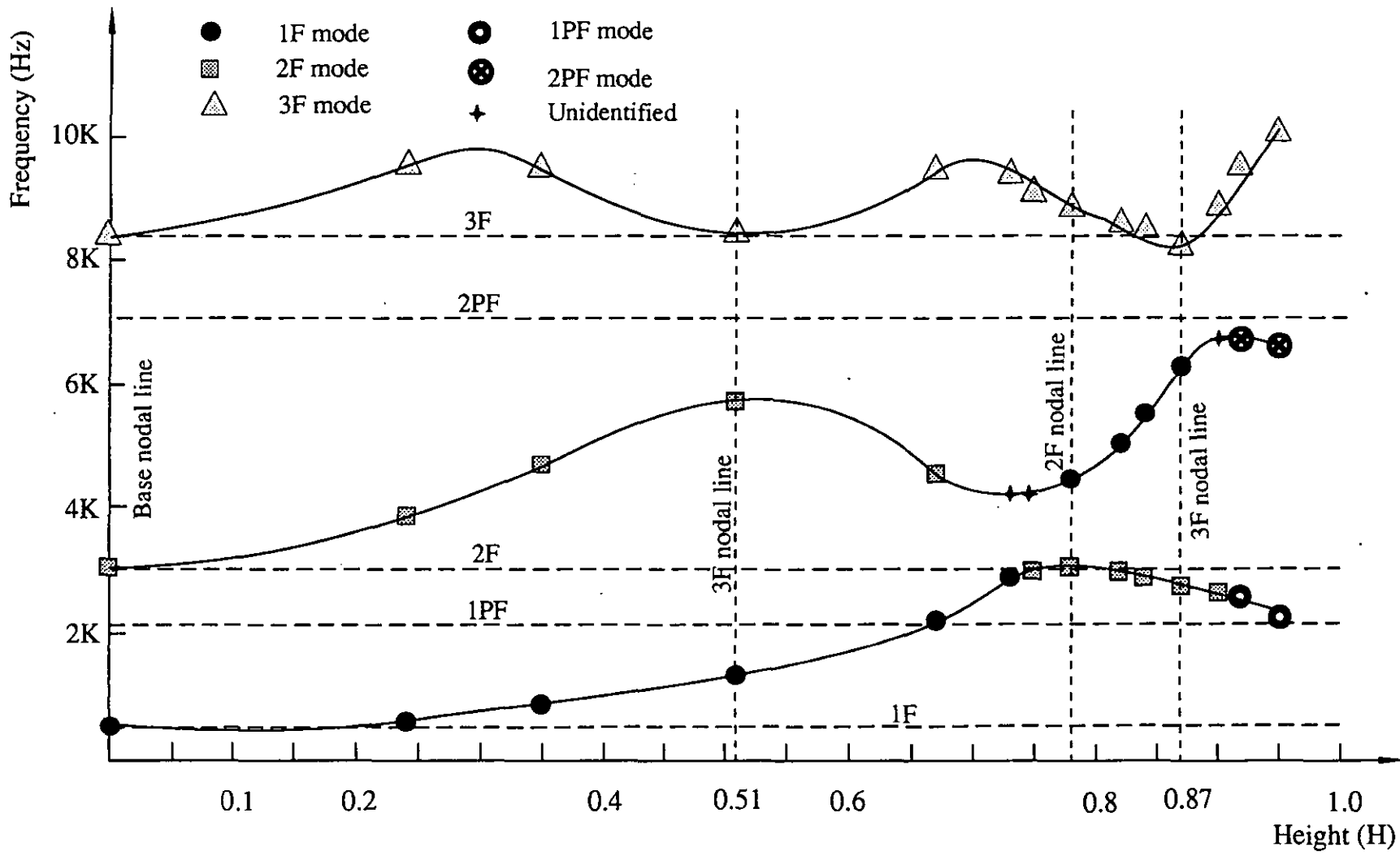
Figure 6.28 The variation of flap modes with the height of the lacing wire
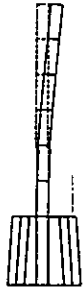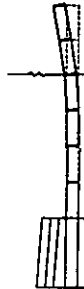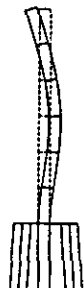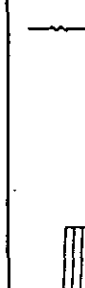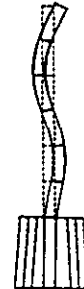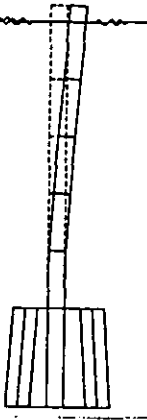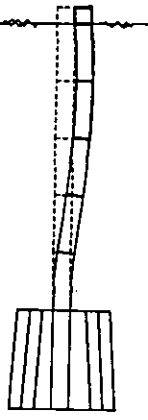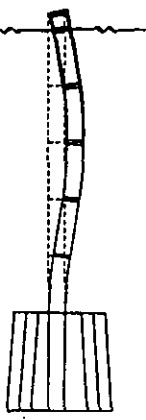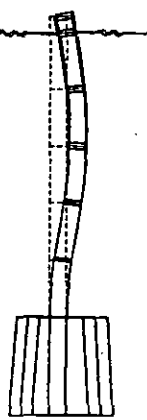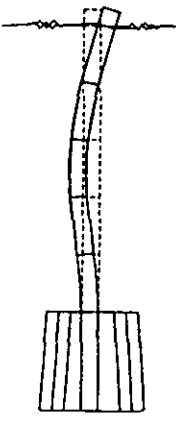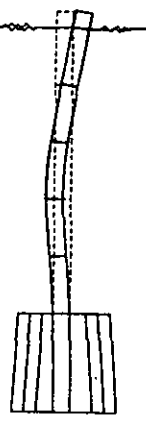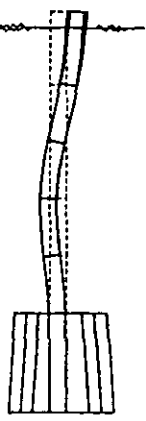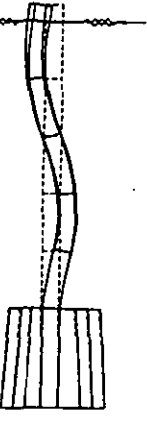
	FE Models and Relative Lacing Wire Height					
	APL1NB	APL14NB	APL13NB	APL10NB	APL8NB	APL12NB
	0%	51%	67%	78%	90%	95%
Freq. /Mode	495/1F	1308 /1F	2155/1F	4470/1F	6750/2PF	6662/2PF
Freq. /Mode	3060/2F	5710/2F	4489/2F	3054/2F	2629/1PF	2243/1PF
Freq. /Mode	8420/3F	8444/3F	9488/3F	8890/3F	8910/3F	10103/3F

Figure 6.29   The effects of the location of the lacing wire on the flap mode shapes
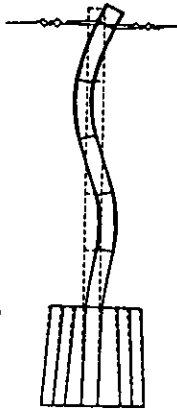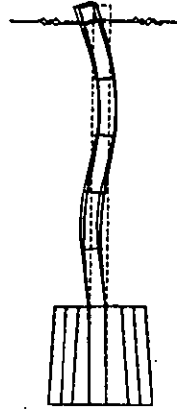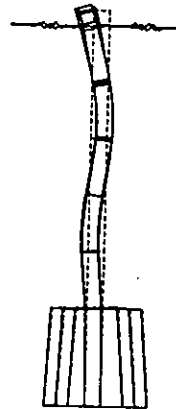
Stiffness / Natural frequency (Hz)			
N/m	2.9×10^5	2.9×10^6	1.5×10^7	2.9×10^7
Hz	813 / 1F	1750	2157	2243 / 1PF
Mode Shape (APL12NB)				

a) The 1F mode changes into the 1PF mode

Stiffness / Natural frequency (Hz)			
N/m	2.9×10^5	7.0×10^6	1.5×10^7	2.9×10^7
Hz	3118 / 2F	4530	5710	6660 / 2PF
Mode Shape (APL12NB)				

b) The 2F mode changes into the 2PF mode

Figure 6.30   Variation of flap modes due to the change of lacing wire stiffnesss

	Stiffness / Natural frequency (Hz)		
N/m	2.95×10^5	1.5×10^7	2.9×10^7
Hz	8540 / 3F	9260	10100 / 3F
Mode Shape (APL12NB)			

c) The 3F mode remains as the 3F mode

Figure 6.30   Variation of flap modes due to the change of lacing wire stiffnesss
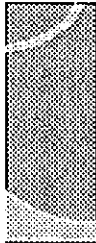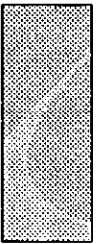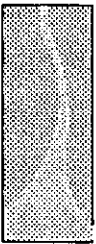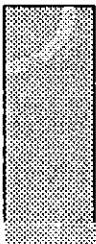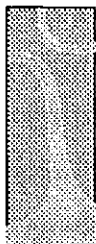
MODE	1	2	3	4	5
ESPI	2369 2542	4022 3934	4910 5017	7763	9954
ASPRT20	2530	4320	4820	7900	10900
ASPRT21	2591	4364	4730	7893	10315

Figure 6.31 Modes of vibration of blade K with loaded lacing wire by initial study
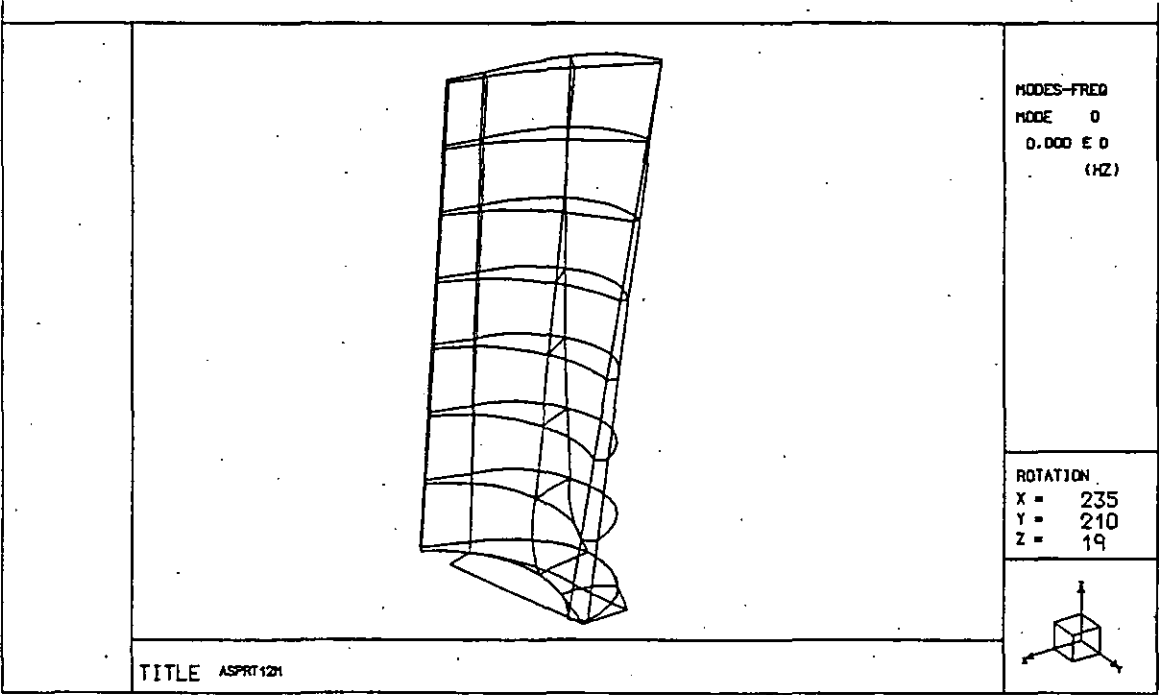
Figure 6.32 FE model ASPRT12 of blade K with root
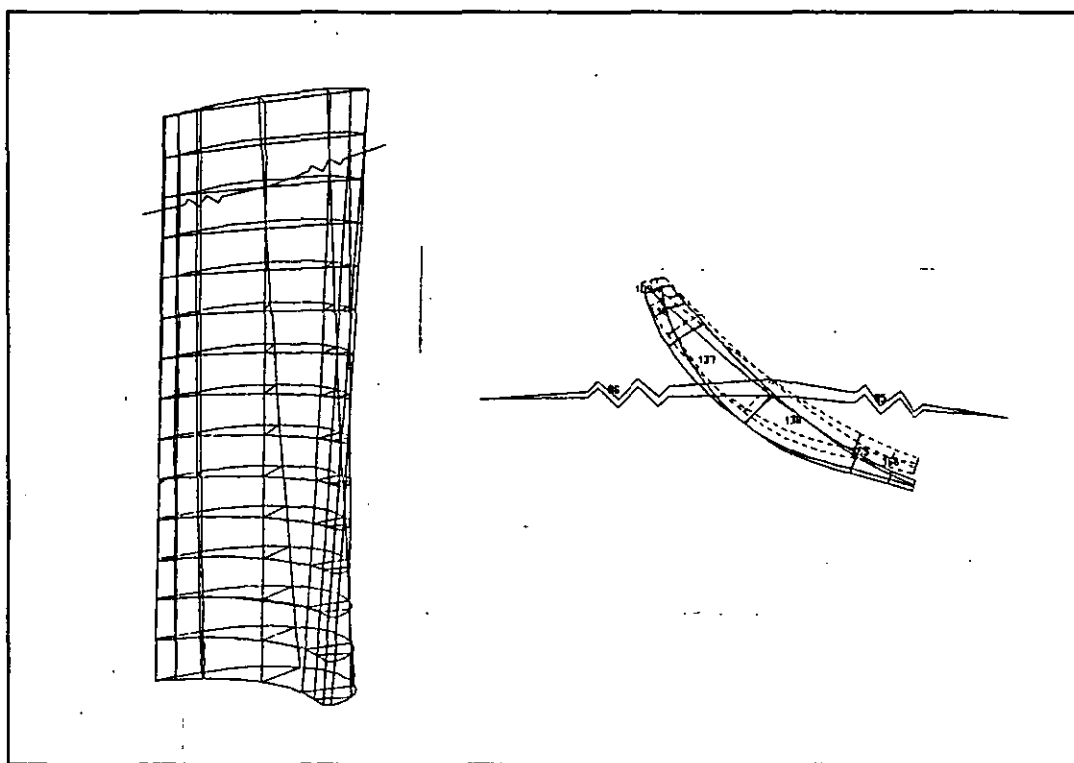
Figure 6.33 Initial FE modelling of lacing wire
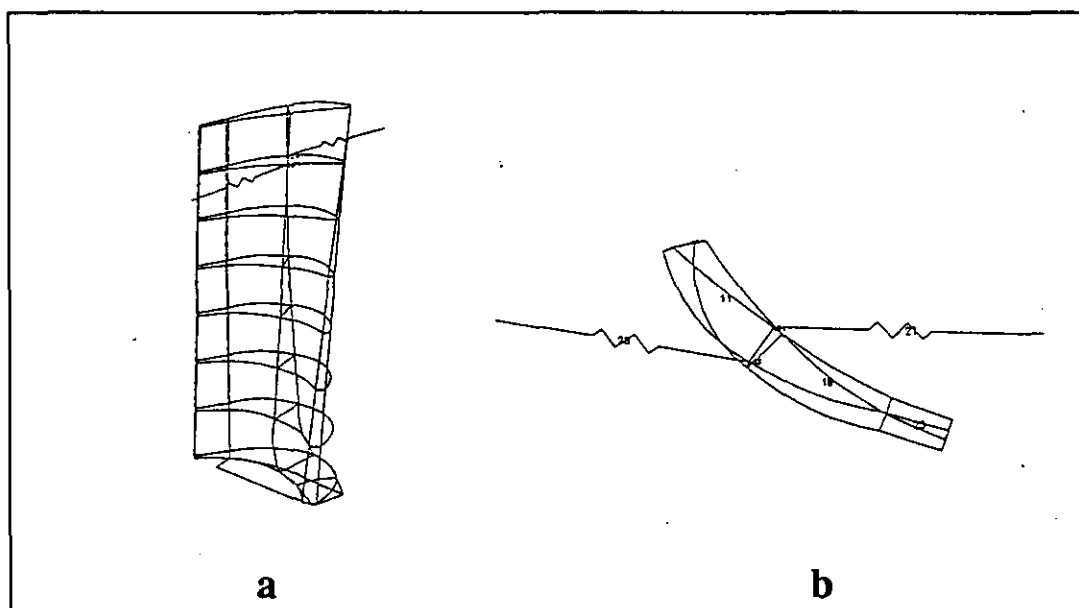
Figure 6.34 FE modelling of lacing wire in model ASPRT21
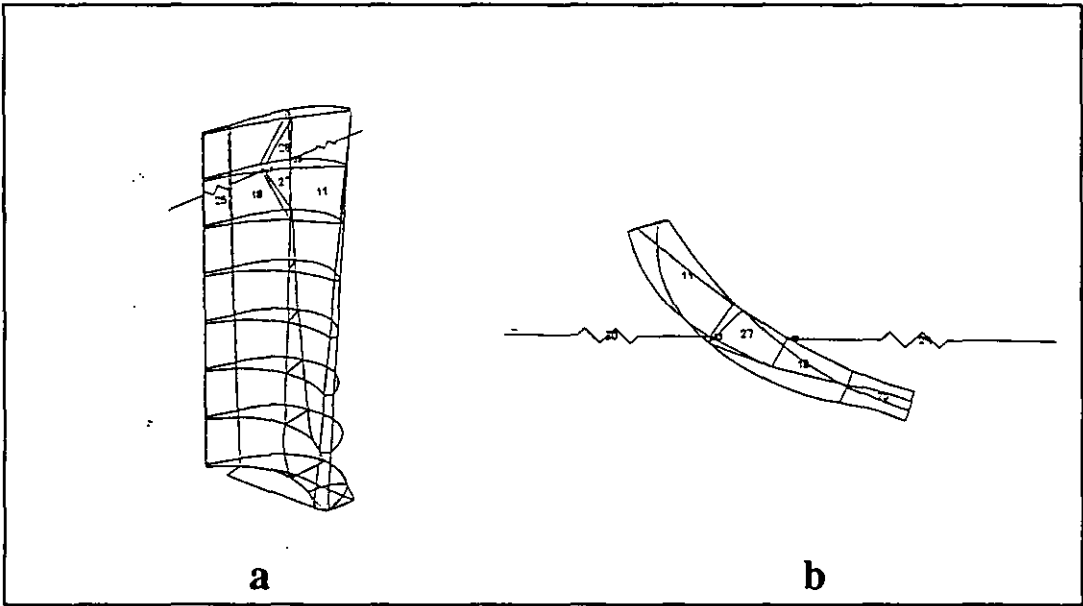
Figure 6.35 ASPRT32, the FE model of blade K with root and lacing wire

10315 Hz

7893 Hz

4370 Hz

4364 Hz

2591 Hz
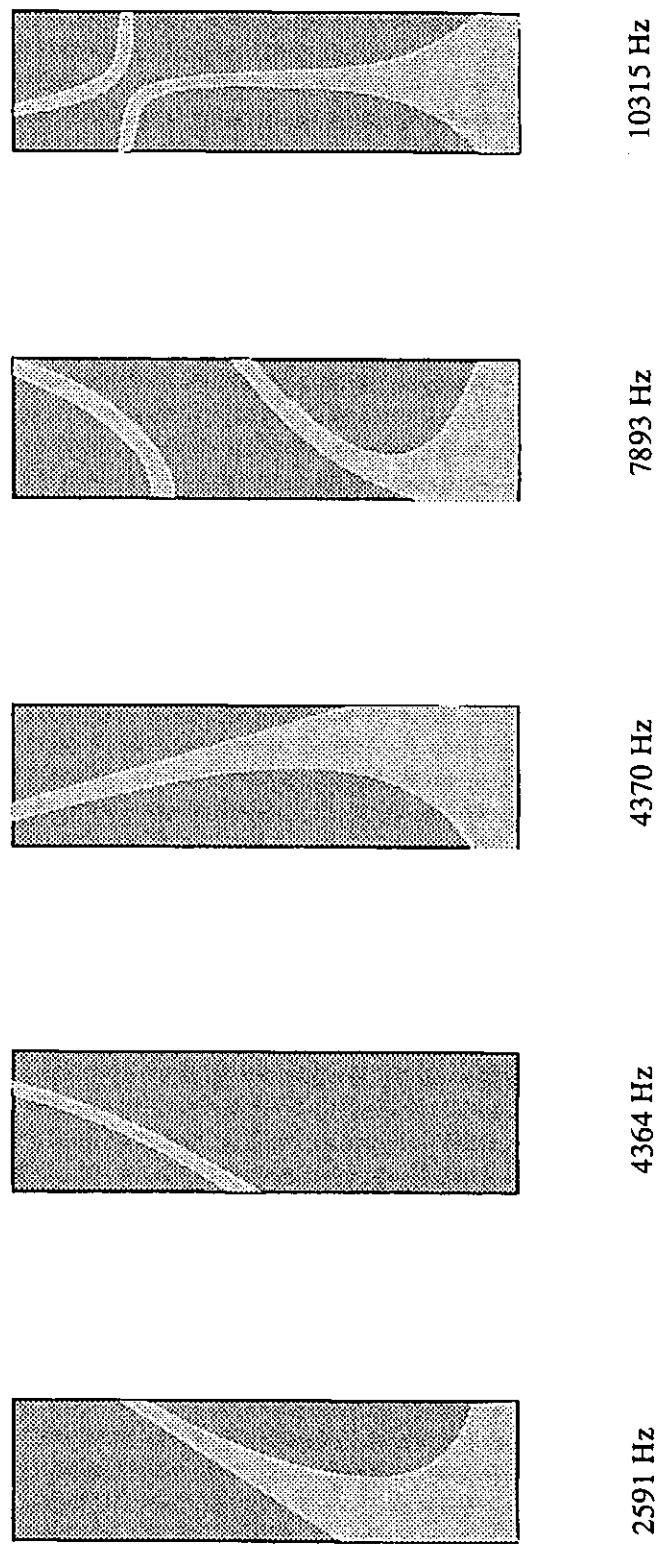
Figure 6.36 The natural frequencies and mode shapes of FE model ASPRT32
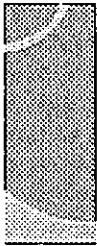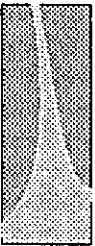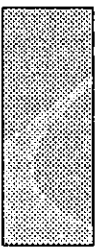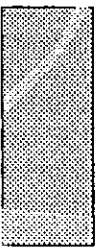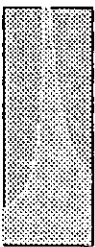
MODE (Hz)	1E	2F	1T	4	5	2T
ESPI						
	2575	4170	4845	7777	7881	10032
FE						
	2539	4181	4618	7189	8782	10418

Figure 6.37 Modal patterns for blade K with a loaded lacing wire
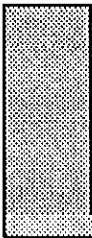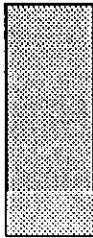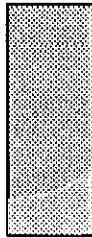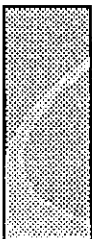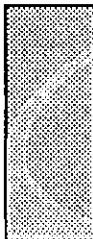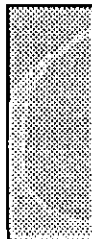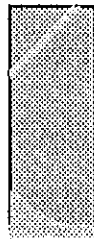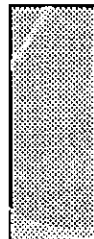
MODEL		AS12	AS41	AS42	AS43	AS44	AS45	AS32
SPRING STIFFNESS	Kx MN/m	0.00	1.34	1.56	3.16	9.60	30.0	67.2
	Ky kN/m	0.00	7.90	8.80	18.7	56.7	177.0	397.0
MODE SHAPE FREQUENCY (Hz)	1F	1220	1914	1991	2302	2421	2416	2581
	1E	2480	2541	2559	2814	3812	4304	4386

Figure 6.38 The effect of lacing wire stiffness on the 1F and 1E modes of blade K

Chapter 7

Study into Laced Bladed Packets

7.1 Introduction

In previous Chapters the vibration characteristics of a single turbocharger blade with and without lacing wire were studied. Its natural frequencies and mode shapes have been identified. Finite Element Models of blade K and other supporting simplified models have been set up. Considerable knowledge of experimental and theoretical techniques used in investigations has been achieved.

However, as indicated by Ewins [57] in 1976, the vibration characteristics of turbomachine blades as measured under operating conditions are usually found to be extremely complex and often quite different from theoretical predictions. The reason for this, firstly, is that the intricate geometry of a blade, which is demanded for aerodynamic performance, makes it a very difficult component to analyse as discussed in previous Chapters. Consequently, predictions for the modes and frequencies of a single cantilevered blade may not always be very accurate. Secondly, it is the existence of multiple interactions between each blade and all the other blades in the same stage, due to coupling through the disk and, often, shrouds or lacing wires linking adjacent blades. Admission of these interactions expands the natural frequencies of the vibration of the assembly into a frequency range, where for a single blade there are only two or three. Since the blades will spend their working lives as components of a complete bladed disk assembly, and not as isolated components, it is clearly necessary to have an understanding of all these assembly modes, and to know what their natural frequencies are.

Finally, it is known that these already complex vibration characteristics (of blades in an assembly) can themselves be markedly affected if all the blades in one stage are not exactly identical to each other but differ very slightly, as they inevitably will in practice.

223

The aim of this chapter is to establish the understanding of vibration characteristics of turbine blade packets linked by lacing wire. Since it is proposed here to consider a complete assembly incorporating many blades, it is clear that some compromise must be made if finite element modelling is to be undertaken. This leads to the concept of a simplified but representative model of a bladed packet, and it is upon this that the present studies are based.

Our primary interest here lies in studying how the blades interact with each other. Hence, we are not specifically interested in the precise details of their aerodynamic profiles since we are not trying to predict their exact mode shapes and frequencies but rather to see how the natural frequencies of a bladed packet relate to those of a single blade. It would seem reasonable to base our studies on blades which have a somewhat simpler profile than the real components (for ease of computation), always provided that they remain dynamically representative of the real thing.

In seeking a suitable simplified model of a bladed packet, it was decided that the following features should be retained by the model:

■   a 3 dimensional blade possessing flap, edgewise and torsional modes;

■   principal axes of the blades staggered with respect to those of the disk;

■   the possibility of coupling between flap and edgewise motion, and between torsion and bending;

■   lacing wire connecting the blades.

Similarly, a number of other features were considered to be of secondary interest to the primary aim of this study, and thus not demanding retention in this model, such as:

224

■   complex blade profiles, serving only aero-dynamic functions;

■   the effects of centrifugal stiffening and high temperatures, both of which influence the exact values of the natural frequencies (as do the complex profiles).

From these considerations, a group of rectangular blades (APL1 type) connected by lacing wire with a setting angle (stagger angle) of 35 degree was provided. Lacing wire threaded through blades and was attached to them in three ways:

a)   lacing wire resting in the holes,

b)   lacing wire was super-glued in the holes and

c)   lacing wire was brazed into the holes.

Both finite element analysis and experiments were carried out. The effects of lacing wire and the vibration behaviour of the bladed packet were studied.

7.2   Finite Element Model of Laced a Bladed Assemblies

7.2.1 Setting Up of AGP F.E. Models

The investigation into bladed assemblies started with F.E. modelling. Again straight rectangular cross section blades (F.E. model APL1) were used to form the multi-blade structure in order to understand the basic characteristics of the packeting without being confused by the complex profile of the blades. The F.E. models of laced bladed assemblies were named as AGP#N, where # represented a serial number. One of the models, AGP14N was plotted in Figure 7.1.

The setting angle α as shown in Fig.7.1 was chosen to be 35 degrees in view of the requirement of the experimental model. The springs were located on the central axis of the blades and were 15mm away from the tip of the blades. The results of the latest improvement in spring-blade connection discussed in Section 6.5.4.3 were used here and it can be seen that springs in different arches are in line. Eight 16-noded brick elements (37130 type) were used for each blade and three spring elements (37100 type) were employed to link these blades together. There was no mass associated with this type of element. The stiffness of the springs, from eq.(6.6), eq(6.16) and eq.(6.19) in Chapter 6, were $K_x = 6.31 \times 10^7$ N/m (longitudinal), $K_y = 3.638 \times 10^5$ N/m (lateral) and $K_t = 303$ Nm/rad (torsional). There were two values for lateral stiffness depending on phase relations of the blades. It was found that they did not make significant differences on mode shapes and natural frequencies, hence eq. (6.16) was used.

The root block was not modelled in this model as this did not affect the blade-wire interaction. However, it was found later that the inclusion of the root block in the FE model was essential because the experimental results revealed that there was much less constraint on the root blocks and they were also more flexible than expected. Therefore they were modelled using three 16-noded brick element in FE models named as AGPB#N, where # denoted a serial number.

7.2.2 Vibration Behaviour of Laced Bladed Packets

The theoretical analysis was carried out on bladed packets with the number of blades ranging from two to ten. The lacing wire was considered as massless spring. When blades were linked up by springs, it was found that many more modes were generated. Further study indicated that assemblies of packaged blades vibrate with all the mode shapes identified for individual blades but produce clusters of natural frequencies for each fundamental mode. Each sub-mode is unique by having

a different phase relation to others in the same cluster. In fact for an N bladed packet, there are N natural frequencies for each fundamental blade frequency. This was also reported in both Bernante et al [16] and Salama and Petyt [160]. The increase in the number of natural frequencies arises as each assembly can exhibit nodal points along its axis resulting in different blades being in phase or out of phase with each other. Among N natural frequencies, the lowest one is associated with in phase vibration, where displacements of all blades are in the same direction, whilst the rest are out of phase.

Figure 7.2 shows a top view of a seven bladed assembly in a typical vibration mode. The blades in the packet exhibited the 1E, 1T and the combination of the two modes. The phase relation is reflected by the S shape of the lacing wire and the variation of the torsional mode shape of the blades. It suggests that the mode shape of the blades in the same packets may be different from each other due to the coupling through lacing wire.

Figure 7.3 illustrates the significance of the nodal points along a nine bladed assembly for all the natural frequencies associated with the fundamental first flap frequency for a single blade.

It can be clearly seen that for this mode the lowest natural frequency is approximately same as the single blade unlaced frequency as all the blades vibrate in unison with no interaction of the lacing wire. However the second natural frequency associated with this mode has a much increased value with half the blades' vibration out of phase with the other half, about a nodal point mid-way along the axis.

To classify these modes a sub-mode classification is developed based on the number of nodal points along the blade assembly. Nodal points represent phase

relationships among the blades, therefore the number of nodal points is unique to each mode in the same cluster. For the nine bladed assembly illustrated in Figure 7.3 the second mode associated with the first flap natural frequency was classified as the 1F-1 mode, as there was only one nodal point along the axis. With 8 nodal points the ninth mode was called 1F-8 while the first mode was named 1F-0 as there was no nodal point associated with this mode. This system of classification works well for all modes so long as no coupling occurs between mode clusters. The example illustrated in Figure 7.2 was therefore the 1T-2 mode for the seven blades system.

7.2.3 Effects of Blade Multiples on Natural Frequencies

Whilst the number of modes was increased for each fundamental mode cluster by the increase of the number of the blades in the assembly, the range of natural frequencies could also be altered in a large scale. This was found especially significant with the first fundamental flap mode. To investigate this phenomenon the chart illustrated in Figure 7.4 was developed for all the natural frequencies for the first flap modes of the assemblies comprising of from two to ten laced blades with the lacing wire located at 84% of the blade height.

In this chart it can be seen that the 1F mode is at 543Hz for the single blade but the second mode (1F-1) of the 1F cluster for the two bladed assembly was found at 7750Hz. In general as the number of blades increases the frequency range covered by each cluster is increased. A similar observation was reported by Salama and Petyt [160].

It was also found from this chart that as the number of blades in the assembly increases the 1F-0 mode remains the same but other modes show a trend of decreasing in their natural frequency for each sub-mode in the cluster. For instance

228

the second natural frequency for a two bladed assembly, when the two blades are vibrating out phase is at 7750Hz whereas the equivalent mode for the nine bladed assembly has a natural frequency of 2081Hz. This is because the effective mass is increased due to the increase of the number of blades but the stiffness of lacing wire is not. Consequently the natural frequency of the same sub-modes decreases whilst the number of blades increases, as natural frequency is inversely proportional to the square root of the effective mass.

In addition, the gaps between natural frequencies in the cluster become narrower as the number of blades increases. In consequence, it was found very difficult to separate the specific modal clusters i.e. 1F, 1E, 1T etc., as their frequencies overlap with each other.

The above findings are also applicable to the 2F and 3F mode clusters and repeat discussions are not necessary.

The effect of blade multiples on natural frequencies is very significant on the 1F mode cluster as discussed above but not that much on other mode clusters such as the T modes and the E mode. Table 7.1 gives all natural frequencies, classified under mode clusters, of AGPB15N which is the F.E. model of the experimental model ASSE1.

Natural Frequencies (Hz) of AGPB15N					
1F	1E	1T	2F	3F	2T
478	1751(1F)	2763	2870	7656	8874
4638	1871(1F)	2765	2891	7665	8852
7465	1943	2770	2900	7682	8882
8838	2199	2774	2939	7757	8918

Table 7.1 Natural frequencies of bladed packet ASSE1 by FE analysis

It shows that the maximum width of the natural frequency bands of mode clusters is 448 Hz except for the 1F cluster. This actually indicates the degree of involvement of the lacing wire in blade vibration. The more the lacing wire is involved in the vibration of a fundamental mode, the bigger the alteration of the natural frequencies of the mode cluster will take place. Out of phase modes of the 1F cluster, i.e. 1F-n, n > 0, directly have lacing wire stretched and compressed, hence the stiffness of lacing wire is actively involved in the assembly. Therefore the natural frequencies are altered according to the number of nodal points along the lacing wire, which is the axis of the assembly. The more the number of nodal points is, and the more stiffness of lacing wire is involved, the higher the natural frequency of the mode in the 1F cluster will be. On the other hand, the natural frequency ranges of other clusters like the 1E and the T modes are not as wide as the 1F cluster since lacing wire is not involved in a great deal in the vibration.

Contrary to the wide frequency band of the 1F cluster, the 2F and 3F clusters show quite narrow band in Table 7.1. The reason is that the lacing wire in AGPB15N model is located at 84% of the blade height. Figure 6.28 reveals that this location is very close to the second nodal line of the 3F mode, hence the involvement of lacing wire in this mode is very limited. It can also be seen that the interfacing of the 2F mode with lacing wire in this region is very little as the result of the wire being close to the 2F nodal line at H = 0.78. This is also the region where the 1PF mode is likely to occur. The lacing wire acts like a hinge in the PF modes with small deformation, hence very weak involvement.

The understanding of the effect of blade multiples offers some basic parameters which give the possibility of controlling the distribution of natural frequencies to design engineers. The variation of the number of blades will change

230

the width of gaps and the location of natural frequencies in the 1F mode cluster. The thickness of the lacing wire decides its stiffness and the latter also has a strong effect on the natural frequencies of some clusters.

7.2.4 Effects of Different Lacing Wire Height on Flap Modes

The effect of lacing wire height on the modes of vibration of a 4 bladed packet was studied using finite element method. The lacing wire was located along the central line at 24%, 35%, 51%, 67%, 78%, 84%, 89% and 95% of the blade height. Following the same definition used for single laced blade and the sub-mode classification for multi-blade modes, modes of vibration were identified and listed together with their natural frequencies in Table 7.3.

In order to assist the discussion about the large amount of data presented in Table 7.3, the natural frequencies of the 1F, 2F and 3F mode clusters are plotted against the height of lacing wire in Figure 7.5 (a), (b) and (c) respectively.

The variation of the frequencies of the 3F cluster in Figure 7.5c is very similar to that of the 3F mode of a single blade shown in Figure 6.28. The frequencies are largely increased if lacing wire is placed away from nodal lines, i.e., near H = 0.2, H = 0.7, especially at the free end, whilst they are very close to the ones of a free-standing blade when lacing wire is located at nodal line positions. It is very interesting that all higher sub-modes converge to the 3F-0 mode at H = 0.84, which is about the position of the second nodal line of the 3F mode of free-standing blade. This confirms that more restraint is introduced into the system if lacing wire is located at positions with large vibration amplitude.

The distribution of sub-modes within each flap mode clusters is clearly demonstrated. The frequency of fundamental sub-modes, i.e., nF-0, n = 1,2,3, vary

231

a little with the height of the lacing wire, because their vibration is in phase hence the involvement of the lacing wire is very weak. The frequencies of higher sub-modes, i.e., nF-m, m > 0 and n = 1,2,3, are generally higher than that of the

RELATIVE LACING WIRE HEIGHT								
Mode	0.24	0.35	0.51	0.67	0.78	0.84	0.89	0.95
1F-0	471	480	476	475	477	478	478	479
1F-1	628	802	1120	3806	4030	4638	5292⊗	5558 2PF-1
1F-2	700	910	1250	5240	6090	7466	7192 2PF-2	6616 2PF-2
1F-3	721	937	1280	5690	6690	8840	7361 2PF-3	6762 2PF-3
2F-0	2950	3050	2906	2993	2926	2939	2963	2977
2F-1	3616	4114	4390	2628	2929	2870	2873	2666
2F-2	4331	5229	6080	2704	2931	2891	2820	2722
2F-3	4607	5647	6630	2722	2927	2990	2843	2759
3F-0	7742	7547	7558	7654	7693	7672	7716	7761
3F-1	8123	7706	7645	8027	7819	7682	7890	8600
3F-2	8711	8009	7954	9000	8289	7758	9160	9800
3F-3	9005	8201	8312	9728	8882	7657	9790	10040

⊗ = a mode shape between the 1F and the 2PF-1 modes

Table 7.3   F.E. prediction of natural frequencies (Hz) of a four-bladed packet with the lacing wire located at different height

fundamental sub-mode (nF-0). Figure 7.5 shows that the increase of the frequencies of higher sub-modes from that of the fundamental one is proportional (may not be

linearly) to the number of nodal point along the lacing wire. The more nodal points in the sub-mode, the larger the increase of the frequency. This is because the stiffness is higher in higher sub-mode vibration.

The variation of frequencies of the 1F and the 2F clusters are also similar to that of a single blade. The frequencies of higher sub-modes in the 2F cluster are significantly increased at about H = 0.5 where large amplitude occurs for the 2F mode. Then they drop sharply and stay very close to the 2F-0 mode in the region H > 0.6. This is the same response as in the case of a single blade where the 2F mode, at H > 0.78, remains in low frequencies and finally transforms into the 1PF mode at H > 0.92, of which the frequency is lower than that of the 2F mode (Figure 6.28). In addition, the springs attached to the blade are fixed to the ground in single blade case and the stiffness of the restraint provided to the free end of the blade is big enough for the 1PF and the 2PF modes to take place. But in multi-bladed system, the lacing wire is attached to blades only and the flexibility of the end blades reduces the stiffness of the restraint provided to the blades by the lacing wire. Therefore, the mode switching does not really take place in the 2F cluster. In the 1F cluster, the frequencies of the two higher sub-modes rise from about 1200 Hz at H = 0.5 to as high as 8900 Hz (1F-3) at H = 0.84 before they transform into the 2PF-2 and 2PF-3 sub-modes and drop back to about 6700 Hz when H > 0.84. The 1F-1 mode rises to 5558 Hz and switches into the 2PF-1 mode at H = 0.95. Unlike the other two higher sub-modes, its frequency does not follow the pattern of rising up and then falling down to the 2PF modes against the increase of the lacing wire height. This is because the stiffness of the lacing wire in the 1F-1 mode is not big enough to raise its frequency higher than that of the 2PF-1 mode when H is smaller than 0.84, but it is enough for the 2PF-1 mode to take place when H is 0.95.

Generally, the effects of the lacing wire height on packeted blades are same as those on a single laced blade. The natural frequencies of the flap mode clusters

can be significantly altered by the position of the lacing wire. Due to different stiffnesses associated with sub-modes in each cluster, the degrees of alteration are also different. The 1F and the 2F clusters transform into the 2PF and the 1PF clusters respectively, when the lacing wire is placed at the free end of the blades.

7.3 Experimental Investigations

Experimental investigations into multi-bladed assembly were carried out to study the interaction between the lacing wire and the blades. The study started from straight cross-section, rectangular blades in order to avoid unnecessary complicated results because of the intricate geometry of turbocharger blades. The experimental model is named ASSE1 which meant the first model of a bladed assembly.

7.3.1 Design Criteria of ASSE1

There were five rectangular blades, at a distance of 25mm from each other, mounted in a holding block with a lacing wire passing through four of the blades leaving one blade standing-by as a reference as shown in Figure 7.6. Every blade was bolted down by two bolts beneath the blade in the blade holding block. Small steel blocks were wedged into gaps between the roots of blades. Then both the roots and wedges were compressed by bolts at two ends of the blade holding block. A setting angle of 35° was introduced to the blades in order that ASSE1 could be properly viewed by ESPI.

The rectangular blade and its root block were machined from one piece of metal. The dimensions of the blade were 91mmx31mmx5mm which were same as those of APL1 model. The lacing wire hole, 3.2mm in diameter, was 15mm away from the top of the blade on the central axis, which was similar to that of the blade

K of which the hole was 13mm away from the top. The design of the root block, with the thickness of 15.9mm, was different from that of the APL1 model as the limited distance between blades and wedging blocks in between blades did not allow thick root blocks. The blade holding block was 210mm long, giving two long shoulders for clamping, 95mm high, giving the blades right height so that they could be viewed by ESPI properly, and 29mm wide. Both blades and blade holding block were made of mild steel.

7.3.2 ESPI Testing on A Group of Cantilevers Linked by the Lacing Wire

The Loading Frame

A loading frame was made in order to apply load to every segment of the lacing wire. Strain gauges were wired to the frame to measure the load applied. The four bladed packet ASSE1 loaded using the loading frame with strain gauge instrumentation is shown in Figure 7.7.

The block holding the blades under the frame is fixed to the testing bench. A piano string loop is hooked on each segment of the lacing wire and fixed on a bolt screwed in the top beam of the frame. The beam is supported by two columns at the two ends. By adjusting the depth of the bolt, tension can be applied to the string and the load can be applied to each lacing wire segment.

Four strain gauges were attached to the top and the bottom of the top beam of the frame, forming a full bridge. The bridge was calibrated against the load and then was used to apply 2100 N force on three segments of the lacing wire. The load was gradually applied into each segment in turn to achieve approximately equal load

on each segment.

Testing

ASSE1 was mounted in front of VIDISPEC with an angle so that a maximum area of the rectangular blades could be viewed. The frequency signal generated by a 3330A automatic synthesizer was amplified and then fed into an electro-magnetic exciter with the capacity of 22 lb excitation force. The excitation was introduced into the assembly via a fine push rod which was pressed onto one of the blades in the assembly. During tests, the excitation frequency was changed manually sweeping through the whole frequency range whilst the modal pattern of the response of the assembly was observed and when necessary, recorded by a reel to reel video recorder for further analysis.

Vibration coupling via the lacing wire was affected by the interaction between the wire and the holes. In this study four ways of connection between the lacing wire and blades were employed to find out their influence on the interaction. They are:

a)   loose lacing wire rested in the holes on rectangular blades without being loaded;

b)   loose lacing wire rested the holes unloaded after being loaded,

c)   the lacing wire was loaded up and

d)   the lacing wire was soldered in the holes without being loaded.

Experiments were carried out on ASSE1 with different connections and monitored

236

natural frequencies were listed under cases B, C, D and E in Table 7.2 (on page 273).

7.4 F.E. Model of ASSE1 --- A Group of Rectangular Cantilevers Linked by the Lacing Wire

To compare the results from ESPI tests on ASSE1 with the finite element prediction, the F.E. model of ASSE1, AGPB15N, was constructed and is shown in Figure 7.8. Same as AGP14N model the blades in AGPB15N were composed of 10 16-noded (37130 type) brick elements.

As discussed in Chapter 6, it was assumed that the friction, between the lacing wire and the holes in blades, resulted from the centrifugal load on the lacing wire when rotating at 18,000 rpm, was considered so big that no slippage took place between the lacing wire and the holes. This assumption was applied to multi- bladed assembly too. Therefore, spring elements of 37100 type were employed to simulate the lacing wire. The stiffness for different degrees of freedom were same as those used in AGP#N models, which were $K_x = 6.31 \times 10^7$ N/m (longitudinal), $K_y = 3.638 \times 10^5$ N/m (lateral) and $K_t = 303$ Nm/rad (torsional). Springs were located 15mm below the top of and on the central axis of the blades.

In ESPI test, the centrifugal force in the blade due to its rotation was not simulated, but a force was applied to the lacing wire in the assembly in order to achieve the friction between the lacing wire and the blade. Therefore, the centrifugal force in blades was not modelled in AGP#N models and the interaction between the lacing wire and the blades was reflected by the modelling of the spring.

7.4.1 Root Modelling

237

It was found very difficult to model the restraint around the root blocks of the blades in ASSE1 as the blocks were separated by wedges in between them and also bolted down onto the holding block.

The initial approach considered that the root blocks were rigidly integrated into the holding block forming a fixed end condition for each blade in the assembly. So blades in AGP#N models were treated as cantilevers with the bottom cross-sections of blades fixed on earth. The natural frequencies of AGP14N, model of a four-bladed assembly, were found higher then those from ESPI tests on ASSE1, which proved that the real system was much more flexible then expected.

The further approach took the root blocks into consideration. The root block of the blades was modelled by 3 brick elements as it was found in the study into the single blade vibration that the root was a very important factor of the structure. The restraint was applied to the bottom plane of the root blocks and the effects of the wedges in between root blocks in the ASSE1 assembly were not considered. The mesh of the model was shown in Figure 7.8.

7.5 Summary of the Analysis on ASSE1

Results obtained from F.E. analysis on ASSE1 together with results obtained from four different ESPI tests are listed in Table 7.2. Analysis are classified under the headings A, B, C, D and E, which are described as follows:

A   F.E. results on AGPB15N. No simulated centrifugal force.

B   ESPI results on ASSE1. Loose wire resting in the holes without being loaded.

C   ESPI results on ASSE1. Loose wire resting in the holes unloaded after being loaded.

D   ESPI results on ASSE1. Loose wire being loaded up.

E   ESPI results on ASSE1. Wire being soldered into the holes without loading.

As it was a 4 bladed assembly, there were generally four sub-modes of vibration found in each mode cluster. Mode clusters were presented in the table by the natural frequencies of their lower and upper boundaries identified by mode classification and number of natural frequencies in the cluster. For instance the 2T mode cluster in case B was found between 8227 Hz and 8473 Hz with four sub-modes in the frequency band. In case of two modes coupled together, identification of coupled modes was given and the number of sub-modes could be more than four in the cluster.

7.5.1 Effects of the Interface between the Lacing Wire and the Blades

Several significant effects of the lacing wire being loaded up and the interface between the lacing wire and the blades were found from the analysis on ASSE1. Firstly, the broadening of the natural frequency band (NFB) of mode clusters of ESPI tests against the F.E. modelling as shown in the Table 7.2 gave the indication of the interface. The NFB of the 1E cluster in case A is narrower than any other relevant NFB in cases from B to E, and the narrowest NFB of 608Hz for the 1T+2F cluster in case D among all ESPI tests is still much wider than the NFB of 176Hz in case A. On the other hand, when the interface was weak, such as at the 2T mode when the lacing wire passed through the relatively stationary area on the blades, the

difference of the width of the NFBs among cases B to E was not significant. The NFB of the 2T mode was found in between 244 Hz (case B) and 178 Hz (case D).

Secondly, intensive mode coupling took place because of the interface. It was found in Table 7.2 that there was no coupling occurring in case A but different degree of coupling was observed in the rest of the cases at the 1T+2F mode clusters. For example, 8 1T+2F sub-modes were found in case C in the NFB between 2753 Hz and 3374 Hz. The 1T and the 2F clusters were well separated in F.E. results though both the 1E and the 2F modes were influenced by the 1T mode.

Apart from broadening the NFB and increasing the coupling of mode clusters, another effect of the interface is the mode splitting phenomenon. Several split modes were presented in Table 7.2. The 1F-1 mode in case C split into two similar modes at 5080Hz and 5742Hz and more than eight natural frequencies were found in the 1T+2F family clusters in cases D and E. As discussed in Section 7.5.5 the mode splitting is resulted from the mistuning and coupling. As an experimental model the blades in ASSE1 was neither designed with great accuracy nor manufactured with great care. Minor differences among blades were expected. Furthermore, the way that the blades were mounted in the assembly, i.e. using wedges in between blades which were bolted down individually, also created differences in boundary conditions to the blades. These mistuning factors meet the condition of mode splitting under excitation and the splitting signifies the coupling between the blades and the lacing wire.

In addition, natural frequencies of some modes went higher as a result of the interface. The typical indication can be found on the 1F-1 mode which is at 5080Hz (5742Hz) in case C, at 6018Hz in case D and at 5033Hz in case E. They are higher than the relevant natural frequency of 4385Hz in case B and 4638Hz in case A.

7.5.2 Effects of the Lacing Wire Being Loaded Up by Simulated Centrifugal Force

The effects of loading were found to be

a)   stiffening up the system and

b)   locking the wire into the blades.

The natural frequencies of the 1F-0 mode at 856Hz, the 1F-1 mode at 6018Hz and the central natural frequency (CNF) of the 1E cluster at 1923Hz, when the system was under loading as shown in Table 7.2 D, were higher than corresponding frequencies of other cases. This revealed that the loading stiffened the system and pushed some natural frequencies higher.

Loading also increased the degree of locking between the wire and the blades. Hence, the degree of the interface was increased. Therefore, the conclusions made on the features resulting from the interface were also true on the loading.

The third important effect of the loading was that the locking resulting from loading remained after the load was removed, if the load was big enough. The photograph in Figure 7.9 recorded the remaining deformation of a lacing wire resulting from the loading of 700 N force upwards on each of the three arches.

The existence of the plastic deformation of the lacing wire makes the interface between the lacing wire and the blades in case C different from that in case B. It can be seen in Table 7.2 B and C that the degree of coupling between the 1T and the 2F clusters increased, the split of the 1F-1 mode took place and the NFB of the 3F cluster was wider in case C compared with case B.

241

Helping to find out the reason of the increased degree of locking, two diagrams are drawn in Figure 7.10 B and C associated with case B and case C respectively. The interface, or the locking in case B comes from the clearance between the lacing wire and the holes on the blades. In addition, misalignment of the holes also contributes to the interface. In case C, plastic deformation took place under the loading and the wire remained bent as shown in Figure 7.10 C. The attachment of the lacing wire to the blades was strengthened by the locking effect arising from the deformation of the lacing wire. Therefore, the degree of locking was increased.

The effect of plastic bending of the lacing wire on the degree of locking suggested that once the bladed disk had gone through the full speed running, the deformation of the lacing wire would not be restored and the vibration characteristics of the assembly should be presented by case C instead of case B plus the effects of loading.

7.5.3 The Effect of the Lacing Wire Being Fully Locked

In comparison of case C, D and E in Table 7.2, it was found that the width of the NFBs in cases C and D were similar. For example, the NFB of the 1E cluster covered 632Hz in case C and covered 711Hz in case D whilst the 1T+2F cluster covered 621Hz in case C and 608Hz in case D. It was also found that the NFB of mode clusters in case E were wider than the relevant ones in cases C and D. For instance the width of the 1E cluster in case E was 1163Hz which was much wider than 771Hz in case D. The same evidence can be found at the 3F cluster.

The above analysis showed that the degree of locking in case E was larger than that in cases C and D when the lacing wire was brazed into the blades. This proved that soldering the wire into blades offered the maximum degree of locking.

242

The connection between the lacing wire and the blades was fully constrained at all degrees of freedom. The analysis also revealed that the degree of locking in case C and case D was very similar to each other. This feature suggested that the locking effect resulting from plastic deformation when the loads were removed was almost same as the one when the lacing wire was loaded up. Therefore, the effect of loading was mainly the increase of certain natural frequencies in case D, instead of changing the width of NFBs in case C.

7.5.4 Nonlinear Stiffness of the Deformed Lacing Wire

The transformation of a straight lacing wire into arched segments between blades has altered its stiffness. There is considerable centrifugal force acting on the lacing wire in rotating bladed packets. The curvature of a deformed lacing wire segment between two blades is affected by their vibration amplitude. It was thought necessary to investigate these factors and their effects on the stiffness of the lacing wire.

The loading condition on one segment of a deformed lacing wire is illustrated in Figure 7.11. The angle between the slope at the ends of the segment and the horizontal reference axis is assumed to remain constant because the centrifugal force acting on the neighbouring segments is the same. The interface between the lacing wire and the blades is considered hinged because the clearance between them allows small rotational motion. This angle should be zero as shown in Figure 7.11a. It can be seen in Figure 7.9 that the deformed lacing wire is very similar to a cosine curve. However, an arch shape segment with non-zero angle at two ends was used in this study, as shown in Figure 7.11b, in order to simplify the analysis.

The aim of this study is to investigate the linearity of the stiffness of the deformed lacing wire, thus it is not necessary to obtain the accurate value of the

stiffness. Although the deflection curves in diagram a and b are different, it was considered that this difference would not change the nature of stiffness, i.e., being linear or nonlinear.

It is considered that the force-displacement relation of the arch shown in Figure 7.11c is nonlinear. The load applied will change the geometry of the arch. The internal bending moment is the function of the geometry. This means that the stress in the beam is the function of the geometry. Therefore, if the change of geometry during loading is taken into account, much more accurate force-displacement relation can be obtained.

Large deformation Finite Element Analysis was chosen to carry out this study. The 10 kN load is applied in 10 steps with 10 iterations in each step. The stiffness matrix is updated in every iteration to account for the geometry change.

One end of the segment is fixed and the other is only free to move in x direction. The segment is 25 mm long and the height of the arch is 5 mm. The lacing wire has a circular cross-section of 3.1 mm diameter. In order to simplify the analysis, a rectangular cross-section as shown in Figure 7.11c was used. Its dimension was chosen to provide the same second moment of area as the circular cross-section. The calculation of equivalent cross-section is given below.

If I_c and I_r are the second moments of area of the circular and the rectangular cross-sections shown in Figure 7.11 respectively, then

$$I_c = [\pi d^4]/64 \text{ and } I_r = [bh^3]/12$$

where d is the diameter of the lacing wire, b and h are the width and the height of the rectangular cross-section. Let them be equal, the dimensions of the rectangular

cross-section have the following relation:

$$bh^3 = [3\pi d^4]/16$$

Given d = 3.1 mm, the equation above becomes

$$bh^3 = 54.40 \text{ (mm4)}$$

If h is 3 mm, the value of b obtained is 2.015 mm. Therefore, h = 3 mm and b = 2 mm are used.

Linear quadrilateral elements in high mesh density are used in order to accommodate large deformation. 20 and 4 elements are used in longitudinal direction and through the depth of the beam respectively to ensure that the elements are not ill-deformed. It was treated as a plane stress problem.

The result of the analysis is given in Table 7.4 and is also plotted in Figure 7.12. The force-displacement relation can be clearly seen to be nonlinear. The change of the stiffness with the load is very significant. Comparing the stiffness at 0.18 mm and -0.2 mm displacement, the deviation found is 13.5%.

This analysis confirms that the longitudinal stiffness of a lacing wire under centrifugal loading is larger in tension than that in compression. Therefore, the lacing wire possesses nonlinear stiffness due to its deformation caused by the centrifugal loading. The effect of the nonlinear stiffness of the lacing wire on the vibration of the bladed packet is discussed in section 7.6.3.

Load kN	Displacement mm	Stiffness kN/mm
-5	-1.56	3.205
-4	-1.11	3.604
-3	-0.747	4.016
-2	-0.442	4.525
-1	-0.208	4.808
0	0	
1	0.180	5.556
2	0.335	5.970
3	0.473	6.343
4	0.594	6.734
5	0.704	7.102
6	0.803	7.472
7	0.894	7.830
8	0.978	8.180
9	1.056	8.523
10	1.129	8.857

Table 7.4 Nonlinear force-displacement relation of the deformed lacing wire

7.5.5 Mistuning

In practice, any group of nominally identical blades will in fact possess small differences. These will be evident as small variations in the various dimensions of the blades and in their fixing and so they may not be readily expressed by a single quantity. The theoretical analysis carried out in this study does not take into account

246

the factor of mistuning but experimental results have indicated its effects.

The blades and their mounting into the holding block in the bladed packets used in this study inevitably possess mistuning because of the way they were manufactured and built. Therefore the effects of mistuning is discussed in this section, largely based on the published information.

It is well-known that the vibration characteristics of a bladed disk assembly may be significantly altered by mistuning. The nature and extent of such alterations from the tuned state are not easy to predict in advance for all categories of mistuned assemblies. As the F.E. analysis in this work was carried out by using the commercial package PAFEC, in which the modelling of mistuning is not available, the effects of mistuning has not been studied theoretically. In this section, the concept of mistuning and its possible effects on the bladed disk assembly is discussed by referencing previous reports by other workers.

For many years now, a lot of research workers in the area of the vibration of bladed disks and designers of advanced turbomachines have given serious thought to the problem termed mistuning or sometimes detuning. The problem is that under certain excitation conditions, the nominally identical blades on a rotor stage do not experience equivalent response amplitudes. Another aspect of the problem is the natural frequency "splitting" phenomenon in which a pair of modes with close natural frequencies and similar characteristics are formed in place of an apparently single mode of vibration in the perfect, or tuned, system. This is contrary to theoretical predictions made on the assumption that all the blades on a stage, having been designed to the same specifications, are practically identical. But in reality, the inevitable small differences among such blades can greatly affect their vibration characteristics when they are coupled together. Thus, although the deviations of blade properties from their nominal values may be small and within tolerance limits,

247

they cannot always be ignored altogether.

Many studies into mistuning problems were reported and the one by Ewins [56] discussed the mode splitting by using receptance coupling at the junction between two connected components, such as the junction between blades and the disk of the bladed disk assembly, which are referenced for the following conclusions.

It has been shown that when the system is detuned by admitting small dimensional variations between one blade and the next, some of the modes split into distinct but similar pairs. In general, a random detuning of the blades will cause all the so-called double modes to split in this way. An interesting feature found in the study into the frequency determinant of a tuned system is a number of "double" or coincident pairs of roots to the frequency equation. This in turn signifies that the system has two modes of vibration at such a frequency. When the blades lose their identity, it is found that the coincident pairs of roots of the tuned case are replaced in this case by pairs of close roots, which explains the mode splitting phenomena.

Exceptions to the regular splitting behaviour were also encountered when two double modes themselves have close natural frequencies. Detuning does not produce the uniform splitting effect for these modes. Only those modes which are separated by a gap which is greater than the frequency split will exhibit an orderly splitting effect.

The effect of some blades suffering excessive amplitude from others under certain excitation because of mistuning is not discussed in this thesis since the research was not focused on the system with excitations.

7.5.6 The Limitation of the F.E. Modelling

Reasonable agreements between results obtained from F.E. modelling and from ESPI testing were found in Table 7.2 A and B, which confirmed that the F.E. model AGPB15N was a close representation of the experimental model ASSE1. The central natural frequency (CNF) of the 1E mode cluster is at 1975Hz in case A whilst it is at 1820Hz, 1852Hz, 1932Hz and 1841Hz in cases B, C, D and E respectively. The difference of the CNF is 6.6% between case A and C which represents the unloaded assembly. The same conclusion could be verified by other clusters such as the 1T+2F and the 3F clusters for which the differences are 6.9% and 1% respectively.

It was also found that the F.E. model AGPB15N was more rigid than the experimental model ASSE1 at some modes. The CNF of the 1E cluster in case A is the highest in all of the cases. This difference reflected the errors in the boundary conditions applied to the F.E. model. In reality, each blade was bolted down at the bottom of the root by two bolts. The distance between the two bolts is smaller than that of the width of the root block. In FE modelling, all degrees of freedom on the bottom plane of the root block were restrained, thus the restraint applied to the edgewise mode was across the whole width of the block. This is certainly a more rigid condition than that in ASSEM1. In addition, at higher frequency range the NFB of the 2T cluster in case A was higher than the 2T NFB in any other cases, which suggested that more elements were required for better modelling of the high frequency modes.

The above discussion revealed that the F.E. model AGPB15N was able to represent the experimental assembly ASSE1. It could provide the mode shapes and the natural frequencies, some of which needed to be modified, of the modes of vibration of its physical model. Furthermore, the techniques used in developing the F.E. model were proved by the good agreement between results obtained from both theoretical and experimental analysis. The same techniques then can be used to build

249

up the F.E. models of the real system.

As centrifugal force was not considered in the programme, some values of calculated natural frequencies were lower, such as those of the 1F mode cluster. The capability of modelling the interface between the lacing wire and the blades within the F.E. package PAFEC was very limited in dynamic analysis. Only linear spring coefficients were employed in the programme as stated in Section 7.2. This limitation greatly constrained the study into the interface by F.E. analysis. Consequently, AGPB15N could not provide information on the effects of locking, such as mode splitting and the broadening of the NFB of some modes.

7.6 Response of Packeted Blades to Excitations

7.6.1 Engine Order Excitation

Probably the most common type of steady excitation of blade vibration is that which is generated by circumferential non-uniformities in the flow of the working fluid [10] and [40]. These non-uniformities, or maldistributions, are the inevitable consequences of necessary obstructions in the flow - bearing support struts, inlet nozzles, combustion chambers etc. - and although the variations which they introduce are static, blades on a rotating disk experience their effects as time-varying dynamic loads at frequencies which are multiples of the rotation speed. For example, a single blocked nozzle passage generates a single pulse which becomes a periodic force with many harmonic components - once per revolution being the fundamental - exerted on the blading.

The total excitation which such non-uniformities exert on a bladed assembly is quite complex, since all the blades are subjected to the some pattern of excitation

forces but at various phase differences owing to their different locations around the disk. Any flow distribution can be considered as the superposition of several sinusoidal components. It may be shown that each such sinusoidal component of excitation will be seen by the blades at a different frequency - a $\cos(n\theta)$ variation being felt as fluctuations at n times the rotation speed - and this we refer to as an nth engine order excitation (or nEO). Since the different components of an actual non-uniformity excite at different frequencies, we may conveniently consider just one at a time.

7.6.2 Bladed Packet Vibration Responses

Possible resonance responses of blades to engine order (EO) excitations can be predicted using Campbell Diagrams, in which the natural frequencies of the blades concerned are plotted against the rotating speed of the bladed disk with EO excitations. The same technique may be used to study the response of a bladed packet to engine order excitations as the packet may be considered as part of a bladed disk assembly. To investigate the response of bladed packets, the Campbell diagram of a four bladed packet with the lacing wire at 89% of blade height was plotted in Figure 7.13 using the FE results listed in Table 7.3.

Natural frequencies of the flap modes (including the pinned-fixed modes), edge mode and torsional modes are plotted in the diagram. Possible resonances are indicated when engine order excitations coincide with the natural frequencies of the packet.

However, the study on the mode shapes of mode clusters of bladed packets reveals that nodal points are exhibited along the lacing wire. This means that, in order for a particular sub-mode to be excited into resonance, not only the frequency of the excitation has to be close to the natural frequency of the sub-mode, but also

251

the spatial pattern of the excitation contains a component of the mode shape of the sub-mode. For instance, the resonance of the 1F-2 mode of a four bladed packet will occur if the engine order excitation varies twice in the span of the packet width. Therefore, not all of the modes will be excited.

The above conclusion can be extended to bladed disk assemblies, in which the blades may be linked into several packets by shrouds or lacing wires. In this case, the nodal points along the lacing wire are reflected by the number of nodal diameters of the disk modes. An nEO excitation will excite a mode of bladed assembly into resonance only if that mode has a component of n-nodal diameters in its mode shape. Resonance will then occur at a speed Ω_n, which is given by $\Omega_n = f_0/n$, where f_0 is the natural frequency (cycle per minute) of the mode in question. The implications of this rule for a tuned system are that each mode of the assembly can only be excited into resonance by one particular engine order. For example, the 4-diameter mode can only be excited if there is a $\cos 4\theta$ component in the 'shape' of the excitation source. Similarly, a given engine order excitation will produce no response in a non-compatible mode, even when the frequency of its excitation ($n\Omega_n$) corresponds exactly with the natural frequency of that mode.

Engine order excitations are proportional to the number of nozzles in turbomachines and it is not uncommon to find more than 10 nozzles in turbochargers. This suggests that the number of EO excitations can be very high. On the other hand, the number of the modes of vibration will increase with the number of the blades in each packet, which in most cases is more than ten. Therefore, even having considered the rule discussed above, it must be said that a resonance free speed zone in the case of rotating blades bound into packets, by shrouds or lacing wires, cannot be achieved [198]. Hence, the bladed packets must be able to operate under resonant conditions. The reduction of vibration stress using damping elements such as lacing wires is confirmed from many operating machines.

7.6.3 Control of Blade Vibration Responses by Lacing Wires in Rotating Bladed Packets

Having established the vibration characteristics of bladed packets, the effects of lacing wires and resonant responses of bladed packets to major excitations, the control of blade vibration responses by lacing wires is better understood.

The control of dynamic stress at resonance is not the subject of this study but relative reports could be found. Wachter et al [198] measured the vibration amplitudes at resonances of low pressure runner blades on an industrial turbine with and without lacing wires in position. The maximum dynamic stress with lacing wires in position was found 55% less compared to that of the free standing blades despite that they were measured under different running speed. The achieved reduction in dynamic stress was as high as 80% compared to that of resonances at about the same speed. For three blades from a first stage turbine of a 6000 to 7000 hp unity, Chubb [36] found that the stresses are consistently reduced by a ratio of about 5:1 by the introduction of lacing wires. These findings confirmed the advantages of blade packeting using tip or mid-span shrouding/lacing wires, especially when blades are operating under resonance conditions. However, the reasons for the reduction of resonance stresses were not explained.

It is considered in this study that the control of forced vibration responses by lacing wires is achieved by

- ■ friction damping at low rotating speed;
- ■ increase of blade stiffness, thus reduction of amplitude;
- ■ nonlinear stiffness of deformed lacing wires; and possibly,
- ■ micro-friction damping

253

At low running speed, the coupling between the lacing wire and the blades is weak as slippage occurs between them. The weak coupling will not strongly modify natural modes of vibration of blades in the packet, but the slippage can dissipate energy due to friction. In this case, the natural frequencies of cantilever blades will not be altered too much but blade vibration amplitude at resonance, hence the dynamic stresses, will be reduced.

Bielawa [17] studied the general slippage characteristics of shroud segment interfaces using Coulomb friction. He found that the energy dissipation due to inter-shroud segment rubbing tended to an amplitude squared dependency and was thus similar to classic structural damping.

At high running speed, the lacing wire is locked with blades due to large centrifugal force. The coupling between the lacing wire and blades generates far more modes of vibration than those in case of free standing blades, depending on the number of blades in the packet. Generally, for a packet with N number of blades, there will be (N-1) number of out-of-phase sub-modes and 1 in-phase sub-mode in each mode cluster corresponding to the fundamental mode of the free standing blade.

The natural frequencies of flap modes are largely altered and their distribution is related to the position and the stiffness of the lacing wire. Some may transform into or coupled with other modes. This alteration and transformation of natural modes of vibration may be used to control the region of resonance of some modes. As discussed in Chapter 6, the 1F and the 2F modes may transform into the 2PF and 1PF modes respectively if the location of the lacing wire is relatively high. This transformation actually alters the critical position where largest dynamic stress occurs. Hence, it is possible to move the critical position away from the hole for a lacing wire. This will certainly reduce the chance of fatigue failure of blades with lacing wires.

The understanding of the alteration of natural frequencies of blade modes using a lacing wire also provides the opportunities for designing some modes to be separated from or coupled with others. The mode coupling/de-coupling could be considered as a means of transferring dynamic stress from one critical area on the blade to some other areas, or to reduce undesired resonance stress due to certain modes. For instance, the coupling between the 1F and the 1T mode could reduce the amplitude of the 1F mode, hence transferring some of the bending stress into shear stress.

The nonlinearity of the stiffness of the deformed lacing wire is identified in this study. At high running speed, the segments of the lacing wire between blades are deformed into segments of arches by centrifugal force. The stiffness of these segments varies with the relative displacement of the blades, i.e. they are functions of relative blade amplitudes. The larger the relative amplitudes are, the larger the difference in stiffness is. Because the relative amplitudes are different for the lacing wire segments in the same packet, due to the phase relations in out-of-phase sub-modes in each flap mode cluster, the nonlinearity introduces 'dynamic mistuning' into the stiffness of the packet.

It is also understood that natural frequencies of blades in packets vary with the stiffness of the lacing wire. As a result, the effect of the dynamic mistuning is that the natural frequencies also undergo small periodic oscillation with vibration amplitudes of the blades, even when excitations remain at constant frequencies. This fluctuation of natural frequency will reduce the energy transmitted into blades from the excitation source. Therefore the response of blades at resonances, hence the stress at resonances will be reduced.

Apart from the features discussed above, the possibility of microslip between the lacing wire and the blades should not be ruled out. There are some reports

discussing relative vibration motions at the interfaces between shroud segments [169, 170], the excessive wear at the shroud interfaces and its consequences, though the direct discussion on the microslip of lacing wires is not found. These studies confirmed that the nature of vibratory motion at the interfaces could be a microslip type and their rubbing action provides important damping assuring the structural integrity of fans.

It is almost certain that microslip takes place when the bladed assembly runs beyond such a speed under which the full slippage can not take place any more. Its existence when the lacing wire is fully locked in blades is not completely impossible. The relative displacements at the interfaces may vary from blade to blade and this variation is attributed to different mode shapes and vibration amplitudes of each blade in the packet. The difference in amplitudes results in varying normal loads and therefore the friction forces at the interfaces will vary. This variation will assist in the reduction of resonance responses and hence, together with friction damping, will contribute to the reduction of dynamic stresses. Further study should be carried out to fully establish the nature of the microslip of lacing wires and its effects in turbine blade vibrations.

7.7   Conclusion

The vibration behaviour of bladed packets bound by a lacing wire was studied in this Chapter using finite element modelling, which was verified by experimental results obtained by ESPI tests. Their dynamic characteristics were identified. The effects of the lacing wire on multi-blade vibration were investigated. Responses of blades with a lacing wire to excitation were analysed.

The study revealed that the application of a lacing wire could largely increase

the stiffness of some modes, for example, flap modes. The blade amplitudes become smaller in a stiffer packet.

Because the natural frequencies of the flap modes can be altered largely by the application of a lacing wire, more flexibility is provided to design engineers to make different modes coupled or de-coupled. As a result, the dynamic stress at certain area on blades could be reduced.

The nonlinearity of the deformed lacing wire was identified in this Chapter. The stiffness of the lacing wire varies with vibration amplitudes of blades. This means that the natural frequencies undergo oscillations because they are the functions of the lacing wire stiffness. The oscillation is considered to have large contributions in the reduction of dynamic stress at resonances.

The friction and microslip of the lacing wire were also discussed although detailed analysis was beyond the scope of this study. It is considered that microslip exists even when centrifugal force is fairly high. Further study should be carried out to investigate the nature of microslip and its effects on the reduction of dynamic stress.
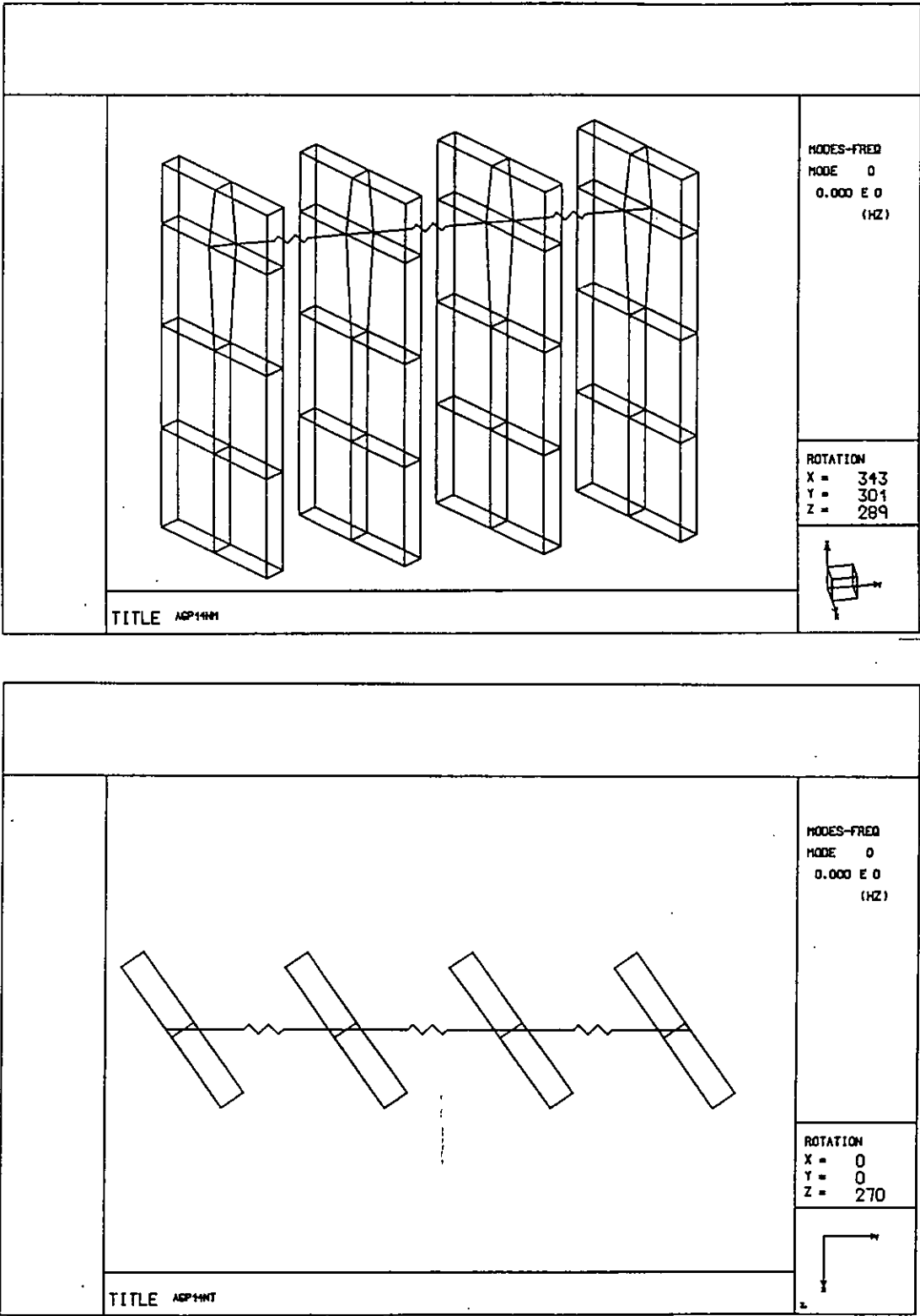
Figure 7.1   The finite element model of a 4 bladed packet
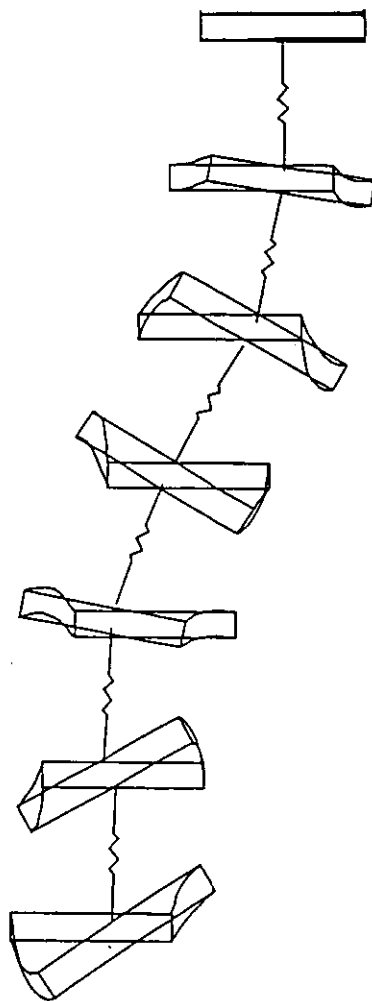
Figure 7.2   One sub-mode in the 1E+1T cluster of a seven bladed packet
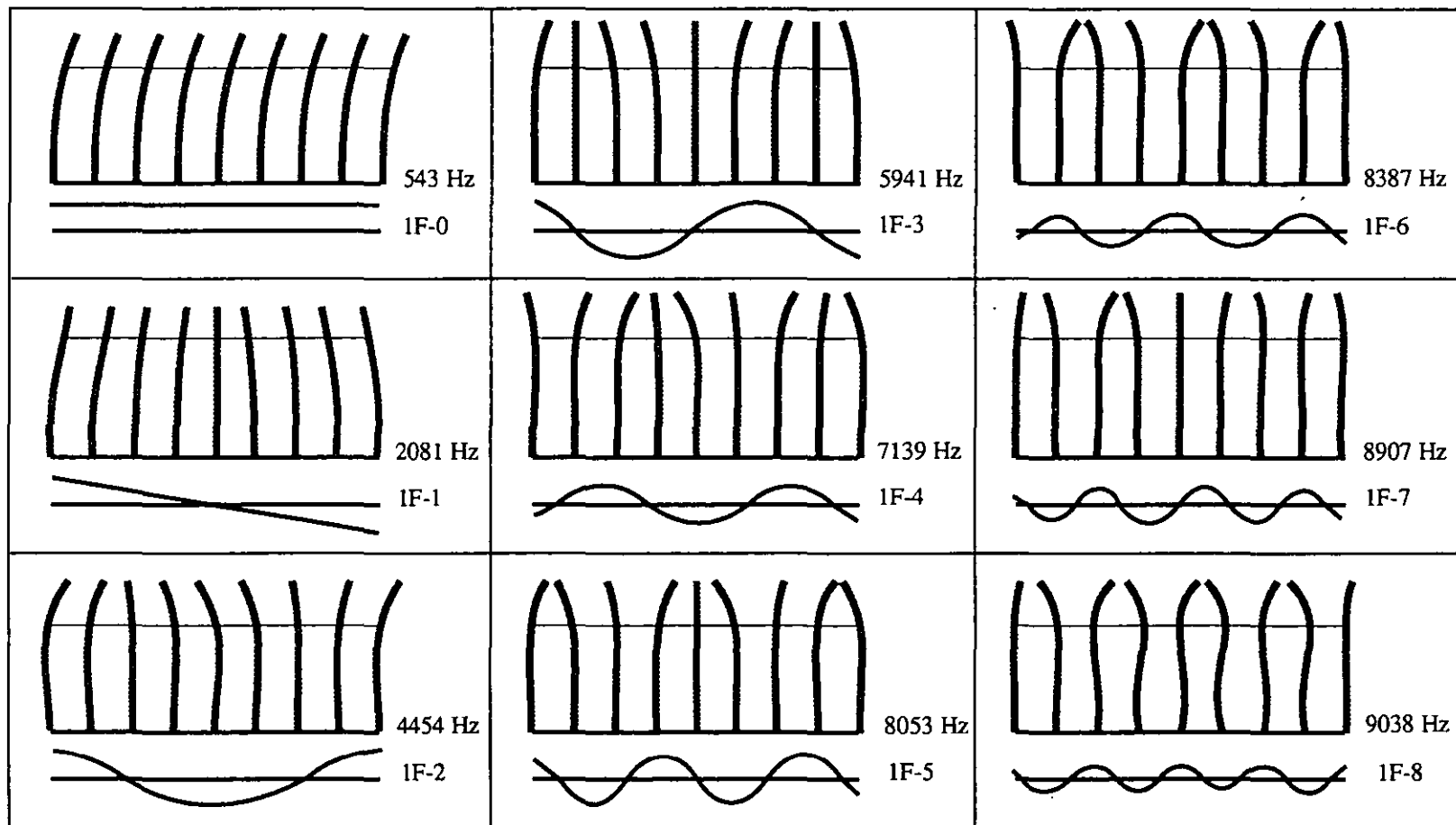
Figure 7.3 Classification of a nine bladed packet vibrating at the 1F cluster frequencies
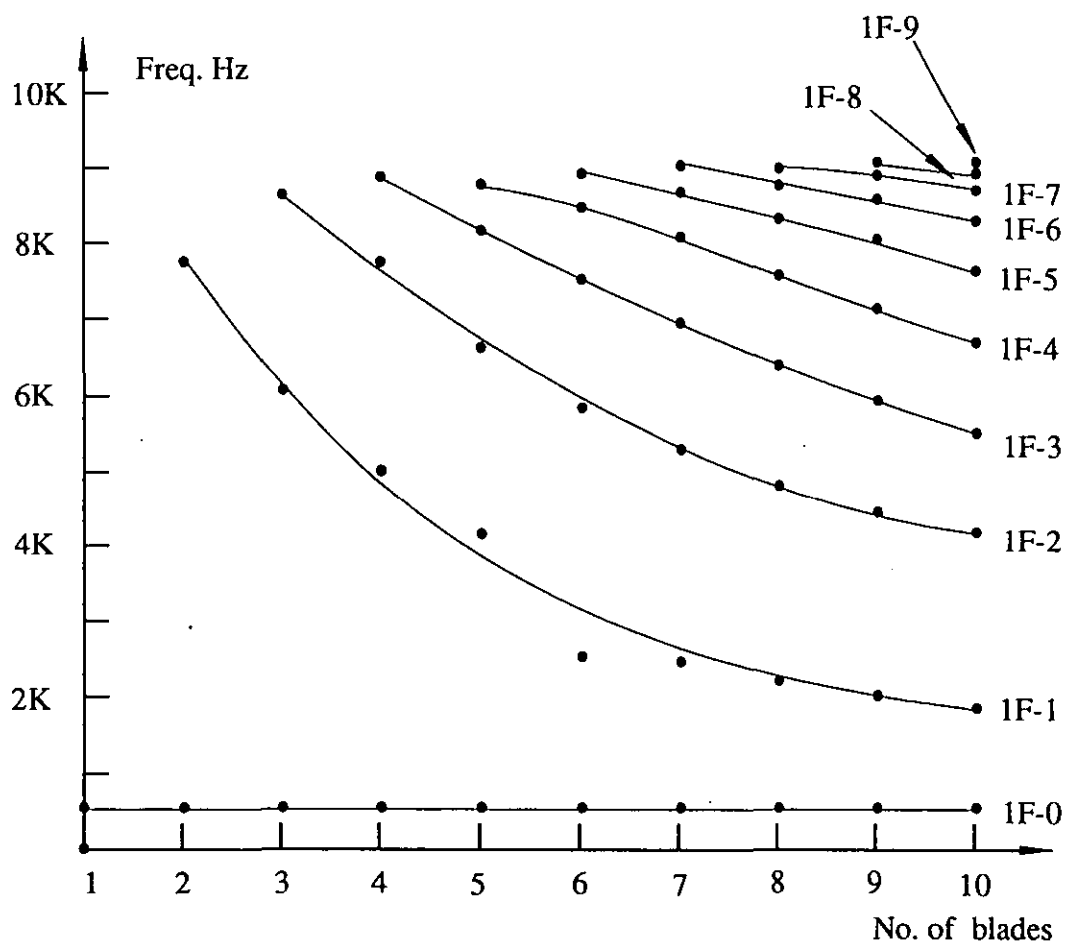
Figure 7.4 Effect of blade number on 1F mode frequencies
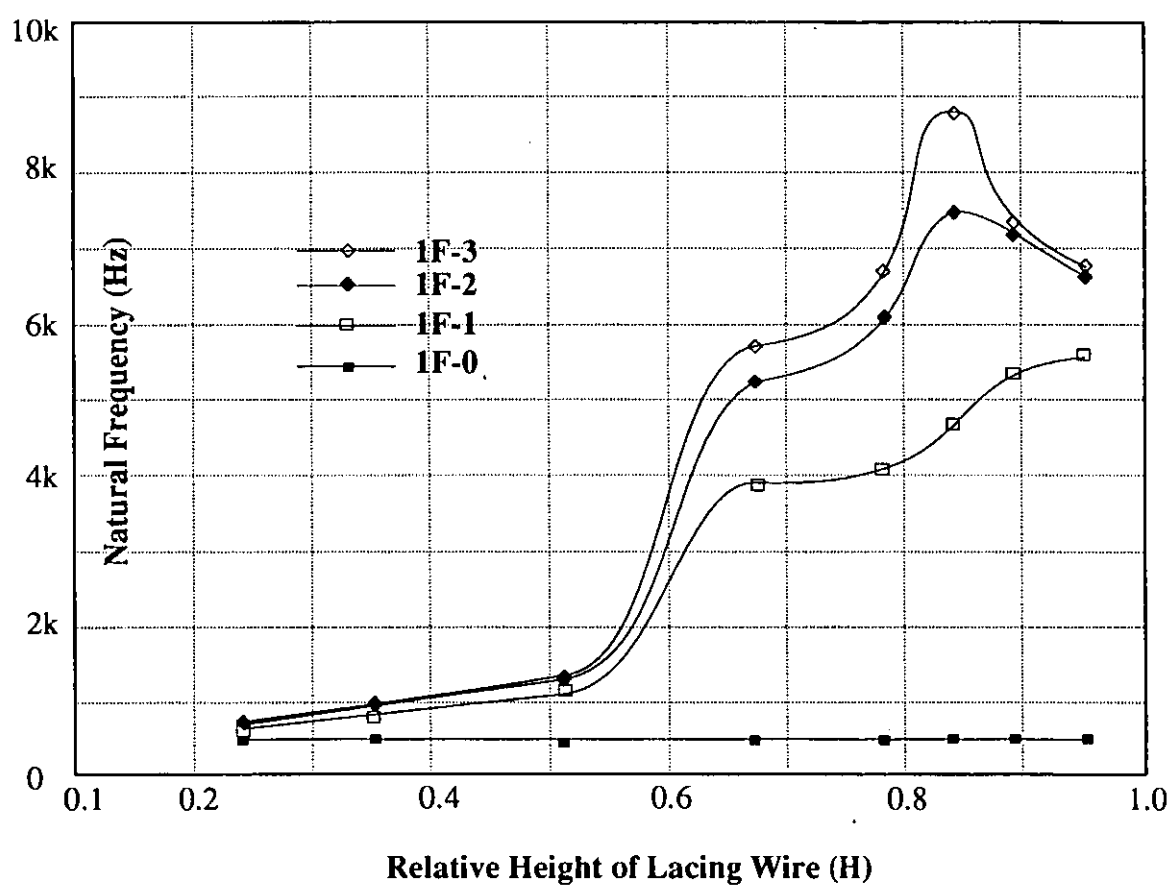
Figure 7.5(a) Variation of the natural frequencies of the 1F mode cluster with the lacing wire height

262
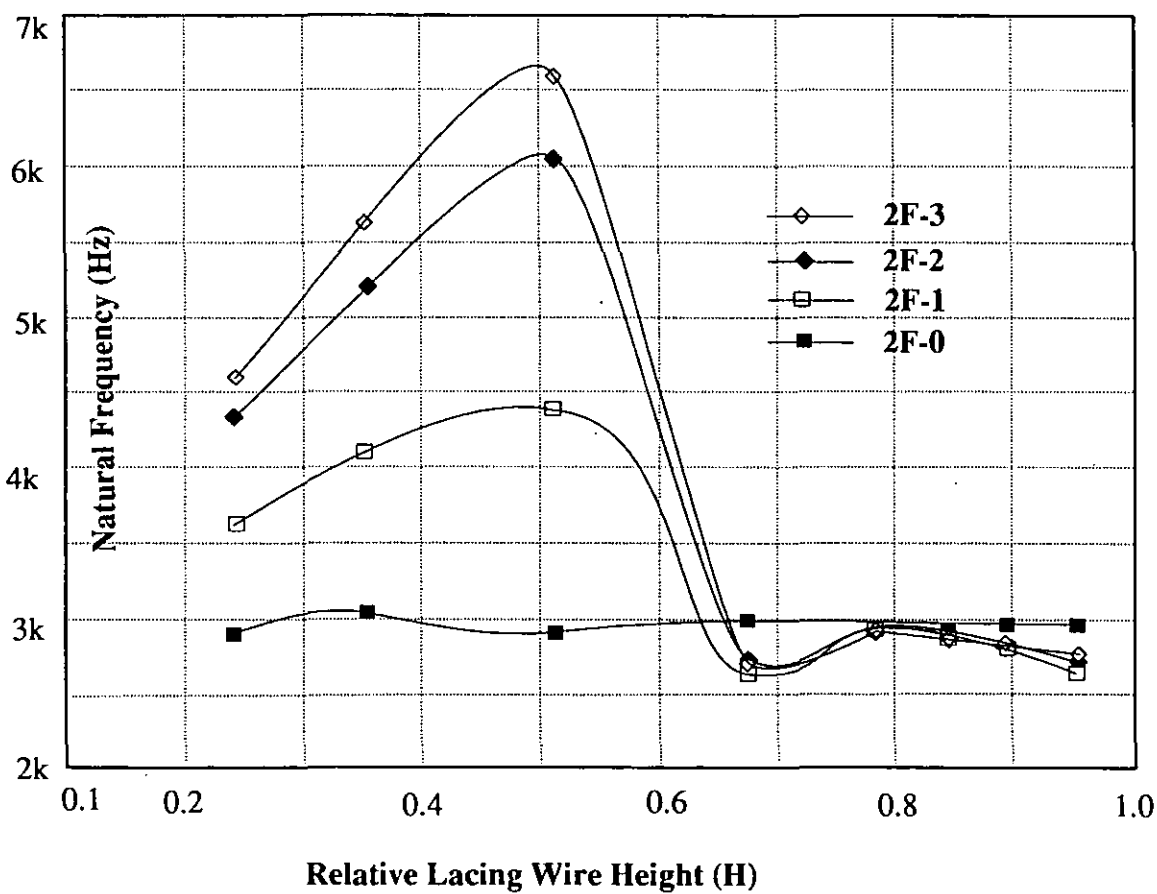
Figure 7.5(b) Variation of the natural frequencies of the 2F mode cluster with the lacing wire height
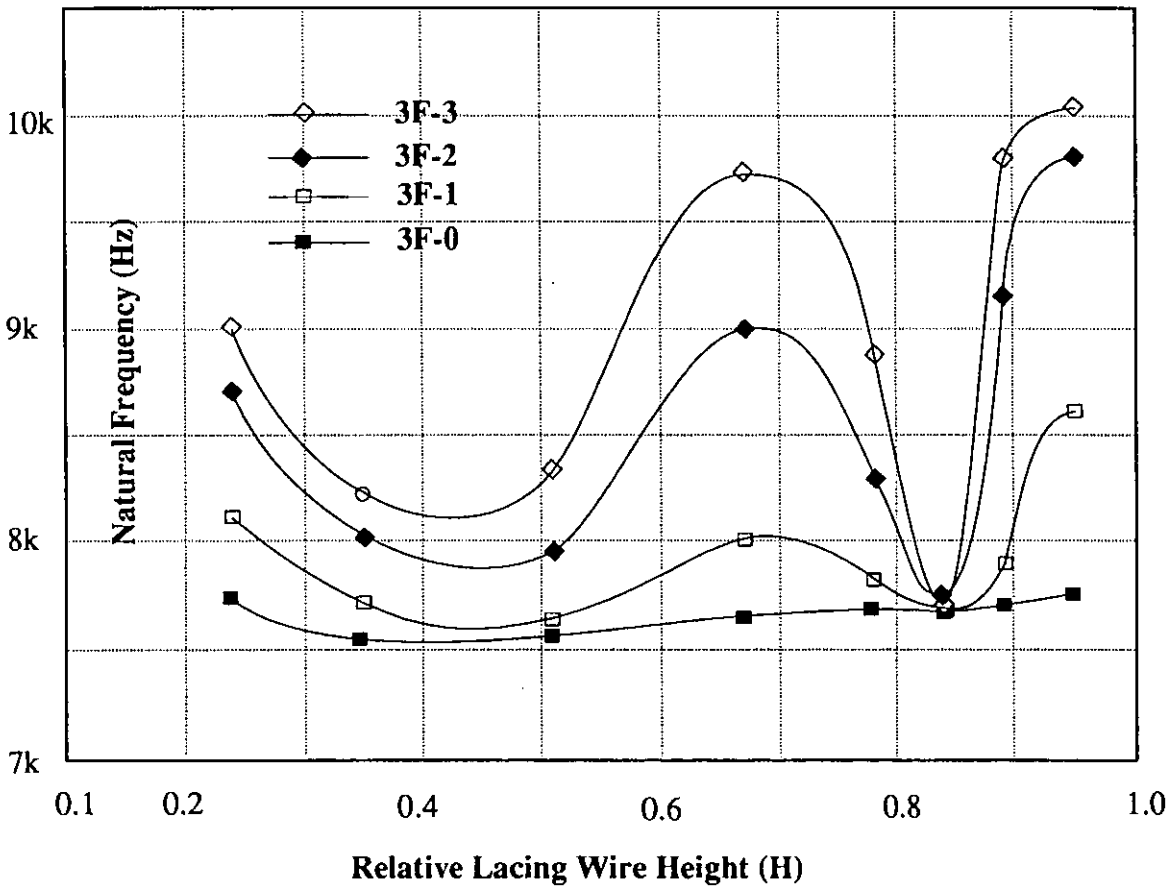
Figure 7.5(c) Variation of the natural frequencies of the 3F mode cluster with the
lacing wire height
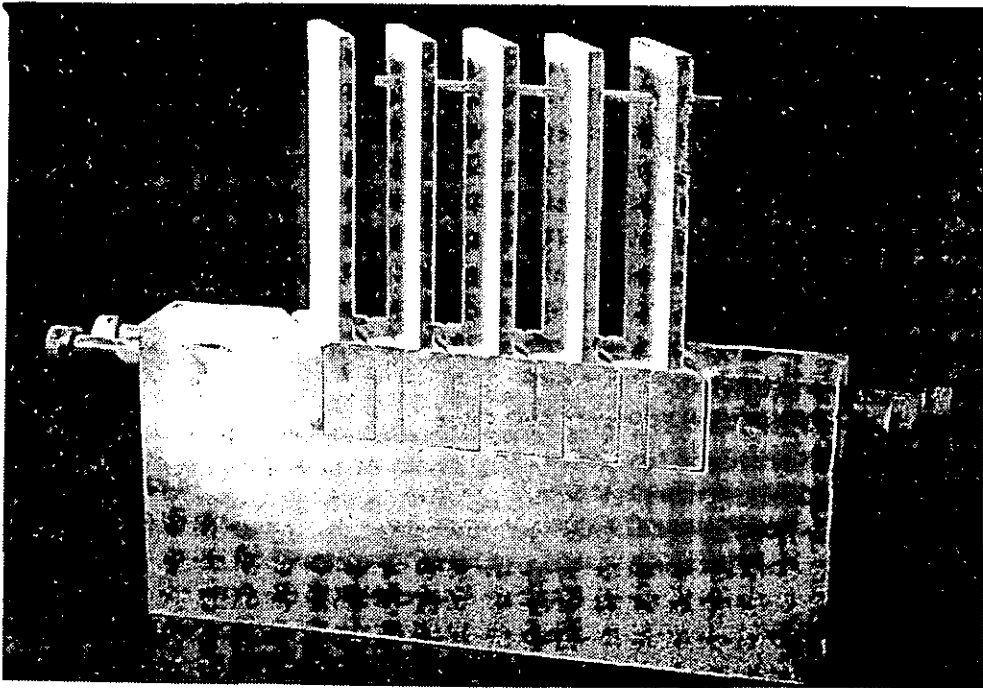
Figure 7.6   Experimental model of a four bladed packet ASSEM1
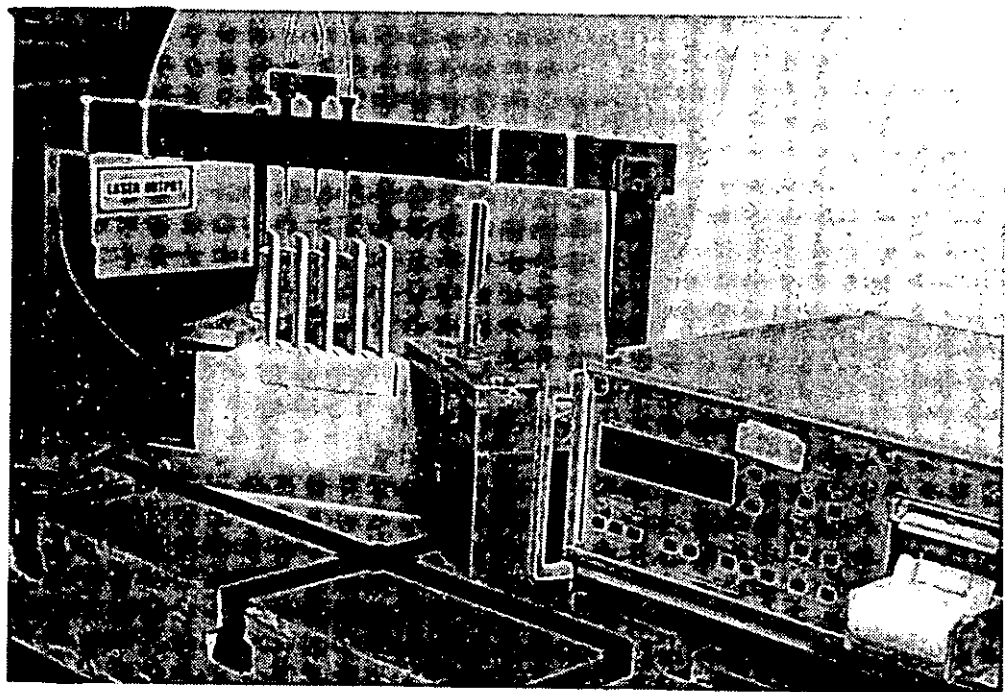
Figure 7.7   The loading frame applying simulated centrifugal force to the lacing wire in ASSEM1

266
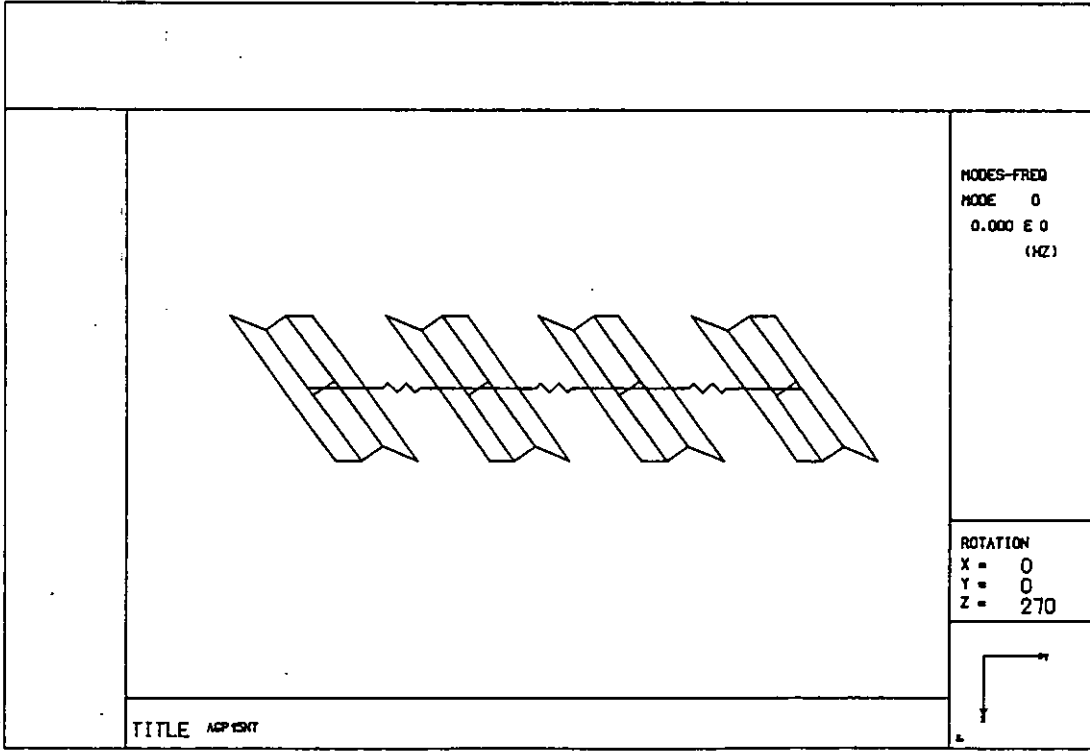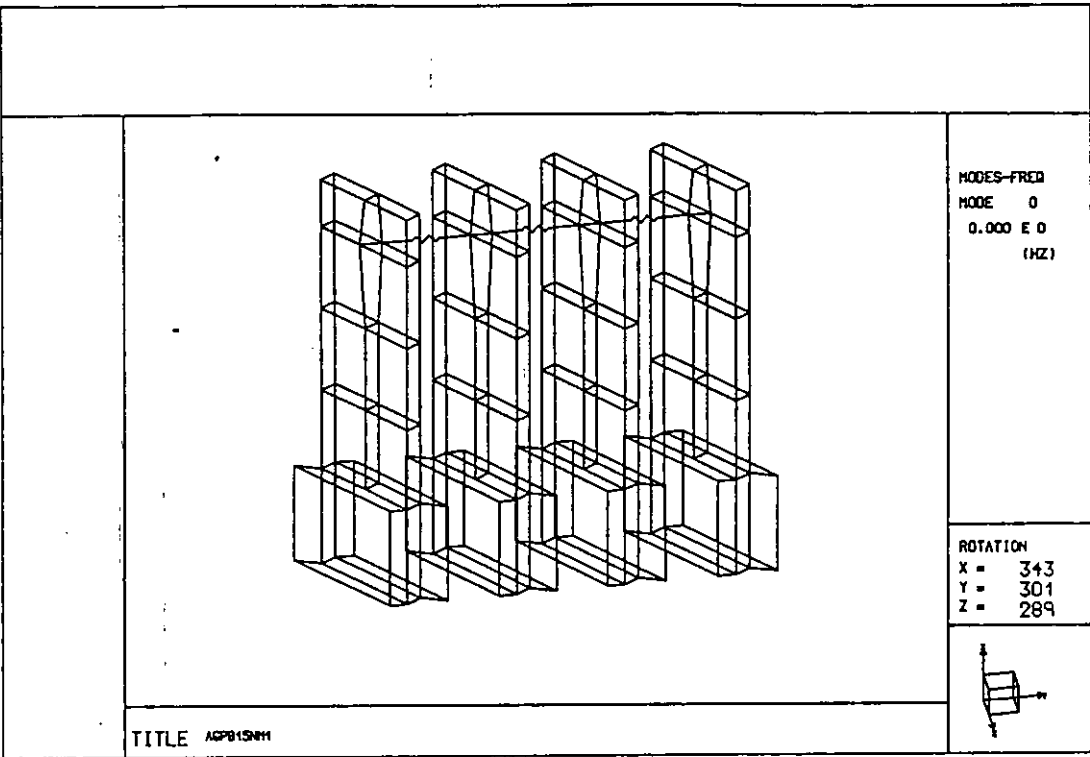
Figure 7.8   The finite element model AGPB15N of the four bladed packet ASSEM1

267
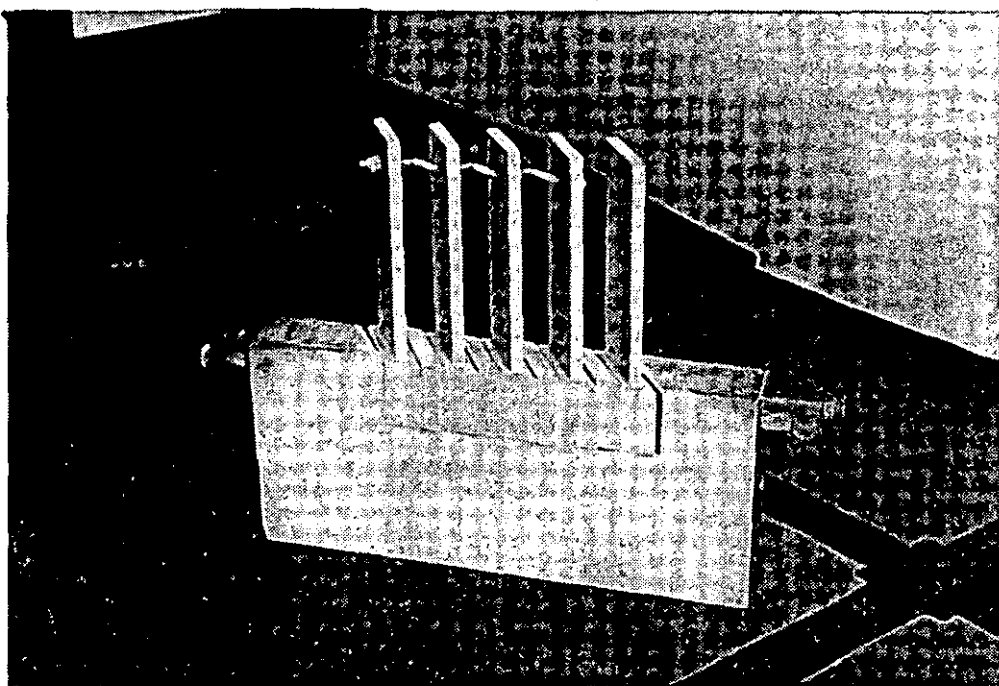
Figure 7.9   Plastic deformation of a lacing wire due to loading

B

C
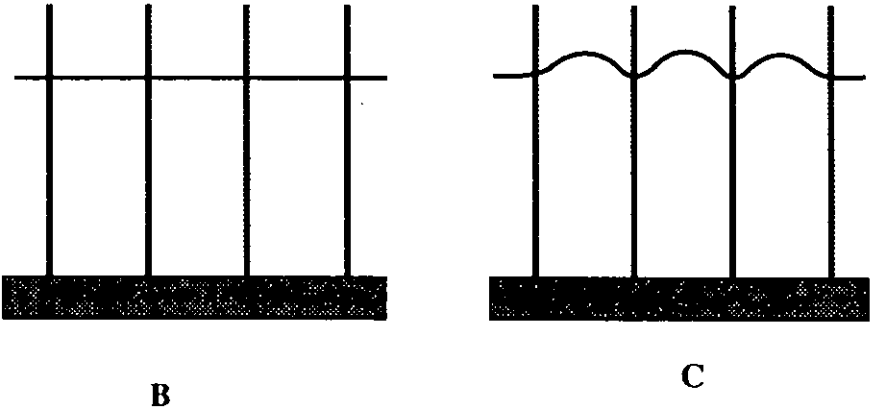
Figure 7.10 Deformed and un-deformed lacing wire in a blade packet
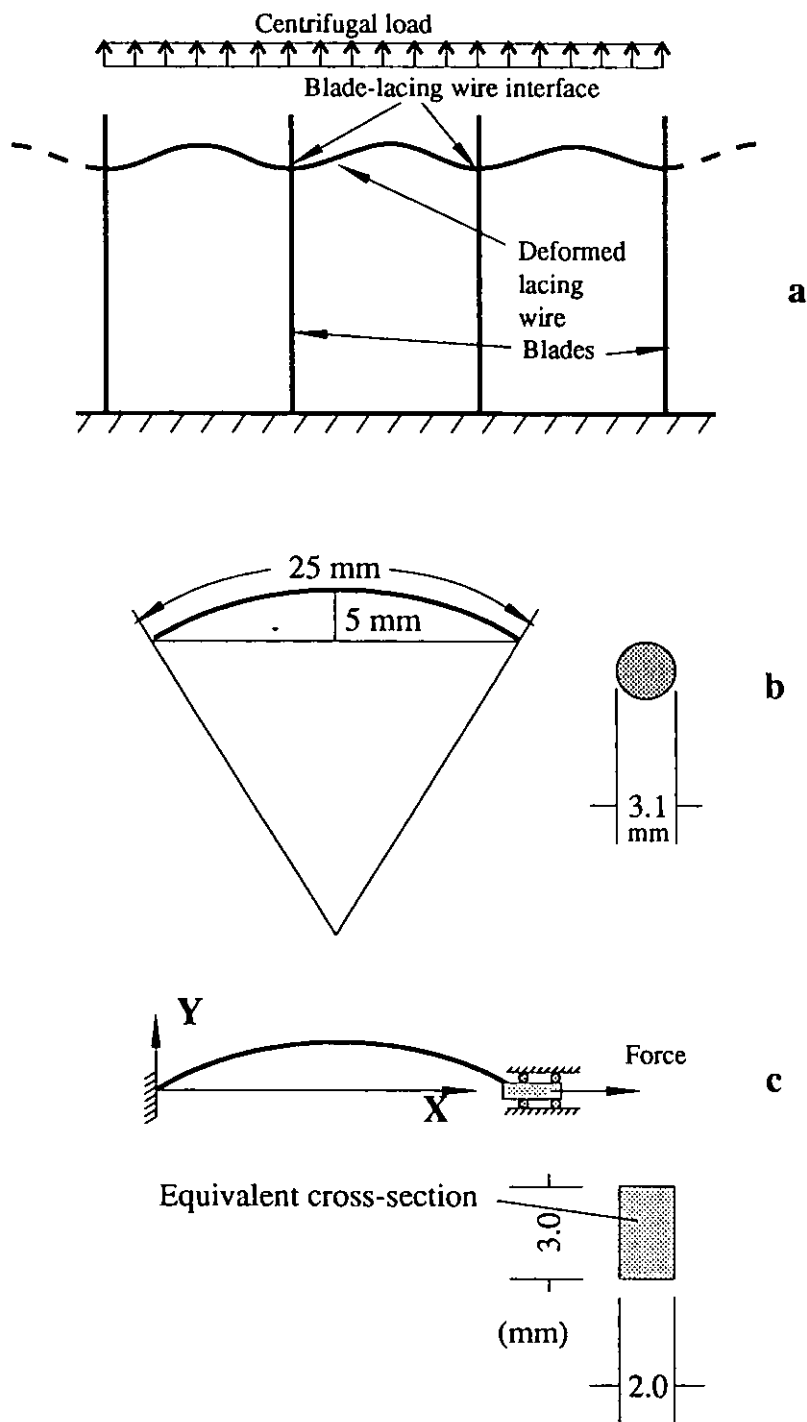
Figure 7.11 Analysis of a deformed lacing wire segment
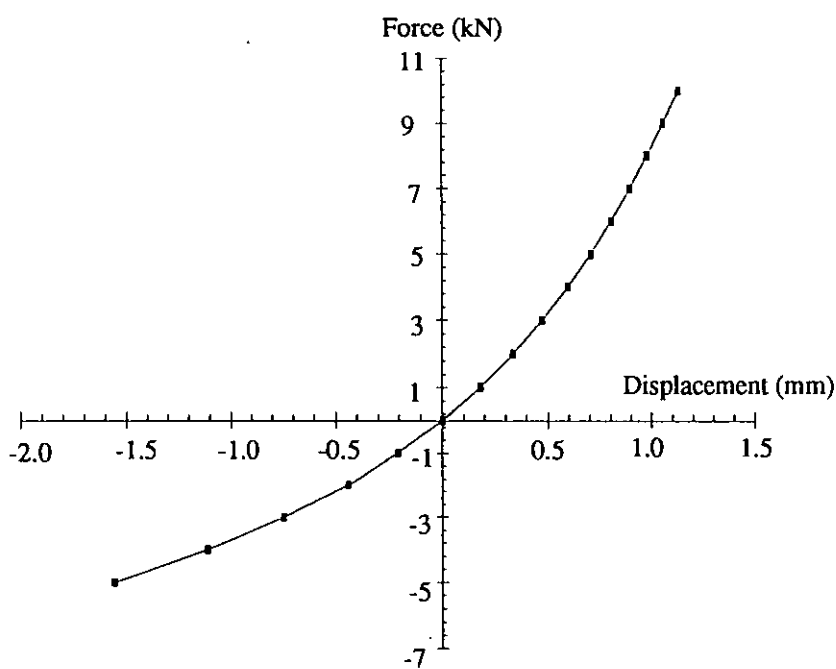
Figure 7.12 Nonlinear stiffness of deformed lacing wire
caused by centrifugal loading
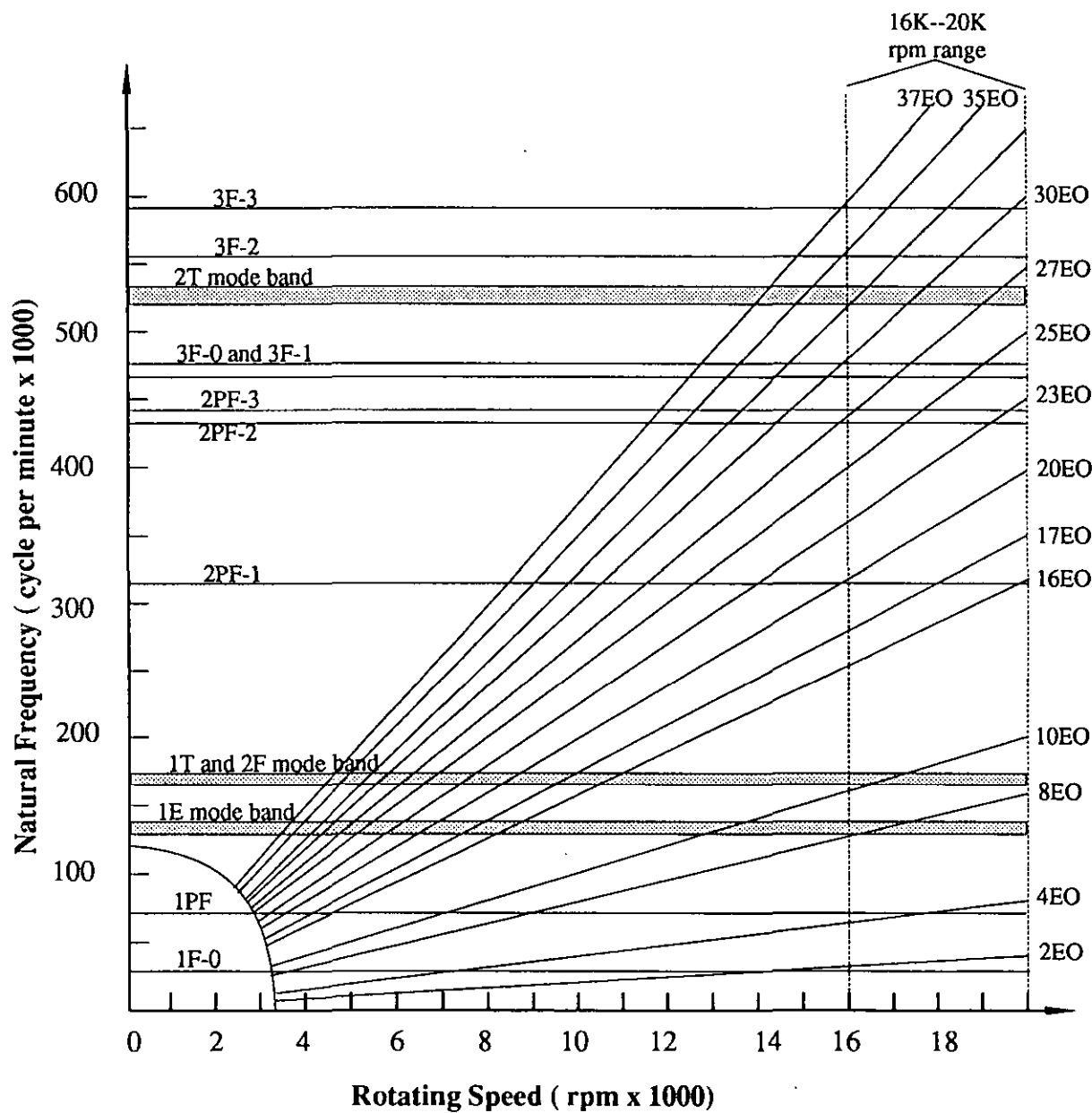
Figure 7.13 Campbell diagram of a simplified blade with a lacing wire at 89% of its height

A	B	C	D	E
FE	ESPI	ESPI	ESPI	ESPI
NO LOADING	NO LOADING	UNLOADED AFTER LOADING	LOADED	SOLDERED
Freq.(Hz) Mode	Freq.(Hz) Mode	Freq.(Hz) Mode	Freq.(Hz) Mode	Freq.(Hz) Mode
478 —— 1F	471 —— 1F	475 —— 1F		479 —— 1F
			856 —— 1F	1260 ┐
1751 ┐	1536 ┐	1536 ┐	1568 ┐	├ 1E x 4
├ 1E x 4	├ 1E x 4	├ 1E x 4	├ 1E x 4	2423 ┘
2199 ┘	2105 ┘	2168 ┘	2279 ┘	
2763 ┐	2725 —— 1T		2713 ┐	2723 ┐
├ 1T x 4	2726 —— 1T	2753 ┐	├ (1T + 2F)	├ (1T + 2F)
2774 ┘	2852 ┐	├ (1T + 2F)	│ x 11	│ x 9
2870 ┐	├ (1T + 2F)	│ x 8	3321 ┘	│
├ 2F x 4	3339 ┘ x 6	3374 ┘		3411 ┘
2939 ┘				
4638 —— 1F	4385 —— 1F	5080 —— 1F		5033 —— 1F
		5742 —— 1F	6018 —— 1F	
	7054 —— 1F	7242 —— 1F	7384 —— 1F	7580 ┐
7455 —— 1F		7584 ┐	7758 ┐	├ 3F x 4
7656 ┐		├ 3F x 4	│	│
├ 3F x 4	7926 ┐	7980 ┘	├ 3F x 4	8144 ┘
7757 ┘	├ 3F x 4		│	
	8021 ┘		8187 ┘	
	8227 ┐	8304 ┐	8471 ┐	8435 ┐
	├ 2T x 4	├ 2T x 4	├ 2T x 4	├ 2T x 4
	8473 ┘	8524 ┘	8649 ┘	8679 ┘
8838 —— 1F				
8874 ┐				
├ 2T x 4			9180 —— 1F	9366 —— 1F
8918 ┘				

Table 7.2 Modes of vibration of ASSE1 by FE analysis and ESPI tests

273

Chapter   8

Conclusion

8.1   Conclusions

The work of this thesis has sought to provide a better understanding of the dynamic characteristics of turbine blades, which are free-standing or in packets and has identified the effects of coupling through lacing wire.

1.   The fundamental vibration modes of blade K have been identified. The effects of taper and pretwist on mode shapes have been shown by studying 7 simplified model blades, each of which represents a fundamental geometric feature of blade K.

2.   One effect of changing the geometry of a blade is that coupled modes of vibration can be generated. The study has revealed that two coupled modes occur outside of the frequency band between the two uncoupled natural frequencies alone, while the latter disappear.

3.   An experimental technique of mode separation has been developed and successfully applied to identify coupled modes of simplified blades and blade K.

4.   The study has shown the contribution of the setting angle of lacing wire to the coupling between the flap and edgewise modes. The displacement of the blade in one direction will result in a pulling force from lacing wire to generate

displacement in the other direction. This contribution assists the coupling when the natural frequency of the 1F mode rises close to that of the 1E mode, due to the stiffening by lacing wire.

5.	The study has shown that both modal testing and ESPI techniques are polarized in detecting displacements. They may see vibration motion in one direction while the blade is moving in the other due to the pretwist of the blade, hence giving false information. Thus thorough understanding of the techniques used is required for correct interpretations.

6.	The finite element analysis has proved to be a very useful tool in the modelling of blading.

7.	F.E. model of a single blade K with loaded lacing wire has been developed and justified by experiments using ESPI technique. Its modes of vibration have been identified and their mode shapes are presented. This has provided a useful tool for further study into the high dynamic stress areas on turbine blades with aero-dynamic profile, in relation to the lacing wire hole which creates stress concentration.

8.	Connecting blades into packets generates far more modes than those of free standing blades. It has been shown that for a N blade packet, there will be N sub-modes in each of mode clusters which correspond to the fundamental modes of the free standing blade. These sub-modes differentiate themselves by having different phase relations to each other, the fundamental one being every blade in phase. .

9.	The blade motion will be out of phase in the remaining (N-1) sub-modes in every cluster. The degree of out of phase can be measured by the number of nodal points along lacing wire. The more nodal points there are, the larger the degree of out of phase, and the higher the natural frequency of the sub-mode. This reflects the

contribution of lacing wire stiffness to packet modes.

10. The stiffness and the location of lacing wire have been seen to have strong effects on flap modes. The employment of lacing wire has been shown to largely increase the natural frequencies of flap modes by increasing the stiffness of the blade packets. Locating the lacing wire between the blade root and approximately 60% of blade height stiffens the second flap mode with consequent frequency increase. In general the third flap mode increases natural frequency for all height of locations of the lacing wire other than at the normal flap mode nodal locations.

11. The alteration of the natural frequencies of flap modes could be used to avoid resonant responses to known major excitations.

12. Mode switching and natural frequency crossing due to the lacing wire have been found. The study has revealed the transformation of flap modes of a free-standing blade into pinned-fixed modes. When the lacing wire location is changed from the bottom of the blade to the top of the blade, the 1F mode switches into the 2PF mode while the 2F mode switches into the 1PF mode. Frequency switching of the two modes occurs when the lacing wire is located near the nodal line of the 2F mode.

13. It has been found that the stiffness of a deformed lacing wire exhibits nonlinearity. The value of stiffness varies with the relative vibration amplitudes of blades. For vibration modes other than the in-phase sub-modes within a single packet of blades, there are different relative amplitudes creating a system with several different relative stiffnesses. It is considered that this dynamic variation of stiffness at different part of the packet will create 'dynamic mistuning'.

14. One possible feature of 'dynamic mistuning' is that the value of stiffness of

deformed segments of a lacing wire undergoes fluctuations. Variation in stiffness amplitude is proportional to the relative amplitude of the blades and this causes instantaneous fluctuation in natural frequency. It is believed that this mode of oscillation contributes to the reduction of vibration amplitude and offers a method for reducing dynamic stress levels.

8.2 Outline of Future Work

The areas where future research work should be concentrated are given in the following sections.

Dynamic Mistuning

The dynamic mistuning in stiffness caused by the nonlinearity of deformed lacing wire combined with the variation of relative amplitude in out-of-phase vibrations of blade packets is a new concept. Its full dynamic characteristics have yet to be established. Its effect on the vibration response of blade packets to major excitations needs to be exploited. Further study should be carried out to gain insight into this feature.

The End Blades in Packets

The effects of grouping blades into packets has been studied in this thesis. However, experiences have shown that it is the blades at the ends of the blade packets that are more prone to failure. The vibration characteristics of end-blades should be further investigated.

Optimization in Blade Packet Design

In the body of this thesis, the study has been focused on establishing the understanding of the vibration of blade packets. It has not been possible to study the packet as part of a bladed disk assembly. In order to provide a base for optimization in the design of blade packets on bladed disks, further work is required to investigate the following subjects:

■   The effect of the number of blades and the number of packets on a bladed disk.

■   The effect of using different lacing wire configurations.

■   The effect of different stiffness and mass ratios between lacing wire and the blade.

■   The location of lacing wire relative to the critical areas on blades

■   The methods of blade location within the disk

8.3   Other Related Areas of Interest

Microslip

Other important areas in the application of lacing wire are the friction and microslip. The dynamic characteristics of friction and microslip interfaces between lacing wire and the blade are to be established. Their effect on the reduction of dynamic stress should be studied.

Other Inter-Blade Coupling Elements

Lacing wire is only one of the inter-blade coupling elements used in turbomachinery. The understanding of its function and the expertise gained in this work can be used to study other types of coupling elements, such as snappers and

lashing pins. The vibration response of blade packets with other coupling elements requires a thorough investigation.

References

1   Afolabi, D., "Vibration of Mistuned Bladed Disc Assemblies" Ph.D. Thesis, University of London (Imperial College) 1982.

2   Afolabi, D., "Effects of Random Mistuning on the Vibration of Coupled Turbomachine Blades" Report No. 8201, 1982, Imperial College, London.

3   Afolabi, D., "The Frequency Response of Mistuned Bladed Disk Assemblies", Proc of the Tenth Biennial Conf on Mechanical Vibration and Noise, Vibrations of Blades and Bladed Disk Assemblies, Cincinnati, Ohio, Sept 10-13, 1985.

4   Afolabi, D., "The Eigenvalue Spectrum of a Mistuned Bladed Disk", Proc of the Tenth Biennial Conf on Mechanical Vibration and Noise, "Vibrations of Blades and Bladed Disk Assemblies", Cincinnati, Ohio, Sept 10-13, 1985.

5   Afolabi, D., "A Note on the Rogue Failure of Turbine Blades" J Sound & Vib Vol. 122 No. 3, 1988, pp 535-545.

6   Ahmad, S., Irons, B.R. and Zienkiewicz, O.C., "Analysis of Thick and Thin Shell Structures by Curved Finite Elements", Intl. J. of Numerical Methods in Eng., Vol. 2, 1979, pp. 419-451.

7   Anderson, R.A., "Vibrations in Uniform Beams According to the

Timoshenko Theory", J of Appl. Mech, Vol 20, Trans. ASME Vol 75, 1953, pp 504-510.

8   Ansari, K.A., "Nonlinear flexural Vibrations of a Rotating Myklestad Beam," American Institute of Aeronautics and Astronautics Journal, Vol. 12, No. 1, 1974, pp. 98-99.

9   Ansari, K.A., "Nonlinear Vibrations of a Rotating Pretwisted Blade," Computers and Structures, Vol. 5, No. 2/3, 1975, pp. 101-118.

10   Armstrong, E.K., Williams, D.D., "Some Intake Flow Maldistribution Effects on Compressor Rotor Blade Vibration". J. Sound & Vibration, Vol. 3, 1966.

11   Arvind, K, Gupta, M., "Vibration of Tapered Beams", Journal of Structural Engineering, Vol. 111, No. 1 January, 1985, pp 19-37.

12   Bancroft, D., "The Velocity of Longitudinal Waves in Cylindrical Bars", Physical Review, Vol 59, 1941, pp 588-593.

13   Banerjee, J. R., Williams, F. W., "Exact Bernoulli-Euler Dynamic Stiffness Matrix for a Range of Tapered Beams", International Journal for Numerical Methods in Engineering, Vol 21, 1985, 2289-2302.

14   Banks, D.O., Kurowski, G.J., "The Transverse Vibration of Doubly Tapered Beam", Trans of ASME, Journal of Applied Mechanics, March 1977, pp. 123-126.

15   Bendiksen, O.O., "Mode Localization Phenomena in Large Space

References

Structures" AIAA Paper No. 86-0903, 1986.

16   Bernante, R., Macchi, A., Magneschi, " Effect of Packeting on Turbine Blades Vibrations", Proc of the Conf. on Rotordyn Probl in Power Plants, Rome, Sep 28-Oct 1. 1982, pp 247-257.

17   Bielawa, L.R. "An Analytic Study of the Energy Dissipation of Turbomachinery Bladed-Disk Assemblies Due to Inter-Shroud Segment Rubbing", Trans. of ASME, Journal of Mechanical Design, Vol. 100, April 1978, pp 222-228.

18   Bogdanoff, J. L., Goldberg, J. E., Marcus, L., "Linear Vibration of a Pinned Rotating Blade", Journal of the Aerospace Sciences, Aug. 1961, Vol 28, No.8, pp 593-601.

19   Bogdanoff, J. L., Lafayette, I., "Influence of Secondary Inertia Terms on Natural Frequencies of Rotating Beams", Journal of Applied Mechanics, Dec. 1955, pp 587-591.

20   Boley, B. A., Chao, C. C, "Some Solutions of the Timoshenko Beam Equations", Journal of Applied Mechanics, Dec. 1955, pp 579-586.

21   Bossak, M. A., Zienkiewicz, O.C., "Free Vibrations of Initially Stressed Solids with Particular Reference to Centrifugal Force Effects in Rotating Machinery," Journal of Strain Analysis, Vol. 8, No. 4, 1973, pp. 245-252.

23   Boyce, W. E., Providence, R. I., "Effect of Hub Radius on the Vibrations of Uniform Bar", J of Applied Mech, Trans. ASME, Vol 23, no. 2, 1956, pp 287-290

References

---

24   Butkovic, M., "Vibrations of Blades with Damping Wire," Intl Conf. on Rotordynamic Problems in Power Plants, Sept. 1981, pp. 237-245.

25   Butters, J. N., Leendertz, J.A., " Holographic and Video Techniques Applied to Engineering Measurement", Trans of the Institute of Measurement and Control, Vol 2 No 12 Dec 1971.

26   Carnegie, W., "Vibrations of Pretwisted Cantilever Blading", Proc. Inst. Mech. Engr., Vol 173, 1959, p 343.

27   Carnegie, W., "Vibrations of Rotating Cantilever Blading: Theoretical Approaches to the Frequency Problem Based on Energy Methods", Journal Mechanical Engineering Science, Vol 1, No 3, 1959.

28   Carnegie, W., "A Note on the Application of the Variational Method to Derive the Equations of Dynamic Motion of a Pre-Twisted Cantilever Blade Mounted on the Periphery of a Rotating Disc Allowing for Shear Deflection, Rotary Inertia and Torsion Bending", Bull. Mech. Engng Educ. 1966, Vol 5, pp 221-223.

29   Carnegie, W., "The Application of the Variational Method to Derive the Equations of Motion of Vibrating Cantilever Blading Under Rotation", Bull. Mech. Engng Educ. 1967, Vol 6, pp 29-38.

30   Carnegie, W., Stirling, C., Fleming, J., "Vibration Characteristics of Turbine Blading Under Rotation -- Results of An Initial Investigation and Details of a High Speed Test Installation", Appl. Mech. Convention, Proc. Inst. Mech., Engrs. Paper No. 32, 1966.

References

31 Carnegie, W., Thomas, J., "Natural Frequencies of Long Tapered Cantilevers", Aero. Q. Vol 18, 1967, p 309.

32 Cranch, E. T., Adler, A. A., "Bending Vibrations of Variable Section Beams", Journal of Appl. Mech., Vol. 23, 1956, pp. 103-108.

33 Chapman, G. M, Wang, X., "Interpretation of Experimental and Theoretical Data for Prediction of Mode Shapes of Vibration Turbocharger Blades", Journal of Vibration, Acoustics, Stress, and Reliability in Design, Trans of ASME, Vol 110, pp 53-58, Jan. 1988.

34 Chen Chu, "The Effect of Initial Twist on the Torsional Rigidity of Thin Prismatical Bars and Tubular Members", Proc 1st US Nat Cong. of Appl. Mech, 1951, pp. 265-269.

35 Chree, C., "The Equations of an Isotropic Elastic Solid in Polar and Cylindrical Coordinates, Their Solution and Application", Transactions of the Cambridge Philosophical Society, Vol. 14, 1889, p 250.

36 Chubb, S. B., "Evaluation of Wire Lacing for the Control of Gas Turbine Blade Vibration", ASME Paper, n 67-VIBR-47, 1967.

37 Cmolnickov, B. L., "Calculation of free Vibration of a Closed Frame System of Periodic Symmetry," Proceedings of Leningrad Institute of Technology, No. 210, 1960.

38 Connor, W. A., Swain, E., Bellamy, A.G. and Chapman, G. M., "Excitation of Turbine Blade Vibrations in Large Turbochargers", 3rd International Conference on Turbochargers, I. Mech. E., London, 1986.

References

39   Conway, H. D., "Calculations of Frequencies of Truncated Pyramids",
        Aircraft Engr., Vol 18, 1946, p. 235.

40   Danforth, C. E., "Distortion-Induced Vibration in Fan and Compressor
        Blading". J. Aircraft, Vol. 12, No. 4, April 1975.

41   Davis, R. M., "A Critical Study of the Hopkinson Pressure Bar",
        Philosophical Transactions of the Royal Society, Series A, Vol 240, 1948,
        pp 375-457.

42   Deak, A. L., Baird, R. D., "A Procedure for Calculating the Frequencies of
        Steam Turbine Exhaust Blades", Trans, ASME, Vol. 85, 1963, p. 324.

43   Dengler, M. A., Goland, M., "Transverse Impact of Long Beams, Including
        Rotatory Inertia and Shear Effects", Proc. of the First US National Cong.
        of Applied Mechanics, 1952, p179.

44   Dewey, R. P., Rieger, N. F., "Survey of Steam Turbine Blade Failures",
        EPRI Report No. CS-3891, Final Report of RP1856-1, March 1985.

45   Edited by Diaz-Tous, I. A., Lansing, N. F. The Proceedings of the
        Conference "Steam Turbine Blade Reliability Seminar and Workshop", Los
        Angeles, California, March 18-20, 1986.

46   Dokainish, M. A. and Rawtani, S., "Vibration Analysis of Rotation
        Cantilever Plates", International Journal for Numerical Methods in Eng.
        Vol 3, 1971, pp. 233-248.

47   Dokainish, M.A. and Rawtani, S., "Pseudo-Static Deformation and

References

Frequencies of Rotating Turbomachinery Blades" AIAA J. Vol 10, 1972, pp. 1397-1398.

48   Dolph, C. L., "On the Timoshenko Beam Vibrations", Quarterly of Applied Mathematics, Vol. 12 1954, pp. 175-187.

49   Downs, B., "Transverse Vibrations of cantilever Beams Having Unequal Breadth and Depth Tapers", J of Applied Mechanics, Trans of the ASME, Dec, 1977, pp 737-742.

50   Dye, R. C. F., Henry, T. A, "Vibration Amplitudes of Compressor Blades Resulting From Scatter in Blade Natural Frequencies", Trans of the ASME, J of Eng for Power, July 1969, pp. 182-188.

51   El-Bayoumy, L. E., Srinivasan, A. V., "Influence of Mistuning on Rotor Blade Vibration", AIAA Journal, Vol. 13, 1975, pp. 460-464.

52   Ellington, J. P., McCallion, H., "The Vibration of Laced Turbine Blades" J. Roy. Aero. Soc., Vol. 61, 1957, p. 563.

53   Edited by Ewins, D. J., Srinivasan, A. V., "Vibration of Bladed Disk Assemblies", Ninth Biennial Conference on Mechanical Vibration and Noise of Design and Production Engineering. ASME Technical conferences, 1983.

54   Ewins, D. J., "The Vibration of Bladed discs", Ph.D Thesis, Cambridge university, England, 1966.

55   Ewins, D. J., "The Effects of Detuning Upon the Forced Vibrations of

Bladed Disks", J Sound Vib, Sept 1969, pp 65-79.

56   Ewins, D. J., "Vibration Characteristics of Bladed Disc Assemblies", J of Mech Eng Sci, 1973, Vol 15 No 3 pp 165-186.

57   Ewins, D. J., "Studies to Gain Insight into the Complexities of Blade Vibration Phenomena", Proc of I Mech E Conf on Vibrations in Rotating Machinery, Sept. 1976, p 165-172.

58   Ewins, D. J., "Blade Disc Vibration--A View of Techniques and Characteristics," Proc of the ISVR Conf. on Recent Advances in Structural Dynamics, Southampton. July 1980, pp 187-210.

59   Ewins, D. J., Modal Testing: Theory and Practice, Research Studies Ltd and John Wiley & Sons Inc, 1985

60   Ewins, D. J, Imregun, M., "Vibration Modes of Packeted Bladed disks", Journal of Vibration, Acoustics, Stress, and Reliability in Design, Transactions of the ASME, April, 1984, Vol. 106, pp 175-180.

61   Ewins, D. J., Han, Z. S., "Resonant Vibration Levels of a Mistuned Bladed disk", Journal of Vibration, Acoustics, Stress, and Reliability in Design, Transactions of the ASME, Vol. 106, 1984, pp 211-223.

62   Fabunmi, J. A., "Forced Vibrations of a Single Stage Axial Compressor Rotor", Ph.D. Thesis, MIT, 1978.

63   Fleeting, R., Coats, R., "Blade Failures in the HP Turbines of RMS Queen Elizabeth II and Their Rectification", Trans. Instn. Marine Engr., Vol. 82,

1970, p. 49.

64   Frank, W., Schaden Spiegel, Vol 25, No. 1, 1982, p. 20

65   Fu, C. C., "Computer Analysis of a Rotating Axial-Turbomachine Blade in
        Coupled Bending-Bending-Torsion Vibrations", International Journal for
        Numerical Methods in Engineering, Vol. 8, 1974, pp. 569-588.

66   Goodier, J. N., Griffin, D. S.,"Elastic Bending of Pretwisted Bars", Int
        Journal of Solids and Structures, Vol. 5, 1969, pp. 1231-1245.

67   Griffin, J. H., Hoosac, T. M., "Model Development and Statistical
        Investigation of Turbine Blade Mistuning," IBID pp. 204-210.

68   Grinsted, B., "Nodal Pattern Analysis," Proc.I Mech. E., Vol 166, No. 3,
        1952, pp. 309-321.

69   Halvorsen, W.G., Brown, D.L., "Impulse Technique for Structural
        Frequency Response Testing", Sound and Vibration, Nov. 1977

70   Henry, R., Lalanne, M., "Vibration Analysis of Rotating Compressor
        Blades", Trans of the ASME, J of Eng for Ind, August. 1974, pp.
        1028-1035.

71   Hodges, C. H., "Confinement of Vibration by Structural Irregularity," J of
        Sound and Vib, Vol. 82, 1982, pp. 411-424.

72   Hodges, C. H., Woodhouse, J., "Vibration Isolation from Irregularity in a
        Nearly Periodic Structure: Theory and Measurements," J of The Acoustical

Society of America, Vol. 74, 1983, pp. 894-905.

73   Housner, G.W., Keightly, W.O., "Vibration of Linearly Tapered Cantilever Beams," Proc. ASCE, 88, (EM 2), p. 95, 1962.

74   Huang, T.C, "Effect of Rotatory Inertia and Shear on the Vibration of Beams Treated by the Approximate Methods of Ritz and Galerkin", Proc. 3rd US Natl. Cong., Appl. 1958, Mech., ASME, pp 189-194.

75   Huang, T. C., "The Effect of Rotatory Inertia and of Shear Deformation on the Frequency and Normal Mode Equations of Uniform Beams with Simple End Conditions", Trans. ASME, J of Appl. Mech., Dec. 1961, pp. 579-584.

76   Huang, Wen-hu, "Free and Forced Vibration of Closely Coupled Turbomachinery Blades", AIAA Journal Vol 19, 1981, pp. 918- 924.

77   Hudson, G. E., "Dispersion of Elastic Waves in Solid Circular Cylinder", Physical Review, Vol 63, 1943, pp 46-51.

78   Hutchinson, J. R, Zillmer, S. D., "Vibration of a Free Rectangular Parallelpiped," ASME Journal of Appl. Mech., Vol. 50, 1983, pp. 123-130.

79   Hutchinson, J. R., Zillmer, S. D., "On the Transverse Vibration of Beams of Rectangular Cross-Section", Journal of Applied Mechanics, Jun 1986 Vol 53, pp. 39-44.

80   Idem, "The Effect of Substantial Pretwist on the Stiffness Properties of Thin Beams of Cambered Section", Journal of Appl. Mech., Trans.

ASME, Vol. 46, 1979, pp. 341-344.

81   Irons, B. M. "Structural Eigenvalue Problems: Elimination of Unwanted Variables", AIAA J, Vol. 3, 1965, p. 961.

82   Isakson, G., Eisley, G. J., "Natural Frequencies in Coupled Bending and Torsion of Twisted Rotating and Non-Rotating Blades," NASA CR-65, 1964, p. 77.

83   Jadvani, H. M., "Vibration of Turbine Blades," Ph.D. Thesis, Indian Institute of Technology, Delhi, 1982.

84   Jones, R., Wykes, C., "General Parameters for the Design and Optimization of Electronic Speckle Pattern Interferometers", Optica Acta. Vol 28, no 7, 1980, pp. 949-972.

85   Kielb, R. E., "Aeroelastic Characteristics of a Mistuned Bladed Disk Assembly," Ph.D Thesis, Ohio State University, 1981.

86   Edited by Kielb, R. E., Rieger, N. F., "Vibrations of Blades and Bladed disk Assemblies", Tenth Biennial conference on Mechanical Vibration and Noise. ASME Conference, 1985.

87   Klein, L., "Transverse Vibrations of Non-Uniform Beams", Journal of Sound and Vib. Vol. 37, 1974, pp. 491-505.

88   Krishna Murty, A. V., "A lumped Inertia Force Method for Vibration Problems", Aero. Quarterly, Vol. 17, 1965, pp. 127-140.

89   Krishna Murty, A. V., Prabhakara, K. R., "Vibrations of Tapered
      Cantilever Beams and Shafts", Aeronautical Quarterly Vol. 20, 1969, pp.
      171-177.

90   Krupka, R. M., Baumanis, A.N., "Bending-Bending Mode of a Rotating
      Tapered-Twisted Turbomachine Blade Including Rotary Inertia and Shear
      Deflection", J Engng Ind., ASME Vol 91, 1969, p 1017.

91   Lacitignola, P., Valentini, E., Morani, D., "Applications of Holographic
      Interferometry to the Study of Blade Vibrations in Turbomachines",
      Quaderni Pignone, Vol 42, 1986.

92   Lang, K. W., Nemat-Nasser, S., "An Approach for Estimating Vibration
      Characteristics of Nonuniform Rotor Blades", AIAA J., Vol 17, 1979, p
      995.

93   Lee, H. C., "A Generalized Minimum Principle and its Application to the
      Vibration of a Wedge with Rotatory Inertia and Shear", Journal of
      Applied Mechanics, Trans of ASME, June 1963, pp 176-180.

94   Lee, H. C., Bishop, R. E. D., "Applications of Integral Equations to the
      Flexural Vibrations of a Wedge with Rotary Inertia and Shear", J. Franklin
      Inst., Vol 227, 1964, p 327.

95   Leissa, A. W., Vibration of Shells, NASA SP-288, U.S. Government
      Printing Office, 1973.

96   Leissa, A. W., MacBain, J. C., Kielb, R. E., "Vibrations of Twisted
      Cantilevered Plates --- Summary of Previous and Current Studies", Journal

References

of Sound and vibration, Vol. 96, No. 2, 1984, pp 159-173.

97   Leissa, A. W., Lee, J. K., Wang, A.J., "Rotating Blade Vibration Analysis Using Shells," ASME Paper No. 81-GT-80.

98   Leissa, A. W., Lee, J. K., Wang, A.J., "Vibrations of Twisted Rotating Blades", Trans of the ASME, J of Vib, Acoustics, Stress, and Reliability in Design, April 1984, Vol 106, pp 251-257.

99   Lindberg, L. M., "Vibration of Non-Uniform Beams", The Aero. Quarterly, Vol 14, 1963, pp. 387-395.

100   Lisicki, A., "Vibration of Rotating Twisted Blades", Archiwum Budowy Maszyn, Vol. 15, No. 3, 1968, pp. 355-382.

101   Lo, H., Goldberg, J. E., Bogdanoff, J. L., "Effect of Small Hub-Radius Change on Bending Frequencies of a Rotating Beam", J of Appl. Mech., Trans. Vol 27, No. 3, 1960, pp 548-550.

102   Lo, J. and Renbarger, J., "Bending Vibrations of a Rotating Beam", Proc. of the 1st US National Cong. on Appl. Mech. 1952, pp. 75-79

103   Lokberg, Ole, "Electronic speckle pattern interferometry", Phys Technol, Vol 11, 1980, pp16-22.

104   Mabie, H. H., Rogers, C. B., "Transverse Vibrations of Tapered Cantilever Beams with End Loads", J. Acoust. Soc. Amer., 36, p 463, 1964.

105   MacBain, J. C., "Vibratory Behaviour of Twisted Cantilevered Plates",

Journal of Aircraft, Vol 12, April 1975, pp 343-349.

106   MacBain, J. C., Genin, J., "Effect of Support Flexibility on the
       Fundamental Frequency of Vibrating Beams", J of The Franklin Institute.
       Vol 296, No 4, 1973, pp 259-273.

107   MacBain, J. C., Homer, J. E., Stange, W. A., Ogg, J. S., "Vibration
       Analysis of a Spinning Disk Using Image-Derotated Holographic
       Interferometry", Experimental Mechanics, Jan. 1979, pp 17-22.

108   MacBain, J. C., Kielb, R. E., Leissa, A. W., "Vibrations of Twisted
       Cantilevered Plates--Experimental Investigation", Trans of the ASME, J of
       Engineering for Gas Turbines and Power. Jan. Vol 107, 1985, pp 187-196.

109   Martin, A. I., "Some Integrals Relating to Vibration of Cantilever Beams
       and Approximation for the Effect of Taper on Overtone Frequencies",
       Aero. Q., Vol 7, 1956, p 109.

110   Mayer, J. F., "Vibration Characteristics of an Axial Blading with Different
       Types of Coupling Links", Rotordynamics' 92, Proc of the International
       Conf. on Rotating Machine Dynamics, Venice 28-30 April 1992, pp 278-
       286.

111   McKenna, J., "on the Lateral Vibration of Conical Bars," SIAM Journal
       on Appl. Mathematics, Vol. 21, 1971, pp 256-278.

112   Mead, D. J., "A General Theory of Harmonic Wave Propagation in Linear
       Periodic Systems with Multiple Coupling," J Sound Vib., Vol. 27, No. 2,
       1973, pp. 235-260

References

113   Mendelson, A., Sendler, S., "Analytical Determination of Coupled Bending Torsion Vibrations of Cantilever Beams by Means of Station Functions", NACA TN 2185, 1949.

114   Mendelson, A., Sendler, S., "Analytical and Experimental Investigations of Effect of Twist on Vibration of Cantilevers", NACA TN 2300, 1951.

115   Meller, A. G., "Survey of Determination of Natural Frequencies and Modes of Vibrations of Compressor Blades", Recherches Aeronautique, No. 22, 1951, pp. 55-66.

116   Meyer, F., "Mathematische Theorie der Transversalen Schwingungen Eines Stabes von Veranderlichen Querchnitt", Ann. der Physik und Chemie, Vol 33, 1888, p 661.

117   Miklowitz, J., "Flexural Waves in Beams According to the More Exact Theory of Bending", NAVORD Report 2049, 1953.

118   Miyaachi, T., Hoshiya, S., Sofue, Y., Amihoshi, S., Iwabu, T., Takeda, K., "On the Vibration of Axial-Flow Turbomachine Blades: Part I: Natural Frequency, Mode and Vibratory Stress Distribution", National Aerospace Laboratory, NAL TR-176, 1969.

119   Montoya, J., "Coupled Bending and Torsional Vibrations in a Twisted, Rotating Blade", Brown Boveri Review, Vol. 53, No. 3, 1966, pp. 216-230

120   Myklestad, M. O., "A New Method of Calculating Natural Modes of Uncoupled Bending Vibration of Airplane Wings and Other Types of Beams", J of Aeronautical Sci. Vol. 11, 1944, pp. 153-162.

References

121   Nagarajan, P, Alwar, R.S, "A Three Dimensional Approach To Blade Packet Vibrations", Journal of Sound and Vibration, Vol. 95, No. 3, 1984, pp. 295-303.

122   Nagamatsu, A., Michimura, S., "Vibration of Blade of Rotating Impeller," Theoretical and Appl. Mech., Vol. 26, 1978, pp. 327-338.

123   Namura, K., Okabe, A., Ikeuchi, K., "Turbine Blade Assemblies and Their Vibration Characteristics" Proc. of the Inst. of Mech. Engr on Vib. in Rotating Machinery, Sept 1992, Univ. of Bath, England.

124   Nobuo, I., "A Technique for Computing Natural Frequencies of Trapezoidal Vibrators", J. Aero. Sci., Vol 24, 1957, p. 239.

125   "PAFEC 75", PAFEC theory manual, PAFEC Ltd, 1984.

126   Data Preparation User Manual (Level 6.2), PAFEC Ltd 1984

127   PIGS USER MANUAL (level 4.1), PAFEC Ltd, 1984

128   Peterson, M. R., Alderson, R. G., Stockton, R. J., Tree, D. J., "Three-Dimensional Finite Element Techniques for Gas Turbine Blade Life Prediction," AGARD Report No. CP-248, 1979.

129   Petricone, R. D., "Vibration Characteristics and Deformation due to Centrifugal Loading of Low-aspect Ratio Compressor Blades," Sc.D. Thesis, Stevens Institute of Technology, Hoboken, New Jersey, 1970.

130   Petricone, R. and Sisto, F., "Vibration Characteristics of Low Aspect Ratio

Compressor blades," Trans ASME, Journal of Eng for Power, Vol. 93, 1971, pp. 103-112.

131 Pfeiffer, R., "Blade Vibrations of Continuously Coupled and Packeted Steam Turbine LP-Stages", Proc of The Tenth Biennial Conf on Mechanical Vibration and Noise, "Vibrations of Blades and Bladed Disk Assemblies", Cincinnati, Ohio, Sept 10-13, 1985.

132 Plunkett, R., "Free and Forced Vibration of Rotating Blades", J. Aero. Sci. Vol 18, 1951, p 278.

134 Pnueli, D., "Natural Bending Frequency Comparable to Rotational Frequency in Rotating Cantilever Beam", J of Appl. Mech., Trans. ASME, Vol 39. No 2, 1972, pp. 602-604.

135 Powell, R. L., Stetson, K. A., "Interferometric Vibration Analysis by Wavefront Reconstruction", J of the Optical Society of America. 1965, Vol 55, no 12, pp 1593-1598.

136 Prohl, M. A., "A Method of Calculating Vibration Frequency and Stress of a Banded Group Turbine Buckets", Trans. ASME, Vol. 80, 1958, p. 169.

137 Provenzale, G. E., Skok, M. W., "A Cure for Steam- Turbine-Blade Failures", Combustion Jul 1974 p 30-36.

138 Putter, S, Manor, H., "Natural Frequencies of Radial Rotating Beams," Journal of Sound and Vibration, Vol. 56, No. 2, 1978, pp. 175-185

139 Rao, J. S., "Fundamental Torsion Vibration of a Cantilever Beam of

References

Triangular Cross Section with Uniform Taper", Proc. 10th Cong. ISTAM, p. 66 1965.

140   Rao, J. S., "Effect of Taper on Uncoupled Natural Frequencies of Cantilever Beams," Ph.D Thesis, I.I.T., Kharagpur, India, 1965.

141   Rao, J. S., Vibration of Turbine Blades, DSc Thesis, I.I.T.,Kharagpur, India, 1971.

142   Rao, J. S., "Natural Frequencies of Turbine Blading -- A Survey", Shock Vib. Dig., Vol 5, n 10, 1973, p 1.

143   Rao, J. S., Blade Group Forced Vibration -- Computer Program, Tech. Memo. 76 WRL M23, Rochester Institute of Technology, Rochester, New York, 1976.

144   Rao, J. S., "Turbine Blading Excitation and Vibrations", Shock Vib. Dig., Vol 9 n 3, 1977, p 15.

145   Rao, J. S., "Turbomachine Blade Vibration", Shock Vib. Dig., Vol 12 n 2, 1980, p 19.

146   Rao, J. S., "Turbomachine Blade Vibration", Shock Vib. Dig., Vol 15 n 5, 1983, p 3.

147   Rao, J. S., Belgaumkar, B. M., Carnegie, W.,"Torsional Vibration of a Cantilever Beam of Rectangular Cross Section with Uniform Taper", BMEE, 9, 1970, p. 61.

148   Rao, J. S., Carnegie, W, "Non-Linear Vibration of Rotating Cantilever Beams", The Aeronautical Journal of the Royal Aeronautical Society, Feb. 1970, Vol. 74, pp 161-165.

149   Rao,J. S., Carnegie, W., "Determination of the Frequencies of Lateral Vibrations of Tapered Cantilever Beams by the Use of Ritz-Galerkin Process", BMEE, Vol 10, 1971, p. 239.

150   Rao, J. S, Carnegie, W, "Non-Linear Vibration of Rotating Cantilever Blades Treated by the Ritz Averaging Process", Aeronautical Journal, Sept. 1972, pp 566-569.

151   Rao, J. S., Carnegie, W., "Torsional Vibration of Pretwisted Tapered Cantilever Beams Treated By Collocation Method", Ind. J. Pure and Appl. Physics, 10, p. 566, 1972.

152   Rao, J.S., Carnegie, W., "Numerical Procedure for the Determination of the Frequencies and Mode Shapes of Lateral Vibration of Blades Allowing for the Effects of Pre-Twist and Rotation", Int. J. Mech. Engng Educ. Vol 1, 1973, p 37.

153   Rao, J. S., Kulkarni, S. V., Subrahmanyam, K. B., "Applications of the Reissner Method to a Timoshenko Beam", Trans. ASME, J. Appl. Mechs., Vol 48, 1982, p 672.

154   Rao, J.S., Rao, D.K.,"Equations of Motion of Rotating Pre-Twisted Blades in Bending-Bending-Torsion with Effects of Warping, Shear, Rotary Inertia, etc.", Proc. Silver Jubilee Conf., Aeronautical Soc. of India, Bangalore, pp. 4-13, 1974

155   Rawtani, S., Dokainish, M. A., "Vibration Analysis of Pre-Twisted Cantilever Plates," Trans. of the Canadian Aero. and Space Ins., Vol. 2, 1969, pp. 95-100.

156   Rawtani, S., Dokainish, M. A., "Natural Frequencies of Rotating Low Aspect Ratio, Turbomachinery Blades," AIAA Paper No. 71-374, 1971.

157   Reissner, E., Washizu, K., "On Torsional Vibrations of a Beam with a Small Amount of Pretwist," Journal of the Japan Society of Aerospace Eng. Vol. 5, pp. 330-335.

158   Rosard, D. D., "Natural Frequencies of Twisted Cantilevers", J. Appl. Mech., Trans. ASME Vol 20, 1953, p 241.

159   Rubinstein, N., Stadter, J. T., "Bounds to Bending Frequencies of a Rotating Beam," J of the Franklin Inst. Vol. 294, No. 4, 1972, pp. 217-229.

160   Salama, A. L., Petyt, M., "Dynamic Response of Packets of Blades by The Finite Element Method", Trans. of The ASME, Journal of Mechanical Design. Vol. 100. Oct. 1978, pp 660-666.

161   Schilhansl, M. J., "Bending Frequency of a Rotating Cantilever Beam", J of Appl. Mech., Trans. ASME, Vol 25, no 1, 1958, pp 28-30.

162   Singh, B. R., Nandeeswariah, N. S., "Vibration Analysis of Shrouded Turbine Blades", J. Inst. Engr. Ind., Vol. 40, 1959, p. 16.

163   Sikora, J. P., Mendenhall, Jr. F. T., "Holographic Vibration Study of a

Rotating Propeller Blade", Experimental Mechanics, June 1974, pp 230-232.

164   Smith, D. M., "Vibration of Turbine Blades in Packets", Proceedings of the 7th International Congress of Applied Mechanics, 1948, Vol.3, pp 178-192.

165   Sollmann, H., "Influence of the Centrifugal Force on the Eigenfrequency of Moving Elastically Clamped Blades," (In German), Maschinenbautechnik, Vol. 27, No. 1, 1978, pp. 37-39.

166   Soares, Oliverio D. D., Fisica, Centro de., "Electronic Speckle Pattern Interferometry (ESPI) for Dynamic Studies", SPIE Vol 699, 1986, Laser and Opto-Electronic Technology in Industry, pp. 10-20.

167   Sreenivasamurthy, S., Ramamurti, V., "Effect of a Tip Mass on the Natural frequencies of a Rotating Pre-Twisted Cantilever Plate," J of Sound and Vib., Vol. 70, 1980, pp. 598-601

168   Srinivasan, A., Frye, H. M., "Effects of Mistuning on the Resonant Stresses of Turbine Blades," ASME Struct Dynamic Aspects of Bladed disks, 1976, pp. 57-75.

169   Srinivasan, A.V., Lionberger, S. R., Brown, K. W., "Dynamic Analysis of an Assembly of Shrouded Blades Using Component Modes", Trans. of the ASME, Journal of Mechanical Design. Vol. 100. 1978, pp 520-527.

170   Srinivasan, A. V., Cutts, D. G., "Dry friction Damping Mechanisms in Engine Blades", Journal of Engineering for Power, Trans of the ASME, April 1983, Vol. 105. 1983, pp 332-341.

References

171 Stange, W. A., MacBain, J. C., "An Investigation of Dual Mode Phenomena in a Mistuned Bladed Disk", Trans ASME J Vib Acous Stress Relia in Desn, Vol 105, 1983, pp 402-407.

172 Steele, Jeffrey, M., "Blade Code for Utility Blading Analysis", Proc. of Steam Turbine Blade Reliability Seminar and Workshop, March 1987, Los Angeles, California.

173 Stodola, A., "Steam and Gas Turbines", McGraw-Hill, 1927.

174 Stratford, B.S., "Rogue Blades", Report, Rolls-Royce Research Centre, 1966, Derby, England.

175 Sutherland, R.L., "Bending Vibration of a Rotating Blade Vibrating in the Plane of Rotation", J of Applied Mech., Trans. ASME, Vol 16, no. 4, 1949, pp. 389-394.

176 Sutherland, R. L., Goodman, L. E., Vibration of Prismatic Bars Including Rotary Inertia and Shear Deflections, Univ. of Ill., 1954

177 Swaminatham, M., Rao, J. S., "Vibrations of Rotating Pretwisted and Tapered Blades", Mech. Mach. Theory, Vol 12, n 4, 1977, p 331.

178 Targoff, W. P., "The Associated Matrices of Bending and Coupled Bending Torsion Vibration", J. Aero. Sci Vol 14, 1947, p 579.

179· Targoff, W. P., "The Bending Vibrations of a Twisted Rotating Beam", Proc. 3rd. Midwestern Conf. Solid Mech., 1957, p 177.

References

180   Taylor, J. L., "Natural Vibrational Frequencies of Flexible Rotor Blades", Aircraft Engr., Vol 30, 1958, p. 331

181   Thomas, D. L., "Standing Waves in Rotationally Periodic Structures," J Sound Vib, 1974, Vol. 37, No. 2, pp. 288-290.

182   Thomas,J., Belek, H. R., "Free Vibration of Blade Packets", Journal Mechanical Engineering Science. Vol. 19, no. 1, 1977.

183   Thomas, J., Dokumaci, E., "Simple Finite Elements for Pretwisted Blading Vibration", Aero. Q. Vol 25, 1974, p 109.

184   Thomas, J., Sabuncu, M., "Finite Element Analysis of Rotating Pretwisted Asymmetric Cross-Section Blades," ASME Paper 79-DET-95, 1979.

185   Thomas, J., Mota Soares, C. A., "Finite Element Analysis of Rotating Shells," ASME Paper No. 73-DET-94, 1973.

186   Thomas, J., Mota Soares, C.A., "Dynamic Analysis of Rotating Turbine and Compressor Blading", Vibrations in Rotating Machinery, Proc. of the I Mech E Conf. Cambridge, Sept. 1976, pp 231-237.

187   Thomson, W. T., "Matrix Solution for the Vibration of Non-Uniform Beams", Journal of Appl. Mech., Vol. 17, 1950, pp. 337-339.

188   Thomson, W. T., Theory of Vibration with Applications, Prentice-Hall, 1972.

189   Timoshenko, S., Strength of Materials, Part II, Advanced Theory and

Problems, Van Nostrand, New York, 1930

190   Timoshenko, S. P., Vibration Problems in Engineering, Van Nostrand
       Publications, 1955

191   Timoshenko, S. P., Goodier, J. N., Theory of Elasticity, McGraw-Hill
       Publications, 1961

192   Tomar, J. S., Sahu, A. R., "Bending Vibrations of a Wedge Shape Beam in
       a Centrifugal Force Field," Journal of the Aeronautical society of India,
       Vol. 27, No. 3, 1975, pp. 125-132.

193   Ucmaklioglu, M., "Vibration of Shells with Applications to Hollow
       Blading," Ph.D. Thesis, University of Durham, 1978.

194   Uflyand, Y. S, "The Propagation of Waves in the Transverse Vibration of
       Bars and Plates", Prikladina Matematika i Mekhanika, Vol 12 May-June,
       1948, pp 287-300.

195   Vet, M., "Torsional Vibration of Beams Having Rectangular Cross
       Sections", J. Acoust. Soc. Amer., 34, p. 1570, 1962.

196   Vierck, R. K., Vibration Analysis, Second Edition, Harper & Row
       Publishers, 1979.

197   Vorobyew, Yu. S., Gontarovskiy, P. P., "Utilization of Variational Methods
       in the Calculation of Rotor Blades and Propeller Vibrations," English
       translation of Dinamika i Prochnost Mashin, 1972, pp. 37-43.

303

References

198   Wachter, J., Bechmann, J., Wolter, I., " Investigation of Turbine Blade
        Vibration due to Flow Distortion and Damping Effects", Proc of I Mech E
        Conf on Rotating Machinery, 1979, C190/79, pp 173-184.

199   Walker, K. P., "Vibrations of Cambered Helicoidal Fan blades," J of
        Sound and Vibration, Vol. 59, 1978, pp. 35-37.

200   Walker, P. B., "Simple Formulae for Fundamental Natural Frequencies of
        Cantilevers", R&M 1831, 1938.

201   Wang, H. C., "A General Treatment of the Transverse Vibration of
        Tapered Beams," Ph.D. Thesis, Univ. of Ill, 1956.

202   Wang, J. T. S., "Equations for the Vibration of a Rotating Blade,"
        Mechanics Research Communications, Vol. 1, No. 5/6, 1974, pp. 341-346.

203   Wang, J. T. S., Mahrenholtz, O., Bohm, J., "Extended Galerkin's Method
        for Rotating Beam Vibration Using Legendre Polynomials," Solid
        Mechanics Archives, Vol. 1, No. 4, 1976, pp. 341-365.

204   Ward, P. F., "Transverse Vibrations of a Rod of Variable Cross Section",
        Phil. Mag., Vol 25, 1913, p 85.

205   Wauer, J., "The Influence of the Centrifugal Force Divergence on the
        Natural Vibrations of Rotating Turbine Blades," (In German), Forschung
        im Ingenieurwesen, Vol. 39, No. 6, 1973, pp. 191-198.

206   Weaver, F. L., Prohl, M. A., "High Frequency Vibration of Steam Turbine
        Buckets", Trans, ASME, Vol. 80, 1958, p.181.

References

207   Weidenhammer, F., "Coupled Bending Vibrations of Turbine Blades in a Centrifugal Field," (In German), Ingenieur-Archiv, Vol. 39, No. 5, 1970, pp. 281-290.

208   Whitehead, D. S., "Torsional Flutter of Unstalled Cascade Blades at Zero Deflection," R & M 3429, 1964, University of Cambridge, Cambridge, England.

209   Whitehead, D. S., "Research Note: Effect of Mistuning on Forced Vibration of Blades with Mechanical Coupling", J Mech Eng Sci, Vol 18, 1976, n 6.

210   Wildheim, "Natural Frequencies of Rotating Bladed Discs Using Clamped-Free Blade Modes", Trans. ASME, J of Vib. Acous. Str. and Reliability Design, 1983, Vol. 105, pp. 416-424.

211   Wrinch, D. M., "Lateral Vibrations of Bars of Conical Type", Proc. Roy. Soc., Vol 101, p 493, 1922